NASA TECHNICAL TRANSLATION

NASA TT F- 16171
TT 73-58027

PHYSICS OF COSMIC RAYS

V. S. Murzin

(NASA-TT-F-16171) PHYSICS OF COSMIC RAYS (NASA) 285 p HC $8.75 CSCL 03B

N75-15584

Unclas
G3/93 07737

Translation of "Fizika Kosmicheskikh Luchey,"
Moscow, Moscow University Press, 1970, pp 1-282

FEB 1975

NATIONAL AERONAUTICS AND SPACE ADMINISTRATION
WASHINGTON, D.C. 20546 DECEMBER 1974

Translated for the National Aeronautics and Space
Administration and the National Science Foundation
Washington, D.C., by Franklin Book Programs, Inc., 1974

CONTENTS

Preface

Chapter 1. Introduction
1. Cosmic-ray physics as an independent branch of science. 2
2. Principal stages of studying cosmic-ray physics. 4

PART ONE
Interaction of High-Energy Particles with Nuclei and Atoms

Chapter 2. Electromagnetic interactions
1. Elementary processes. 9
2. Ionization. 10
3. Bremsstraalung 15
4. Interaction of protons with matter 18
5. Radiation length unit and critical energy 20
6. Scattering of electrons , ... 23
7. Restrictions at high energies 23
8. Electron-photon showers 24
9. Spatial divergence of particles in a shower 26
10. Experimental study of cascade showers 38
11. Measurements based on the properties of electromagnetic interactions. 42

Chapter 3. Elementary particles
1. Methods of determination of particles' masses 46
2. Muons 49
3. Neutrinos 61
4. Strong-interaction particles 64
Questions and problems. 70

Chapter 4. High-energy nuclear interactions
1. Major Properties 71
2. Kinematics of collision between relativistic particles 72
3. Inelastic collisions 77
4. Methods for studying nuclear interactions in cosmic rays ... 91
5. Investigation of nuclear interactions 102
6. Nature of shower particles 107
7. Number of shower particles 109
8. Angular distribution of shower particles. 110
9. Transversal momentum. 116
10. Inelasticity coefficient 117
11. Energy spectra of the created particles 121
12. Interaction of nuclei at high energies 126
13. Theoretical interpretation of multiple production of particles 129
Questions and problems 136

PART TWO

Interaction of Primary Radiation with Magnetic Fields and Matter

Chapter 5. Primary cosmic radiation
1. Basic definitions 138
2. Basic properties of primary cosmic rays 140
Questions and problems. 146

Chapter 6. Interaction of the primary radiation with the magnetic field of the earth
1. Geomagnetic effects 146
2. Motion of charged particles in a magnetic dipole field 148
3. Practical application of the theory 158
Questions and problems 167

Chapter 7. Motion of particles in the internal permitted region (capture region)
1. Geometry of the capture region 167
2. Particle sources in the capture region 168
3. Radiation belts of the earth 169
4. Instruments for studying radiation belts 178
5. Experimental investigation of radiation belts 180
Questions and problems. 188

Chapter 8. Stability and variation of cosmic radiation
1. Conservation of mean intensity 188
2. Variations of cosmic rays 195
3. Variations of different origins 200
4. Mechanism of solar-connected variations 204
Questions and problems. 210

Chapter 9. Interaction of cosmic rays with the terrestrial atmosphere
1. The atmosphere 211
2. Cosmic ray penetration through the atmosphere 212
3. Nuclear cascade processes in the atmosphere 215
4. Pions in the atmosphere 223
5. The muons 225
6. The electron-photon component 232
7. The neutrinos 235
8. Extensive atmospheric showers 236
9. Determination of energies of particles generating showers ... 257
Questions and problems. 259

PART THREE

Origin of Cosmic Rays

Chapter 10. Origin of cosmic rays

1. Introduction 260
2. Possible sources of cosmic rays 262
3. Cosmic-ray acceleration mechanism 264

Appendices 270

References. 276

P r e f a c e

This course in "Cosmic-Ray Physics" (Fizika Kosmičeskih Lucej) is intended for advanced undergraduate students. The smallness in volume of this text-book does not allow us to expound several important aspects of the subject. The special situation of the course "cosmic-ray physics" relative to other study courses leaves its imprints on its contents. Lectures on cosmic rays are often given before the students study a course in "Interaction of Particles with Matter". For this reason, the present text-book involves a brief survey of the theory of electromagnetic interactions, mainly at high energies. The book also only gives a general background on elementary particle physics since the student will, in the future, be given a special course on this subject.

The author finds it useful to include in the present text-book a list of references on original experimental and theoretical papers since the next stage of studying cosmic rays is the acquaintance with review articles which give detailed bibliographies. The preparation of students for reading review articles is one of the main targets of the present text-book. For this reason, special attention is paid to the explanation of the terminology. Each chapter of the book is provided with a special list of references, where, in particular, the principal surveys written in Russian are quoted.

A limited number of problems is listed at the end of each chapter. Some of them are simply based on the application of the formulae and tables involved in the corresponding chapter. In many cases, it is required to give an explanation of the solutions since this simplifies the understanding of one or another aspect of the physical phenomenon concerned. An extensive collection of problems on cosmic-ray physics is available in : "Collection of Problems in Nuclear Physics" (Sbornik Zadač po Jadernoj Fiziki, M., Fizmatgiz, 1963) by S.V. Skackov et al.

The author owes a particular debt of gratitude to G.T. Zacepin and I.L. Rozental' for reading through the manuscript and making several valuable suggestions. He is also grateful to L.I. Dorman, G.B. Ždanov, I.P. Ivanenko, C.N. Kuznecov, L.I. Caryceva, C.I. Syrovatskij and G.B. Hristiancen for useful comments on separate parts of the book.

The author would like to express his thanks to L.F. Marčenko for assistance in preparing the manuscript for publication.

Chapter 1

INTRODUCTION

1. Cosmic Ray Physics as an Independent Branch of Science

Cosmic rays are stable particles and atomic nuclei created and accelerated to high energies somewhere outside the Earth in the immense universe space.

The study of cosmic rays has its own characteristic features. It can be considered, at the present time, as an independent branch of physics. The characteristic features of a given independent branch of science are the particular subjects of research and the specific methods of investigation as well as the theoretical and practical value of this branch of science.

The objectives of research in cosmic ray physics are: (a) the processes leading to the generation and acceleration of cosmic rays, (b) the cosmic particles, their nature and their properties, and (c) the effects, caused by cosmic particles in the cosmic space, in the atmospheres and crusts of the Earth and other planets.

Studies on cosmic ray physics make use of methods and instruments, developed by nuclear physicits. Examples of these methods are the method of magnetic analyses of the momenta of particles and the method of determination of the penetration power of radiation by measuring its absorption in various materials. These methods are modified when applied to investigations on cosmic ray physics. The Earth's magnetic field is used as a natural analyser for the momenta of cosmic particles (the so-called latitutde-effect method). The terrestrial atmosphere is used as an absorber. The phenomena caused by cosmic rays sometimes extend over an area of tens of thousands of square meters. Their analyses require instruments having dimensions in hundreds of meters. A great number of methods and technical devices are common between cosmic-ray physics and other branches of science, such as construction of high-mountain stations, exploitation of balloons, rockets and artificial satellites. The wide application of these methods brings cosmic-ray physics close to geophysics.

Finally, it is worthwhile to write several words on the great theoretical and practical value of cosmic-ray physics. This branch of knowledge plays an important role in the study of the interaction of elementary particles at high energies. Most of the elementary particles that we now know have been discovered in cosmic rays. For a long time, processes occuring at energies higher than 10^9 eV could be studied only in cosmic rays, and even now the range of energies exceeding 10^{11} eV has not been reached by means of accelerators. Here, cosmic-ray physics prevails without competance. In the last few years, cosmic ray physics penetrated into many other branches of science, from archeology to astronomy and problems of cosmic flights. Other applications of cosmic ray physics will be clearer in the future. For all these reasons, cosmic-ray physics has the right to be considered as an independent branch of physics.

We shall now try to identify the place occupied by cosmic-ray physics relative to other branches of science. In 1927, it has been established that cosmic rays are fluxes of high-energy particles. Since then, the problem of studying the properties of cosmic particles and their interaction has occupied many physicists. It was realized that investigations on cosmic rays carried a nuclear aspect, and cosmic-ray physics was becoming closer and closer to nuclear physics. A great number of publications appeared in this direction. Although considerable success is already achieved in these studies, much more is still expected. This direction of research may be called "Study of Intersection of Particles at High Energies".

There is another direction of research on cosmic rays which involves a large class of phenomena related to the interaction of cosmic rays with different cosmic objects, mainly with plants. Researches of this kind are concerned with the study of the interaction of cosmic-ray particles with the Earth's magnetic field (and possibly of other planets) and of the penetration of cosmic rays through the atmospheres and matters of the planets. The interaction of charged cosmic-ray particles with the magnetic fields of planets is responsible for the latitude effect of the cosmic radiation and for the existance of the radiation belts. The interaction of cosmic rays with the atmosphere is responsible for the creation of extensive showers of cosmic rays. Muons which are observed deeply underground are a consequence of the presence of the atmosphere. This part of the subject is to be called "Interaction of Cosmic Radiation with Cosmic Bodies".

Another important direction of research on cosmic-ray physics is what we shall call "Studies in the Cosmic Space". In this part, theories on the origin of cosmic rays are analysed. This direction of research is mainly devoted to the study of cosmic rays in their sources before they become influenced by the Earth and its atmosphere. Here, cosmic-ray physics borders astrophysics, solar physics, radio astronomy and plasma physics. In this respect, the boundaries of cosmic-ray physics become wider, and the term "cosmic rays" in a wider sense means any type of gas in the cosmic space, which exists in a state far from thermodynamic equilibrium, and the collisions of its particles with one another may be ignored (P. Morrison, 1960).

Consequently, cosmic-ray physics involves a number of problems which are closely related to each other and which stand on the cross roads of nuclear physics, astrophysics, cosmic-space physics and geophysics.

It may be more logical to start the study on cosmic rays by studying their origin. This probably will be the approach which will be followed in the near future. At present, the problem of the origin of cosmic rays is still at the guessing stage, which can be only checked by the analysis of the interaction of cosmic-ray particles with the terrestrial atmosphere and with the Earth's magnetic field. Only very recently, radio astronomy made it possible to study cosmic rays at their origins. For this reason, we start our course on cosmic ray physics by considering their interaction with atomic nuclei.

2. Principal Stages for Studying Cosmic Ray Physics

The discovery of cosmic radiation was related with the investigations of electric conductivity of gases. In 1900, Wilson discovered a spontaneous current in a gas held under the action of an alectric field. This phenomenon was interpreted as an ionization induced by the radioactivity of the Earth. However, when the ionization chamber in which the current was measured was screened by a thick layer of lead, a residual current was always registered.

The assumption that an ionization was self induced by thermal agitation was rejected as improbable after carrying experiments in which temperature was varied. Wilson tentatively suggested that the ionizing agency might be a radiation of extra-terrestrial origin. This point of view was not met with approval at that time.

In 1910-1911, experiments were made in which chambers were raised in balloons. It was expected that the ionization would decrease with height if the reason for ionization was the radioactivity of the Earth. Hess, Gockel and Kolhorster carried out such experiments and found that the ionization current was slightly damped at the beginning but then increased rapidly. In 1962, the 50th anniversary of this event was celebrated. In July 28, 1914, just before the First World War, Kolhorster discovered that the ionization current at 9.2 km was tan times greater than at the surface of the Earth. It was concluded that radiation came from above to below. The radiation was called the Hess radiation from above.

Three postulates were suggested to explain the origin of this radiation. These postulates are: 1) there exists a radio-active gas in the upper layer of the atmosphere, 2) electrons are accelerated by the influence of the electrical processes in the atmosphere (the so-called thunderstorm theory, which was soon rejected) and 3) the radiation is cosmic.

In 1922-1925, Mellikan measured the absorption coefficient of the radiation from above in lead. He found that this absorption coefficient was close to the absorption coefficient of gamma-rays. This was considered to be consistant with the first postulate. However, L.V. Mysovskij measured the absorption coefficient of the radiation from above under the water of Lake Onega. He found that the absorption of this radiation in water is much less than the corresponding absorption of gamma-rays. Therefore, it was concluded that the absorption of the radiation from above strongly depends on the material of the absorber. This was an indication that the properties of this radiation are significantly different from the properties of gamma rays.

In 1927, D.V. Skobel'cyn carried out a series of investigations on the Compton effect. His aim was to chekc the Klein-Nishina formula. In his experiments, he used a Wilson cloud placed, for the first time in history, in a strong magnetic field. In this way, he was able to measure the momenta of the particles of radiation. In some of the slides, he observed the tracks of particles which had no relation with the gamma-ray sources. The monenta of these particles were much greater than the momenta of the radio-active contaminations. He concluded that these tracks must have been due to cosmic rays passing through the chamber. This was a proof for the corpuscular nature of cosmic rays.

At that time, investigations on the radiation from above were carried out mainly by geophysicists. After Skobel'cyn's discovery, the subject attracted the attention of nuclear physicists. This stage of development of cosmic ray physics may be called "Stage of Accumulation of Experimental Data on Cosmic Rays". During this period of time, cosmic-ray showers were discovered. The dependence of the intensity of cosmic rays on altitude was carefully studied. It was found that the intensity of cosmic rays has a maximum at an altitude of ~20 km.

In 1932, Anderson discovered positrons in cosmic rays. Slightly later, the theory of creation of pairs was developed. Of great importance was the experiment that led to the discrimination of cosmic rays into hard and soft components. This experiment consisted in the following. Two counters were placed a small distance apart one above the other and connected to a coincidence circuit. A lead filter was put between the two counters (Figure 1a). The number of coincidences corresponding to different thicknesses of the lead filter were recorded. The dependence obtained from this experiment is given in figure 1.b. At the beginning of the curve, the number of coincidences rapidly decreases with increasing thickness, then, after the thickness reaches 10 cm, the rate of decrease of the number of coincidences becomes much smaller. Cosmic-ray particles absorbed in 10 cm of Pb were called soft, while the others were called penetrating or hard. The ratio of numbers of soft and hard particles depends on the altitude. At sea level, the number of soft particles is approximately one-third the total number of cosmic-ray particles.

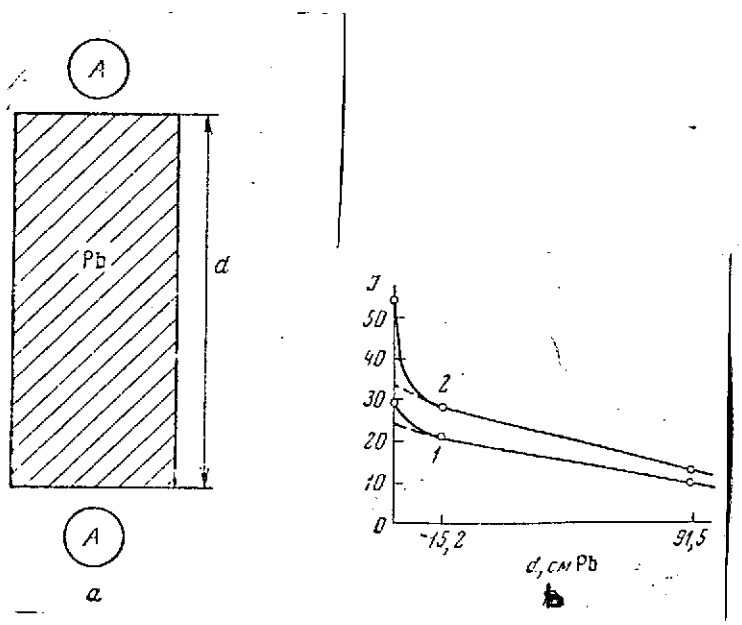

Fig. 1 - Absorption curves for cosmic-radiation particles in lead (discrimination into soft and hard components): (a) the scheme of the experiment (d is the thickness of the lead filter and AA are the gas-discharge counters), (b) dependence the number of coincidences on the thickness of lead: 1) 76 cm.Hg (sea level) 2) 52 cm.Hg (3200 m above sea level).

It was found later that this phenomenological descrimination has a deep physical meaning and corresponds to a differentiation between particles of different nature. It was established that soft cosmic-ray particles are electrons and positrons. These particles loose the main part of their energy in emitting photons while they are decelerated in the fields of the atomic nuclei. The hard particles are muons (μ-mesons). Their mass is approximately two-hundred times the mass of the electron. They are absorbed much more slowly since their bremsstraalung is rare. The principal role in their deceleration is played by the ionization losses. Muons were discovered in 1937 by Anderson and Neddermeyers. It was found that these particles are unstable. They decay into electrons during a mean time $\tau_o \simeq 2 \times 10^{-6}$ sec.

During this stage, there was a hope to construct a well-composed picture for the processes that take place in cosmic rays. The grounds for this hope was the electromagnetic cascade theory of showers, developed at that time and found to be consistant with the observation. The theory was able to predict the existance of the maximum of the intensity of particles when protons or electrons are incident on matter. This maximum had been observed in the altitude dependence of cosmic rays, and this was considered as a proof for the generation of cosmic rays. It was thought that primary cosmic rays consist of electrons. When the latitutde effect of cosmic rays was discovered, according to which the intensity of the cosmic radiation depends on the geographical latitude of the place of observation, the effect was explained as being a result of the influence of the Earth's magnetic field. This indicated that cosmic rays are fluxes of charged particles. Everybody was convinced that the principal role in cosmic rays was played by electromagnetic processes. No one cared to consider the role of nuclear processes.

Nature, however, was preparing a great surprise to physicists. The discovery of neutrons and protons in cosmic rays, and the anomalies of the development of showers in air, shaked their faith in the correctness of their interpretation of the phenomena that occur in cosmic rays. In the earlier post-war years (1945-1949), Soviet physicists discovered the nucelar cascade process and the electronic-nuclear showers, formed by particles at very high energies. These showers are composed not only of electrons, but also of protons, neutrons and pions (π-mesons), which have masses 275 times of the electron mass and have been discovered in 1947. The highly-effective generation of gamma-photons by protons and neutrons was found to take place through the formation of a neutral pion (π^0-meson), which decayed after about 10^{-16} sec. into two gamma-photons. Finally, a series of experiments, carried out in the statosphere in 1949, proved the fact that there are no electrons in the primary radiation and that the primary radiation consists mainly of protons. The year 1951 witnessed the discovery of Kaons (K-mesons) having a mass 966 times that of the electron mass. Subsequently, the discoveries of new particles took a shower-like character. Each year brought in newer and newer particles. The properties of these particles were so unexpected, that they were called strange particles by physicists who by now are accustomed to anything. The term "strangeness" was introduced in physics and used on equal footing with the terms "spin", "magnetic moment", etc.

Four years later, a new excitement took place. It was found that the law of conservation of spatial parity was violated in a given type of interaction, known as the weak interaction.

The rapid development of accelerators enabled us to artificially create these new particles and to study them in laboratory conditions. Recently, completely new formations were discovered by means of accelerators. These are groups of two or more strongly-interacting particles such as pions and kaons. These particle-systems have a very short life time $\tau \sim 10^{-20} - 10^{-23}$ sec.

During all these years, rockets have been intensively used for the investigation of cosmic rays outside the limits of the atmosphere. By means of rockets, we could measure the intensity of cosmic rays at heights reaching 150 km, where the atmosphere is practically non-existing. A new facility for studying primary cosmic rays became available in 1957, when physicists were offered such a powerful research device as artificial satellites. The first satellite flights registered an increase in the itnesity of cosmic rays, especially in the polar zones. Later, zones of radiation of tremendously high intensity were discovered at large altitutdes over the Earth. The speed of the counts in the first experiments were so high that the counters were spoiled and registration stopped. Later measurements indicated that that the fuluxes of cosmic-ray particles at these zones is hundreds of millions of times greater than the expected fluxes of cosmic radiation. In 1958, V.S. Vernon and A.I. Lebedinskij were able to interpret these phenomena.

These are the principal stages of the development of cosmic-ray physics. We now believe that the picture for propagation of cosmic rays is becoming clearer and clearer, exactly the same as we thought 25 years ago. We have learned that the principal role in these phenomena is played by nuclear processes. However, who knows what kind of surprise nature has in store for us.

PART ONE

INTERACTION OF HIGH-ENERGY PARTICLES WITH NUCLEI AND ATOMS

Types of interaction

In modern physics, four types of interactions are recognized. Amongst them, only three types have to be considered in nuclear physics[1] : 1) the strong interaction, 2) the electromagnetic interaction, and 3) the weak interaction.

The strong interaction takes places between protons, enutrons, pions, kaons, and hyperons. At high energyies, this interaction leads to the multiple

---

1) The fourth type is gravitational interaction. At present, there is a tendency to consider another "intermediate" type of interaction, e.g., the semi-strong interaction.

generation of mesons. If the intensity of the strong interaction is characterized by a dimensionless constant G^2/hc, analogous to the constant $\alpha = e^2/hc$ of the electromagnetic interaction, then this constant will be approximately equal to 15. The quantity G will have the physical meaning of a "nuclear charge". The carriers of the strong interactions are the mesons. The strong-interaction processes are distinguished by their very short time $\sim 10^{-22} \div 10^{-24}$ sec. (the so-called "nuclear time").

The electromagnetic interaction is the most studied type of interaction. It is present between particles possessing electrical charges. The carriers of this interaction are the phonons. The constant of the electromagnetic interaction $\alpha = e^2/hc = 1/137$. The characteristic time of the electromagnetic interaction is by tens of thousands times greater than the nuclear time.

Examples of the weak interaction are the following reactions :

the β-decay of the neutron : $n \rightarrow p + e + \vec{\nu}$

the μ-decay : $\mu \rightarrow e + \nu + \vec{\nu}$

The constant of the weak interaction $(g/\hbar c)^2 (\hbar/\mu c)^{-4} \sim 10^{-12} - 10^{-13}$. Such a small value for the constant of the interaction is responsible for the fact that the weak processes proceed very slowly, during times $\gg 10^{-10}$ sec, and sometimes, e.g. in the decay of the neutron, during 1000 sec on the average. The weak interaction is the most universal type of interaction. It is inherent to all particles, except photons.

CHAPTER 2

ELECTROMAGNETIC INTERACTION

1. Elementary Processes

At the present time, only the theory of electromagnetic interaction is well developed. For this reason, various properties of the elementary particles are determined by means of electromagnetic processes. We shall first give a brief account of the elementary processes which take place when a particle or a photon approaches an atom. Later, we shall consider the phenomena, which take place when high-energy electrons or photons pass through a thick layer of matter (the cascade theory).

Different interaction processes of a charged particle with an atom will occur, depending on the distance at which the charged particle approaches the atom. For quantitative characterization of the approach distance, one often uses the impact parameter b. One can distinguish the following three cases :

1. The impact parameter is so large as compared with the dimensions of the atom that it reacts as a whole upon the field of the incident particle. In this case the atom may be excited or ionized.
2. The distance of approach is such that the incident particles interact with the separate electrons of the atom. In this cass, one of the electrons may acquire enough energy to be released from the atom. Such an electron is called a δ-electron. Evidently, this effect is considered as a component of the process of ionization.
3. If the particle is interacting with the coulomb field of the nucleus or the atomic electrons, then an extremely important role will be played by the curvature of the particle's trajectory under the influence of this field. This curvature means that the particle acquires a transversal acceleration. According to classical electrodynamics, and acceleration leads to radiation, with an intensity proportional to the square of the acceleration. This process is known as bremsstraalung.

When photons interact with atoms, one also has to distinguish between the following three cases :

1. The photon interacts with the atom as a unit. This interaction takes place at very low photon energies and is known as photo-effect. In photo-effect, the photon is totally absorbed and its energy is transferred to one of the atomic electrons.
2. The photon interacts with the "free electrons". Such an interaction takes place when the energy of the photon is much greater than the binding energy of the electron in the atom. The photon transfers part of its energy and momentum to the electron. This phenomenon is known as the Compton effect.
3. The photon interacts with the Coulomb field of the nucleus (or the atomic electrons). The photon creates an electron-position pair. Naturally, this process takes place only when the photon energy is greater than $2m_e c^2$. The nucleus acquires the momentum excess.

All these phenomena have been studied in other courses. Therefore, we shall not give the derivation of the formulae, describing these processes. We shall only give the results which will be useful for future discussions.

2. Ionization

The simplest type of electromagnetic processes is the excitation and ionization of the atoms. For pratical purposes, it is very important to know everything about the ionizational energy losses of different particles. The first calculation of ionizational losses was made by Bohr /1/ on the basis of classical considerations. More exact calculations on this subject can only be done on the basis of quantum mechanics. Such calculations were carried out by Bethe /2/. He found that the total energy loss of a particle of charge $\pm ze$ along a path of length 1 cm on the ionization of the atoms is represented by fig. 2 and given by the following equation

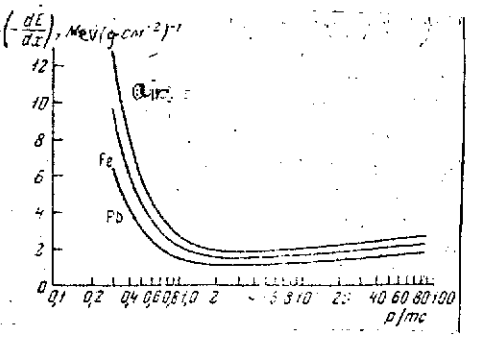

Fig. 1. The dependence of the specific ionizational loss of energy on the quantity p/mc calculated by Bethe's formula (p is the momentum, and m is the mass of the particle).

$$-\left(\frac{dE}{dx}\right)_i = 2\pi n Z z^2 r_0^2 \frac{mc^2}{\beta^2}\left[\ln\frac{2mc^2}{I^2(Z)}\cdot\frac{\beta^2}{(1-\beta^2)}W_m - 2\beta^2 - \delta\right], \qquad (2.1)$$

where δ is a correction depending on the density of the medium, n is the number of atoms per cubic centimeter, $r_0 = e^2/mc^2$ is the classical radius of the electron, Z is the atomic number of the material, W_m is the maximal energy that the incident particle can transfer to the electron[1] and I(Z) is the ionization potential.

The ionization potential enters the formula inside the logarithmsign. Therefore, it is unnecessary to know the exact dependence of I on Z. Generally, the consideration is confined to the empirical formula $I(Z) = I_0 Z$, where I_0 is a proportionality constant.

Experiments show that I_0 varies from 9 to 12 eV for different elements. Table 1 gives the values of the ionization potentials for some atoms.

---

1) For very high energy particles, $W_m = pc = E$. In general

$$W_m = \frac{E^2 - (Mc^2)^2}{Mc^2\left(\frac{M}{2m} + \frac{m}{2M} + \frac{E}{Mc^2}\right)}.$$

Table 1

	Element					
	Be	C	Air	Al	Cu	Pb
I, eV	64	78	94	166	323	826
I_0, eV	16	13	12,8	12,8	11,1	10

Let us analyse equation (2.1). The purpose of our analysis is to make the formula more convenient for practical use keeping the required accuracy in the area of high energies.

Step 1 : Formula (2.1) is related to the loss of energy on a path of length 1 cm. We note that the specific weight of any material may be represented as

$$\gamma = nAm_p,$$

where n is the number of atoms in 1 cm^3, A is the mass number and m_p is the mass of a proton. For not very heavy nuclei, $A \approx 2Z$, and thus $\gamma \approx n \cdot 2Zm_p$. Consequently, if we define the ionization loss at a path of 1 g/cm^2, then

$$\left[\left(\frac{dE}{dx}\right)_i\right]_{g/cm^2} = \frac{1}{\gamma}\left[\left(\frac{dE}{dx}\right)_i\right]_{cm}$$

almost does not depend on the properties of the medium. Indeed, the dependence on Z remains only inside the sign logarithm, i.e. becomes very weak.

Step 2 : The energy of the ionizing particles also only enters the expression of the energy loss inside the logarithm sign. Therefore, the ionization loss of a high-energy particle, i.e. when $\beta \sim 1$ (practically, when $B > 0.96$), will weakly (logarithmically) depend on the energy. Consequently, we may rewrite equation (2.1) in the form of

$$\left[-\left(\frac{dE}{dx}\right)_i\right]_{g/cm^2} = \pi r_0 \frac{mc^2}{m_p} z^2 L_{ion}(Z, E), \qquad (2.2)$$

where $L_{ion}(Z,E)$ is the so-called ionization logarithm, which is a slowly varying logarithmic function of Z and E. Accordingly, the energy loss by particles of unit charge in 1 g of a material will almost be the same for all materials if the energy of the particle is sufficiently large ($\beta \approx 1$). In order to illustrate this fact, we give in table 2 the values of the energy losses of different materials on ionization by particles having energy $E \sim 2 \div 3\ Mc^2$. These values are often practically used and they should be well remembered. The ionization logarithm slowly increases with increasing energy. Therefore, the losses increase with energy. Such an increase is related with the relativistic contraction of

Table 2

Material	Energy loss MeV cm^2/g
Air	1.8
Aluminium	1.65
Iron	1.50
Lead	1.20

the field in the longitudinal direction and with the consequent increase of the distance of approach at which the ionization and excitation of the atoms are possible. However, in dense gases, liquids and solids, the density effects become important. The atoms of the medium become deformed by the influence of the field of the incident particle. As a result, the medium becomes polarized. The induced electric field will be in the opposite direction with respect to the field of the incident particle.

At a certain distance from the line of motion of the particle (depending on the density), the field of the incident particle is completely compensated, and the energy losses due to far collisions increase with energy. Mathematically, this result is expressed by the fact that the quantity δ ,which describes the density effect, increases logarithmically with energy. At sufficiently high energies (for example, in argon, at muon energies higher than 10^4 GeV)

$$\delta = -\ln(1-\beta^2) - \varphi,$$

where φ is a constant depending only on the properties of the medium. The term $\ln(1-\beta^2)$ in the equation for δ completely compensates the increase of the first term in equation (2.1).

The logarithmic increase of the energy loss is weaker than in the case when the density effect is not taken into account. However, this loss continues by the influence of the near collisions, which lead to great losses in energy. This is clear from the fact that the maximal energy transfer W_{max} is proportional to the initial energy (when $E \gg Mc^2$).

The ionization losses are strongly (quadratically) dependent on the charge of the incident particle. This property of the ionization losses is useful in determining the charge of the particle. For example, a moving nucleus of iron (Z = 26) looses energy on ionization 676 times more than the energy lost by a proton.

In order to make use of this ionization loss property, it is necessary to learn how to measure it. In deriving his formula, Bethe started from the assumption that the energy loss is due to excitation of atoms and to ionization (i.e. tearing off an electron from the atom and imparting some of the energy to the electron). The instruments used for the registration of the particles, e.g. the photoemulsion, ionization chambers, proportional counters, etc., do not measure the ionization loss of energy, but measure only ionization, i.e. the number of ions produced by the penetrating particle. However, theory and experiment show that the ratio of the energy lost for the excitation of an atom, W_e , and the energy lost for ionization, W_i,does not depend on the incident energy. Since W_e/W_i = constant, then

$$\frac{dE}{dx} = W_i + W_e = W_i\left(1 + \frac{W_e}{W_i}\right) = CW_i. \qquad (2.3)$$

Since the total energy, lost for the tearing off of electrons from atoms is proportional to the number of ions, then $W_i = k_i$ and

$$\frac{dE}{dx} = Cki = V_0(Z)\, i, \tag{2.4}$$

In other words, the energy loss is proportional to the number of ions. The quantity V_o does not depend on Z.

The validity of the previous relation has been checked experimentally. A number of the energy experimental measurement results, in electron-volts, lost on the formation of a pair of ions in gases, is given in table 3.

Accordingly, we are able to determine the ionization loss by measuring ionization.

Table 3

Particle	Air	H_2	O_2	Ar
α-particle	35,0	36,0	33,2	25,8
Proton	33,3	35,3	31,5	25,5
Electron	35,0	38,0	32,2	27,0

An important property of the ionization loss follows from table 3. In each collision act, only a very small portion of energy is lost on the average. However, in several cases of near collisions, the torn off electrons acquire considerable amounts of energy. Such electrons are called δ-electrons. In principle, the δ-electron may escape with a very large amount of energy. However, the probability of a large energy transfer is small. The probability of energy transfer is inversely proportional to the square of the energy of the δ-electron, ε^2,

$$P(\varepsilon)\, d\varepsilon = Q \frac{d\varepsilon}{\varepsilon^2}. \tag{2.5}$$

With increasing thickness, x, of the layer of matter, penetrated by the particle, the probability of a large transfer of energy to the δ-electron increases. Therefore, $Q \sim x$. Expressing x in units of g/cm^2, then

$$Q = 0,15 \frac{Z}{A} z^2 x \text{ Мэв}. \tag{2.6}$$

when $\beta \sim 1$.

The existance of δ-electrons, to which considerable energy is transferred leads to a logarithmic increase in the energy loss even if the density effect is taken into consideration. This is a consequence of the increase of the maximal transferable energy W_{max}.

In practice, the value of the quantity W_{max} often cannot be measured because of the limitations on the dimensions of the counters. For example, in a proportional counter of dimension 5 cm at atmospheric pressure, the maximal energy released in the gas does not exceed a few kiloelectron-volts. The high-energy δ-electrons lose the main amount of their energies in the walls of the container. Analogous phenomena (although caused by different reasons) are observed in

Wilson's chambers and in photo-emulsions where ionization is measured by counting the number of drops or grains. In this case, the instruments are also unable to register the energy W_{max}. Therefore, when one calculates the energy loss due to ionization, one replaces the quantity W_{max} in equation (2.1) by the maximal value W_o of the energy measured, which is almost independent of the initial energy. Under these ionization conditions, the energy measured experimentally does not increase with the incident energy and passes through a plateau. This effect is illustrated in figure 3. The existance of δ-electrons leads to strong fluctuations of the ionization loss.

The magnitude of the fluctuations of the energy loss in thin layers is

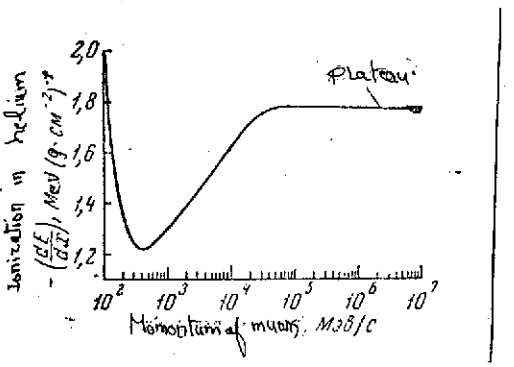

Fig. 3. The influence of the density effect on the ionization energy loss in a detector with limitations on the transferred energy (W_o = 1 KeV).

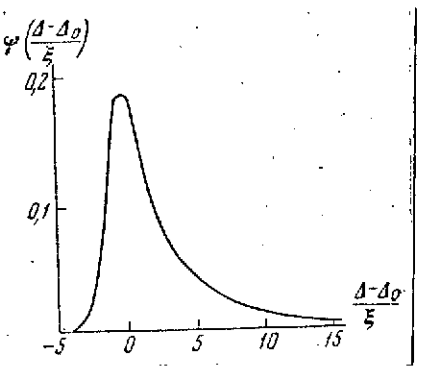

Fig. 4. Fluctuations of the energy loss due to ionization (Landau's curve).

calculated by Landau [3]. In a thin layer, the probability of formation of a delta electron of high energy is small. When the thickness of the layer is increased, the fluctuations almost do not change because, parallel with the number of collisions, the probability of large transfers of energy increases. Consequently, the fluctuations have a standard distribution. Figure 4 shows the differential probability of the energy loss from its most probable value . We must note the asymmetry of the curve of the energy loss. This forces us to distinguish between the most probable energy loss, which corresponds to the maximum of Landau's curve, and the mean energy for which the ordinate divides the area enclosed by the curve into two equal parts.

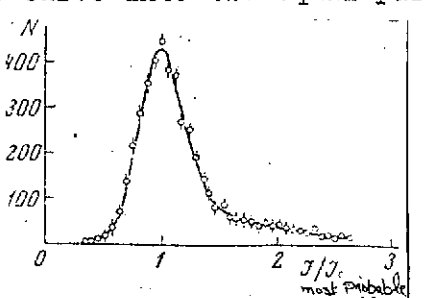

Fig. 5. Differential spectrum of ionization for muons at the sea level, measured by a proportional counter. The theoretical curve of the fluctuations of the ionization losses in calculated by Landau's theory and multiplied approximately by 2.

Landau's distribution is valid for widths x, for which the condition $Q < 0.05\ W_{max}$ is fulfilled. Figure 5 shows the distribution of ionizations, measured by a proportional counter.

3. Bremsstraalung

3.1. Screening

The phenomenon Bremsstraalung occurs during an interaction of a charged particle with the Coulomb field of a nucleus or the field of atomic electrons. The electric field of a nucleus is considered a Coulomb field if the impact parameter of the collision is much larger than the dimensions of the nucleus. When the impact parameters become of the same order of magnitude as the dimensions of the atom, the screening effect of the field of the nucleus due to atomic electrons becomes important. For impact parameters larger than the atomic radius, screening will be at a maximum, or as it is usually expressed, screening will be complete.

The radius of the atom, according to the Thomas-Fermi model, is equal to

$$a = 137\,\frac{h}{mc}\,Z^{-1/3}. \tag{2.7}$$

The condition for complete screening therefore becomes

$$b > 137\,\frac{h}{mc}\,Z^{-1/3}. \tag{2.8}$$

Since the effective impact parameter of the collision depends on energy, the previous condition imposes a definite restriction on the energy of the electrons. It is found that screening is complete if the energy of the incident particle

$$E \gg 137 mc^2 Z^{-1/3}. \tag{2.9}$$

The numerical values of the quantity $B = 137\ mc^2\ Z^{-1/3}$ for different materials can easily be calculated by using equation (2.9) (see table 4) /5/.

Table 4

Material	B(MeV)
Hydrogen	68.5
Carbon	38.0
Lead	15.0

The expression for the probability of Bremsstraalung was first obtained by Bethe and Heitler in 1934 by applying the Born approximation.

In the case of complete screening, the probability of radiation in the field of the atomic nucleus of a photon with energy E' by an electron of energy E along a length 1 cm is given by

$$W_e(E, E')\,dE' = 4n\alpha Z^2 r_0^2\,\frac{dE'}{E'}\,\ln 183 Z^{-1/3}. \tag{2.10}$$

The probability $W_e(E,E')$ is calculated for a track of an electron in a material of length 1 cm. When an electron passes through an atom, it will be subject to bremsstraalung not only in the field of the nucleus, but also in the field of the atomic electrons. One may assume that the probability of radiation in the field of an electron is approximately equal to the probability of radiation in the field of a nucleon. Denoting this probability by W_e^H, one obtains $W_e = W_e^H Z^2 + W_e^H Z$ because the number of electrons in the atom is equal to Z. Consequently

$$W_e(E, E')\,dE' \approx 4n\alpha Z(Z+1)\,r_0^2 \frac{dE'}{E'} \ln 183 Z^{-1/3}. \tag{2.11}$$

3.2. Introduction of radiational unit of length

Equation (2.11) can be written in a simple form if one introduces a special notation for part of this expression that does depend on energy, namely

$$4n\alpha Z(Z+1)\,r_0^2 \ln 183 Z^{-1/3} = \frac{1}{t_0}. \tag{2.12}$$

It is easy to see that the quantity t_o has a dimension of length [cm] and is therefore called the radiational length unit (see Sec. 5).

3.3. The radiation energy

The probability that an electron radiates a photon is given by

$$W_e(E, E')\,dE' = \frac{1}{t_0} \cdot \frac{dE'}{E'}. \tag{2.13}$$

Let us consider some of the consequences of this formula. When energy E' of the radiated phonon decreases, the probability of radiation W_e increases indefinitely. This means that the number of low-energy photons, obtained during a unit track is very large. The total radaition energy, however, remains finite. This energy can easily be calculated by means of the following expression

$$-\left(\frac{dE}{dx}\right)_e = \int_0^E W_e(E, E')\,E'dE' = \int_0^E \frac{1}{t_0} \cdot \frac{dE'}{E'} E' = \frac{E}{t_0}. \tag{2.14}$$

Accordingly, the relative energy loss on bremsstraalung is a constant quantity and does not depend on energy

$$-\frac{1}{E}\left(\frac{dE}{dx}\right)_e = \frac{1}{t_0}. \tag{2.15}$$

Integrating this expression, one easily derives a law according to which the energy of the electron decreases when it penetrates through matter :

$$-\frac{dE}{E} = \frac{dx}{t_0}, \quad E = E_0 e^{-x/t_0}, \tag{2.16}$$

where E_o is the initial energy of the electron. We see that, along a path of 1 radiational unit, the energy of the electron decreases e times regardless of the value of the electron's initial energy E_o. It seems at first sight that the penetration power of the electron does not increase with increase in energy and that it looses 2/3 of its energy on passing a path length of 1 radiational unit. Here, the difference between ionizational losses and losses on bremsstraalung is clear.

The energy spent on ionization is usually transferred to atomic electrons in small portions and is rapidly dissipated into the thermal motion of atoms. The energy is then lost irreversibly. What happens is the so-called dissipation of energy. In the case of bremsstraalung, the photon on the contrary has a large probability to carry out an amount of energy comparable to the energy of the electron. Therefore, in the case of bremsstraalung, a splitting of energy takes place; the energy is distributed between a small number of high-energy photons. The energy then remains with high-energy particles, though of different nature. In order to prove this, let us consider the differential probability of transfer of a given amount of energy from an electron to a number of photons. The total energy transferred to photons of energy in the interval between E' and E' + dE' along a path of 1t units is equal to

$$W(E, E')E'dE' = dE'. \tag{2.17}$$

This expression does not depend on the energy of the photon in the approximation under consideration. Consequently, the energy transferred along a path of 1t-units to photons of energies varying from 0 to $\frac{1}{2}E$ is equal to the energy transferred to photons of energies in the interval from $\frac{1}{2}E$ to E. In the first case, however, a large number of low-energy phonons are created, while, in the second case, only one or two photons are created. On a path of a t-unit, half of the energy will then on the average be transferred to low-energy photons and half to high-energy ones.

We have thus shown that, in bremsstraalung, the energy is not lost irreversibly into thermal motion but is "exchanged" with photons whose energies are capable with the energy of the incident electron. This leads to a strong fluctuation in energy losses since the electron can be stopped at once, producing a high-energy photon and can create a large number of photons and gradually loose its energy.

3.4. Bremsstraalung by heavy particles

Up till now, we considered processes of radiation by electrons. We shall now consider how heavy particles loose their energy on bremsstraalung. It is known from classical electrodynamics that energy E lost on radiation is proportional to the square of acceleration, w^2. If the electric intensity of the electrostatic field of nucleus Z is equal to $\mathcal{E}$, then

$$mw = e\mathcal{E}; \quad \mathcal{E} = \frac{Ze^2}{r^2}$$

and then

$$E \sim \frac{e^2}{m^2} \cdot \frac{Z^2 e^4}{r^4}.$$

The energy lost on bremsstraalung will then be inversely proportional to the square of the mass of the particle :

$$-\frac{1}{E}\left(\frac{dE}{dt}\right) = \left(\frac{m_e}{m}\right)^2. \tag{2.18}$$

Accordingly, a muon with mass 200 m_e will loose on bremsstraalung an energy 40,000 times less than the energy lost by an electron.

4. Interaction of Photons with Matter

4.1. Compton-effect

The Compton effect consists of a collision of a photon with free electrons. In the limiting case of very large energy photons, $E' \gg m_e c^2$, the Compton effect can be described by the Klein-Nishina equation. The same equation was also obtained by I.E. Tamm :

$$\sigma_G = \pi n Z r_0^2 \frac{m_e c^2}{E'}\left(\frac{1}{2} + \ln\frac{2E'}{m_e c^2}\right) \tag{2.19}$$

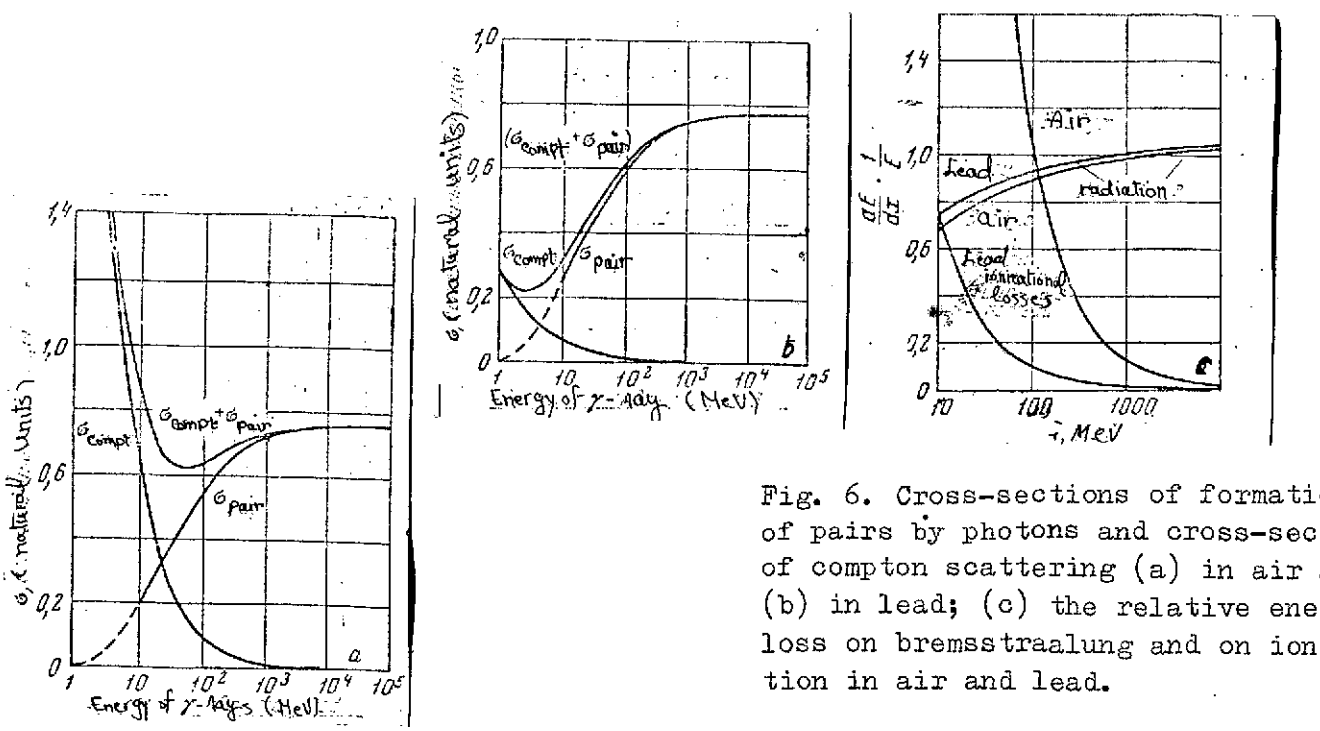

Fig. 6. Cross-sections of formation of pairs by photons and cross-section of compton scattering (a) in air and (b) in lead; (c) the relative energy loss on bremsstraalung and on ionization in air and lead.

Consequently, the probability of the Compton effect decreases as the energy of the photon increases (see fig. 6). The cross-section of the Compton effect is proportional to the atomic number of the medium. If we neglect the relatively weak logarithmic dependence of the cross section on the energy, as we have already done in the case of ionizational losses, we obtain the following equation for the probability of the Compton effect (calculated for a track of length 1 cm).

$$\sigma_{\text{C}} = K \cdot \frac{Z}{E'}.$$

For a track of length 1 radiational unit, the cross-section of the Compton effect is inversely proportional to Z

$$\sigma_{\text{C}} t_0 = ZCt_0 = \frac{ZC'}{Z^3} \sim \frac{1}{Z}, \qquad (2.20)$$

where t_o is the radiational unit.

4.2. Creation of pair

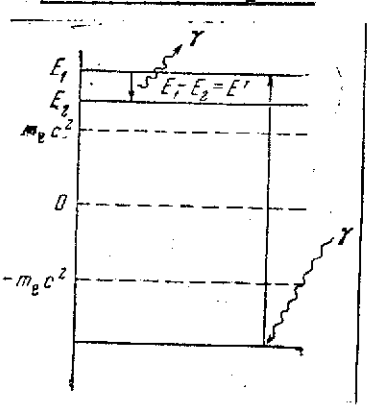

Fig. 7. Illustration for the processes bremsstraalung and creation of pair.

The creation of an electron-positron pair takes place in the field of the atomic nucleus or the atomic electrons. This process is similar to the process of bremsstraalung and is, in some sense, an inverse to it. Indeed, let us have a look at the diagram given in Fig. 7. Bremsstraalung is a transition of an electron from state E_1 of positive energy to state E_2 of lower energy, accompanied by a radiation of a photon of energy E'. The process of creation of a pair can be regarded as an absorption of a photon of energy $E' > 2m_e c^2$ followed by a transition of an electron from a state of negative energy to a state of positive energy. The mathematical expressions describing bremsstraalung and pair creation are therefore very much similar. The probability that a photon of energy E' forms along a track of length 1 cm an electron of energy E and a positron of energy E' - E, in the case of complete screening is given by

$$W_{\text{p}}(E', E)\, dE = 4n\alpha Z(Z+1)\, r_0^2 \frac{dE}{E'} \cdot \frac{7}{9} \ln 183 Z^{-1/3}. \qquad (2.21)$$

Introducing the radiational unit t_o, as in the case of bremsstraalung, we obtain

$$W_{\text{p}}(E', E)\, dE = \frac{7}{9} \cdot \frac{1}{t_0} \cdot \frac{dE}{E'}. \qquad (2.22)$$

This expression does not depend on the energies of the electron and positron. This is expected since, on the average; the energy is divided on equal footing between the electron and positron. The photon disappears after the creation of the pair, and one of the particles carries out more than one half of the photon energy. Accordingly, the energy here is transferred in large portions as in the case of bremsstraalung.

We shall now calculate the total cross-section of the formation of a pair along a track of 1 cm length. For this purpose, it is necessary to integrate the expression W_p (E',E) over all possible electron energies

$$\sigma_p = \int_0^{E'} W_p(E', E)\, dE = \frac{7}{9} \cdot \frac{1}{t_0}. \tag{2.23}$$

Consequently, the total cross-section of formation of a pair does not depend on the energy of the photon in the case of complete screening (the high-energy limit $E' \gg 137\, m_e c^2 Z^{-1/3} \gg m_e c^2$). When $E' < 2m_e c^2$, this cross-section must be equal to zero (Fig. 6). Consequently, the absorption of photons at high energies takes place due to the formation of pairs and at low energies due to the Compton effect.

5. Radiational Length Unit and Critical Energy Synonyms: radiational unit, cascade unit, shower unit, t-unit

We shall now consider some of the properites of the t-unit :

$$t_0 = [4n\alpha Z(Z+1)\, r_0^2 \ln 183 Z^{-1/3}]^{-1}. \tag{2.24}$$

We shall use this quantity as a unit of length for calculating different processes. The relative energy loss along a 1 cm track due to bremsstraalung is equal to

$$-\frac{1}{E}\left(\frac{dE}{dx}\right)_e = \frac{1}{t_0}. \tag{2.25}$$

In order to obtain the energy loss along a track of 1 t-unit, one has to multiply all the terms in equation (2.25) by t_o. One then obtains

$$-\frac{1}{E}\left(\frac{dE}{dt}\right)_e = 1; \quad dx = t_0 dt. \tag{2.26}$$

Similarly, the absorption of photons due to the production of a pair on a track of length t cm will be equal to

$$(\sigma_p)_t = \frac{7}{9} = \sigma_0 \tag{2.27}$$

Consequently, if we choose the t-unit as a scale of length, then both the process of bremsstraalung and the formation of pairs will be described exactly in the same manner provided that the condition of complete screening will apply. This will be achieved due to the fact that the properties of matter will be involved in the measurement scale of the track length.

We now turn to the formula for the ionizational energy losses. The relative energy loss along a 1 cm track is equal to

$$-\frac{1}{E}\left(\frac{dE}{dx}\right)_i = \frac{Z \cdot \text{const}}{E} \tag{2.28}$$

If t-units are used in the calculation, this energy loss is increased by t_0 times :

$$-\frac{1}{E}\left(\frac{dE}{dt}\right)_i = \frac{Z \cdot \text{const}}{E}\, t_0 = \frac{\text{const}}{ZE} \tag{2.29}$$

since t-unit is inversely proportional to Z^2. Using the notation $\frac{\text{constant}}{Z} = \mathcal{E}$ one may rewrite the previous equation in the following manner

$$-\frac{1}{E}\left(\frac{dE}{dt}\right)_i = \frac{\varepsilon}{E} \tag{2.30}$$

It is easy to see that the quantity $\mathcal{E}$ has the dimension of energy loss on a 1 t-unit.

What are the properties of the quantity $\mathcal{E}$? In order to answer this question, we have to combine equation (2.30) with the equation that describes the energy loss on bremsstraalung

$$-\frac{1}{E}\left(\frac{dE}{dt}\right)_e = 1$$

We see that, if we put $E = \mathcal{E}$ in the equation which describes the ionization losses, the energy loss due to ionization will be equal to the energy loss due to bremsstraalung (see Fig. 6). The quantity $\mathcal{E}$ is therefore called critical energy. When $E < \mathcal{E}$, the loss due to ionization is greater than that due to bremsstraalung and when $E > \mathcal{E}$, the radiational losses predominate. From the definition of the critical energy, it follows that

$$\varepsilon Z = \text{const.} \tag{2.31}$$

This relation is approximate since we are considering the ultra-relativistic case. It is interesting to see how this relation applies in actual conditions. Table 5 gives the values of the t-unit, the critical energies [7] and the products of $\mathcal{E}Z$. The fifth column in table 5 shows that equation (2.31) applies within an accuracy of 13%.

Table 5

Material	Z	t_0, г/см²	ε, Мэв	εZ
Water	7,23	36,4	65	470
Air	7,37	37,1	81	600
Carbon	6	43,3	76	456
Aluminium	13	24,3	40	500
Iron	26	13,9	21	550
Lead	82	6,4	7,6	620
Average..				555±75

In conclusion, it is necessary to say some words on the computation of the t unit. The equation we obtained for t_o follows from the consideration of the cross-sections of bremsstraalung and pair production. Both these cross-sections are calculated in the Born approximation, however, is not accurate for the purpose of considering media with large atomic numbers. One thus has to introduce a correction that depends on Z. Such a correction must enter the definition of t_o. It is almost the same for both the processes of bremsstraalung and pair production and is equal to $1 + 0.12\ (Z/82)^2$. The next difficulty in computing the t-units consists in the fact that it is necessary to know the exact form-factor of the atom. At large values of Z, the atom is however well described by the Thomas-Fermi theory. We thus arrive to the following conclusions:

1. The energy loss by electrons may be considered constant at energies higher than the critical energy such as for light and heavy materials

$$E > \varepsilon \quad \text{(condition } A\text{)}.$$

2. The cross section of the process of pair production by photons may be considered independent of energy if the condition of complete screening is fulfilled, i.e. if

$$E \gg 137 m_e c^2 Z^{-1/3} \quad \text{(condition } B\text{)}. \tag{2.32}$$

The numerical values of energy, which correspond to these two conditions are given in table 6. Consequently condition A is stronger for air while condition B is stronger for lead. Accordingly, the limiting expressions for the processes of bremsstraalung and pair production can be applied when conditions A and B are fulfilled. At lower energies, it is necessary to take into consideration the ionization losses in light materials, and the dependence of the absorption cross section of photons on energy in heavy material.

Table 6

Material	Condition	
	A(MeV)	B(MeV)
Air	66	40
Lead	7.6	15

6. Scattering of Electrons

Until this moment, we have considered the energetical problem of interaction of electron and photons with matter. There is also a geometrical problem which needs to be considered, namely the scattering of particles. In each act of bremsstraalung, formation of pairs or Rutherford scattering, charged particles acquire some angle with respect to the initial direction of motion.

The change in the direction of motion of an electron due to bremsstaalung, or the angle of flight of a pair is equal, in order of magnitude to

$$\theta_{rad} \approx \frac{m_e c^2}{E}. \tag{2.33}$$

The Rutherford scattering leads to a considerably large deviation. It is well-known that the mean square angle of Rutherford scattering is equal to

$$\sqrt{\overline{\theta_R^2}} = 0{,}7\,\frac{E_s}{E}\sqrt{t/t_0}, \tag{2.34}$$

where E_s = 21 MeV and t_o is thellength of the shower unit. Comparing the two types of scattering, we obtain

$$\frac{\theta_{rad}}{\theta_R} \sim \frac{m_e c^2}{E}\cdot\frac{E}{0{,}7E_s\sqrt{t/t_0}} = \frac{m_e c^2}{0{,}7E_s\sqrt{t/t_0}} \tag{2.35}$$

Substituting $t \simeq t_o$, we obtain $\theta_{rad}/\theta_R \simeq 1/30$. Along a track of length 1 t-unit, the Rutherford scattering is then roughly 30 times greater than the radiational scattering. It follows from the expression of $\sqrt{\overline{\theta^2}}$ that the scattering in heavy materials will be strong even if condtion B is fulfilled. Indeed, in lead, where condition B requires that $E > 15$ MeV, the scattering angles will be very large. In light materials, where condition A is stronger, the scattering angles will be much smaller than $\sqrt{\overline{\theta^2}} \sim \frac{1}{5}$ when this condition will be fulfilled.

7. Restrictions at High Energies

The cross-section calculated by Bethe and Heitler are concerned with the interaction with separate atoms. In this particular case, there is no restrictions on the validity of these expressions in the high energy region. L.D. Landau and I.Ja. Pomerančuk however showed that this theory is not valid at high energies for the interaction with atoms in a medium. The reason for the failure of the theory is the following. The radiation of low-energy photons takes place as a result of interactions at distances much longer than the dimensions of the atoms. When the energy increases, this effective distance increases and becomes, at sufficiently high energy, greater than the length of the shower

unit. At this distance, electrons and photons are essentially absorbed, and this is not considered in the Bethe-Heitler theory which deals with isolated atoms. With increasing energy E of the electron, deviation from theory becomes more important for the radiation of photons of higher energies; multiple scattering lead to an even stronger effect. In lead, at $E > 5 \times 10^3$ GeV the theory is not valid even when the energy of the radiated phonons is approximately equal to E. The greatest deviation from theory however occurs at low photon energies whose spectrum behaves as $dE'/\sqrt{E'}$ (compare with eq. (2.13)).

The effects described above lead to the decrease of the energy losses of electrons and photons. The length of the track along which an energy of the order of E is lost on radiation increases with E. In this case, the penetration power of electrons and photons increases. This could be formally described by assuming that the length of the t-unit increases with energy.

8. Electron-Photon Showers

Synonyms: Electromagnetic cascades, electron-photon showers, cascade showers.

8.1. Introductory remarks

Electron-phonon showers are produced when high-energy electrons or phonons penetrate through thick layers of matter. They occur as a result of a large number of separate interactions and, hence, are not elementary processes. The ability of electrons and photons to create showers is, however, used to measure one of the most important properties of the motion of the particles, namely their energies. Consequently, further description of the experiments on cosmic rays is not possible to carry on without having a theory that connects the measured properties of showers with the energy of the primary particles.

8.2. Electromagnetic cascade theory

It is clear from the above-mentioned arguments that a high-energy electron incident on a layer of matter is responsible for a whole series of processes. During the first t-unit, photons will occur due to bremsstraalung, and their energies will be of the same order of magnitude as the energy of the electron. The resulting photons will subsequently create electrons and positrons through the process of pair production. It is not possible experimentally to descriminate between electrons and positrons. We shall only consider the number of charged particles and for definition call them, electrons.

At a depth of a few t-units, we shall accordingly have a large number of electrons and positrons. An electron-photon shower will occur. As the number of particles increases, their energy decreases and finally reaches a critical value. The particles will then start to be absorbed as a result of ionizational losses. Photons, available in the shower will partially compensate the loss of electrons, yet the shower will sooner or later die down. This is how an electron-photon shower develops.

The quantitative description of the electron-photon cascade is given by the electromagnetic cascade theory. The main purpose of the electromagnetic cascade

theory, i.e. the theory of penetration of charged particles through matter, is to search for the functions which dtermine the distribution of particles at a given depth t in a matter of atomic number Z in terms of energies and scattering angles measured from the shower axis, defined as the direction of motion of the initial particle.

In many cases, however, it is sufficient to confine oneself to a one-dimensional problem, i.e. to neglect the transversal extension of the shower and the angular distribution of the particles. This is possible because the longitudinal dimensions of the shower are much larger than the transversal ones. As we have already seen, the particles scattered at large angles (of the order of one radian) have energies near the critical value. When such particles pass a track of length 1 t-unit, they are absorbed as a result of ionization losses. The transversal dimensions of the shower are thus in the order of one t-unit (more precisely $\sim t_o E_s/\mathcal{E}$). The longitudinal dimensions of the shower are measured in tens of t-units.

If one disregards the spatial distribution of particles in the shower, the problem is then reduced to the search of a function that describes the distribution of particles of different energies in different depths. Let us denote the average number of electrons in the energy interval from E to E + dE at a depth t by $P(t,E)dE$ and the average number of photons by $\mathcal{P}(t,E')dE'$. We shall confine our consideration to the average number of particles and not consider fluctuations. We shall derive the equations of the cascade theory by introducing the following assumptions.

1. It is possible to neglect all processes other than bremsstraalung by electrons and pair production by photons.
2. The solution of the equations is given when expressions derived in the limit of complete screening can be used for the corresponding cross-sections.

These assumptions are valid if conditions A and B, mentioned previously, are fulfilled. The assumption that ionizational losses are absent means that we are considering energies greater than $\mathcal{E}$. This condition is stronger for lighter materials; in heavier materials the neglect of ionizational losses does not cause any restrictions on the validity of the solutions because the heavier the matter the stronger the condition of complete screening. Consequently, for light materials the next approximation will be to account for ionizational losses while in heavier materials, the subsequent approximation will be to account for the energy dependence of the photon absorption cross-section. At even lower energies, one has to take the Compton effect into consideration. The approximate account of this effect in light materials can be achieved by setting in the course of calculation the absorption coefficient equal to $\sigma_r + \sigma_c$.

Accordingly, we confine our consideration to the one-dimensional problem, i.e. neglect the Coulomb scattering, and use asymptotic expressions for the cross-sections of various processes. This latter simplification is possible when the energy of the cascade electrons $E \gg \mathcal{E}$ in materials with small Z and when $E \gg 137\, m_e c^2 Z^{-1/3}$ in materials with large Z. How can these restrictions be removed will be sicussed below.

8.3. Kinetic equations of the cascade theory

The balance of the number of particles with energies between E and E + dE at a given depth t when passing through a layer of thickness dt will be determined by the following expressions.

1. The increase in the number of electrons due to pair production by photons is given by

$$\left.\frac{\partial \mathscr{P}(E,t)}{\partial t}\right|_{\mathrm{p}} = 2\int_{E}^{\infty} \Gamma(E',t)\, W_{\mathrm{p}}(E',E)\, dE'. \tag{2.36}$$

2. The decrease in the number of photons due to this process is

$$\left.\frac{\partial \Gamma(E,t)}{\partial t}\right|_{\mathrm{p}} = -\int_{0}^{E} \Gamma(E,t)\, W_{\mathrm{p}}(E,E')\, dE'. \tag{2.37}$$

3. The variation in the numbers of electrons and photons as a result of bremsstraalung is given by

$$\left.\begin{aligned}
&\left.\frac{\partial \mathscr{P}(t,E)}{\partial t}\right|_{\mathrm{e}}^{+} = \int_{E}^{\infty} \mathscr{P}(t,E')\, W_{\mathrm{e}}(E',E'-E)\, dE';\\
&\left.\frac{\partial \mathscr{P}(t,E)}{\partial t}\right|_{\mathrm{e}}^{-} = -\int_{0}^{E} \mathscr{P}(t,E)\, W_{\mathrm{e}}(E,E')\, dt';\\
&\left.\frac{\partial \Gamma(t,E)}{\partial t}\right|_{\mathrm{e}} = \int_{E}^{\infty} \mathscr{P}(t,E')\, W_{\mathrm{e}}(E,E')\, dE.
\end{aligned}\right| \tag{2.38}$$

Consequently, one may write the following kinetic equations for the cascade theory

$$\left.\begin{aligned}
&1)\ \frac{\partial \mathscr{P}}{\partial t} = 2\int_{E}^{\infty} \Gamma(t,E')\, W_{\mathrm{p}}(E',E)\, dE' +\\
&+\int_{E}^{\infty} \mathscr{P}(t,E')\, W_{\mathrm{e}}(E',E'-E)\, dE' - \int_{0}^{E} \mathscr{P}(t,E)\, W_{\mathrm{e}}(E,E')\, dE
\end{aligned}\right| \tag{2.39}$$

(at lower energies, when $E < \mathcal{E}$, it is necessary to include another term to account for the ionizational losses, namely

$$\left.\frac{\partial \mathscr{P}(t,E)}{\partial t}\right|_{t} = \frac{\partial \mathscr{P}}{\partial E}\cdot\frac{\partial E}{\partial t} = -\varepsilon\frac{\partial \mathscr{P}}{\partial E}, \tag{2.40}$$

but, when $E \gg \mathcal{E}$ this term is not important);

$$2)\ \frac{\partial \Gamma}{\partial t} = \int_E^\infty \mathscr{P}(t, E') W_c(E', E)\, dE' - \int_0^E \Gamma(t, E) W_p(E, E')\, dE'. \tag{2.41}$$

If the term that accounts for the ionizational losses were absent, the resulting expression would be nothing else but an integral equation. In this case, it is possible to obtain a solution by using the method of functional transformations. This method was first applied by L.D. Landau in 1938.

The Laplace-Mellin functional transformations consist in replacing the unknown function P(t,E) by another function $P^*(t,s)$, related to function P by definite relations. As a result of this replacement, integral equations (2.39) and (2.41) are transformed into differential equations. The differential equations are analytically solved and function $P^*(t,s)$ is found. One then obtains function P(t,E) from function $P^*(t,s)$ by means of the inverse transformations. Details on the solution of the cascade equations are given in a number of monographs [5, 8, 9].

The Laplace-Mellin transformation is given by

$$\begin{aligned} \mathscr{P}^*(t, s) &= \int_0^\infty E^s \mathscr{P}(t, E)\, dE; \\ \Gamma^*(t, s) &= \int_0^\infty E^s \Gamma(t, E)\, dE. \end{aligned} \tag{2.42}$$

The star (*) is usually not written, but one has always to be aware that functions $P^*(t,s)$ and P(t,E) are not identical even if S = E. We now apply these transformations to the equations of the cascade theory. For this purpose we multiply the equations by E^S and integrate from 0 to ∞. Let us show, as an example, what happens with the first term in equation (2.39)

$$\begin{aligned} &\int_0^\infty 2E^s \int_E^\infty \Gamma(t, E') W_p(E', E)\, dE' dE = \\ &= \int_0^\infty E^s 2 \int_E^\infty \Gamma(t, E) \frac{7}{9} \cdot \frac{dE'}{E'}\, dE. \end{aligned} \tag{2.43}$$

We make the following change in variables

$$\begin{aligned} E' &= E''; \quad dE' = dE''; \\ E &= \eta E''; \quad dE = E'' d\eta; \\ \eta &= \frac{E}{E''}; \end{aligned}$$

Then,

$$\int_0^\infty \eta^s E''^s 2 \int_1^0 \Gamma(t, E'') \frac{7}{9} dE'' E'' d\eta = \frac{14}{9} \int_0^\infty \Gamma(t, E'') E''^s dE'' \int_1^0 \eta^s d\eta =$$

$$= \frac{14}{9} \cdot \frac{1}{(s+1)} \Gamma(t, s) = B(s) \Gamma(t, s)$$

(we dropped the star). We transform the other terms in an analogous manner. We obtain the following differential equations for functions P(t,s) and Γ(t,s)

$$\begin{cases} \dfrac{\partial \mathcal{P}(t, s)}{\partial t} = A(s) \mathcal{P}(t, s) + B(s) \Gamma(t, s); \\ \dfrac{\partial \Gamma(t, s)}{\partial t} = C(s) \mathcal{P}(t, s) + D(s) \Gamma(t, s). \end{cases} \tag{2.44}$$

Here

$$A(s) = \int_0^1 \frac{1-\eta^s}{1-\eta} d\eta; \quad B(s) = \frac{14}{9} \cdot \frac{1}{s+1};$$

$$C(s) = \frac{1}{s}; \qquad D(s) = \frac{7}{9} = \sigma_0.$$

In order to solve equations (2.44), it is necessary to know the boundary conditions. If a single electron of energy E_0 falls on the boundary of the layer of matter under consideration, the boundary conditions will then be written in the following form

$$\begin{cases} \mathcal{P}(0, E) = \delta(E_0 - E); \\ \Gamma(0, E) = 0 \end{cases} \qquad \begin{cases} \mathcal{P}(0, s) = E_0^s; \\ \Gamma(0, s) = 0. \end{cases} \tag{2.45}$$

Of particular interest will also be the following boundary conditions

$$\begin{cases} \mathcal{P}(0, E) = 0; \\ \Gamma(0, E) = a/E. \end{cases} \tag{2.46}$$

This will be the spectrum of photons obtained in an accelerator, since they occur there as a result of bremsstraalung.

In the system of differential equations under consideration, the variable is t whereas s enters as a parameter. Our system is thus a system of first-order equations with constant coefficients. This system can easily be solved. The solution may be written in the form of

$$\begin{cases} \mathcal{P}(t, s) = a_1(s)\, e^{\lambda_1(s)t} + a_2(s)\, e^{\lambda_2(s)t}; \\ \Gamma(t, s) = b_1(s)\, e^{\lambda_1(s)t} + b_2(s)\, e^{\lambda_2(s)t}. \end{cases}$$

where λ_1 and λ_2 are the roots of the following algebraic equations

$$\begin{vmatrix} -A(s) - \lambda, & B(s) \\ C(s), & -D(s) - \lambda \end{vmatrix} = 0;$$

$$\begin{cases} \lambda_1 = \frac{1}{2}\sqrt{(A-D)^2 + 4BC} - \frac{A+D}{2}; \\ \lambda_2 = -\frac{1}{2}\sqrt{(A-D)^2 + 4BC} - \frac{A+D}{2}; \end{cases}$$

while constants a and b are related together by

$$\frac{a_1}{b_1} = \frac{B}{A+\lambda_1}; \quad \frac{a_2}{b_2} = \frac{B}{A+\lambda_2}.$$

There remains only two undefined parameters which are to be determined from the boundary conditions. Obtaining functions $\mathcal{P}(t,s)$ and $\Gamma(t,s)$ in this manner, we use the inverse transformation to obtain functions $\mathcal{P}(p,E)$ and $\Gamma(t,E)$:

$$\mathcal{P}(t, E) = \frac{1}{2\pi i E} \int_{\delta - i\infty}^{\delta + i\infty} E^{-s} \mathcal{P}^*(t, s)\, ds.$$

In practice, one often does not deal with the number of particles of a given energy but with the number of particles of energies exceeding a given value

$$N(t, E) = \int_{E}^{E_0} \mathcal{P}(t, E)\, dE. \tag{2.47}$$

Function N(t,E) is called integrap spectrum. The solution of the cascade equations (for a single incident electron) for this function can be obtained by means of the saddle-point approximation [6] and has the form of

$$N(t, E) = \frac{H(s)}{s} \cdot \frac{\exp\left[s \ln \frac{E_0}{E} + \lambda_1(s)\, t\right]}{\sqrt{2\pi \lambda_1''(s)\, t}} \tag{2.48}$$

Since $\lambda_2 < 0$, the corresponding term in the solution given by equation (2.48) rapidly decreases with increasing t and does not lead to a considerable contribution to the quantity N(t,E) when $t \gg 1$. In this expression, t is related to s by the following equation

$$t = -\frac{1}{\lambda_1'(s)} \ln \frac{E_0}{E}. \tag{2.49}$$

Values of functions $\lambda_1(s)$, $\lambda_1'(s)$ and $\lambda_1''(s)$ are tabulated and given in the monographs /5,8/. Function $\lambda_1'(s)$ can be approximated by

$$\lambda_1'(s) \approx \frac{1}{2}(1 - 3/s),$$

while function $\lambda(s)$ satisfies the following relations :

$$\lambda_1(s) = 0 \text{ при } s = 1;$$
$$\lambda_1(s) > 0 \text{ при } s < 1.$$

From the equation for t, it is clear that $\lambda_1'(s)$ is always negative, $\lambda_1'(s) < 0$, while $\lambda_1''(s) > 0$. Function H(s) is positive and decreases monotonously :

$$H(s) = \frac{\sigma_0 + \lambda_1(s)}{\lambda_1(s) - \lambda_2(s)}$$

All these functions appear in the course of inverse transformation from s to E.

We now find the position of the maximum of the number of particles for energies $> E$. The position of the maximum is determined by function $\exp\left[s \ln \frac{E_0}{E} + \lambda_1(s) t\right]$, since the other functions are monotonous.
The extreme value of this function is given by the root of the equation :

$$\frac{\partial}{\partial t}\left[s \ln \frac{E_0}{E} + \lambda_1(s)\, t\right] = \frac{\partial \varphi}{\partial t} = 0;$$
$$\frac{\partial \varphi}{\partial t} = \lambda_1'(s) = 0$$

The latter condition is satisfied when s = 1. Consequently, the position of the maximum is given by the relations :

$$t_{max} = -\frac{1}{\lambda_1'(1)} \ln \frac{E_0}{E} = 1{,}01 \ln \frac{E_0}{E}. \tag{2.50}$$

$$N_{max} = \frac{H(1)}{1} \cdot \frac{\exp\left[\ln \frac{E_0}{E} + \lambda_1(1)\, 0{,}01 \ln \frac{E_0}{E}\right]}{\sqrt{2\pi \lambda_1''(1) \ln \frac{E_0}{E}}} = \frac{0{,}137}{\sqrt{\ln \frac{E_0}{E}}} \cdot \frac{E_0}{E} \tag{2.51}$$

8.4. Account for ionizational losses

Until now, we have considered energies $E > \mathcal{E}$ for light materials and $E > 137\, m_e c^2 Z^{-1/3}$ for heavy ones. Experimentally, the lower limit of measured

energy depends on the properties of measuring device. This minimal energy is often close to zero as, for example, in the case when particles are registered by an ionization chamber. It is therefore necessary to remove the restrictions on the values of energy E. In light materials, we have to take the ionizational losses of the electron into consideration and to set the absorption coefficient of photons equal to a constant since the total absorption coefficient due to the Compton effect and pair production is essentially constant up to an energy much less than the critical energy ($\sim 0.1\,\mathcal{E}$). The number of particles at the maximum and the position of the maximum when the ionizational losses are taken into account are given by

$$N(E_0, t_{Max}, 0) = \frac{0.3}{\sqrt{\ln \frac{E_0}{\varepsilon}}} \cdot \frac{E_0}{\varepsilon};$$

$$t_{Max} = \ln \frac{E_0}{\varepsilon}. \qquad (2.52)$$

The dependence of the number of electrons of energy $E > 0$ on t is shown in figures 8a and b for carbon and iron.

8.5. Heavy materials

The distribution of the number of electrons of $E > 0$ by depth in lead is shown in Figure 8c.

For heavy materials, one has to take into account the variation of the absorption coefficient of photons with energy. This leads to the result that t_{max} and N_{max}

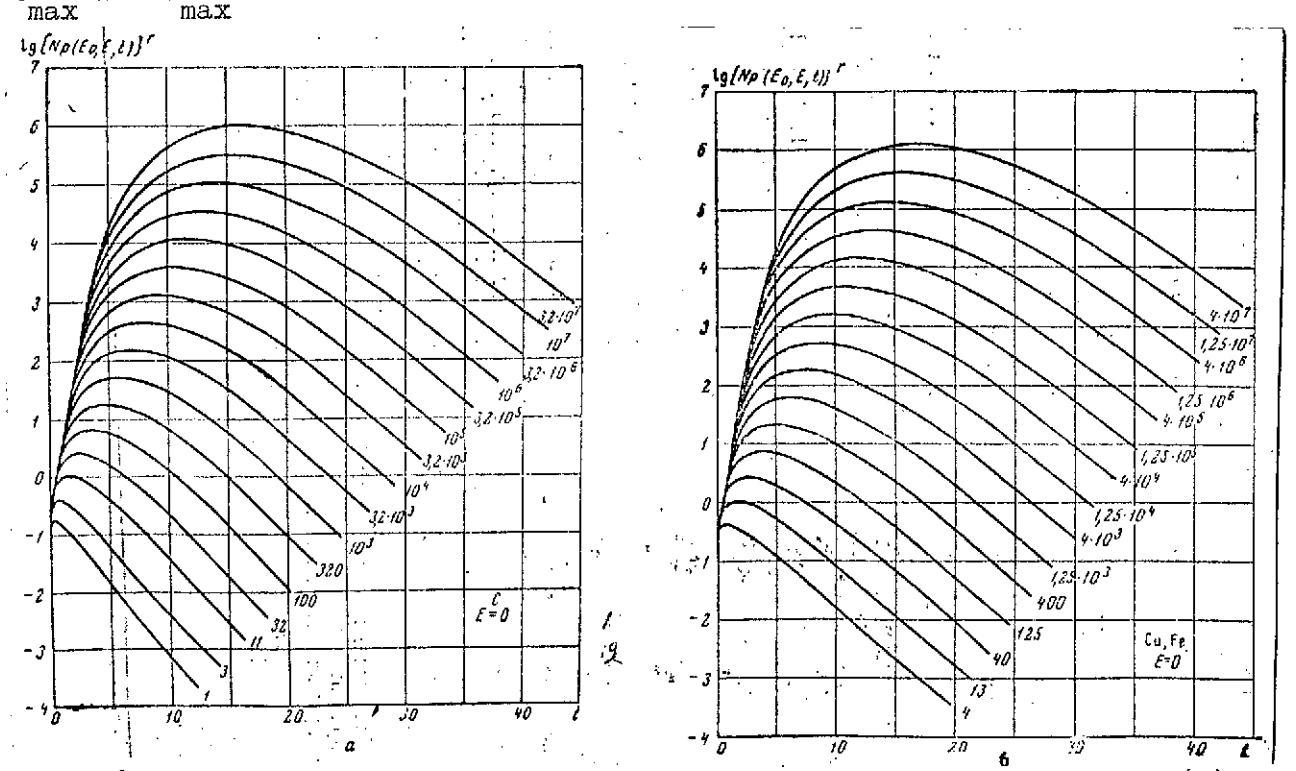

Figs. 8a,b. Cascade curves for primary photons at different energies (a) in carbon, (b) in iron. The numbers on the curves are the values of the quantity $E_0/0.437$.

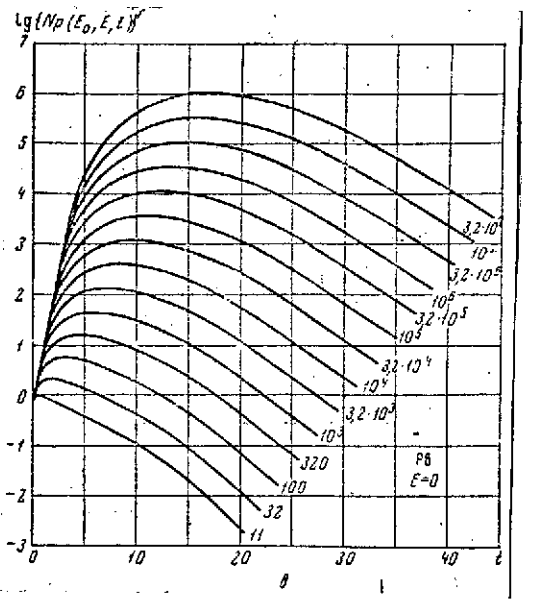

Fig. 8,c. Cascade curves for initial photons at different energies in lead. The numbers on the curves are the values of the quantity $E_0/0.437\,\varepsilon$.

depend on energy in a more complicated manner than they do for light materials

$$t_{max} = K_1\left(\frac{E_0}{\varepsilon}\right)\ln\frac{E_0}{\varepsilon};$$
$$N_{max} = K_2\left(\frac{E_0}{\varepsilon}\right)\frac{1}{\sqrt{\ln\frac{E_0}{\varepsilon}}}\cdot\frac{E_0}{\varepsilon}. \qquad (2.53)$$

For lead, the values of K_1 and K_2 are given in table 7.

Table 7

E_0	$5\cdot10^8$, eV	10^9, eV	10^{10}, eV
K_1	1,4	1,33	1,29
K_2	0,172	0,180	0,200

Comparing these expressions with those obtained for light materials, we see that the number of particles at the maximum of the cascade in lead, at a given value of E_0/ε, is less than in the light materials. This means that the cascade curve is extended to larger depths. Actually, the area under the cascade curve is constant. By definition, this area is equal to

$$S = \int_0^\infty N(t)\,dt.$$

On the other hand, the particles of the shower loose an energy of $N(t,0)\ dt$ in a layer of thickness dt at depth t. The total energy loss is then equal to $\int_0^\infty N(t,0)\,\mathcal{E}\,dt = E_0$, i.e. the initial energy of the electron. Therefore

$$S = \int_0^\infty N(t,0)\,dt = E_0/\varepsilon. \tag{2.54}$$

Consequently, for a given value of $E_0/\mathcal{E}$, the area enclosed under the cascade curve is constant.

Since the cascade curve at a given value of $E_0/\mathcal{E}$ has a maximum, whose value in lead is less than in light materials, then the cascade curve must extend towards larger depths. The physical reason is that low-energy photons in lead (see Fig. 6b) have smaller absorption coefficients and hence larger penetration power. They will penetrate deeper and hence extend the cascade curve. The penetration power of photons is greater than that of electrons, and thus the number of electrons at large depths will decrease in the same way as the number of phonons, i.e. in the following manner

$$N_\gamma(t) = e^{-\sigma_{min} t},$$

where σ_{min} is the minimum of the absorption coefficient of photons and is given by the slope of the cascade curve in Figure 8c :

$$\sigma_{min} = \operatorname{tg} \alpha,$$

because $\ln N = -\sigma_{min}\, t$. In light materials $\sigma_0 = 7/9$ (at $t \gg 1$), while in lead $\sigma_{min} = 0.23$ (see Figure 6c).

8.6. Energy spectrum

Let us rewrite the solution of the cascade equation, given by equation (2.48), as

$$N(t, E) = \left(\frac{E_0}{E}\right)^s \frac{H_1(s)\, e^{\lambda_1(s)t}}{s\sqrt{2\pi\lambda_1''(s)\,t}} \sim \frac{1}{E^s}.$$

We see that parameter s, which has been formally introduced, defines the shape of the spectrum of electrons in the shower. As it has already been mentioned, parameter s depends on t. Consequently, the spectrum varies with variation in depth. At the maximum of the shower, s = 1 and the spectrum $N(t_{max}, E) \sim 1/E$. Before the maximum, $s < 1$ and the spectrum slopes more gently, i.e. it involves a large number of high-energy electrons. After the maximum, the spectrum is sharper and the energy of the electrons is less. At the maximum of the shower, almost 80% of the electrons have an energy less than the critical energy and 50% have an energy less than $\frac{1}{3}\mathcal{E}$.

The following function is often used

$$\mathscr{P}(E) = \int_0^\infty N(t, E)\, dt.$$

It is called the equilibrium spectrum. In the cascade theory, it is shown that $\mathscr{P}(E) \sim 1/E$ if $E \ll E_0$.

8.7. Method of moments

The introduction of equilibrium spectrum is connected with a solution method for the cascade equation which was first developed by S.Z. Beln'kij, and called the method of moments. Recently, I.P. Ivanenko [10] applied this method and successfully solved the equations for the cascade theory.

We call the quantity

$$\overline{t^n}(E_0) = \frac{\int_0^\infty N(E_0, t)\, t^n dt}{\int_0^\infty N(E_0, t)\, dt}$$

the n-th moment of function $N(E_0, t)$. We can easily show that the moments of the electron distribution functions are related with each other through the following recurrence relation

$$\{\overline{t^n}(E_0, 0)\}^p = \frac{n}{E_0} \int_0^{E_0} [\mathscr{P}(E_0, E)\, \{\overline{t^{n-1}}(E, 0)\}^p + \Gamma(E_0, E)\, \{\overline{t^{n-1}}(E, 0)\}^p]\, dE$$

Here $\mathscr{P}(E_0, E)$ and $\Gamma(E_0, E)$ are the equilibrium spectra of the electrons and photons respectively. It is clear that the first moment is directly expressed in terms of the equilibrium spectra :

$$\{\overline{t}(E_0, 0)\}^p = \frac{1}{E_0} \left[\int_0^{E_0} \mathscr{P}(E_0, E)\, E dE + \int_0^{E_0} \Gamma(E_0, E)\, E dE \right].$$

Our problem is, consequently, reduced to the determination of the shape of the equilibrium spectrum. The equilibrium spectrum can be more easily obtained than the cascade curves themselves. This can be done by integrating the cascade equations over depth from the very beginning. The solution of the resulting equations was obtained by I.E. Tamm and S.Z. Belen'kij.

If we expand the unknown function which gives the dependence of the number of electrons on depth in series of orthogonal polynomials, for instance Laguerre polynamials, we then obtain

$$N(x) = A_0 + A_1 L_1^i(x) + A_2 L_2^i(x) + \ldots;$$
$$L_n^i(x) = e^x \frac{x^{-i}}{n!} \cdot \frac{d^n}{dx^n} (e^{-x} x^{n+i}), \quad i = 0, 1, 2 \ldots$$

These polynomials are orthogonal with weight $x^i e^{-x}$, and coefficients A_n are

related to the moments of function N(x). The expansion will be the better, the smaller the mean square deviation

$$M = \int_0^\infty e^{-x} x^i \left[A_0 + A_1 L_1^i(x) + A_2 L_2^i(x) + \ldots - N(x)\right]^2 dx.$$

The minimum of the mean square deviation is defined by the conditions :

$$\frac{\partial M}{\partial A_n} = 0.$$

Using these conditions, one can evaluate all coefficients of A_n. Cascade curves given in Figure 8, are computed by using the method of moments.

8.8. Method of statistical trials, or Monte-Carlo method

There exists an alternative method for obtaining cascade curves. This method is known as the method of statistical trials or the Monte-Carlo method. It resembles a practical experiment more than a calculation. The method consists in the following. Suppose that we know from theory or from general practical considerations, the properties of the elementary processes we are interested in, and we want to know the result of several repetitions of these processes. This is the problem which one meets in the cascade theory.

We know all of the probabilities of the elementary processes and want to find the number of particles and their distribution in different depths. Let us consider a photon of energy E_o incident on a layer of matter and try to predict its future. We know that a photon with energy $E_o \geqslant 137\, m_e c^2 Z^{-1/3}$ has an absorption cross-section with the creation of a pair $\sigma = 7/9$ in t-units. Let us divide this t-unit into ten parts. The probability of creation of a pair in such a layer will then be $7/90 \simeq 8/100$ (see figure 9.a).

Let us prepare a cylinder with well-balanced axes and mark on it ten

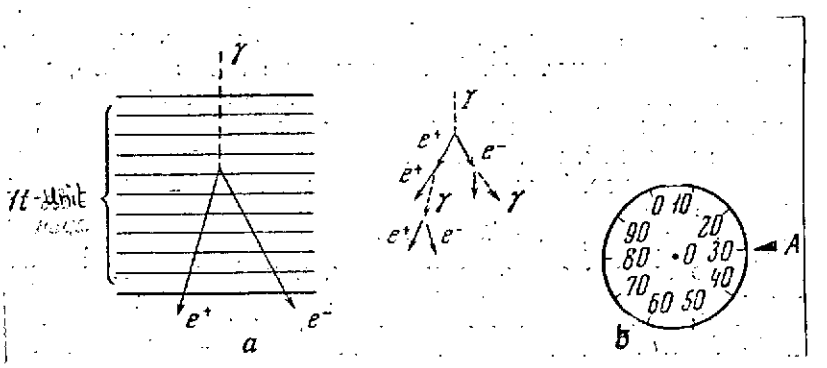

Fig. 9a,b - Illustration of method of statistical trials.

divisions (figure 9b). Let us rotate this cylinder and then suddenly stop it and read the number in front of pointer A. We now assume that if the pointer indicates to one of the numbers 1 - 8 then the photon have created a pair,

otherwise it has passed without interaction. In the latter case we repeat our experiment letting the photon pass through the next 0.1 t-unit. In this manner we find in which layer the photon has created a pair.

We now have to determine the energy of the particles produced. We know that the energy is distributed among the particles with equal probability. Let us divide the interval of possible values of energy into 100 divisions and try to find the energy of the electron. We again rotate our cylinder. Assuming that it has stopped with the pointer indicating number 10 means that the electron has energy 1/10 E_o and the positron 9/10 E_o. Repeating this experiment (this is equivalent to many photons falling on our filter), we find how many pairs are created in each layer, and consequently find the number of the particles. Naturally, in order to calculate the whole shower, one has to determine the future of each electron and photon until it is removed from the cascade. Such a consideration has to be repeated many times and the result is then summed. In this method, one can easily take into account the energy dependence of the absorption coefficient of photons, for example. We assume that in the shower under consideration at a given depth t, a photon has appeared with an energy whose absorption cross-section is half its asymptotic value. By rotating our cylinder, we will then assume that the photon will be absorbed if the pointer stops in the interval between 1 and 4 and not between 1 and 8, and so on. Solving problems by the Monte-Carlo method is very cubersome, and in many cases it is useful to use computers in the calculation. When the problem is not very complicated, one can sometimes do without the use of computers. Onviously, it is also not necessary to rotate a cylinder. It is sufficient to use a set of tables of random distributed numbers from 01 to 99.

9. Spatial Diversion of Particles in a Shower

The distance r by which an electron is shifted from the shower axis is determined by the Coulomb scattering along a track of length approximately 1 t-unit (see Sec.6, Chap. 2). When $r \ll t_o$ (t_o is the length of the t-unit),

$$r \sim \langle \theta \rangle \sim \frac{E_s}{E}, \tag{2.55}$$

i.e. the distance of the particle from the axis is inversely proportional to its energy. It follows from equation (2.48) that the number of electrons having energy $> E$ at depth t is given by

$$N(>E, E_0, t) = f\left(\frac{E_0}{E}, t\right). \tag{2.56}$$

Substituting expression E in terms of r into equation (2.56), we find that for particles having an energy greater than E and, consequently, at a distance from the axis less than r

$$N(E_0, <r, t) = f\left(\frac{E_0 r}{E_s}, t\right). \tag{2.57}$$

From this rough consideration, we can conclude that the number of particles in a circle of radius r at depth t is proportional to the product $E_o r$. More accurate calculations support this conclusion. If we choose r to be approximately equal to 100 um, then $E \sim 1$ GeV. Consequently, in calculating function f, we can use cross-sections derived from the assumption of complete screening and neglect ionizational losses.

Concrete results can be obtained by solving three-dimensional kinetic equations, written for the first time by L.D. Landau. They may be represented in the following manner

$$\left\{\begin{aligned} &\left(\frac{\partial}{\partial t}+\theta\frac{\partial}{\partial r}\right)\mathcal{P}(t,\theta,r,E)=-A\mathcal{P}+B\Gamma+\\ &\quad+\frac{E_s}{4E^2}\left(\frac{\partial^2}{\partial\theta_1^2}+\frac{\partial^2}{\partial\theta_2^2}\right)\mathcal{P}+\varepsilon\frac{\partial\mathcal{P}}{\partial E};\\ &\left(\frac{\partial}{\partial t}+\theta\frac{\partial}{\partial r}\right)\Gamma(t,\theta,r,E)=C\mathcal{P}-\sigma_0\Gamma. \end{aligned}\right. \tag{2.58}$$

Here A, B and C are integral operators corresponding to bremsstraalung and pair production and σ_o is the absorption coefficient of photons calculated in t-units. Operators A, B and C are given by equations (2.36 - 2.38), i.e.

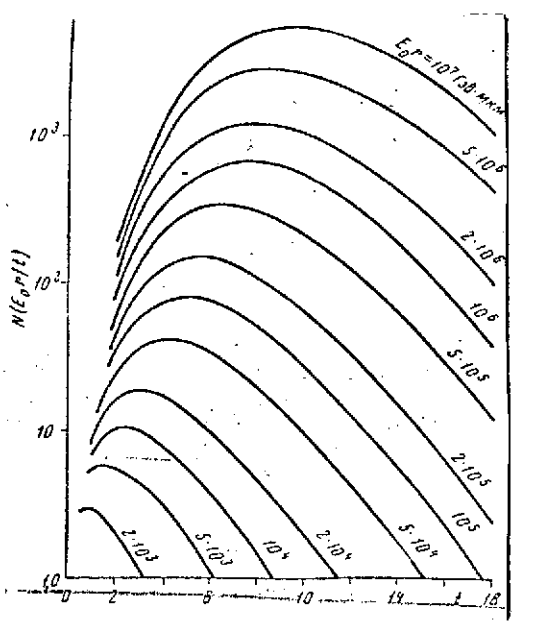

Fig.10. Number of electrons in a circle of radius r for a shower produced by electrons (theoretical curves).

and so on. Calculations by Pinkaw, Nishimura Kidom and others [12*] establish the relation between the number of particles in a circle of radius r and the quantity $E_o r$ for different depths t. Curves for $N(r) = f(E_o r, t)$ for photo-emulsion are given in figure 10. The experimental verification of these calculations was made by Pinkaw et al [13] and showed that both theory and experiment agreed with each other in a wide range of energy, equal to severn times E_o (E_o was determined by the longitudinal extension of the cascade).

10. Experimental Study of Cascade Showers

10.1. Earlier work

Cosmic particle showers were first observed by D.V. Skobel'cyn. While studying cosmic-ray particles by means of Wilson's chamber, he observed on some of the plates, two or three particles that occured simultaneously. The number of these events was too large to be considered as an accidental coincidence. He therefore concluded that these particles were correlated with each other, i.e. entered in the composition of a shower.

Soon after the discovery of showers, Rossi studied them by using counters. The experimental device used by Rossi was very simple (figure 11). Three Geiger counters were placed in such a way, that in order to have them work simultaneously, at least two particles should have fallen. Over these counters, he placed a

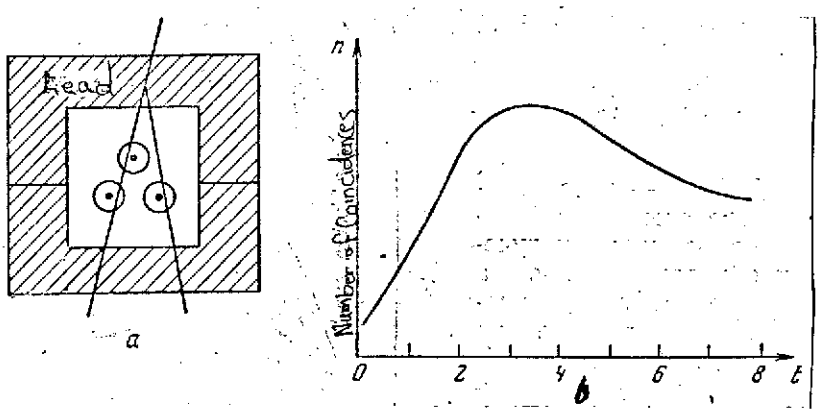

Fig. 11 - Rossi's Experiment for measuring cosmic-particle showers: a) the scheme of the experimental device; b) Rossi's curve.

layer of lead whose thickness had been previously measured. He studied the dependence of the number of coincidences of discharge in the three counters on the thickness of the lead filter. As a result, he obtained the so-called Rossi curve, which had a maximum when the lead thickness was three-four t-units. When the number of coincidences was increased, i.e. when not three but, say, six counters were used, the maximum of the curve was observed for larger filter thicknesses. The reason for this was that, in order to have the system work, more particles had to be incident on the matter, i.e. more shower energy was required and therefore the maximum was shifted deep down to satisfy the relation $t_{max} = \ln (E_o/\mathcal{E})$. Consequently, Rossi's experiment qualitatively supported the cascade theory.

Quantitative comparison between theory and experiment requires accurate measuring devices. For this purpose, it is convenient to use ionization chambers (for measuring the total intensity or bursts). The first of such experiments

was carried out by Schindler in 1931. These experiments gave negative results because of lack of accuracy in the performance of the experiment. Schindler and later Young and Street in their experiments on hills, did not observe a maximum in the curve describing the dependence of ionization on the filter thickness. They measured ionization by means of ionization chambers covered from above by layers of lead of different thickness (figure 12a).

The reason of the failure of these experiments was discovered by S.N. Vernov. At the maximum of the shower, nearly 80% of the electrons have an energy less than the critical energy. Such electrons are very strongly scattered. On consequence, at a depth of a few t-units in lead, almost half of the electrons move in the reverse direction. Hence, in order to perform the experiment correctly, one has to not only put the filters above the chamber but also beneath it. Furthermore, it is well known that the ionization loss is inversely proportional to Z whereas bremsstraalung and pair production does not depend on Z. If the walls of the chambers are made of a light material (for example, aluminium) and are not very thin, the ionization losses will then sharply increase and the number of particles will decrease. This will lead to an underestimation of the number of particles coming out of lead (transitional effect). For this reason, more than half the particles were not registered in Schindler's experiments.

The magnitude of the transitional effect can be evaluated theoretically, though one may find a great deal of difficulties in the course of calculations.

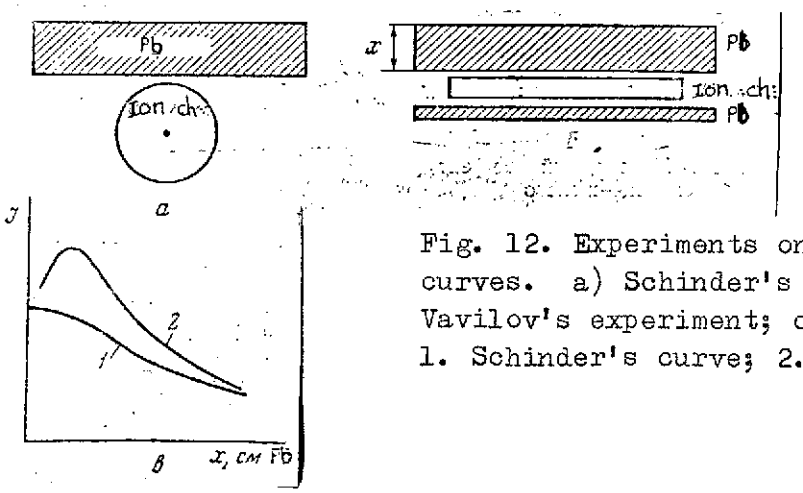

Fig. 12. Experiments on the study of cascade curves. a) Schinder's experiment; b) O.N. Vavilov's experiment; c) experimental results: 1. Schinder's curve; 2. Vavilov's curve.

Figure 13 shows the dependence of the transitional effect lead-iron on the thickness of the iron layer.

Accurate experiments in which the errors made by Schindler were eliminated were carried out by O.N. Vavilov. He used a very thin plane chamber with walls made of duraluminium having a thickness of 0.4 mm (figure 12b). O.N. Vavilov found that the addition of lead below the chamber increased the current in it by 40%. Only a few percent of the particles were absorbed in the thin walls of

the chamber. As a result of this experiment, O.N. Vavilov obtained a clear maximum in the curve of the dependence of ionization on the absorber thickness (figure 12c). The position of the maximum and the shape of the cascade curve were in good agreement with the cascade theory in which these curves were evaluated by assuming a certain shape for the spectrum of the cosmic electrons.

10.2. Modern experiments [10, 14]

More accurate results were obtained in experiments by Panovskij and others. The arrangement of these experiments was similar to the corresponding experiments by O.N. Vavilov, but, as a source of high-energy particles, they used Berkeley's synchrotron which gave bremsstraalung photons with energy $E < 330$ MeV and spectrum $\sim 1/E$.

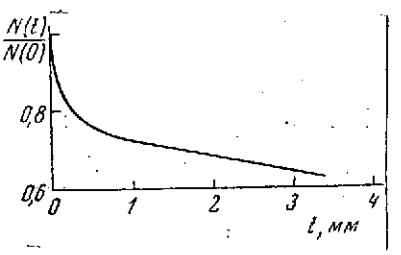

Fig. 13. Transitional effect lead-iron

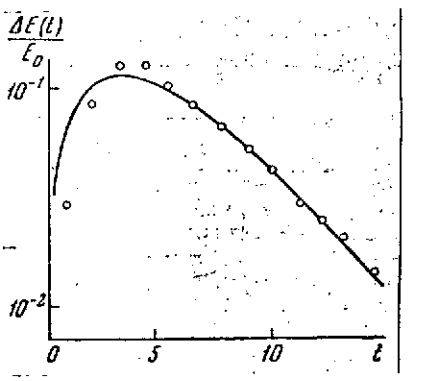

Fig.14. Verification of cascade theory by means of an accelerator: Dependence of energy separated in a therma luminophore on the lead thickness when 1 GeV electrons falls on the absorber (circles); calculation by means of the method of moments (solid curve).

Comparing the experiment for graphite with the cascade theory showed a good agreement between theory and experiment, except for large thickness, where the experimental results showed a more gentle decrease than theoretical predictions. The reason for this was that, in the calculation the absorption coefficients of photons were calculated in the limit of complete screening instead of using the minimal values of cross-sections which were less by 15%.

Nielsen et al. in USA used the electron accelerator in Stanford to check the calculation of the electromagnetic cascades at energies near 1 GeV. As a radiation detector, they used thermal-luminescence dose meters and lithium fluoride LiF which has the property of accumulating energy of ionizing radiation. In practice, this latter material was used to fill up thin walled tubes which were placed under absorbers of different thicknesses. After being radiated, the tubes were taken out of the block of matter where they were exposed. If

they are subsequently heated, they start to illuminate giving a quantity of light proportional to the energy saved during the exposion period to radiation. Luminescence does not occur at room temperature (about 5% of the emergy is radiated during one year of preservation). Therefore, by placing a tube full of LiF in a block of lead, iron or any other material, one can determine the distribution of ionization over depths in the absorber when electrons of a given energy fall on the material, i.e. one can measure the mean cascade curve. After radiation, one can also discharge separate parts of the tube, and measure the energy saved in each part. In this manner, one can find the distribution of ionization in transversal directions.

Experiment (figure 14) shows that there was good agreement between the observation and the cascade curves calculated by I.P. Ivanenko and B.E. Samosudov [10] by using the method of moments.

The verification of the cascade theory in the high-energy region was carried out in cosmic rays by means of an experiment performed on the Pamirs mountain (at a height of 3860 m above sea level) [14]. The experimental instrument consisted of an iron block of thickness ~ 40 t-units. Within each few t-units, the block contained an ionization chamber that worked according to Nielsen's scheme. Such an instrument was called an ionization calorimeter. The instrument gave the instantaneous ionization distribution (and consequently the number of electrons) for all thicknesses in the case when an electron or photon of energy greater than 10^{11} eV had fallen on it. The transitional effect, i.e. the absorption of electrons in the walls of the chambers, was absent because the chambers were made of the same material as the filter, i.e. of iron. Cascade curves for electrons and photons of energy $10^{11} \div 10^{12}$ eV in iron were obtained. The resulting experimental curves were in good agreement with the theoretical ones. One can therefore conclude that the cascade theory agrees with the experiment in a range of energy extending to at least 1000 GeV.

An analogous experiment was carried out on the Tien Shan mountain in 1964 [15] where a more developed instrument (fig. 15a), in which ionization chambers separated from each other by 3t-units, was applied (all were placed in 10 rows). The cascade curve in iron, obtained by this experiment compared to the theoretical curve is shown in figure 15b.

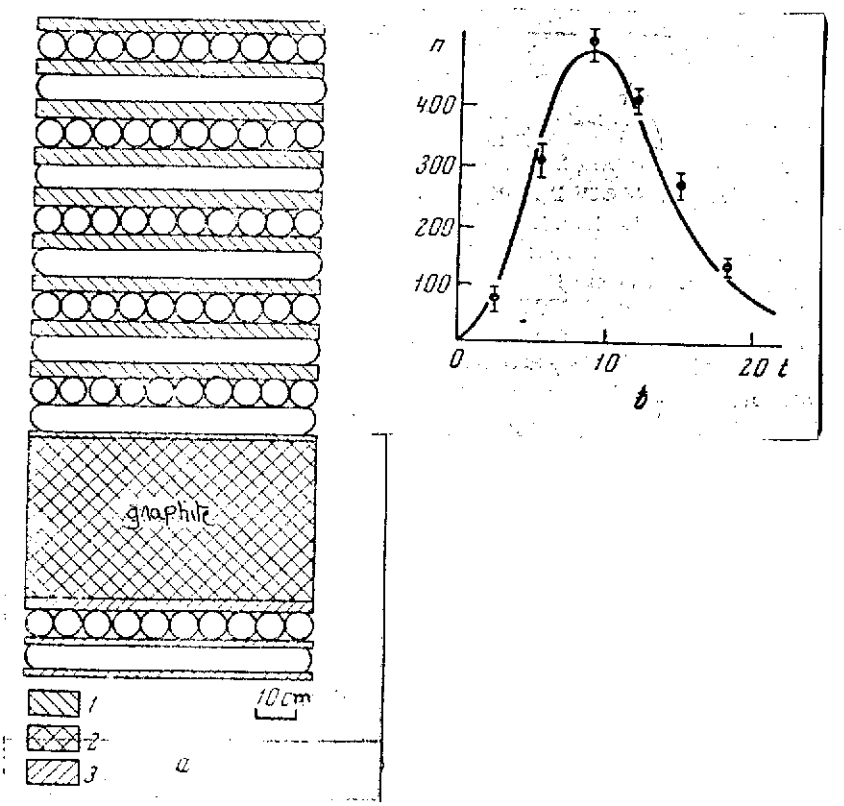

Fig. 15. Determination of the form of the cascade curve by means of an ionization chamber (see Chapter 2 [15*]): a) Experimental instrument (1. iron, 2; graphite, 3; lead); b) Experimental points on the theoretical curve.

11. Measurements Based on the Properties of Electromagnetic Interactions

11.1. Measurement of particle energy [12, 13, 16]

The Multiple scattering method [13]

We can determine the energy of a particle by studying its multiple scattering in an emulsion. Equation (2.34) gives :

$$\alpha(t) = \sqrt{\overline{\theta^2}} = k_0 \frac{E_s}{E} \sqrt{t}.$$

In order to determine the multiple-scattering angle, we divide the track of the particle into separate cells. The result of measuring α_t on a cell of length t is reduced to cell of length 100 um (α_{100})

$$\alpha_{100} = \alpha_t \frac{\sqrt{100}}{\sqrt{t}}. \qquad (2.59)$$

Equation (2.59) may then be written as

$$\alpha_{100} = \frac{k}{p\beta c}. \tag{2.60}$$

When $B \ll 1$, $pBc = 2E$ and $E = \frac{k}{2\alpha_{100}}$ while when $B \sim 1$, $pBc = E$ and $E = \frac{k}{\alpha_{100}}$. Constant k is called the scattering constant and is equal to 27 MeV. degrees/ $(100\ \mu m)^{\frac{1}{2}}$ if α_{100} is expressed in degrees.

If the mass of the particle is known, it is then possible to use this method to energies up to 10 GeV. The restriction on the value of energy measured is due to the various deformations of the emulsion and the inaccuracy in preparing the coordinate system of the microscope. It is possible to increase the higher limit of the energy measured in the case when there are several particles moving in parallel at small distances from each other ($\sim 20 \div 30\ \mu m$). In this case, one measures the relative scattering of two particles. The deformation of the emulsion and the other impediments in this case act on the two tracks in the same manner and hence have no influence on their relative scattering.

Utilization of the characteristics of longitudinal development of a cascade

Equations (2.50) and (2.51) show that it is possible to determine the energies of the photons and electrons from the knowledge of the position of the cascade maximum, the number of electrons at the maximum and the area under the cascade curve. The position of the cascade maximum depends logarithmically only on energy and hence, plays only a subsidiary role. In order to reach the cascade curve's maximum, one needs a layer of matter of considerable thickness, much thicker than required to determine the energy by the area under the cascade curve. The multiple-scattering method, considered above, is valid below a certain energy and good only for charged particles. The methods to be described below work better for higher energies and are valid for both electrons and photons.

The instrument can be constructed either on the basis of the photo-emulsion method or using radio engineering. In the first case, photo-emulsion rouleaus of thickness reaching few t-units are assembled out of emulsion layers of thickness 600 - 1000 μm. In the process of assembling, a coordinate set is plotted on the surface of each layer by a photographic manner. Each of the layers is later developed separately and stuck on a glass plate. One can then observe the development of the cascade from one plate to another and find the position of the maximum. One can then measure the intensity of blackening photometrically and find the corresponding number of particles by a calibration prepared in advance. These rouleaus are mainly applied for investigating nuclear processes measuring the energies of photons appearing in them.

In order to measure the energies of phonons coming from the atmosphere or created in the instrument's material, one applies emulsion chambers consisting of

separate layers of emulsion, separated by thin disks made of a material having a large atomic number (lead, tungsten, tin, etc., the thickness of the metal layers is 1 ÷ 3 t-units) (figure 16). By means of this system, one can simply collect considerable thicknesses of matter. The dimensions of emulsion chambers sometimes reach several square meters in area and one meter in thickness. They can include tens of layers of emulsion. If the photon has an energy ~ 100 ÷ 500 GeV, then the number of particles at the maximum can be determined either by direct counting or by means of photometric methods.

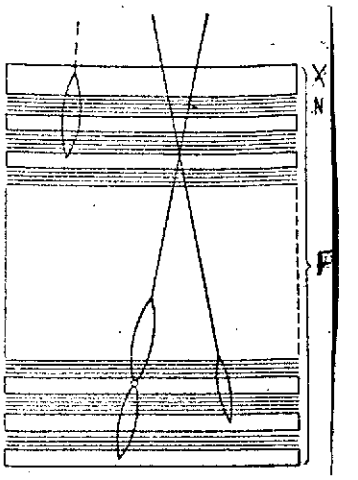

Fig. 16. Emulsion chamber and photon- and nuclear-active-particle-cascades occuring in it: X - X-ray films; N - nuclear emulsions; F - filters (60 t-unit Pb).

Showers produced by photons with energies near 5×10^3 GeV are seen by the naked eye or through a lens, as specks or dashes. X-ray films are sometimes used instead of nuclear emulsions and often in combination with them. In this case, the density of blackening is determined by photometric methods. The film is calibrated in advance by using a well-studied electron source, so that the correspondence between the number of particles and the intensity of blackening is established.

The radio-engineering version of the experiment for the determination of the photon and electron energies has already been described in Section 10. The instrument consists of a series of ionization chambers inserted between layers of iron (figure 15). Sometimes lead is used as an absorber. In this case, however, a transitional effect takes place in the iron or brass walls of the chambers and one must take this into account on determining energies. The instrument enables one to calculate the energy by measuring the area under the cascade curve. In order to find the energy from the position of the maximum, it is sufficient to have only two-three rows of ionization chambers and to choose the absorber's thickness according to the predictions of equation (2.52) and in accordance with the range of the energy measured.

11.2. Utilization of the transversal development of the shower [12, 13]

Equation (2.57) and the curves given in figure 10 enables one to determine the energy of the photon in terms of the number of particles in a circle of radius r. Usually one considers radii in the range 50 ÷ 100 μm. Particles moving within such a circle have an energy 2 ÷ 1 GeV and hence, are sharply

collimated. They can easily be separated from the randomly dispersed low-energy particles and from the particles in the background. In the application of the present method, photo-disks of an emulsion thickness of 50 ÷ 100 μm are usually covered with appropriate layers of lead. Shower particles move almost perpendicular to the emulsion plane and are therefore seen under the microscope as short dashes. An example of the sketch of collimated shower particles in an emulsion under lead is shown in figure 17.

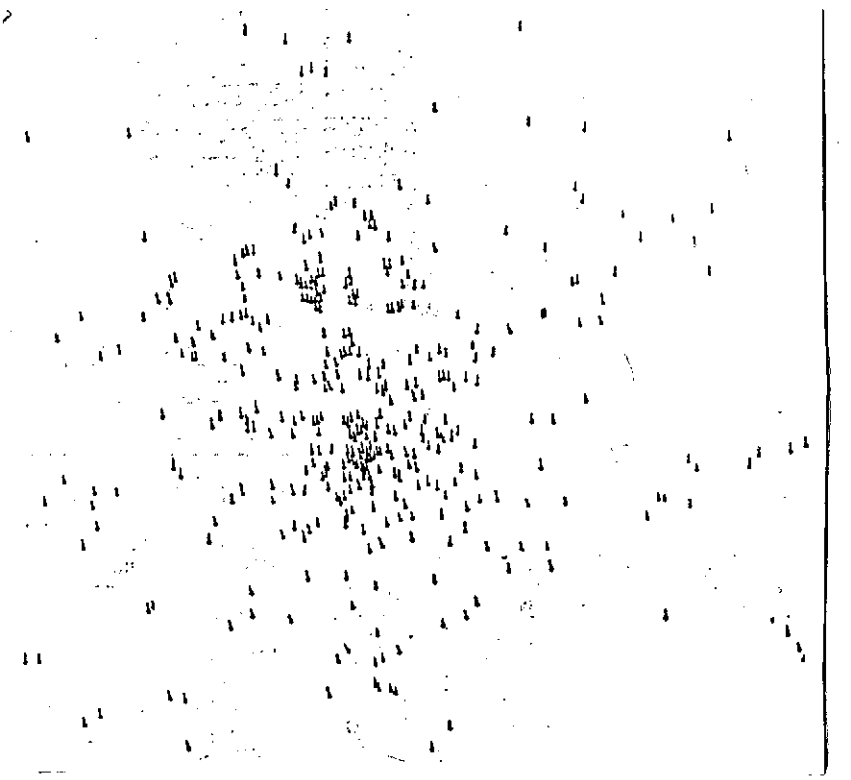

Fig. 17. A sketch for the transversal cross section of an electron-photon shower in an emulsion.

Questions and Problems

1. Find the number of δ_2-electrons with energy > 1 MeV, created by a relativistic alpha particle in 1 g/cm^2 of aluminium.
2. How much energy is lost on ionization by a proton of energy 3 GeV when it penetrates through 1 m of water (100 g/m^2) and 100 g/m^2 of lead ?
3. Find the energy lost on ionization by a singly-charged relativistic particle when it passes through the whole atmosphere.
4. What is the number of ion pairs produced in argon by an alpha particle of energy 5 MeV ?
5. Find the behaviour of functions (2.50) and (2.51) when $E \rightarrow E_o$ and explain your results.

6. Calculate the approximate value of the critical energy in mercury ($Z = 80$).
7. Find the position of the maximum, the total number of particles and the number of particles having energy exceeding 100 MeV at the cascade maximum in lead when the initial energy is 10 GeV.
8. Calculate the mean square scattering angle of electrons having energies exceeding 1 GeV.
9. What is the thickness of lead required for an experiment to determine the energy of photons in the range of 10^5 GeV ?

CHAPTER 3

ELEMENTARY PARTICLES

1. Methods for the Determination of Particle Masses

The mass, m, is the most important characteristic of a particle. It is the common factor that relates energy, E, of the particle to its momentum **p** and also relates both of these quantities to velocity :

$$mc^2 = \sqrt{E^2 - p^2}; \tag{3.1}$$

$$p = \frac{mc\beta}{\sqrt{1-\beta^2}}; \tag{3.2}$$

$$E = \frac{mc^2}{\sqrt{1-\beta^2}}. \tag{3.3}$$

Consequently, by measuring any two of the three quantities β, E and **p**, one can determine the mass of the particle.

Measurement of momentum

The momentum of a particles can be determined by measuring the radius of curvature ρ of the trajectory of the particle in a magnetic field. For singly-charged particles, the following relation between the particle's momentum and the magnetic intensity $\vec{B}$ holds :

$$B\rho = \frac{c}{e}p.$$

If B is given in ersteds and pc in electron-volts, then

$$pc = 300B\rho.$$

In practice, the trajectory of a particle is observed in Wilson's chamber, in a spark chamber or by means of a magnetic spectrometer. Figure 18 shows a

snapshot obtained by means of Wilson's chamber in a magnetic field in the Pamirs Alpine Station [1*]. By means of such a method, accurate work can lead to the measurement of momenta up to 50 GeV/c.

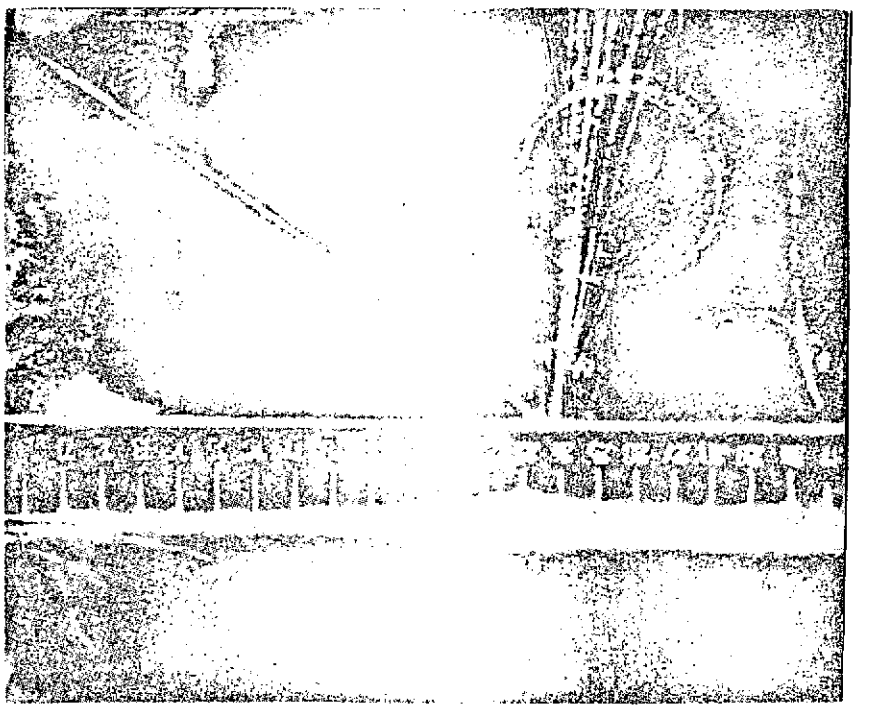

Fig. 18 Snapshot of a shower in Wilson's chamber in a magnetic field.

Momenta can also be measured in magnetic spectrometers, in which a number of points on the particle's trajectory in the magnetic field are fixed by means of Geiger counters of small diameters (a few mm) or spark chambers.

In order to determine the particle's mass, the measurement of momentum is combined with the measurement of the ionization path. The instrument, shown in figure 19, was constructed by A.I. Alihanov and A.I. Alihanjan, and called a mass spectrometer [2*].

The particle's momentum was measured in a magnetic field and the trajectory was determined by means of three rows of Geiger counters working in harmony with each other. The path was also determined by means of Geiger counters interlayed by lead filters. This instrument has the advantage, over Wilson's chamber, of high illumination and short dead time. Its disadvantage is that one cannot see the cause for the stoppage of the particle. The mass can be defined if the stoppage is due to ionization loss. If the stoppage, however, is due to a nuclear

disintegration, then the determination of mass will be erroneous. The counters do not enable one to differentiate between ionization losses and nuclear stoppages.

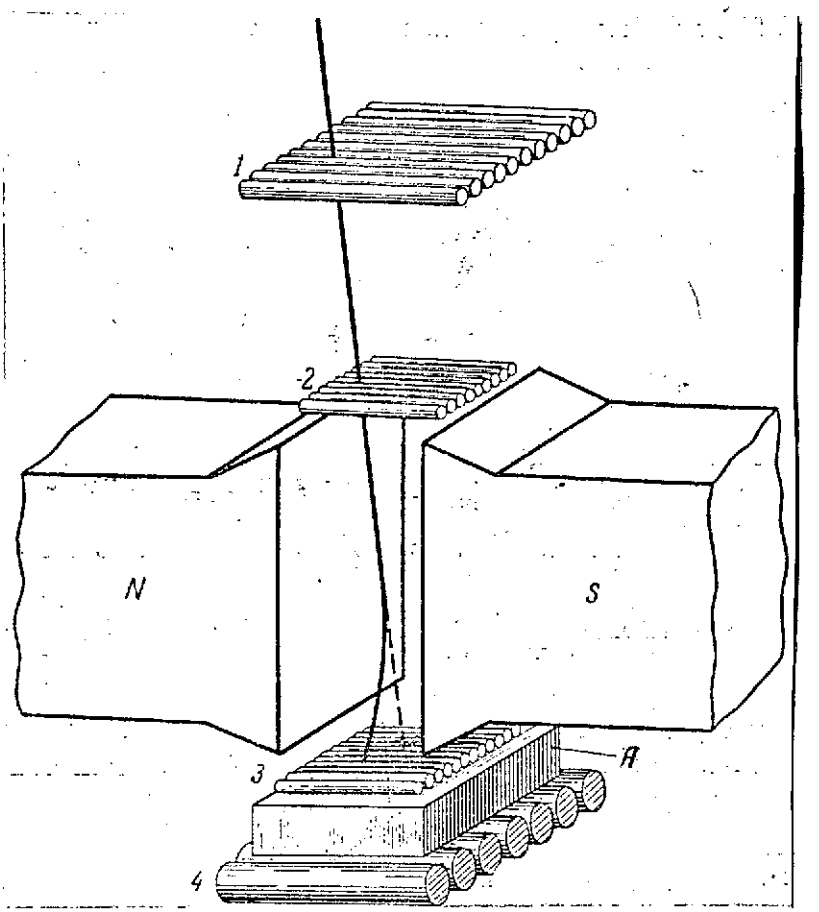

Fig. 19. Magnetic mass spectrometer; A: absorber, 1-4 : Geiger counters.

In a Wilson chamber, the products of nuclear disintegration will be seen if one is dealing with a nuclear stoppage. In the latter instrument, lead discs are put in a Wilson chamber in order to measure the path. The accuracy of measuring momenta can be increased by using spark chambers instead of counters for measuring the curvature of the trajectory.

In order to define the mass of a particle by means of a photoemulsion, one often starts by determining the energy by means of the multiple scattering method (see Section 11, Chapter 2) and the velocity by the magnitude of ionization (by the density of grains in the emulsion). The relation between the density of grains and the quantity $p\beta c$, which is connected with the angle of multiple scattering, is shown in figure 20 for particles having different masses. From this figure, one can easily see that there exists a range of values of $p\beta c$, in which curves corresponding to particles of different masses overlap which unables

this method to give results. At higher energies, ionization becomes exactly the same for particles of any mass because of the density effect.

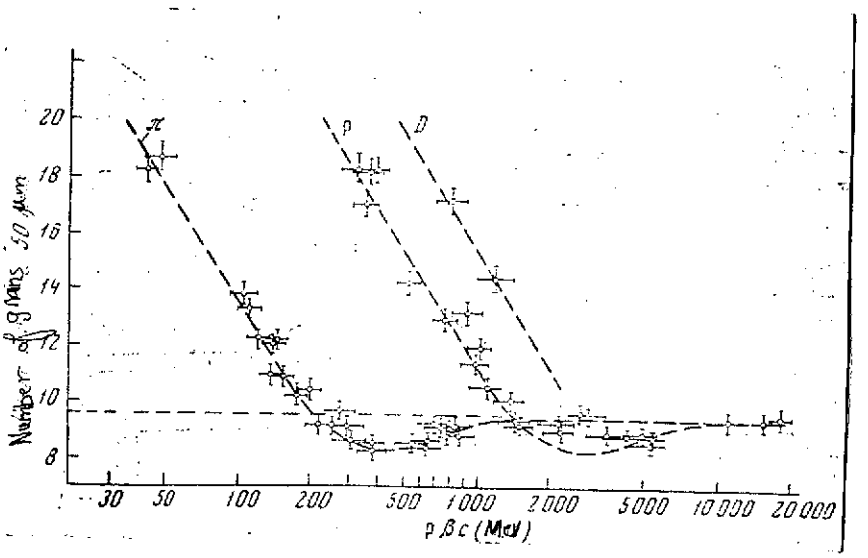

Figure 20. Relation between the density of grains and the quantity pβc for particles of different masses (π : pion, p : proton, D : deuteron).

Low-energy particles are sometimes stopped in the emulsion. In this case, one can utilize the relation between path R and energy E to determine the energy of the particle. This relation can be obtained by integrating equation (2.1) from E to 0. In practice, it is convenient to have a relation between R and the particle's velocity

$$R = mf\left(\frac{\beta}{\sqrt{1-\beta^2}}\right)$$

The measurement of R is then combined with the measurement of ionization in the initial part of the track.

One can use a series of alternative methods for the determination of the particle masses. All these methods, however, are based on equations (3.1-3.3).

2. Muons [3, 4]

Synonyms: mesons (in earlier literature), μ-mesons

2.1. General considerations :

The discovery of μ-mesons initiated the study of weak interaction in cosmic

rays. This particle is best of all called a muon because it belongs to leptons and not to mesons in the modern classification of elementary particles.

The history of the muon [3, 5] can be summarized as follows. In 1935, Yukawa suggested a brave idea, according to which the short-range character of nuclear forces can be understood if one assumes that the quantum of the nuclear field is a heavy photon of a non-vanishing mass. The mass of this quantum must be equal to

$$m \sim \frac{\hbar}{r_0 c} \sim 300 m_e,$$

where r_0 is the range of the nuclear forces. In order to explain the radioactive β-decay, Yukawa proposed that the quanta had to decay spontaneously. This hypothesis was the initiative for the search of such a quanta in cosmic rays. The first snapshot for these heavy particles was obtained in 1937 by Street and Stevenson. They measured the particle's momentum in the magnetic field and the ionization it produced in a Wilson chamber and found that its mass $\mu = 175\ m_e$. Anderson and Neddermeyer at that time showed the mass of the new particle to be in the order of $\sim 200\ m_e$. They found that some of these particles have positive charges and some negative charges. They called the new particles intermediate particles or mesons. After other types of mesons were discovered, these particles became called u-mesons, and now muons.

2.2. Mass and charge of a muon

The exact determination of the mass of a muon was made in cosmic rays by means of the methods, discussed in Section 1, Chapter 3. Later, the mass of the muon was determined by using accelerators. The most accurate value of the mass is $m_\mu = 206.7\ m_e$; $m_\mu c^2 = 105.6$ MeV.

The accurate knowledge of the mass of the muon is necessary for the determination of its magnetic moment and for use in the theory of elementary particles. Observations in which Wilson chamber in a magnetic field or magnetic spectrometers were used showed that there exists positively and negatively charged mesons and that both kinds have the same mass. Negative muons have never been observed.

2.3. Decay of a muon

The proof of the decay of a muon was obtained by means of different independent methods. One of these methods was the study of the difference in the absorption of muons in dense and dilute materials of the same chemical composition. A second method was to observe processes occuring when a muon was stopped in a Wilson chamber or a photoemulsion. A third method was to measure the life-time of a meson by applying methods of radio engineering. In the following we shall consider these three methods respectively:

In 1926, P.V. Mysovskij found that when atmospheric pressure changed, the intensity of cosmic rays changed accordingly. This phenomenon was called barometric effect. This was interpreted as a consequence of the change of thickness of the atmosphere over the place of observation. This interpretation was

checked by putting a layer of matter, say graphite or wood over the instrument, which could be equivalent to the decrease in atmospheric pressure. The thickness of such a layer, expressed in grams per cm^2, is given by

$$\Delta x = \frac{1030\ g/cm^3}{760\ mm\text{-}Hg}\,\Delta p\ mm\text{-}Hg$$

Experiment however showed that this equivalent thickness of dense matter did not compensate the barometric effect. Direct measurements of the absorption coefficient of cosmic rays in air and in dense materials (in wood) gave unexpected results.

The absorption coefficient in air was found to be 1.5 times greater than in wood. This effect of anomal absorption of cosmic rays in air was explained in 1938 to be due to the spontaneous decay of muons. In the presence of muon decay, the absorption of muons would be due to two factors: ionization loss and decay.

Ionization losses depend only on the quantity of penetrated matter and does not depend on the geometry of the track. The number of decaying muons is proportional to time, i.e. to the length of the track. For equal quantities of matter, the length of the track in air is 1000 times that in a dense matter. Therefore, if the life time of a meson is of the same order of magnitude as the time of flight of mesons through the atmosphere, then a considerable part of the mesons will have enough time to decay in the atmosphere, whereas in dense matter, the decay will be insignificant. Experiments on absorption of muons made it possible to determine their life time. The life time of a moving meson with energy E is given by

$$\tau = \frac{\tau_0}{\sqrt{1-\beta^2}} = \tau_0 \frac{E}{\mu_0 c^2}, \qquad (3.4)$$

Consequently, the effect of the decay of muons will be more important for higher energies than for lower ones. Instead of life time, one can introduce the decay path :

$$L_r = \frac{\beta c \tau_0}{\sqrt{1-\beta^2}} = \tau_0 \frac{p}{\mu_0}. \qquad (3.5)$$

Accordingly, the decay path of a muon is proportional to its momentum. Experimentally, one thus has to separate muons of different momenta.

Experiments for the determination of the life time of muons were made by Rossi in 1941. The experiments were undertaken at different heights and at sea level.

Rossi's instrument is schematically illustrated in Figure 21. He chose hard particles which were able to penetrate 196 g/cm^2 lead. The separation of

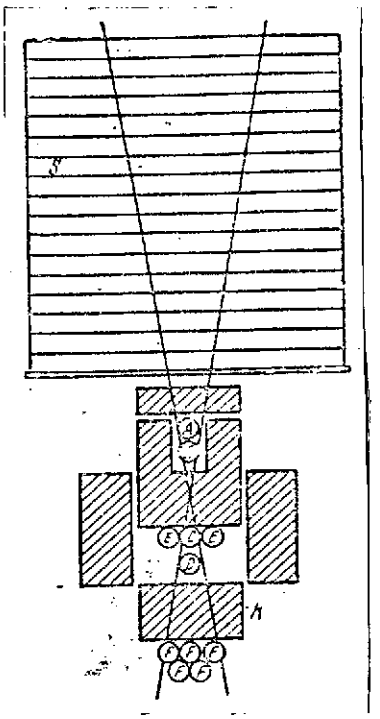

Fig. 21. Rossi's instrument for studying the decay of muons.

these hard particles was achieved by means of counters A, B, C and C which worked in coincidence with one other. This put a restriction on the momenta of the muons; muons with momenta $< 4.5 \times 10^8$ eV/c could not penetrate the filter. Another filter K of thickness 115 g/cm^2 was placed under counter D. Counter F opened the circuit of the instrument if the muon came out of block K. In this manner, particles having momenta $> 5.85 \times 10^8$ eV/c were not registered.

Let us assume that the change in the number of muons between two heights is entirely due to decay. Then, the number of muons at height h, is equal to

$$N_1 = N_0 e^{-h_1/L_r},$$

and at other height h_2 is

$$N_2 = N_0 e^{-h_2/L_r}.$$

It then follows that the decay path is equal to

$$L_p = \frac{h_2 - h_1}{\ln \frac{N_1}{N_2}}.$$

One can therefore determine L_r if one eliminates the ionization loss. The ionization loss can be eliminated by putting a compensating filter S at a high

distance over the instrument. The thickness of such a filter must be equal to

$$\Delta x = (h_1 - h_2)\frac{\sin\alpha}{\gamma_1},$$

where γ_1 is the density of the compensating material (Fe in Rossi's experiment).

Rossi's experiment gave the following results

$$1.\ \frac{L_1\rho_1}{L_1\rho_2} = \frac{\rho_1}{\rho_2},$$

i.e., in agreement with the relativistic formula for the transformation of time.

2. The life time of a muon is equal to $\tau_0 = (2.5 \pm 0.2) \times 10^{-6}$ sec.

The most accurate measurement of the muon life-time was made by using radio-engineering techniques. Observations carried by means of a Wilson chamber and photoemulsion showed that, as a result of the decay of muons, electrons and positrons appeared. Therefore, one can determine the life-time of a muon by measuring the time interval between the moment when the muon stopped and the moment when the electron appears. This method was realized by Rasetti.

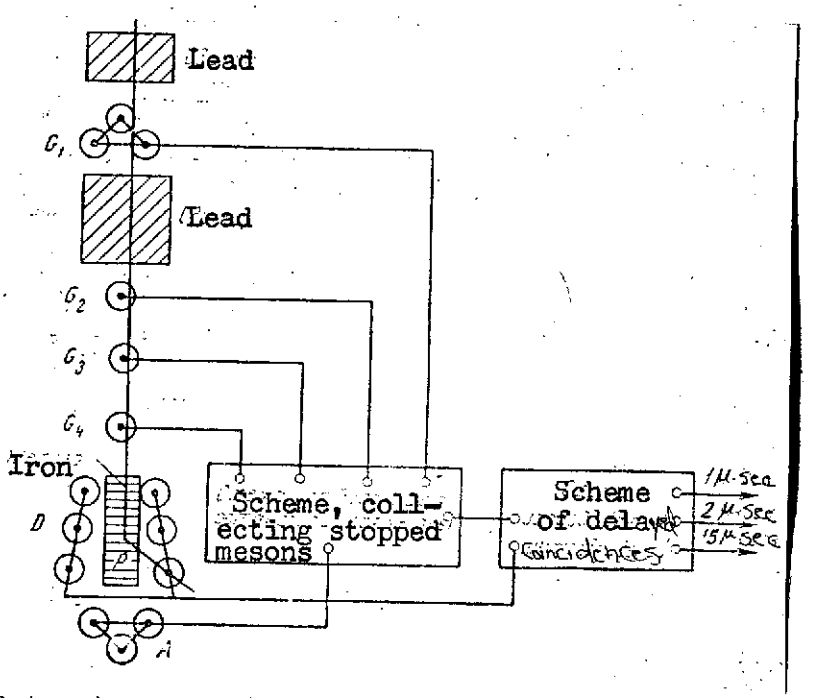

Figure 22. Determination of the life-time of muons by the method of delayed coincidences: G_1 - G_4 are gas-discharge counters and A are anticoincidence-system counters.

The instrument shown in figure 22 registers muons stopped in block P. Group of counters D are switched on with delay varying from tenths to tens of microseconds, and remain switched on for fractions of microseconds. If a decay electron appears during this time, it is then fixed by counters D. In this manner, the number of decays is determined as a function of the delay time. This method is a clever modification of the conventional method for determining the half-life time of decay of radio-active elements. It gives the following results $\tau_{\mu^*} = (2.22 \pm 0.02) \times 10^{-6}$ sec. The most recent (1960) and most accurate value for the muon life time $\tau_{\mu} = (2.212 \pm 0.001) \times 10^{-6}$ sec. Consequently, the decay of a muon is due to a weak interaction.

2.4. Decay scheme of a muon

Early observations already showed that the muon decays with the emission of one charged particle: an electron or positron $\mu^{\pm} \rightarrow e^{\pm} + ?$. What are the other decay products of a muon? Some information can be obtained from the study of the energy distribution of the decay electrons. Indeed, assuming that the muon decays into two particles with masses m_e and m_x, one writes the conservation laws in the form of

$$\begin{cases} p_e = -p_x; \\ \mu_0 c^2 = E_e + E_x. \end{cases}$$

Excluding E_x from these equations, one obtains

$$E_e = \frac{\mu_0^2 c^2 + m_e^2 c^2 + m_x^2 c^2}{2\mu_0}. \qquad (3.6)$$

Consequently, all the electrons must have the same energy in the case of a two-particle decay.

Experiments on the determination of energies of the decay electrons were carried out by Leighton and Anderson, and independently by Ždanov in 1949 in the USSR. Leighton studied the decay of muons stopped in a graphite disk. The momenta of the decay electrons were determined by the curvatures of their trajectory in a magnetic field. It was found that the momenta, and consequently the energies, were distributed by continuous spectra, sharply cut at an energy near 55 MeV. The mean value of the energy of the decay electrons was equal to approximately 35 MeV, i.e. 1/3 of $\mu_0 c^2$. This showed that a muon decayed into more than two particles. The fact that the electron carries out 1/3 of the whole energy means, with a high degree of assurance that the muon decays into three particles. The masses of these particles can be determined by the upper limit of the spectrum of the decay electrons. The energy of the electron will be maximum when the other particles fly in the opposite direction. In this case, one can apply equation (3.6) obtained above assuming that m_x is the sum of masses of decay particles other than the electron. Substituting $E_e = 55$ MeV, $\mu_0 c^2 = 106$ MeV and $m_e c^2 = 0.5$ MeV into equation (3.6) one finds that $\Sigma m_x = 0$.

We know two particles having mass zero: the photon and the neutrino. Special experiments in which attempts were made to observe cascade showers produced by decay photons gave negative results, and photons were not found. Accordingly, a muon decays with an emission of two neutrinos or antineutrinos or with an emission of a neutrino and an antineutrino :

$$\mu^{\pm} \rightarrow e^{\pm} + \nu + \tilde{\nu}.$$

The shape of the spectrum of decay electrons can also answer the question : whether identical neutrinos or a neutrino and an antineutrino are emitted in the decay of a muon. Since the decay of a muon is produced by a weak interaction, it can be treated theoretically in complete analogy with β decay.

Michel used the theory of β decay to calculate the spectrum of the decay electrons. He found that this spectrum was given by

$$N_e(E)\,dE = \text{const}\, E^2 \left[3\,(E_m - E) + 2\rho\left(\frac{4}{3}E - E_m\right)\right] dE.$$

Here E_m is the upper boundary of the decay electron spectrum. Michel's constant depends on the interaction constants for different types of coupling between the particles. It has different values depending on whether the two neutrinos are identical, i.e. indistinguishable, or different i.e. neutrino and antineutrino. In the first case, the parameter is zero and consequently, the spectrum of electrons must vanish at the upper boundary. In the second case, $\rho = \frac{3}{4}$ and the spectrum is sharply cut at $E_m = 55$ MeV. Experiment shows that ρ is near to $\frac{3}{4}$ and consequently, the decay scheme of a muon is in the form of

$$\mu \rightarrow e + \nu + \tilde{\nu}.$$

There are also other types of decay of a neutrino :

$$\mu^{\pm} \rightarrow e^{\pm} + \nu + \tilde{\nu} + \gamma \quad (W = 1{,}4 \cdot 10^{-2})$$

and

$$\mu^{\pm} \rightarrow e^{\pm} + \nu + \tilde{\nu} + e^{+} + e^{-} \quad (W = 2{,}2 \cdot 10^{-5})$$

where W is the probability of the corresponding decay channel.

2.5. Spin of a muon

Since a muon decays into three particles of half-integer spins, they must also have a half-integer spin. Now, it is proved that the muon spin is equal to $\frac{1}{2}\hbar$. This is a very important fact; on the basis of it one has the right to separate muons from the class of mesons which all have integer spins. The muon

that is produced in the decay of a π-meson at rest, is longitudinally polarized, i.e. its spin is either parallel or antiparallel to its momentum.

2.6. Interaction of muons with nuclei

There are two ways to study the nuclear interaction of muons. The first way is to study processes occuring in the collision of rapid muons with nuclei. A muon has an electric charge. When a muon interacts with a nucleus, not only nuclear but also electromagnetic processes can take place. These interactions can lead to reactions of the same type as photo-nuclear reactions, leading to the disintegration of nuclei and to the creation of mesons. Such experiments therefore require not only accurate measurements but also reliable theoretical calculations, since the method is mainly based on determining the deviation of experimental data from theoretical predictions.

The other way is to observe the capture of the stopped muons by nuclei. One expects that positively and negatively charged muons behave in a different manner. This was emphasized for the first time in 1936 by the Japanese physicists Tomonaga and Araki. Positively charged muons will be pushed away by the Coulomb field of the nucleus and will not be able to approach it enough to interact with the nuclear field. Negatively charged mesons after showing down to an energy $\sim$2000 eV will have a velocity comparable to the velocity of atomic electrons. Fermi and Teller showed that, in a dense material, muons reached this energy within a time equal to 10^{-9} sec. After another 10^{-13} sec., the muon is captured in the muonic K-shell of the atom and forms a mesoatom. The K-shell of the muon has a radius 200 times less than the corresponding electronic shell. For heavy nuclei with $Z > 40$, the mesonic K-shell is located at the peripheral part of the nucleus. Therefore, if the muon strongly interacts with the protons, negatively charged muons must always be captured by nuclei. Positively charged muons must all decay.

The different behaviour of positively and negatively charged muons was first observed by Conversi, Pancini and Piccioni in 1945. Their instrument had the following construction (figure 23). Two iron prisms were magnetized in opposite directions. This made muons of a given charge sign focus at the absorber and stop in it while those of the opposite charge scatter aside. By changing the direction of magnetization, they could focus on the absorber either positively or negatively charged muons. Counters D were included in an anti-coincidence scheme. The lower row of counters C was included in a delayed coincidence circuit and could register decay electrons, occuring with a delay from 1 to 4.5 μ sec. It was expected that decay electrons would be absorbed only when positively charged muons were stopped. This assumption was confirmed when experiments were made with an iron absorber. However, when iron was replaced by graphite, the instrument counted equal numbers of decay electrons when either positively or negatively charged muons were stopped. This means that, during its life time, ($\sim$2.2 μ sec.), the muon does not have enough time to interact with light nuclei. It is thus concluded that muons weakly interact with nucleons.

The probability of interaction of a muon with a nucleus increases with increasing Z, whatever the mechanism of interaction is. This will become clear if we take into consideration the increase in the probability of interaction which follows from the increase of the number of protons, i.e. the increase of Z. On the other hand, the probability of interaction is proportional to the probability of a muon to be inside the nucleus. This probability is evidently proportional to the volume of the region in which the wave function of the μ meson is not very small. One expects that this region, as an order of magnitude, has the same dimension as the Bohr orbit; consequently

$$W \sim \frac{1}{V} \sim \frac{1}{r_\mu^3} \sim Z^3.$$

Therefore, the total probability of absorption of a muon $\sim ZZ^3$, i.e. rapidly increases with increasing atomic number. If the two competing processes: decay and absorption of a meson are present, then, for a given ratio of probabilities, the muon capture will occur only in heavy nuclei since the probability of a capture $\sim Z^4$, while the probability of a decay is independent of Z. This explains the different behaviour of muons in light and heavy nuclei observed experimentally by Conversi et al. Accordingly, muons can be the quanta of the nuclear field that Yukawa predicted because the interaction of a muon is 10 ÷ 12 times weaker than what theory requires. The quanta of the nuclear field were

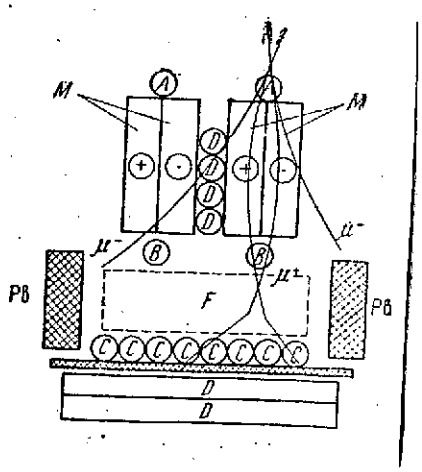

Fig. 23. The experimental scheme for studying the interaction of the stopped mesons of charges with different signs (The direction of magnetization of the bars and the trajectories of the particles are indicated).

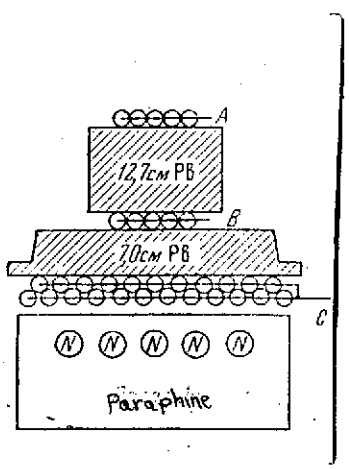

Fig. 24. The experimental scheme for registration of neutrons appearing after absorption of muons in lead (Experiment by Sard et al.).

discovered in 1948 by Powell and Occhialini and called π-mesons. We will, however, continue to speak about muons.

What happens to a nucleus when it captures a negative muon? After a muon capture, the nucleus is given an energy equal to the rest energy of a muon, i.e. 106 MeV. This energy goes into excitation ("heating") of the nucleus, which subsequently "cools down" by emitting neutrons, protons or nuclear fragments. Several authors used Wilson's chamber, photoemulsions and other methods to study charged particles resulting from nuclear distintegrations caused by muons.

George and Evans investigated nuclear disintegrations caused by negatively charged muons. They carried out their experiments in a London underground station in order to avoid disintegrations produced by radio-active particles existing in the atmosphere (neutrons, π-mesons). They prepared the nuclear photographic plates at a depth of 30 m underground (6000 g/cm^2). The authors observed the stoppage of 290 muons. The results are given in table 8. We see from the table that charged particles very seldom appear as a result of muon capture. In 265 cases, charged particles were not observed.

Table 8

Type of reactions following a muon capture	number of cases
Without formation of charged particles	265
Single-ray stars	22
Two-ray stars	3
$>$ 2 rays	0
Total	290

Experiments were made to observe neutrons appearing after a muon capture. One of these experiments was carried out in 1948 by Sard at the University of Washington. The instrument consisted of two rows, A and B, of counters switched on in coincidence, and a row, C, of counters connected together in anticoincidence. He collected negatively charged muons that stopped in a lead block (figure 24). The neutron which flew off from the nucleus could fall into a paraffin block, decelerate up to a thermal velocity and be registered by a boron counter. Counters N were switched on with a delay of 4 μ sec since the deceleration of neutrons up to thermal velocities required a few micro-seconds. The experiment showed that neutrons were emitted after a muon capture. After the lead nucleus captured a muon, two neutrons with energies $<$ 10 MeV were emitted. In light elements (Mg, Ca) the number of neutrons emitted in a single act of capture was 5 times less, i.e. was equal to $\sim$0.4 neutron per muon captured.

All these results could only be understood if a small fraction of the muon

energy went into the excitation of the nucleus. Actually, the binding energy of a neutron in a nucleus is equal to a few MeV and hence a transfer of 106 MeV to a nucleus must lead to the emission of a large number of neutrons. The absence of multi-neutron emissions indicates that a considerable fraction of energy is carried out by a neutral particle different from a neutron.

Furthermore, experiments showed that photons with energies >10 MeV were not observed. All this leads to the conclusion that a large fraction of energy is carried away by a neutrino and that the reaction is in the form of

$$\mu^- + p \rightarrow n + \nu.$$

We see here again the analogy between the interaction of electrons and muons with nuclei :

$$e^- + p \rightarrow n + \nu.$$

2.7. Interaction of high-energy muons

The above-mentioned arguments suggest that muons have either weak or electromagnetic interactions with other particles and nuclei, at least in the not-very-high-energy region. The cross sections of weak interactions are by many orders of magnitude less than the cross sections of electromagnetic interactions. Therefore, the main type of interaction of muons with energies up to 10^3 GeV is the electromagnetic interaction.

The direct creation of electron-positron pairs by muons, their bremsstraalung and electromagnetic-nuclear interaction were studied theoretically and experimentally. The latter processes are described as a photonuclear interaction of virtual photons, formed by the electromagnetic field of a moving muon, with the nucleus. Several authors raised the question on whether there existed an "anomalous" type of interaction of muons, different from the above mentioned types. It is possible that this type of interaction will play an important role in the region of very high energies not yet reached up till now.

In order to observe anomalous interactions, one has to put very severe requirements on the accuracy of the calculations of the cross-sections of electromagnetic interactions, since experimentally, one has in general to find a small difference between the theoretical and experimental cross sections. This was the initiative for many authors to improve the accuracy of the calculated cross sections of electromagnetic interactions by taking various corrections into consideration. For example, in considering bremsstraalung, one has to consider [4] more accurately :

1) the production of photons in the field of the atomic electrons;
2) the radiational corrections;
3) the influence of the medium (the Landau-Pomerančuk effect);
4) the deviations from the first Born approximation.

The analysis of the theoretical results shows that the cross-section of bremsstraalung is now known within an accuracy of 5% [4]. Probably, the accuracy of the theoretical values of the cross-sections of direct creation of an electron-positron pair by a muon is of the same order. We should note that equation (2.10) has a much smaller accuracy because of the simplifications we have used in its derivation.

In the interaction of rapid muons with nuclei, nuclear disintegrations and showers may be produced by the quanta of the nuclear interaction, the π-mesons. The experimental estimation of the cross-section of these processes showed that it is small; $\sigma_n \sim 10^{-30}$ cm^2/nucleon. This is one thousand times less than the cross sections of strong interactions.

In theory, this phenomenon is explained as a process having the same type as photonuclear reactions. The quantitative consideration of this process can, for example, be done by means of the Weizsäcker-Williams method, representing the electromagnetic field of a muon as a flux of photons.

The cross section of interaction of a photon with a nucleus is only known for experiments on accelerators (at energies of a few MeV) where it is equal to $\sigma_{\gamma n} \simeq 10^{-28}$ cm^2/nucleon. If one assumes that the cross section $\sigma_{\gamma n}$ keeps the same value in the high-energy domain, one then finds that the cross section for an electromagnetic-nuclear interaction is equal to $\sigma_n \sim 10^{-30}$ cm^2/nucleon, in agreement with experiments on production of nuclear showers by mesons (Maze-Kessler showers).

Accordingly, the nuclear interactions of muons with nuclei which have been observed up till now, are explained as either weak or electromagnetic interactions and the properties of muons do not differ from the properties of electrons. The only difference between the two particles is in their masses. Table 9 gives a comparison between the properties of muons and electrons.

Table 9

Property	Electrons	Muon
Mass	m_e	207 m_e
Spin	1/2	1/2
Reaction	$e^- + p \to n + \nu$	$\mu^- + p \to n + \nu$
Interaction constant	10^{-13}	10^{-13}
Strong interaction	absent	absent
Weak interaction	present	present
Magnetic moment, theory	1,0011596	1,0011654
Magnetic moment, experiment	1,0011600	1,0011600

According to the modern field theory, the mass of a particle is a result of a given type of interaction. The situation is therefore quite mysterious. While there is no difference between the interaction of muons and electrons,

their masses are quite different. It is possible that some kind of specific interaction of muons will be discovered at energies higher than those available at present. This calls for the particular attention towards muons and makes them an attractive subject of study in the different laboratories. It is expected that many secrets of matter are kept by muons and, indeed, the increase in interest devoted to them has alreayd reaped the fruits of the labour made.

3. Neutrino /9, 10, 11/

3.1. General considerations

Recently, the utilization of neutrinos has become very popular. These are particles having only weak interactions. Some of their properties have already been mentioned above. They were specially "invented" as they were impossible to be observed. However, this property was "invented" quite long ago (by Pauli in the thirties) and since then, many methods were constructed to 'hunt' the neutrinos. In order to illustrate the role played by neutrinos in cosmic rays, the well-known American physicist Morrisson told a story that one of the scientists working on the problem of neutrinos gave a New Year present to one of his friends consisting of a brightly painted match box on which he wrote "in this box, there are at least 100 neutrinos".

Actually, the neutrino current coming from the sun and reaching the earth's surface is very large and approximately equal to 10^{11} cm^{-2} sec^{-1}. This is by several orders of magnitude greater than the intensity of any other component of cosmic radiation. A percentage of solar energy is radiated in the form of neutrinos. The major fraction of neutrinos is created in the depths of the sun. Consequently, the study of neutrinos can provide us with information on the processes which occur in the centre of the sun. Up till now we do not know of any other method to "look" at the depths of the sun.

3.2. Properties of neutrinos

The mass of the neutrino is zero or very close to zero. The neutrino, like the muon, has the interesting property of being longitudinally polarized. This means that the spin of the neutrino, which is equal to $\frac{1}{2}$, is either parallel or antiparallel to its momentum. This property is called helicity and is characterized by the quantum number $H = \pm 1$. The antineutrino has $H = +1$ and the enutrino has $H = -1$. In principle, one can use this property to differentiate between matter and antimatter. Actually, a neutrino is produced in the thermonuclear reaction of fusion of hydrogen into deuterium :

$$p + p \rightarrow d + e^{+} + \nu; \quad E_{\nu} < 0{,}8 \text{ Mev.}$$

If an "anti-sun" existed somewhere in the universe, which consisted of anti-hydrogen, then such an "anti-star" would emit antineutrinos although light that would come from such an object would not differ from light coming from the stars (since $\gamma = \tilde{\gamma}$).

3.3. Two types of neutrinos

Very recently, in the spring of 1962, a very interesting discovery was made. It was found that there existed two types of neutrinos: electronic ν_e and muonic ν_μ . When we concluded that a neutrino was emitted in the decay of a muon, we were proceeding from the "principle of economy". We knew no other weakly interacting particles which had a mass close to zero and with a spin equal to $\frac{1}{2}$. This however does not mean that these particles must be identical to those which appear in a β-decay. This question was treated experimentally by Lederman, Steinberg and others and the experimental idea was suggested by M.A. Markov and B.M. Pontekorvo. They observed on an acceleration the neutrinos emitted in the decay of π-mesons

$$\pi \rightarrow \mu + \nu.$$

and searched for the reactions :

$$\nu + p \rightarrow n + e^+; \quad \nu + n \rightarrow p + e^-;$$
$$\nu + p \rightarrow n + \mu^+; \quad \nu + n \rightarrow p + \mu^-.$$

They found that there were no reactions leading to the production of electrons. Since neutrinos, created in the accelerator, were pairing with muons, the result of this experiment was interpreted as that neutrinos were not capable of producing electrons. Consequently, $\nu_\mu \neq \nu_e$ and pions decay by the reaction :

Neutrinos interact with nucleons, though the cross sections of these processes are small. Typical reactions are the following :

$$\nu_e + n \rightarrow p + e^-; \quad (1) \qquad \nu_\mu + n \rightarrow p + \mu^-; \qquad (3)$$

$$\tilde{\nu}_e + p \rightarrow n + e^+; \quad (2) \qquad \tilde{\nu}_\mu + p \rightarrow n + \mu^+. \qquad (4)$$

Reaction (2) was used by Rajnes and Kouen /11/ to observe neutrinos produced in a reactor. A liquid scintillator, containing hydrogen and cadmium, was radiated by antineutrinos. The resulting positron was annihilated with the production of photons. The neutron was decelerated and captured by the cadmium, giving delayed neutrons with a total energy of 9 MeV. The cross section of reaction (1) was found to be approximately equal to 10^{-43} cm^2.

An alternative method for detecting neutrinos was suggested by B.M. Pontekorvo.. This method utilizes the reaction of neutrino capture by the chlorine nucleus.

$$\nu + Cl^{37} \rightarrow Ar^{37} + e^- - 0{,}8\ Mev. \tag{5}$$

In practice, $C_2\ Cl_4$ is applied, and a small number of the radio-active atoms Ar^{37} is separated from large volumes of this material. Neutrinos from sun will be observed if the nuclear reactions taking place in the depths of the sun are :

$$\begin{aligned} N^{13} &\rightarrow C^{13} + e^+ + \nu; \\ O^{15} &\rightarrow N^{15} + e^+ + \nu; \\ B^8 &\rightarrow Be^8 + e^+ + \nu; \quad E_\nu > 0{,}8\ Mev. \end{aligned} \tag{6}$$

Muonic neutrinos will be observed by means of reactions (3) and (4). Taking the large penetration power of the neutrinos into consideration, one can carry out the experiments deep underground and study the interaction of neutrinos coming from below, i.e. having penetrated the whole thickness of the earth. The muons produced are registered by means of scintillators. The investigation of the interactions of neutrinos by means of accelerators shows that the cross section of the reaction $\nu + n \rightarrow \mu^- + p$ + pions rapidly increases with energy. In experiments on accelerators, the increase of the cross section with energy is expressed by the following relation

$$\sigma \sim 0{,}8 \cdot 10^{-38} E_\nu\ cm^2. \tag{3.7}$$

Where E_ν is expressed in GeV.

3.4. Sources of neutrinos

It is clear from the above discussion that there exists a number of sources of neutrinos in cosmic rays.

Muonic neutrinos are produced in the decay of pions and kaons. In the first case, the neutrino carries up to 46% of the energy of the pion, and in the second case up to 100%. At energies higher than 10^3 GeV, pions do not have enough time to decay in the atmosphere, and hence the number of neutrinos having $E_\nu > 10^3$ GeV must be small. The observation of muonic neutrinos underground enables us to study their interaction at highest energies, because the increase of the energy of the neutrinos increases the path of the muons produced, and consequently the possibility of their registration. If the cross section increases with energy, the experiments described here will then enable us to confirm this increase.

A second source of neutrinos are thermo-nuclear reactions occuring in stars. In this case, neutrinos of lower energies will be produced and they can be measured by means of reaction (5).

4. Strongly-Interacting Particles

4.1. Pions (synonym: π-mesons)

Yukawa's prediction for the existance of the heavy quanta of the nuclear field with mass $\sim 300\ m_e$ was realized in 1947, when Powell and Occhialini discovered π-mesons [12] in cosmic rays by means of an improved version of the photoemulsion method. They observed cosmic-ray particles, stopped in emulsions. Some of these particles emitted at the point of stoppage, a particle that left a thin trace in the emulsion. This suggests that the emitted particle was relatively possible, and this could be possible if emission took place in a decay process. They also succeeded to fix the stoppage of the secondary particle which also decayed, with the production of an electron (this was easily confirmed by studying the scattering of the latter particle). Such a decay scheme was characteristic for a muon. Measurements showed that all of the muon tracks had the same length, nearly equal to 500 μm. It was then concluded that the particle that produced a muon, decayed into two particles: a muon and a neutrino, as was established by means of further special investigations.

The mass of the new particle was easy to calculate. It was found to be equal to 140 MeV. This particle was called a π-meson and later, more simply, a pion. Subsequent experiments showed that the life time of a pion (measured by the method of delayed coincidences) was equal to 2.15×10^{-8} sec. The spin of the pion was found to be equal to zero. It was also found that there existed two types of charged pions having the following decay schemes :

$$\pi^+ \rightarrow \mu^+ + \nu_\mu; \quad \pi^- \rightarrow \mu^- + \bar{\nu}_\mu.$$

π^0-mesons were discovered much later. The existance of π^0-mesons was predicted by B. Rossi and C.N. Vernov on the basis of their analyses of cosmic experiments. The existance of these particles was necessary to explain the appearance of the electron-photon components at large heights in the stratosphere. At that time, it was possible to even give an estimate for the life time of the π^0-meson. It should be quite short. Being a neutral particle, the π^0-meson can decay into two photons, i.e. at the expense of electromagnetic interactions. Consequently, the life time of a π^0-meson $\tau_{\pi^0} \ll 10^{-10}$ sec. Recent experiments showed that the life time of a π^0-meson $\tau_{\pi^0} = 1.2 \times 10^{-16}$ sec.

The proof of the existance of π^0-mesons was obtained by observing the photons are produced by the decay of a π-meson with mass m_π , then the photon spectrum must have a maximum and a definite relation must hold between energies ε_1 and ε_2, located at opposite sides from the maximum and corresponding to equal intensities in the spectrum, and the mass m_π of the pion (see [1], in chapter 4):

$$\sqrt{\varepsilon_1 \varepsilon_2} = \frac{m_\pi c^2}{2}.$$

It was found that the spectrum of cosmic-ray photons satisfied this relation.

A direct proof for the existance of π^0-mesons was obtained in the experiments, carried out by Panovskij et al. on an accelerator. In these experiments, the decay scheme of a π^0-meson was accurately established :

$$\pi^0 \rightarrow 2\gamma$$

and its mass was measured and found to be equal to $m_{\pi^0} = 134.97 \pm 0.05$ MeV/c^2. Accordingly, the π^0-meson is slightly lighter than the charged pions.

We can thus see that there are three types of mesons, forming an isotopic triplet (i.e., the isotopic spin of a pion is equal to I = 1).

4.2. Strange particles [13]

The discovery of π-mesons was a consequence of the natural development of physics. The discovery of heavier particles, in particular hyperons, i.e. particles heavier than a neutron, was completely unexpected. Before hyperons were discovered, it was believed that there was an upper limit to the masses of elementary particles and that all elementary particles had masses lying between the masses of the electron and the neutron.

At the present time, it is impossible to predict whether there is an upper limit for the masses of elementary particles. Particles heavier than a neutron are unified under the common name hyperons. They all have a half-integral spin as the nucleons. Together with nucleons, these particles are called barions.

One of the first-discovered hyperons is the Λ^0-hyperon. It probably was given this name because it formed a characteristic fork when it decayed in a Wilson chamber;

$$\Lambda^0 \rightarrow p + \pi^- + Q \quad (Q = 37 \pm 1 \text{ Mev}).$$

The Σ-hyperons and the so-called cascade hyperons denoted by Ξ^-, were discovered later. All hyperons are unstable; they decay. Table 10 gives some of the properties of hyperons

Table 10

Hyperon's decay scheme	Q, Mev	M/m_e	τ, sec
$\Lambda^0 \rightarrow p + \pi^-$	37 ± 1	2182,7	$(2,505 \pm 0,086) \cdot 10^{-10}$
$\Sigma^+ \rightarrow \begin{cases} p + \pi^0 \\ n + \pi^+ \end{cases}$	115,8 109,9	2327,5 2327,5	$0,81 \cdot 10^{-10} \pm 0,06 \cdot 10^{-10}$ $0,81 \cdot 10^{-10}$
$\Sigma^- \rightarrow n + \pi^-$	—	2340,5	$1,6 \cdot 10^{-10} \pm 0,1 \cdot 10^{-10}$
$\Sigma^0 \rightarrow \Lambda^0 + \gamma$	—	2331	10^{-11} (theoretically) — 10^{-10}
$\Xi^- \rightarrow \Lambda^0 + \pi^-$	67	2586	$1,75 \cdot 10^{-10}$
$\Xi^0 \rightarrow \Lambda^0 + \pi^0$	—	—	$2,8 \cdot 10^{-10}$
$\Omega^- \rightarrow \begin{cases} \Xi + \pi \\ \Lambda + K \end{cases}$	534 595	3260	$(1,3 \pm 0,7) \cdot 10^{-10}$

The majority of hyperons were discovered in cosmic rays (except Σ° and Ξ°). At the present time, all hyperons are produced in accelerators.

The discovery of mesons heavier than a π-meson was as unexpected as the discovery of hyperons. In the earlier stages, these mesons were studied by means of Wilson chamber and nuclear photo-emulsions in cosmic rays. The few observed cases gave the primary information on the decay schemes. All the preliminary classifications of the new particles were based on the study of their decay schemes. It was considered that each of the decay schemes belonged to a given particle. The first discovered heavy meson decayed into three π-mesons and was called a τ-meson. Later came the discovery of the θ-meson which decayed into two π-mesons, as well as the discovery of other mesons. Soon, almost all the Greek alphabet was used. However, at the same time, it was realized that the newly discovered mesons had similar properties (except decay schemes). They almost all had near masses and life times. People began to believe that the heavy measons are the same particle with alternative decay schemes. They called these particles K-mesons. The decay schemes of K-mesons are given in table 11.

Table 11

Type of decay	fraction of cases
$K_{\mu}^{\pm} \to \mu + \nu$	$(63 \pm 8)\%$
$K_{\pi_2}^{\pm} \to \pi^{\pm} + \pi^{\circ}$	19%
$\tau^{\pm} \equiv K_{\pi_3}^{\pm} \to \pi^{\pm} + \pi^{\pm} + \pi^{\pm}$	5,6%
$\tau^{\circ} \equiv K_{\pi_3}^{\circ} \to 3\pi^{0}$ или $\pi^{\pm} + \pi^{\pm} + \pi^{\circ}$	—
$\tau_{\pi_3}^{\pm\prime} \equiv K_{\pi_3}^{\pm} \to \pi^{\pm} + \pi^{\circ} + \pi^{\circ}$	$(1,1 \pm 0,6\%)$
$\theta^{\circ\prime} = K_{\pi_2}^{\circ} \to \pi^{-} + \pi^{+}$	—
$\theta^{\circ\prime\prime} = K_{\pi_2}^{\circ} \to 2\pi^{\circ}$	—
$K_{\mu_3}^{\pm} \to \mu^{\pm} + \pi^{\circ} + \nu$	$(2,5 \pm 1,2\%)$
$K_{e_3}^{\pm} \to e^{\pm} + \nu + \nu$	$(9,0 \pm 4,0\%)$

There are other, rarer decay schemes. The negative K-mesons when stopped are usually captured by the nuclei. The majority of decay schemes is therefore established for positive K-mesons. The masses of these particles were found to be very close to each other :

$$m_{\tau} = (966,1 \pm 0,7)\, m_e; \quad m_{K_{\mu_3}} = (968 \pm 6)\, m_e;$$
$$m_{K_{\mu_2}} = (967,2 \pm 2,2)\, m_e; \quad m_{K_{e_3}} = (963 \pm 10)\, m_e;$$
$$m_{K_{\pi_2}} = (966,7 \pm 2,0)\, m_e; \quad m_{K^{\pm}} = (493 \pm 0,2)\ Mev/c^2;$$
$$m_{K^{\circ}} = (497,8 \pm 0,6)\ Mev/c^2.$$

The equality of masses gives a sound basis for considering all these particles as the same K-particle. Recent measurements of the life times lead to the same conclusion. The life times of all charged K-mesons are close to 1.2×10^{-8} sec while that of the neutral θ^0-meson $\sim 1.0 \times 10^{-10}$ sec.

In which processes are these heavy mesons created? Let us first consider the decay scheme of Λ^0 :

$$\Lambda^0 \rightarrow p + \pi^-.$$

This reaction takes a time $\sim 10^{-10}$ sec., which means that the decay of the hyperon occurs at the expense of a weak interaction. The probabilities of the direct and inverse reactions must be equal. Consequently, in the present case, it is not possible to obtain a hyperon in a rapid interaction of a π-meson with a proton. Experiment shows however, that hyperons and K-mesons are always produced in pairs as a result of the nuclear interaction of π-mesons with protons :

$$\pi^- + p \rightarrow \Lambda^0 + \theta^0.$$

Other hyperons are also created in pairs with K-mesons. In this manner, the following experimental fact is established: hyperons are created in pairs with K-mesons (the associative creation rule).

Another experimental fact is that hyperons are created in pairs either with positive or neutral K-mesons :

$$\pi^- + p \rightarrow \Sigma^- + K^+; \quad \pi^+ + n \rightarrow \Lambda^0 + K^+;$$
$$\pi^+ + p \rightarrow \Sigma^+ + K^+; \quad \pi^- + p \rightarrow \Lambda^0 + \theta^0.$$

For this reasons K^--mesons are more rarely obtained by accelerators than K^+ mesons. Indeed, K^- mesons are obtained only in the process of creation of a $K^- \pm K^+$ pair which requires a large amount of energy.

A third experimental fact is that, in all reactions, the number of barions (particles with masses equal to or greater than the nucleon mass) is conserved.

Although considerable progress has recently been made in the study of elementary particles, it is probably hard to find a courageous scientist that is able to say how many particles actually exist. Each year brings about the discovery of new "elementary" particles.

4.3. Resonances /14/

New members have been added to the family of strongly interacting particles, now called hadrons. These are the extended group of "resonances" and isobars. These particles are very similar to K-mesons and hyperons though they decay at the expense of strong and not weak interactions. Their life times are of the same scale as the nuclear time scale, and only in rare cases exceed 10^{-20} sec. Having such a small life time, their masses cannot be measured with the same

accuracy as the masses of particles with long lives because of the uncertainty principle. For this reason, one of the most important properites of a particle of this group is its width $\Delta\Gamma$ which characterises the dispersion of masses of separate resonances around the average mass. This width is defined by the relation

$$\Delta\Gamma\Delta t \sim \hbar.$$

where Δt is the life time. Resonances occur as bound states of two or more strongly interacting particles. However, the particles in these bound states are so strongly coupled that their individuality is lost so that the resonance appears as a unit formation. A bound state of a barion with a meson is often called an isobar, while a bound state of several mesons is called resonance (or "resonon"). The values of masses of these particles are quite different but their $\Delta\Gamma$'s vary from tens to hundreds of MeV.

Let us follow the analogy between a resonance and a meson. For example, a K-meson sometimes decays according to the following scheme

$$K^\circ \to 2\pi \equiv 0^\circ; \quad \tau \sim 10^{-10} \text{ sec.}$$

while one of the decay schemes for a ω^0 - resonance is

$$\omega^\circ \to 2\pi; \quad \tau \sim 10^{-20} \text{ sec.}$$

What is then the reason for such a difference in life times of these particles, or equivalently, the difference in the character of the forces causing their decay ?

It was found that these particles differed from one another by the quantum number strangeness. By introducing this quantum number, Gell-Mann and Nishigima succeeded to explain the decay properties of K-mesons and hyperons. If there exists a quantum number S, which must be conserved in strong interactions, then a particle with $S \neq 0$ cannot be produced in strong interactions which only just have time to appear during the time of collision of two rapid particles ($10^{-22} \div 10^{-24}$ sec.).

On the other hand, the creation of two particles having a strangeness of opposite signs does not violate the law of conservation of strangeness. Consequently, two of these particles can be produced in strong interactions.

Gell-Mann and Nishigima suggested to give hyperons a negative strangeness $S = -1, -2$ and K^+- and K^0-mesons a positive strangeness $S = +1$. It then becomes evident that hyperons must be produced in pairs with K^+- or K)-mesons. K^-- and $\bar{K}^0$ - mesons have a strangeness $S = -1$, and can therefore be only produced in pairs with K^+- and K^0-mesons, but not with hyperons.

In order to explain the reason for decay of K-mesons and hyperons, it was suggested that strangeness is not conserved in weak interaction and that the change in S does not exceed 1. This explains why K-mesons and hyperons live so long ($\sim 10^{-8} \div 10^{-10}$ sec).

Resonances have S = 0, and hence can be created and annihilated, i.e. torn out by the action of the nuclear (strong) interaction.

We now briefly look at some questions which have recently attracted the interest of physicists working in the field of cosmic-rays physics. We shall consider the following important definitions :

Barionic charge (barionic number) :

This definition is introduced in order to explain the extraordinary stability of barions. In all reactions , the number of barions and antibarions is always constant.

Hyperchange :

Recently, instead of strangeness, one often uses the quantum numberhypercharge, being equal to the sum of the barionic charge and strangeness and denoted by Y.

As mentioned above, the number of "elementary particles" known recently has drastically increased and is now counted in the hundreds. This does not seem satisfy physicists. Every now and then there appears an attempt to reconstruct all the "elementary" particles from more elementary bricks.

4.4. Quarks [15]

One of the attempts to construct "elementary" particles from more elementary bricks is made through the hypothesis of "quarks". "Quarks" are elementary bricks. These are in the number of six: three quarks and three antiquarks. Their properties are stranger than the properties of the strange particles.

The most particular property is the division of the electric charge. We denote the three types of quarks by the small letters p, n and λ . The properties of quarks are given in table 12.

Table 12

Notation for the quark	Electric charge	Strangeness	Barionic number	Spin
p	+2/3	0	1/3	1/2
n	−1/3	0	1/3	1/2
λ	−1/3	−1	1/3	1/2

Combining the different quarks, one can construct all the known particles; for example, the nucleons and hyperons (8 particles) :

Σ^+ — ppλ;	Ω — ppn;
Σ^0 — pnλ;	N — pnn;
Σ^- — nnλ;	Ξ^0 — pλλ;
Λ^0 — pnλ;	Ξ^- — nλλ.

The isobars (10 particles) :

$$\begin{array}{rrrr} \Omega^{-*} - \lambda\lambda\lambda; & \Xi^{c*} - p\lambda\lambda; & \Sigma^{+*} - pp\lambda; & \Delta^{++} - ppp; \\ & \Xi^{-*} - n\lambda\lambda; & \Sigma^{c*} - pn\lambda; & \Delta^{+} - ppn; \\ & & \Sigma^{-*} - nn\lambda; & \Delta^{\circ} - pnn; \\ & & & \Delta^{-} - nnn. \end{array}$$

It was found that each row in this scheme has a characteristic regularity concerning masses, strangenesses, etc. This lead to the theoretical prediction of the existance of the Ω - particle, which was later experimentally confirmed.

One can analogously construct other particles (the mesons and resonances). In this case, one has to use the antiquarks. It is possible in this manner to construct the whole world out of three bricks. There remains only the question, whether quarks exist or not. Recently, a series of experiments were carried out in order to search for these mysterious particles. The simplest experiment was to search for particles having very low ionization powers. Since quarks must have a charge 1/3, their ionization power must be 9 times less than that of a conventional particle. These experiments were not successful. Work on accelerators showed that the mass should not be less than 6 nucleon masses, otherwise they would not be observed in accelerators. In many laboratories, however, experiments are still being undertaken to try to observe quarks in cosmic rays.

Questions and Problems

1. Calculate the maximum energy, in a laboratory system, for neutrinos emitted in the decay of pions and kaons having an energy E.
2. What fraction of neutrinos having an energy E is absorbed when they pass through the diameter of the earth ?
3. What fraction of energy is carried out by the muon in the decay of a π-meson ?
4. (No. 496 from [16]). The source of the solar energy is assumed to be Bethe's carbon cycle, which may be represented by the following reactions :

$$\begin{array}{ll} 1)\ p + C_6^{12} \rightarrow N_7^{13} + \gamma; & 4)\ p + N_7^{14} \rightarrow O_8^{15} + \gamma; \\ 2)\ N_7^{13} \rightarrow e^+ + C_6^{13} + \nu; & 5)\ O_8^{15} \rightarrow N_7^{15} + e^+ + \nu + \gamma; \\ 3)\ p + C_6^{13} \rightarrow N_7^{14} + \gamma; & 6)\ p \rightarrow N_7^{15} \rightarrow C_6^{12} + He_2^4. \end{array}$$

In Bethe's cycle, a flux of neutrinos is produced and falls on the earth. Evaluate this flux, taking the sun's power equal to 3.78×10^{33} erg/sec. and the mean energy of neutrinos $\langle \mathcal{E}_\nu \rangle = \frac{2}{3} E_m$, where E_m is the upper limit of energy of the positronic decay :

$$E_m = 1.2 \text{ MeV for } N_7^{13} \text{ , and } E_m = 1.68 \text{ MeV for } O_8^{15} .$$

5. Consider the chain of decay processes, following the decay of a Ξ^- -hyperon.

CHAPTER 4

HIGH-ENERGY NUCLEAR INTERACTIONS

1. Major Properties

Strong interactions are characterized by a large interaction constant, large reaction cross sections and small interaction times (10^{-23} sec.). Because of the latter property, processes resulting from strong interactions are called rapid processes.

In strong interactions, the isotopic spin and its Z-projection, the strangeness quantum number and other quantum numbers are conserved. At high energies when electromagnetic interactions are negligible, one usually makes no difference between protons and neutrons. In the direct multiple production of mesons, the isotopic invariance means that the three kinds of π-mesons must be created, on the average, in equal numbers and have equal energy distributions and equal mean energies.

The study of nuclear interactions at energies higher than 10^{10} eV is still in the stage of collecting experimental information. Up till now, there is no exact theory for these processes.

The most important experimental characteristics of nuclear interactions are the following :

1. Collision cross section, or total cross section σ_o.
2. Inelastic cross section, or reaction cross section σ_r.

In cosmic-ray physics, inelastic processes are considered to be those, leading to the creation of new particles such as mesons, antinucleons, hyperons, etc. From this point of view, nuclear reactions are classified as elastic (or, more precisely, quasi-elastic) processes, because the particles emitted in these reactions have been present in the nucleus before the interaction. In this sense, low-energy physics is different, since nuclear reactions are considered there as inelastic processes.

3. The inelasticity of nuclear interaction is characterized by the inelasticity coefficient, defined as the energy fraction carried out by all the newly created particles. In practice, the inelasticity coefficient is understood as the fraction of energy, carried by π-mesons because the main part of the separated energy is carried out by these particles namely,

$$\varkappa = \frac{E_\pi}{E}.$$

4. A very important characteristic is the plurality of secondary particles, i.e. the number of the newly produced particles in a single interaction act.
5. The angular, momentum and energy distribution of secondary particles.
6. The nature of secondary particles. It is important to note that all these characteristics depend on the nature of the incident particles, on their energies, and on the radius of the target nucleus (i.e. on its mass number). Direct interactions lead to phenomena, hardly observable in cosmic rays. For this reason, most of the recent studies deal with inelastic processes.

2. Kinematics of Collisions between Relativistic Particles

2.1. General considerations

We shall now consider creation processes of new particles. In the investigations that utilize photo-emulsions, the created particles, which are sometimes called shower particles, form narrow tracks. The plurality, nature, angular distributions and energy spectra of shower particles will be discussed in the following sections.

In describing the interactions, one is met with two problems; a kimatic and a dynamic problem. Kinematic problems involve all phenomena related with the relativistic effects that appear in the motions of the coordinate systems. It is therefore useful to study the interactions in such a coordinate system, where the phenomena have the greatest possible symmetry, and do not depend on the velocity of motion of the system. Such a system is the centre-of-mass, where one usually considers the collision characteristics, i.e. the dynamics of the process.

2.2. Coordinate systems

The most commonly used four coordinate systems are: the laboratory or L-system, the symmetrical, or S-system, the centre-of-mass or C-system and the mirror or M-system. In the L-system, one of the particles is at rest before collision.[1] In the symmetrical system, the numbers of particles emitted in the forward and backward directions are the same. The C-system is defined as the system in which the sum of momenta of the colliding particles is equal to zero, $\sum p_i = 0$.

In the C-system, the collision processes have the maximal degree of symmetry if the colliding particles are identical and also in the case of decay of particles. For example, when two nucleons collide in the C-system, there will be an axial symmetry in the direction of motion of the two nucleons and a plane of symmetry perpendicular to this axis. In the L-system, however, there will be only an axial symmetry. In the case of decay of particles, the C-system in many cases will have a spherical symmetry while the L-system will only have an axial symmetry. Therefore, the solution of many problems is simpler in the C-system than in the L-system. Consequently, it is of great importance to find relation between these two frames of reference.

---

1) An exception is the crossing-beam experiments. When one is studying collisions with atomic nuclei, one has to take into consideration the Fermi motion of the nucleons inside the nucleus (see Section 3).

We shall denote the different quantities in the C-system by putting the sign " $\sim$ " above the corresponding notations. The momentum, for example, will be denoted by $\tilde{p}$, the angle by $\tilde{\theta}$, the velocity by B and so on. In the L-system, the corresponding quantities will be denoted with the same symbols but without the sign " $\sim$ ". The velocity of motion of the C-system with respect to the L-system will be denoted by $\vec{v}$ and $\frac{1}{\sqrt{1-\frac{v^2}{c^2}}} = \gamma$

2.3. Coordinate transformation

It is well known that relativistic mechanics is formulated in a 4-dimensional space, in which the lengths of 4-dimensional vectors are conserved. If the coordinates of the end of a vector in the L-system are x, y, z, ict, and if their corresponding values in the C-system are $\tilde{x}$, $\tilde{y}$, $\tilde{z}$, $ic\tilde{t}$, then the relation between the coordinates of the vector in the two system is given by

$$\left.\begin{aligned} x &= \gamma(\tilde{x} + v\tilde{t}), & z &= \tilde{z}, \\ y &= \tilde{y}, & t &= \gamma\left(\tilde{t} + \frac{v}{c^2}\tilde{x}\right). \end{aligned}\right| \qquad (4.1)$$

Here the C-system is chosen to be such that the $\tilde{x}$ axis coincides with the x axis and the velocity v is in the direction of the x axis.

2.4. Transformation of velocities and angles

By differentiating equations (4.1), one easily obtains the following equations for the transformation of the particles' velocities :

$$\left.\begin{aligned} v_x &= \frac{dx}{dt} = \frac{d\tilde{x} + v d\tilde{t}}{d\tilde{t} + \frac{v}{c^2} d\tilde{x}} = \frac{\tilde{v}_x + v}{1 + \frac{v\tilde{v}_x}{c^2}}; \\ v_y &= \frac{dy}{dt} = \frac{\tilde{v}_y}{\gamma\left(1 + \frac{v\tilde{v}_x}{c^2}\right)}; \\ v_z &= \frac{dz}{dt} = \frac{\tilde{v}_z}{\gamma\left(1 + \frac{v\tilde{v}_x}{c^2}\right)}. \end{aligned}\right| \qquad (4.2)$$

These equations can easily lead to the relation between the angles in the two coordinate systems

$$\left.\begin{aligned} v_x &= v\cos\theta; \quad \tilde{v}_x = \tilde{v}\cos\tilde{\theta}; \\ v_y &= v\sin\theta; \quad \tilde{v}_y = \tilde{v}\sin\tilde{\theta}; \\ \operatorname{tg}\theta &= \frac{v_y}{v_x} = \frac{1}{\gamma}\cdot\frac{\tilde{v}_y}{\tilde{v}_x + v} = \frac{1}{\gamma}\cdot\frac{\tilde{v}\sin\tilde{\theta}}{\tilde{v}\cos\tilde{\theta} + v} \end{aligned}\right| \qquad (4.3)$$

In the case of $\tilde{v} = v$, one obtains the following simple expression :

$$\operatorname{tg}\theta = \frac{1}{\gamma}\operatorname{tg}\frac{\tilde{\theta}}{2}. \tag{4.3a}$$

This expression is also valid at very high energies, when $\tilde{v} \sim v \sim c$. Similarly, one obtains the inverse transformation

$$\operatorname{tg}\tilde{\theta} = \frac{1}{\gamma}\cdot\frac{v\sin\theta}{v\cos\theta - v}. \tag{4.4}$$

2.5. Transformation of energies and momenta

The momentum and energy together form another vector. Its components are :

$\tilde{p}_x c$, $\tilde{p}_y c$, $\tilde{p}_z c$, $i\tilde{E}$, in the C-system, and

$p_x c$, $p_y c$, $p_z c$, $i\tilde{E}$, in the L-system.

Here $\tilde{E}$ and E denote the total energy. In correspondence with the formulae for coordinates, one may write

$$\begin{aligned} &a)\ p_x = \gamma\left(\tilde{p}_x + \frac{v}{c^2}\tilde{E}\right);\\ &b)\ p_y = \tilde{p}_y;\\ &c)\ p_z = \tilde{p}_z;\\ &d)\ E = \gamma(\tilde{E} + v\tilde{p}_x); \end{aligned} \tag{4.5}$$

Here E is the total energy, equal to the sum of the kinetic energy, equal to the sum of the kinetic energy T and the rest energy mc^2 :

$$E = T + mc^2. \tag{4.6}$$

Sometimes, it is required to find the sum of the total energy of particles in the L-system provided that the corresponding quantity in the C-system is known. Summing both sides of equation (4.5,d) over all the particles, and taking into account that the sum of momenta in the C-system is equal to zero, one obtains

$$\sum_i E_i = \gamma c \sum_i \tilde{E}_i. \tag{4.7}$$

2.6. Relation between energy and momentum

The square of a 4-dimensional vector, i.e. the square of its length, is invariant :

$$E^2 - p^2c^2 = m^2c^4.$$

From this, one obtains

$$E = \sqrt{p^2c^2 + m^2c^4}. \tag{4.8}$$

One should also take into consideration the following formula, whose derivations are available in all text-books

$$E = \frac{mc^2}{\sqrt{1-\beta^2}} = \gamma mc^2; \tag{4.9}$$

$$pc = \beta E. \tag{4.10}$$

When $\beta \simeq 1$ (the ultra-relativistic case), the latter equation reads

$$pc = E. \tag{4.11}$$

If the particles moves in the C-system making an angle $\tilde{\theta}$ with the $\tilde{x}$ axis, then $\tilde{p}_x = \tilde{p} \cos \tilde{\theta}$ and

$$E = \gamma(\tilde{E} + v\tilde{p}\cos\tilde{\theta}); \tag{4.12}$$

$$p^2c^2 = E^2 - m^2c^4 = \gamma^2(\tilde{E} + v\tilde{p}\cos\tilde{\theta})^2 - m^2c^4;$$

$$pc = \gamma\sqrt{(\tilde{E} + v\tilde{p}\cos\tilde{\theta})^2 - \frac{m^2c^4}{\gamma^2}}; \tag{4.13}$$

$$v = c\sqrt{\frac{\gamma^2-1}{\gamma^2}};$$

$$\tilde{E} = \sqrt{\tilde{p}^2c^2 + m^2c^4}. \tag{4.14}$$

In this manner, we obtain a formula for transforming the momentum from the C-system to the L-system. It is important to note that the transyersal component of momentum does not change in the transformation of the L-system to the C-system

$$p_y = \tilde{p}_y = \tilde{p}\sin\tilde{\theta} = p\sin\theta. \tag{4.15}$$

Choice of the C-system

How can we find the C-system for a pair of colliding particles having masses m_1 and m_2 ? Assume that particle m_2 was at rest in the L-system before collision. The velocity of motion of the C-system relative to the L-system will then coincide with the velocity of motion of particle m_2 in the C-system. Consequently,

$$\gamma_C = \frac{\tilde{E}_2}{m_2c^2}. \tag{4.16}$$

Usually, one is only given energy E_1 in the L-system, and therefore one has to obtain an expression for $\tilde{E}_2$ in terms of E_1. In the C-system $\tilde{p}_1 = -\tilde{p}_2$ and hence

$$\begin{gathered}
\tilde{E}_2^2 = \tilde{E}_1^2 - m_1^2c^4 + m_2^2c^4; \\
E_2 = m_2c^2 = \gamma_C(\tilde{E}_2 + \tilde{p}_2 v) = \gamma_C(\tilde{E}_2 - \tilde{p}_1 v); \\
-\tilde{p}_1 v = \frac{m_2c^2}{\gamma_C} - \tilde{E}_2; \\
E_1 = \gamma_C(\tilde{E}_1 + \tilde{p}_1 v); \\
\tilde{E}_1 = \frac{E_1}{\gamma_C} - p_1 v = \frac{E_1}{\gamma_C} + \frac{m_2c^2}{\gamma_C} - \tilde{E}_2; \\
(m_2c^2\gamma_C)^2 - m_2^2c^4 + m_1^2c^4 = \left(\frac{E_1}{\gamma_C} + \frac{m_2c^2}{\gamma_C} - m_2c^2\gamma_C\right)^2.
\end{gathered}$$

Solving these equations relative to γ_C, we obtain

$$\gamma_C = \frac{E_1 + m_2c^2}{\sqrt{2(E_1 + m_2c^2)m_2c^2 + m_1^2c^4 - m_2^2c^4}}; \tag{4.17}$$

$$\tilde{E}_2 = \frac{(E_1 + m_2c^2)m_2c^2}{\sqrt{2(E_1 + m_2c^2)m_2c^2 + m_1^2c^4 - m_2^2c^4}}. \tag{4.18}$$

Let us consider some particular cases

a) $m_1 = m_2 = m$:

$$\gamma_C = \frac{(E_1 + mc^2)}{\sqrt{2mc^2(E_1 + mc^2)}} = \sqrt{\frac{E_1 + mc^2}{2mc^2}} = \sqrt{\frac{\gamma_1 + 1}{2}}; \tag{4.19}$$

$$\tilde{E}_2 = \tilde{E}_1 = \sqrt{\frac{(E_1 + mc^2)mc^2}{2}}; \tag{4.20}$$

b) $\gamma \gg 1$, т. е. $E_1 \gg mc^2$:

$$\tilde{E}_1 = \sqrt{\frac{E_1 mc^2}{2}}; \quad \gamma_C = \sqrt{\frac{E_1}{2mc^2}} = \sqrt{\frac{\gamma_1}{2}}; \tag{4.21}$$

the inverse transformation :

$$E_1 = \frac{2\tilde{E}_1^2}{mc^2} = 2\gamma_C^2 mc^2. \tag{4.22}$$

The equations obtained here are often used in the experimental analysis of nuclear interactions.

Recently, one also uses the so-called mirror system of coordinates (the M-system), in which the initial (incident) particle is at rest. In order to carry out the transformation into the M-system, one has to know energy E_o of the particle in the L-system. Then, the relativistic particles become

$$\gamma = \frac{E_0}{mc^2}; \quad \frac{v}{c} = \sqrt{1 - \frac{1}{\gamma^2}};$$

$$\begin{cases} E_M = \gamma (E_L - v p_L \cos\theta_L); \\ p_M = \gamma \sqrt{(E_L - v p_L \cos\theta_L) + \frac{m^2c^4}{\gamma^2}}; \\ \sin\theta_M = \frac{p_L}{p_M} \sin\theta_L. \end{cases} \tag{4.23}$$

2.8. Addition of Lorence factors

If two particles move in a given coordinate system with Lorence factors γ_1 and γ_2, then their relative Lorence factor can be obtained by means of an addition formula, which may be deduced from the velocity addition formula (4.2) :

$$\gamma_{12} = \gamma_1\gamma_2 \pm \sqrt{\gamma_1^2 - 1}\ \sqrt{\gamma_2^2 - 1} \cos\theta, \tag{4.24}$$

where θ is the angle between the direction of motion of the two particles.

3. Inelastic Collisions

3.1. Pion production. Electronic-nuclear showers

The limiting case of inelastic interactions is the reaction with the creation of a single meson. This is the qualitative difference between inelastic interactions from quasi-elastic interactions in which no new particles are created. The number of created mesons increases with increasing energy of the colliding particles. The phenomenon of multiple creation of pions is called an

electronic-nuclear shower[1]. Figure 25 shows examples of electronic-nuclear showers registered in a photo-emulsion and a Wilson chamber.

The name "electronic-nuclear shower" is historically established and stresses the fact that electrons in these showers are produced by the nuclear interaction in the following series of processes.

$$\pi^0 \to 2\gamma \to 2(e^+ + e^-).$$

The electronic-nuclear showers were discovered by Soviet physicists under the supervision of V.I. Veksler and D.V. Skobel'cyn in 1945 - 1949 [2].

In order to produce new particles, a minimum amount of energy is required, which is necessary create the rest masses of the particles produced.

$$T_0 = 2m_\pi c^2 \left[1 + \frac{m_\pi}{4M}\right] = 293 \ Mev.$$

The generation of mesons in the field of nuclei, however, starts at a lower energy. The reason is that the nucleons are moving inside the nucleus. In light nuclei, the values of energy and momentum of a nucleon (the Fermi energy and momentum) are 21 MeV and 216 MeV/C respectively, and weakly depend on mass number A. These quantities are easily determined. Nucleons are particles of spin $\frac{1}{2}$, and according to the Pauli principle, only two protons and two neutrons of opposite spin can occupy the same quantum state. The number of states with momenta less than p_f is equal to the volume in the phase space, divided by $\hbar^3$, i.e.

Since the number of protons is equal to Z, then the maximum values of the momentum is defined by the relations

$$2(4/3\pi)^2 \frac{r_0^3 p_f^3 A}{\hbar^3} = Z \ (\text{protons});$$

$$2(4/3\pi)^2 \frac{r_0^3 p_f^3 A}{\hbar^3} = A - Z \ (\text{neutrons}).$$

The energy of the Fermi motion is defined by

$$T_f = \frac{p_f^2}{2m_p}.$$

If the incident nucleon collides with a nucleon moving in the nucleus in the opposite direction, then the threshold of pion production essentially decreases. In order to estimate the decrease in the threshold energy, one may use the addition formula of the Lorence factors (equation (4.24) of Section 2). If γ_0 is the Lorence factor of the incident particle and γ_f the Lorence factor of the Fermi motion, we then obtain the maximal increase in energy by setting $\cos\theta = 1$:

---

1) Synonyms: penetrating showers, narrow showers (in old hiterature), jets (at high energies), meson showers or mesonic-nuclear showers.

$$\gamma = \gamma_0\gamma_f + \sqrt{\gamma_0^2 - 1}\,\sqrt{\gamma_f^2 - 1}\,;$$
$$\left(\gamma_0 = \frac{E_0}{m_p c^2} \text{ и } \gamma_f = \frac{E_f}{m_p c^2}\right).$$

At threshold kinetic energy $T_0 = 293$ Mev, $\gamma_0 = 1.31$ and $\gamma_f = 1.02$. Then $\gamma_0\gamma_f \simeq \gamma_0$ and the change in the Lorence factor $\gamma - \gamma_0 = 0.17$ which corresponds to increasing the energy by 15%.

At the threshold energy, the cross section of mesor production is very small. In practice, one may consider that the effective generation of mesons starts at an evergy $\simeq 10^9$ eV.

3.2 Geometrical cross-section

With the increase in energy , the number of open reaction channels increases. It becomes possible, for example, to create a number of pions. This must lead to an increase in the value of the interaction cross section. However, if the radius of nuclear interaction does not vary with energy, the maximal possible value of the inelastic (non-diffractive) interaction cross section must be determined by the nuclear dimensions. Assuming that the nucleus can be represented by a sphere having a sharp edge, then the cross section (the so-called geometrical cross section) is equal to

$$\sigma_0 = \pi R^2 = \pi r_0^2 A^{2/3}, \qquad (4.25)$$

where r_0 is the radius of a nucleon and A is the mass number of the nucleus.

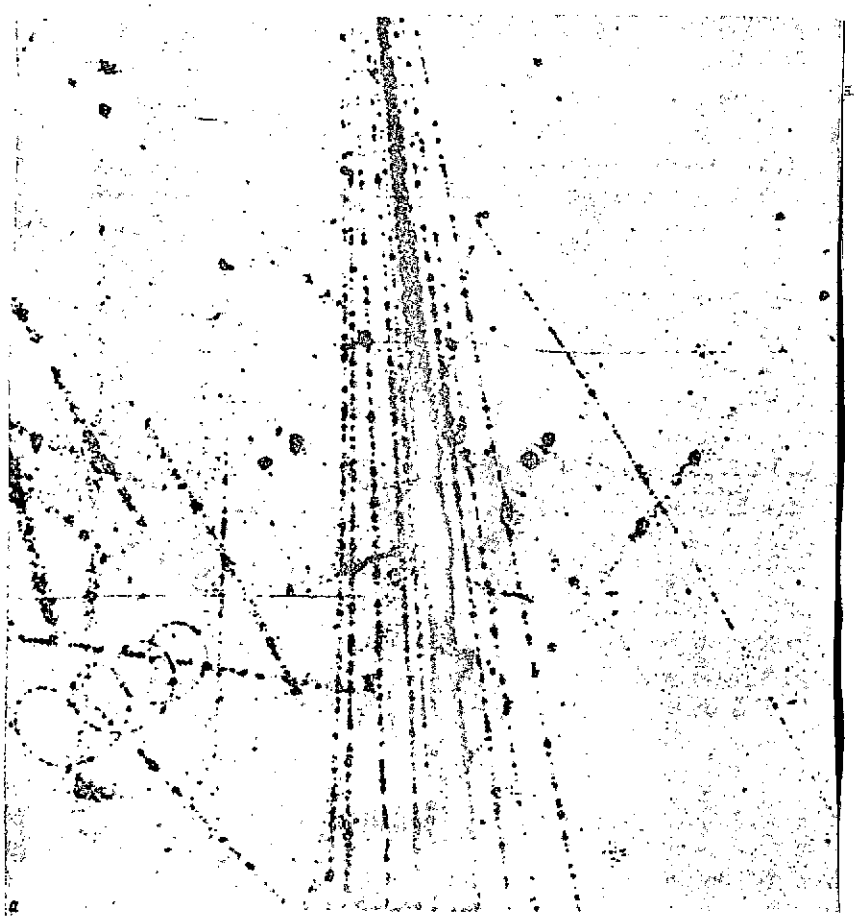

Fig. 25a. Examples of electronic-nuclear showers, registered in Wilson chamber.

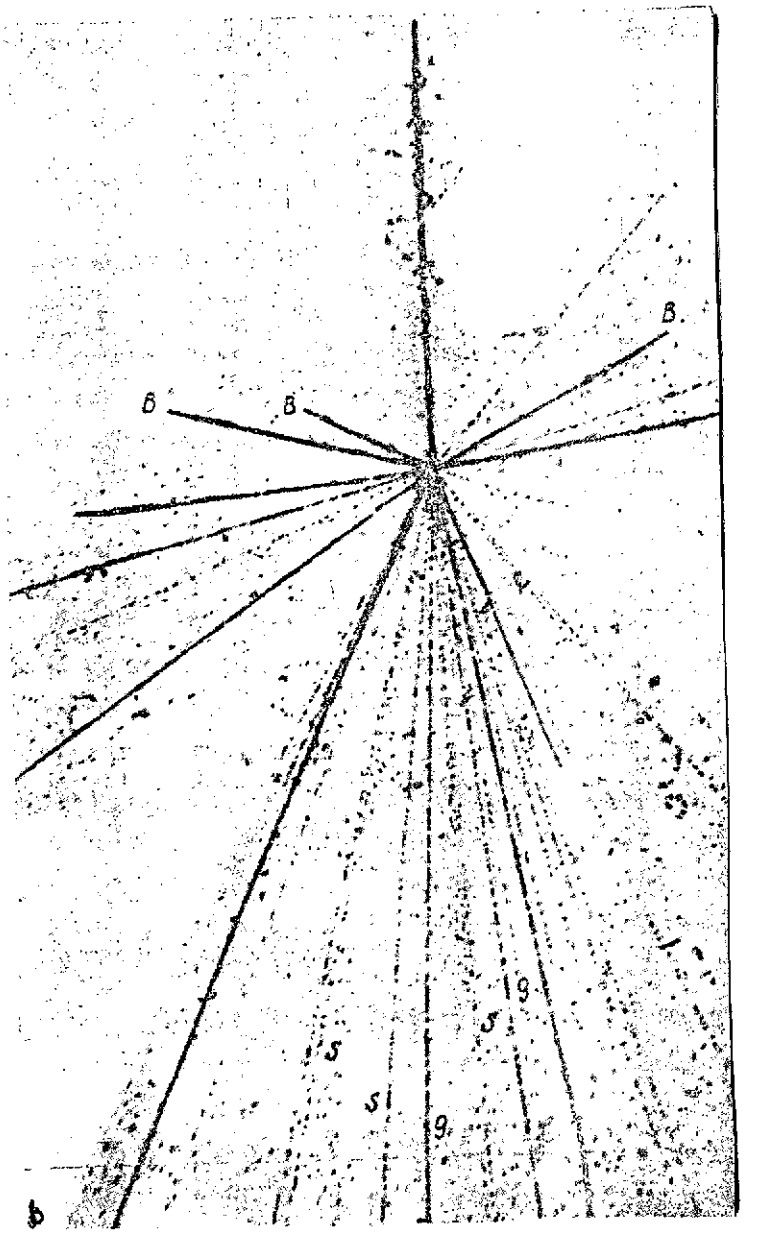

Fig. 25b. Examples of electronic-nuclear showers, registered in a nuclear emulsion (s: shower, g: gray and b: black tracks)

In cosmic rays, besides the cross section, one makes use of the interaction path[1] which is uniquely related to the cross section (for a given material). If n is the number of atoms in 1 g of matter, then

$$\lambda = \frac{1}{\sigma n} \; g/cm^2 \tag{4.26}$$

1) Synonyms: means free path, interaction path and collison path.

The interaction path, defined in this manner, does not depend on matter density. Naturally, it can also be expressed in cm :

$$\lambda = \frac{1}{\rho \sigma n} \text{ cm} \tag{4.27}$$

where ρ is the density. The interaction path that corresponds to the geometrical cross section is called geometrical path. Table 13 gives the values of geometrical paths in a number of materials. In the calculation of these paths, values if radii r_o obtained in the analysis of electron scattering by nucleons in nuclei ($r_o = 1.28$ Fermi) was used. It is clear that the geometrical path is proportional to $A^{1/3}$.

Table 13

Material	Hydrogen	Carbon	Air	Photoemulsion	Iron	Lead
(g/cm^2)	82	75	80	100	125	190

This can easily be seen when one expresses σ and n in equation (4.26) in terms of A, r_o and the nucleon mass m_p.

3.3. Elastic and inelastic cross sections

Elastic interactions, in which no new particles are created, are observed side by side with inelastic interactions, even at very high energies. In the former interactions, the energy of the particles before and after interaction is the same; only the momentum changes. Experiments carried out on accelerators shows that the change in momentum in such processes is not large; the scattering angle does not exceed 7×10^{-3} radians at an incident energy of 20 GeV.

In the case of a collision with a nucleus, one has to consider the scattering by all the nucleus as a unit (coherent scattering). The scattering of the incident particle by separate nucleons of the nucleus leads to an emission of recoil nucleons from the nucleus (δ-nucleons). This process is called quasielastic. Experiment shows that quasielastic scattering is equivalent to elastic scattering by N independent nucleous in the nuceleus, where $N = 1.6\ A^{1/3}$ and A is the mass number of the nucelus ($A \geqslant 8$) /3*/.

3.4. Experimental methods for determining the interaction paths

Let us consider the change in the number of particles, dN, when they penetrate through a layer of matter of thickness equal to dx

$$dN = -N \frac{dx}{\lambda} \tag{4.28}$$

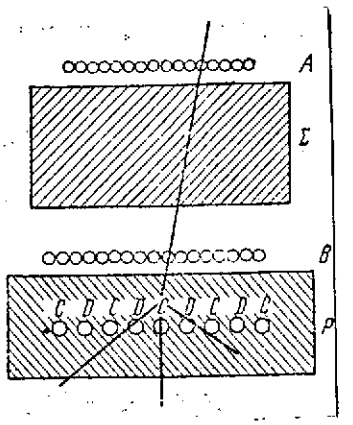

Fig. 26. An instrument for the deterination of the interaction path; Geiger counters are denoted by circles.

Integrating this expression we obtain

$$N = N_0 e^{-x/\lambda}, \tag{4.29}$$

where N is the number of particles that reach a depth x without interaction and N_0 the initial number of particles falling on the absorber.

Equation (4.29) is the basis of the experimental determination of interaction thresholds. The most powerful method for measuring λ is the method of knocking out the beam. It is based on counting the number of particles passing through a given layer of matter of thickness x without interaction and then being subjected to interaction in a detector located below the layer. Figûre 26 shows a typical instrument for studying λ by the method of knocking out the beam.

Counters A serve for separating the cases in which a particle falls on the instrument. Row of counters B enables me to select the cases, when the particle penetrates through layer Σ without interaction (one counter of row B works in harmony with a counter of A). The number of these cases is equal to

$$N = N_0 e^{-x/\lambda}.$$

The number of interactions, n'_{CD}, registered by counters CD (it is required that they simultaneously work in harmony) in unit time t_1 is given by

$$n'_{CD} = \frac{N' W_{CD}}{t_1} e^{-x/\lambda} = N_0 W_{CD} e^{-x/\lambda}$$

(W_{CD} is the probability of registering the interaction by counters CD and t_1 is

the time of measurement). Filter Σ is periodically removed. If the time of measurement without the filter is equal to t_2, then the number of interaction in detectors CD without filter Σ is given by

$$n'_{CD} = \frac{N'' W_{CD}}{t_2} = N_0 W_{CD}.$$

Consequently

$$\lambda = \frac{x}{\ln \frac{n'_{CD}}{n_{CD}}}.$$

Carrying out such an experiment requires that the target thickness, x , is sufficiently small, otherwise the products of interaction in layer Σ will be absorbed and not registered by the counter row B. The presence of these phenomena will decrease the number of registered interactions and accordingly increase the interaction path. Experiments of this type gave values of λ for lead varying from 160 to 200 g/cm^2, and for graphite $\sim$ 85 g/cm^2. Noting that these are overestimated values, one must consider them as upper limits of the interaction paths. Quasi-elastic interaction cross sections in cosmic rays usually cannot be measured because the δ -electrons do not get out of the filter.

Recently, inelastic interaction paths in carbon were measured in Soviet satellites of the "Proton" type (figure 27) [4*]. In this method, the selection of singly-charged initial particles was done by using proportional counters while

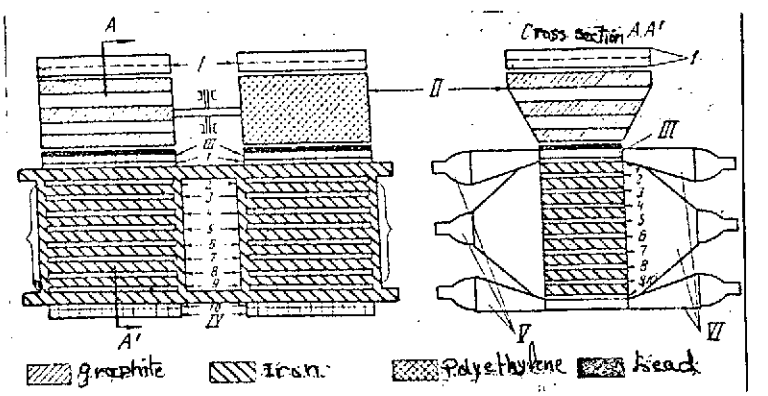

Fig. 27. The scheme of the instrument for investigation of nuclear interactions on the "Proton" satellite; I: proportional counters, 1-10, III, IV: scintillators, II: targets (during flights in the earth program, target places were changed or removed), V: photomultipliers, VI: cones for collecting light from scintellators.

the selection of particles penetrating through the filter without interaction was done by using scintillators. An instrument consisting of scintillators covered by iron layers was used as a detector for the interactions. This instrument has a registration coefficient close to unity ($w \sim 1$). If matter thickness in the instrument $D \gg \lambda$, the instrument will be able to measure the energy of particles subject to the interaction inside itself.

Many studies [5*] were devoted to the determination of the interaction path in nuclear emulsions. In this case, one again uses equation (4.29). One determines the number of interactions occuring at depths exceeding x in an emulsion chamber or an emulsion rouleau. The number of these accidents as a function of x is given by a straight line in a semi-logarithmic scale; the slope of this line is equal to $-\lambda$.

Interaction path of nucleons

Table 14 gives values of inelastic interaction paths of protons obtained in cosmic rays and accelerators at 20 GeV [6].

Table 14

Energy Interval	λ					
	Hydrogen g/cm²	Carbon g/cm²	Air g/cm²	Emulsion cm	Iron g/cm²	Lead g/cm²
Accelerator (20 GeV) [2]	56	90±1	—	36,5±0,5	127±6	199±6
Cosmic Rays 100÷1000 GeV	—	78±5	83±10	35,9±2,9	135±9	192±20

Nuclear transparency

The comparison of the results given in table 14 with the geometrical paths, shows that the measured cross sections are systematically less than the geometrical ones for light and medium weight nuclei. The two cross sections for the nucleon are particularly different. The geometrical cross section of the nucleon is equal to 52 mb and the measured cross section is about 30 mb [1].

---

1) The calculation of the cross sections of nucelon-nucleon and nucleon-nucleus collission lacks consistency. In calculating the cross section given in table 13, it is assumed that the incident particle is a point particle. The neglect of the dimensions of the incident particles leads to a particularly large error in the case of nucleon-nucleon collision. If one takes into account the finite dimensions of both the colliding nucleons, one has to calculate the geometrical cross section by using the following expression

$$\sigma = \pi (2r_0)^2 = 4\pi r_0^2.$$

This difference is explained by the fact that the nucleon is not a "black sphere" but has a "semi-transparent" edge where the density of nuclear matter gradually decays to zero. Such a nucleon structure leads to a similar conclusion about the nucleus, that its edge is also semi-transparent. The larger the nuclear dimensions, the smaller the contribution of the nuclear edge to the cross section. This can be seen on the basis of the following simplified qualitative arguments. Let us define the nuclear transparency by

$$\Pi = 1 - \frac{\sigma}{\pi R^2}, \tag{4.30}$$

where σ is the inelastic cross section and R the geometrical nuclear radius. If the nucleons in the nucleus are closely packed, the nuclear transparency will then be entirely due to the semi-transparent regions of the surface nucleons. If the nucleon has a semi-transparent edge of thickness Δx, then the common semi-transparent area will be equal to $2\pi R \Delta X$, and hence

$$\Pi = 1 - \frac{\pi R^2 - 2\pi R \Delta x}{\pi R^2} = 2\frac{\Delta x}{R} = 2\frac{\Delta x}{r_0} A^{-1/3}.$$

It is clear that the increase of the nuclear radius decreases the role of the nuclear periphery, where the quantity of matter is not sufficient for an

---

(1 Contd).
If r_o = 1.28 fermi, one obtains σ = 200 mb. The experimental cross section is much less : σ = 30 mb. This gives for the effective nucleon radius

$$r_0 = \sqrt{\frac{\sigma}{4\pi}} \simeq 0.5 \text{ Fermi}.$$

Taking into account the finite dimensions of the projectile leads to the following expression for the cross section

$$\sigma = \pi (R_1 + R_2)^2,$$

where R_1 and R_2 are the radii of the colliding particles (see figure 31).

The Indian physicist Oditia found that the latter expression gave correct result if the nucleon radius was set equal to r_o = 0.5 fermi, while the radii of all nuclei were calculated by means of the relation : $R = r_1 A^{1/3}$ where $r_1 = (1.16 \pm 0.03)$ fermi. For deuteron, one has to use r_1 = 1.62 while for the Helium nucleus r_1 = 1.04 fermi (see /6/).

efficient interaction. Consequently, the transparency of the nucleus as a whole falls in proportion with the nuclear radius. The nuclear transparency can be more accurately evaluated by considering the realistic density distribution ρ (r) of the nuclear matter. The function ρ (r) describes the number of nucleons in a unit nuclear volume at distance r from the centre of the nucleus. If the wavelength of the particle is much less than R, then the number of nucleons passing at a distance b from the nuclear centre (see figure 28) without interaction is given by

$$N_b = N_0 e^{-2\sigma \int_0^\infty \rho(r) ds}$$

Averaging over all impact parameters, one obtains

$$\frac{N}{N_0} = 2\pi \int_0^\infty e^{-2\sigma \int_0^\infty \rho(r) ds} b db. \qquad (4.31)$$

The density distribution of nucleons inside the nucleus (the nuclear form-factor) is not sufficiently well known. It is usually assumed that the nuclear-matter distribution in the nucleus coincides with the electric-charge distribution, which has been very well studied by Hofstadter by means of nuclei electron scattering.

Figure 29 shows a typical nuclear shape. It is seen that the nucleus has a spherical region of almost constant density and a surface layer in which the density smoothly decays. The characteristic parameters are : the half-density radius C, the thickness S of the nuclear surface layer, in which the density falls from 0.9 to 0.1 of its value at the centre. Sometimes, the equivalent radius R of homogeneous distribution is introduced, which gives at constant density ρ = constant, the same scattering as the realistic density distribution. Table 15 gives the values of parameters R, C and S for a number of nuclei (in units of fermi).

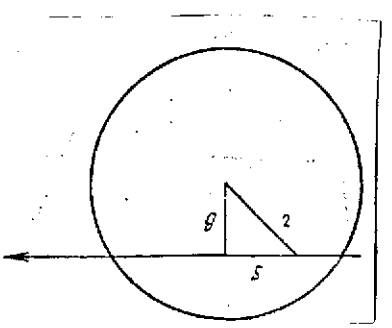

Fig. 28 - Passage of the nucleon through the nucleus.

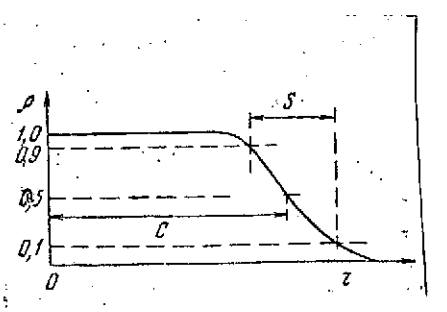

Fig. 29- Distribution of density of the nuclear matter in the nucleus distribution

Table 15

Nucleon	He^4	C^{12}	N^{14}	O^{16}	Ca^{40}	Au^{197}	Pb^{208}
R	2,07	3,11	3,20	3,42	4,55	6,88	7,0
C	1,10	2,30	2,40	2,60	3,64	6,38	6,5
S	1,40	1,85	1,85	1,80	2,50	2,32	2,3

3.5. Determination of nucleon-nucleon collision cross section in cosmic rays [6, 8]

The cross section of inelastic interaction can be defined as the difference between the total cross section and the transparency. Using equation (4.31), one can evaluate the nucleon cross section σ_1 from the value of the cross sections of inelastic collisions with nuclei. The cross section of inelastic collision of a nucleon with a nucleus of mass number A is given by

$$\sigma_A = 2\pi \int_0^\infty \{1 - e^{-2\sigma_1 \int_0^\infty \rho(r)ds}\} bdb. \qquad (4.32)$$

Figure 30 shows the dependence of the nucleon-nucleus interaction cross section σ_A in carbon on the nucleon-nucleon cross section σ_1. Measuring the nucleon-nucleon collision cross sections in cosmic rays is difficult because of

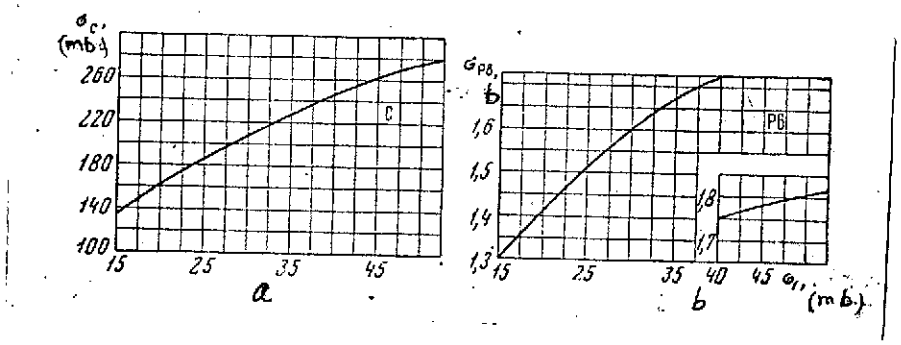

Figure 30. Dependence of the nucleon-nucleus cross section on the nucleon-nucleon cross section for carbon (a) and lead (b).

the small value of this cross section. Equation (4.32) and curves such as those given in figure 30 are therefore used to obtain the elementary cross section in terms of the measured σ_A. In order to measure σ_1 directly, one has to use a liquid-hydrogen target. An alternative method is to compare the cross sections in paraffin and carbon. One applies the method of knocking out the beam firstly with a paraffin target and secondly with a carbon target. The thickness of the

carbon target is chosen such as it includes as much carbon as in the paraffin target. It is clear that this difference in methods could be used to estimate the interaction cross section in carbon. Up till now this method was only applied to energies up to $\sim$60 GeV and yielded cross sections $\sigma_1 \simeq 30$ mb. Almost the same results were obtained by analysing measurements of σ_A in carbon, iron and lead up to energies of 500 GeV.

3.6. Interaction cross section of pions and kaons with nuclei /8/

Interaction cross sections of pions with nucleons were measured on accelerators. At energies around 20 GeV, the pion-nucleon cross section was found to be 1.5 times less than the nucleon-nucleon cross section, i.e. $\sigma_{\pi p} = 20$ mb. The interaction cross section of kaons was found to be even less ($\sim$ 17 mb).

At energies higher than 100 GeV, no measurement of the cross sections of pion interactions with nuclei were made because of the difficulties in the identification of pions in cosmic rays. For this purpose, one therefore has to use indirect methods. Assuming that at cosmic energies the cross section of π-p interaction is equal to 20 mb, one can use equation (4.32) to obtain the cross-section of a π-nucleus collision. It was found, for example, that the inelastic interaction path in air $\simeq 120$ g/cm^2 (as compared with the corresponding quantity for protons).

3.7. Interaction of a nucleus with a nucleus

Alongside protons, one finds heavier nuclei in cosmic rays at large heights (see Chapter 5, Section 2). It appears that if two heavy nuclei collide, their interaction cross section would be equal to $\sigma = \pi (R_1 + R_2) = \pi r_o^2 (A_1^{1/3} + A_2^{1/3})$. It was however found that the experimental values of the cross sections were significantly less than those calculated by using the previous formula. This means that, in order to produce an interaction, the two nuclei must have a minimal amount of overlap. It was found that the experimental values of the cross sections agreed with the theoretical ones if the overlap was set equal to $\Delta R \simeq 0.85 \times 10^{-19}$ (see also the footnote on pp. 84,85). Therefore

$$\sigma_{1,2} = \pi (R_1 + R_2 - 2 \cdot 0{,}85 \cdot 10^{-13})^2. \qquad (4.33)$$

Table 16 gives those values for the interaction paths λ of nuclei in emulsion, measured experimentally and those calculated by using equation (4.33) /9*/.

Table 16

Z	λ, см Experimental	λ, см Calculated
2	20 ±2	20
3÷5	14,9±1,0	16
6÷9	13,9±1,0	13
10	10,9±0,5	10
20	8,7±0,5	9

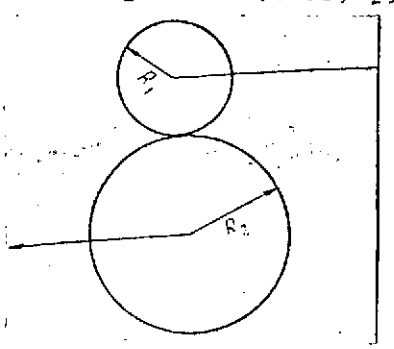

Fig. 31. Collision of two nuclei of different sizes.

3.8. Nature of particles, participating in nuclear interactions in cosmic rays

The results of the previous section provide us with a key to understand the behaviour of various particles in cosmic rays. Since primary radiation consists mainly of protons and nuclei whereas secondary nuclear-active particles are pions and kaons, the these particles must namely participate in nuclear processes. It was however found that different particles are effective in different energy regions. Since K- and π-mesons decay rapidly, their flux in the atmosphere cannot be too large. The life time of a particle depends on its energy (more precisely on its Lorence factor) through the relation

$$\tau = \frac{\tau_0}{\sqrt{1-\beta_C^2}} = \frac{E}{m_\pi c^2}\tau_0 = \gamma\tau_0$$

and the mean decay path

$$l = c\tau = \frac{E}{m_\pi c^2}\tau_0 c. \qquad (4.34)$$

Mesons can contribute to the nuclear interaction only if their decay path is greater than the nuclear interaction path

$$l > \lambda. \qquad (4.35)$$

If ρ is the density of air, then condition (4.35) gives (λ in g/cm^2) :

$$\frac{E_{cr}}{mc^2}\tau_0 c > \frac{\lambda}{\rho}.$$

From this, we find the critical energy above which particles have mainly enough time to interact before decaying

$$E_{cr} \doteq \frac{\lambda mc^2}{\rho\tau_0 c}. \qquad (4.36)$$

For pions at sea level, this energy is equal to

$$E_\pi = \frac{120\ g/cm^2\ 140\ Mev}{1{,}3\cdot 10^{-3}\ g/cm^3\ 2\cdot 10^{-8}\ sec\ 3\cdot 10^{10}\ cm/sec} \approx 20\ GeV$$

As the height increases, this limit also increases because of the decrease in the density of air ρ .

Protons also have an energy limit, below which, protons do not participate in nuclear reactions. This limit is defined by the ionization loss. If the ionization path R is less than the nuclear interaction path λ , then in most

cases the proton will have enough time to stop before having a single collision with a nucleus. Consequently, protons interact with nuclei only at those energies satisfying condition $R_{ion} > \lambda$. This condition starts to be fulfilled at proton kinetic energies around 400 MeV in air and 450 MeV in lead. The most "active" particles, in the sense of nuclear interaction in cosmic rays, are neutrons for which there is practically no energy limit. Consequently, nuclear interactions in cosmic rays at low energies are almost entirely due to neutrons. In this case, the main reactions are quasielastic processes leading to nuclear disintegration not accompanied by emission of new particles[1]. Starting from energies around 400 MeV, protons enter the game, and at energies higher than a few GeV, the ability of protons and neutrons to have an interaction becomes equal. At these energies, the chances of production of electronic-nuclear showers predominate. Finally, at energies higher than 200 ÷ 400 GeV, pions play a considerable role.

3.9. The picture of nuclear interaction

If the energy of the colliding particles in the L-system is not large ($\lesssim 10^9$ eV), then the probability of creating a meson will be small and mainly quasielastic processes will be observed. In this case, a part of the momentum of the incident particle will be transferred to one of the nucleons of the nucleus (δ-nucleon). Moving through the nucleus, this nucleon will make secondary collisions with other nucleons and share the energy if gained with them. After the δ-nucleon leaves the nucleus, the nucleus remains in an excited state and subsequently de-exites emitting protons, neutrons, alpha-particles and heavier fragments in a so-called "evaporation process".

At energies $\gg 10^9$ eV, inelastic processes leading to pion-production predominate. Among the created pions, there are π^0-mesons whose decay give a start to electron-photon showers. For this reason, inelastic processes are often called electronic-nuclear showers, though they would be better called mesonic-nuclear showers. Similarly, as in the case of elastic interactions, a part of the incident energy in inelastic processes is given to nucleons of the target nucleus, which leads to its disintegration. Consequently, the collision of a nucleon with a nucleus passes through two stages, first the generation of π-mesons and the knock out of δ-particles, and second the disintegration of the nucleus by "evaporation processes" which are characterized by the excitation energy U.

The description of nuclear interactions is well established at energies up to $10^{11} - 10^{12}$ and less accurately at higher energies. Up till now, the study of seprate cases of nuclear interactions at energies higher than 10^{14} eV has not been achieved. It is thus not yet clear whether collisions of particles have any special properties at such high energies.

4. Investigation of Nuclear Interactions in Cosmic Rays

4.1. Basic type of instruments

The considerable progress in studying nuclear interactions in cosmic rays is due to methods, enabling us to observe the picture of nuclear collisions and to determine the angular distributions of the particle, created, their number and energy.

The basic type of instruments used to study the most important properties of nuclear interactions in cosmic rays are the following :

1. Photo-emulsions,
2. Wilson chambers,
3. ionization chambers,
4. Geiger counters,
5. Čerenkov and Scintillation counters,
6. spark chambers.

4.2. The photo-emulsion method

One of the most powerful methods of studying nuclear interactions is the nuclear photo-emulsion method. This method was applied by L.B. Mysovskij in 1927. In the forties, a considerable contribution to the development of the method was given by Powell and collaborators [10]. This method has now reached its peak of perfection and photo-emulsion is not only applied in the form of photographic plates but also in the form of rouleaus, consist of a large number of separate layers folded together. The volume of an emulsion rouleau sometimes reaches tens of liters.

In emulsion chambers, the photo-emulsion layers alternate the absorber disks (iron, tungsten or lead). In the process of developing, the emulsion chamber is unpacked into separate layers, stuck on glass and investigated under a microscope.

The advantage of emulsions is that they enable us to see the picture of showers coming into existence, and in many cases to determine the nature of the particles of the shower, their charges and energies (or momenta). By means of emulsion, it was possible to register the interactions of particles having energies $\simeq 10^{14}$ eV. In this manner, the photo-emulsion method enables us to obtain a large amount of information.

It is important, however, to stress that the above-mentioned measurements can be carried out only for particles of not very high energies. The particle energies can be determined only in the region of energies $< 10^{10}$ eV[1]. This limit can be achieved in the concurrence of favourable circumstances.

Another disadvantage of the method is the complicated composition of the emulsion. Table 17 gives the composition of nuclear photo-emulsion produced

---

1) In the cases when relative scattering is measured, the limit of measurable energies can be increased up to $\simeq 250$ GeV (see Chapter 2, Section 11 and Chapter 4, Section 4).

in England and in the USSR by the Soviet Cinema-Institute NIKFI-r. In table 17, the number of nuclei in 1 $cm^3 \times 10^{-22}$ is given [11].

Table 17

Emulsion	Element					
	H	C	N	O	Br	Ag
NIKFI-r	2,93	1,39	0,37	1,06	1,02	1,02
Ilford G-5	3,37	1,36	0,29	1,02	1,02	1,02

Table 18 gives the probability of nucleon interaction with various nuclei in the emulsion of NIKFI-r. This table shows that collisions occur mainly with heavy nuclei of bromine and silver. The contribution of light nuclei however is also significant. Consequently one does not know as a rule with which nucleus the collision takes place in each separate case.

Table 18

Nucleus	H	C	N	O	Br	Ag
Probability of interaction	0,026	0,106	0,031	0,092	0,343	0,400

Usually, when people analyse the phenomena taking place in the emulsion, they consider that it consists of heavy nuclei (Ag and Br; Z = 47 and 35) and of light ones (C, N, O; $Z \simeq 7$). One can rarely show that the reaction occurs on hydrogen. When more than 8 strongly ionizing protons are emitted in a nuclear disintegration, it then becomes evident that the reaction takes place with Ag or Br nuclei. Processes in which only one recoil nucleon is emitted are usually assumed to be nucleon-nucleon processes. These processes exceed in number the expected 3%, which means that they occur not only due to collisions with the protons but also with the peripheral nucleons of the other nuclei.

In constructing experiments with nuclear emulsions, one always has to remember the heavy work necessary to search for the required processes and their measurement. In order to examine a single plate of area 10 x 10 cm^2 and thickness 400 μ, a highly trained examiner needs 10 ÷ 15 days, and needs 30 ÷ 60 minutes in order to measure the scattering of a single particle.

In the last few years, considerable interest was devoted to the investigation of reactions induced by very high energy particles (with $E > 10^{12} \div 10^{13}$ eV). These reactions are extremely rare. A single event with an energy of 10^{13} eV might be obtained by examining several liters of emulsion after being radiated at height of 30 km during several hours. Fortunately, the search for these events is often simplified by the fact that, due to the interactions of

these particles, cascade showers composed of tens of thousands of particles are developed in the emulsion. These showers can be seen by the naked eye or through a lens in the form of dash or spot.

Accordingly the photo-emulsion method has many advantages, but its most serious disadvantage is that it does not enable us to meaaure directly the incident particle energy if it exceeds 10 GeV.

4.3. Wilson's Chamber method

The probability of emergence of a nuclear shower in the gas inside a Wilson chamber is small. Therefore, a necessary element in the experiments using Wilson's chamber are plates of the investigated material-generator. These plates or groups of plates are placed either inside or over the chamber. Since the plates have a considerable thickness, the low energy particles, i.e. the nuclear distingeration products cannot be observed in Wilson chambers, so that attention is concentrated on deeply penetrating particles and electrons. By means of a Wilson chamber with a magnetic field, one can measure particle momenta up to $\lesssim 10^{11}$ eV/c in the best chamber (usually $\sim 30 \div 40$GeV/c). Combining this with the measurements of angular distributions, one can have enough material for studying nuclear interaction kinematics.

4.4. Hodoscopic counters

Geiger counters are successfully used to study several properties of electronic-nuclear showers. In earlier experiments , these instruments were used to study the dependence of the number of showers and single particles on height by S.N. Vernov, N.L. Grigorov, A.M. Kulikov, A.N. Čarahč'jan and others [12*] (figure 32). An instrument of such a type must involve two principal elements: an instrument for collecting the nucleons and an instrument for fixing the showers. The upper lead block serves for absorbing the electrons. Protons which pass through the upper block are capable of producing showers in the lower block. The showers are fixed by the hodoscopic counters. The upper hodoscopic counters are used to register atmospheric showers. These instruments are very simple and permit the radio broadcasting of all the information. They are often used to study cosmic rays by means of balloons raised in the stratosphere.

4.5. Counting ionization chambers

Counting ionization chambers are successfully used to study strongly ionizing particles and nuclear distingerations. If the walls of the chamber are made of light material, say aluminium of thickness $\delta \simeq 1 - 1.5$ mm, then neither pair production induced by photons nor bremsstraalung can occur in such thin walls (because $\delta \ll t_o$, where t_o is the t-unit length). Therefore, atmospheric electrons penetrate the ionization chamber without cascade reproduction in quantity.

If we set the threshold of registration of ionization omenta (the so-called "impulses") equal to two÷three relativistic particles, then the electrons and other rapid particles will not be registered. The chamber will register only

those cases in which a large ionization is produced. More often (in 80% of the cases) this occurs as a result of a nuclear disintegration occuring in

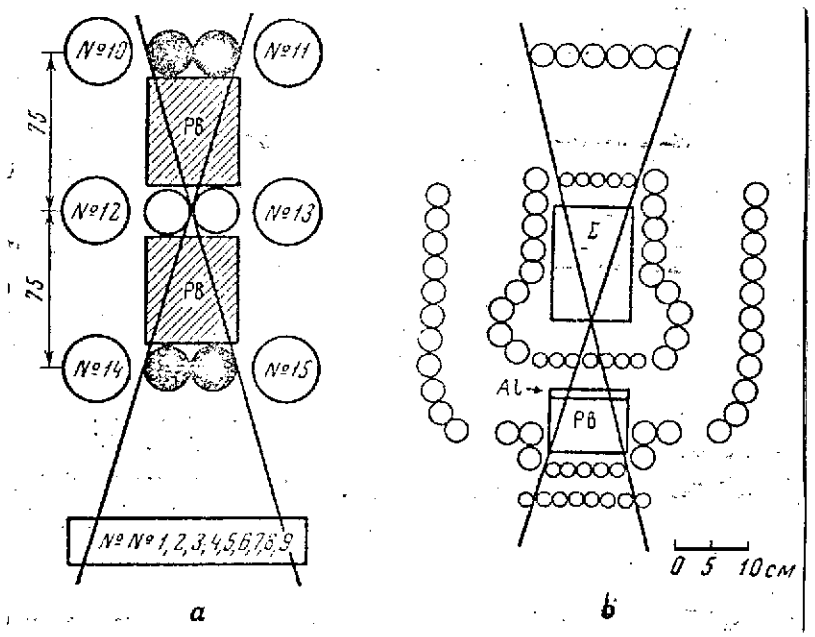

Fig. 32. An instrument with a system of hodoscopic Geiger counters (denoted by circles) for investigating the interaction of particles in cosmic rays.

the chamber's walls. The products of this disintegration (low energy protons and alpha particles) leave the thin walls of the chamber and enter its working volume and cause ionization pulses. By analysing these pulses, one can draw a series of conclusions on the properties of nuclear disintegrations.

High-energy phenomena (electronic-nuclear showers) can also be investigated by means of ionization chambers. It is only necessary to exclude the cases of strongly ionizing particles falling into the chambers. These cases are so numerous and can imitate high-energy events. For example, a low-energy ($\sim$20 MeV) neutron causes a nuclear disintegration capable of producing an ionization, 50 times greater than that caused by a shower of relativistic particles whose generation requires an energy exceeding 50 GeV. Low-energy events can easily be excluded by switching on two ionization chambers in coincidence separated by a small layer of matter. Disintegrations occuring in the walls of one chamber will not then give particles capable of producing events in the second chamber. Such an instrument will mainly register electronic-nuclear showers.

In order to increase the effectiveness of registration of electronic-nuclear showers, a target of a thickness comparable to the nuclear interaction path is placed over the instrument. Electronic-nuclear showers will be generated in this layer.

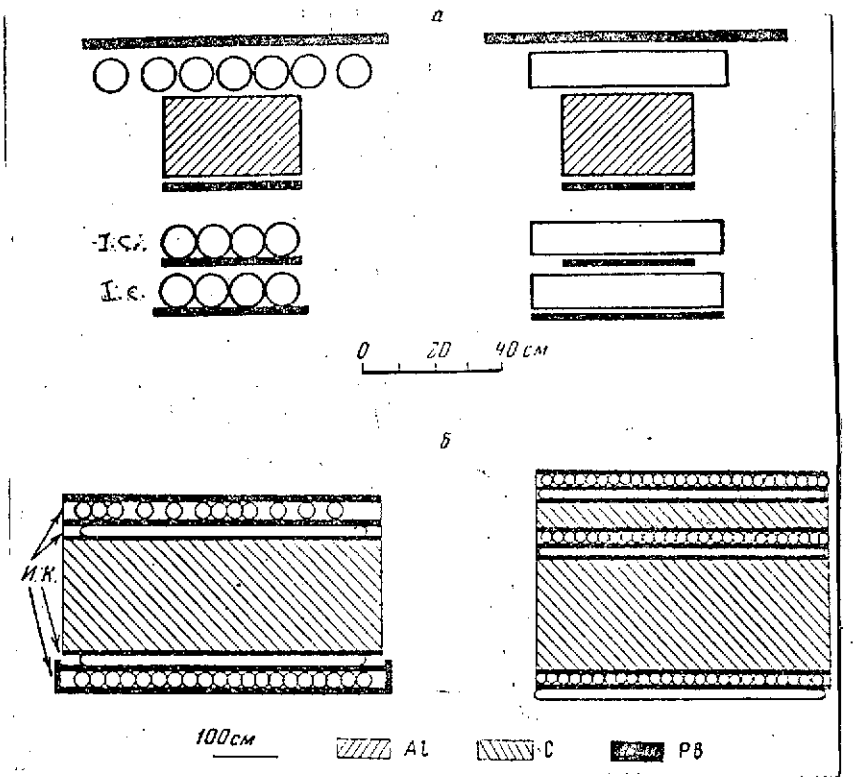

Fig. 33. "Impulsive" instrument. a: aeroplane instrument; b: surface instrument; I.C.: ionization chambers (the thickness of lead over the chambers is 2 ÷ 4 cm).

If the ionization chambers are screened by thin layers of lead (of thickness equal to a few t-units), then photons resulting from the decays of π°-mesons will produce electron-photon showers consisting of large numbers of particles which will easily be registered by the chamber (at $E_{o} \simeq 100$ GeV, the shower may consist of up to 800 particles). Instruments of this type are called "impulsive" (figure 33). In some studies, impulsive instruments having an area tens of square meters were used to study particles with energies up to 10^{4} GeV.

Equation (2.53) enables one to estimate the energy of all photons appearing in an electronic-nuclear shower.

4.6. Ionization calorimeter /6,14/

Impulsive instruments enable one to determine the total energy of photons (i.e. ending in neutral pions) which appear in a nuclear interaction. In many cases, however, it is important to know the energy of the initial particle. In order to measure the initial energy, one applies an instrument involving a large number of ionization chambers, known as the ionization calorimeter (figure 34). This instrument involves rows of ionization chambers alternating with absorber (iron) layers. The total quantity of matter in an ionization calorimeter is by many times greater than the interaction path. Hence, the initial particle and all its descendants interact many times and loose all their energy into ionization mainly through the following chain of processes : electronic-nuclear shower - neutral pions - photons - electron-photon cascade. Ionization is measured by means of a series of ionization chambers separated by distances less than the length of an electron-photon shower. The energy of the initial particle is evidently equal to

$$E_0 = V_0 \int_0^\infty \mathcal{J}(x)\,dx \qquad (4.37)$$

where V_0 is defined in p. 13 .

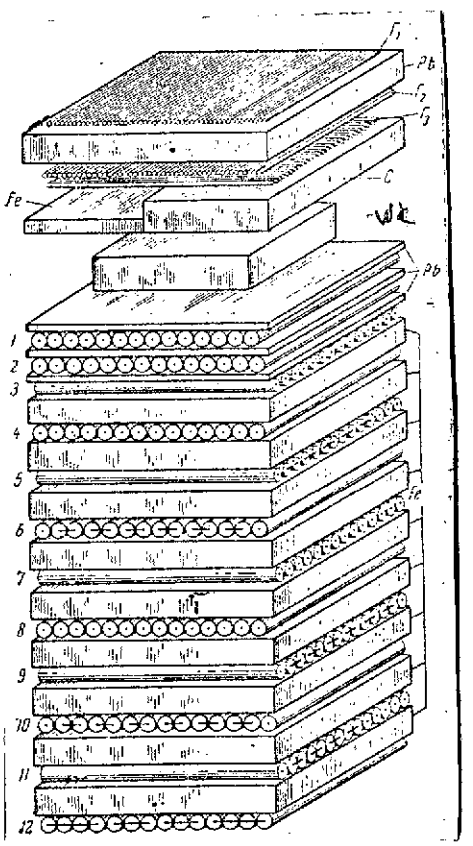

Fig. 34. Ionization calorimeter. $\Gamma_1 - \Gamma_3$: a system of hydoscopic counters; 1 ÷ 12 rows of ionization chambers; W.C. Wilson's chamber.

In the calorimeter, the ionization is measured at discrete levels x_i. Integral (4.37) is therefore in practice replaced by a sum :

$$V_0 \int_0^\infty \mathcal{J}(x)\,dx \rightarrow V_0 \sum_{i=1}^{N} \mathcal{J}(x_i)\,\Delta x_i,$$

where Δi is the thickness of the i th layer $\mathcal{J}(x_i)$ is the ionization per unit length at depth x_i . Usually the thicknesses Δx_i of the absorber layers are chosen equal; Consequently

$$E_0 = V_0 \Delta x \sum_{i=1}^{N} \mathcal{J}(x_i)$$

where N is the number of rows of the ionization chambers.

The ionization calorimeter was used for the first time in the cosmic ray laboratory of Moscow State University by N.L. Grigorov, V.S. Murzin and I.D. Papoport. Čerenkov counters or scintillators can be equally successfully used instead of ionization chambers in ionization calorimters. In this case, liquid or plastic scintillators with photomultipliers are applied. Particularly simple is the construction of instruments with Čerenkov counters, which are often made simply of distilled water. Calorimeters are used in combination with Wilson chambers, hodoscopic counters and other instruments.

4.7. Controlled-photo-emulsion method

The controlled photo-emulsion method was suggested by N.L. Grigorov in 1956 /15*/. It made use of the advantages of both the photo-emulsion and electrical methods. The method practically consists in the following. Three to four emulsion layers are put under lead absorbers of a thickness equal to a few t-units, and under this system the ionization chambers are arranged. The registration of impulses in the ionization chambers enables one to choose events of required energy, and by specifying which chamber is working, one can find the position in the emulsion, where the given shower takes place. If the target is far enough from the emulsion, then photons resulting from the nuclear interaction have enough time to become dispersed over a large distance. One can then register separate photons and measure their energies in the emulsion and also use the ionization chambers (in the form of an ionization calorimeter) to measure the energy of the primary particle.

In the comparison of showers in both photoemulsion and in the chambers, a discrepancy may appear. During the exposure time, a number of showers of comparable energies may pass through the emulsion. Moreover, the accuracy of determining in which chamber the shower occurs is not sufficient. In order to eliminate the accuracy in time and coordinates, two layers of X-ray plates, a fixed and a moveable one, are put under the photo-emulsion. The movable plate is shifted by steps of 1 cm within equal time intervals. Comparing the two plates after their development, one can determine the coordinates within an accuracy of 2 ÷ 3 mm and the time of appearance of the shower and compare between the pictures in the photo-emulsion and the calorimeter. Figure 17 shows an example of the events, registered by means of the controlled photo-emulsion method.

4.8. Spark chambers /16/

At present spark counters and spark chambers are widely used in nuclear investigations. Their role in cosmic experiments also increases every day.

The Spark counter is a plane condenser, between whose plates is found air or another usually inert gas. The plates are given a high potential difference, reaching 10 kv/cm in noble gases. When a charged particle passes through the gap into the gas, a spark break down occurs in the shortest distance between the plates near the place where the particle passed. By photographing the spark, one can determine the place of the particle's passage. In many cases, several

counters are gathered together to assemble a chamber. This is a multi-layer system having tens, or even hundreds of gaps. By means of such an instrument, one is able to follow the trajectory of the particle.

At the present time, impulsive supply of high voltage is used for spark chambers. The voltage pulse is given with a delay of no more than 1 μ sec. Counters filled with neon can register sparks resulting from the simultaneous penetration of several particles. By means of chambers of large discharge intervals, it is possible to make the spark follow the trajectory of the particle up to track slopes $\simeq 40^{\circ}$.

G.E. Čikovani and collaborators suggested a method to construct spark counters, capable of registering particles moving in any direction (isotropic chambers). The investigation of the growth of the spark in the chamber, shows that the spark appears at the points where the incident particles produce ionization, and that the electron showers forming the streamer, move from these points to the electrodes. If the process of growth of the streamer is artificially cut at the very beginning, then the luminous region will be localized near the trajectory of the particle. In this case, the track in the chamber will be composed of short dashes directed along the lines of forces of the electric field. The length of each of these dashes can be reduced to a few millimeters. Spark chambers of this type can have large dimensions. They are used to observe particle showers, and by putting them in a magnetic field, one can measure the momenta of the particles by the curvature of their trajectories (see figure 35). The angle of the trajector slope is determined with an accuracy of 10^{-3} radians.

Spark counters have a number of advantages over Wilson chambers. In particular, spark counters have a small dead time $\simeq 10^{-2}$ sec. (large Wilson chambers of an area $\simeq 1$ m^2 have a dead time measured in minutes). The dimensions of spark counters can be made very large quite easily which is very important in cosmic-ray experiments. Spark counters of an area equal to a few square meters are now being constructed.

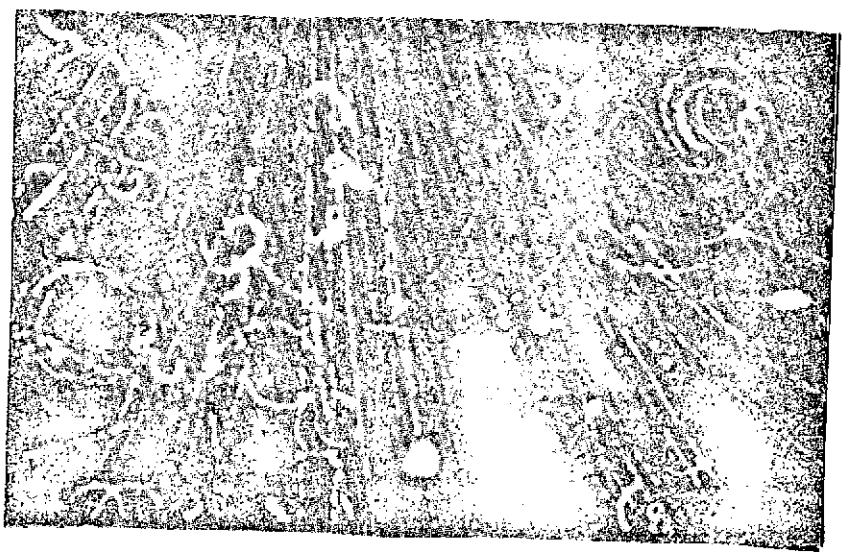

Fig. 35. A photograph of a shower in an isotropic spark counter, placed in a magnetic field. The photograph was obtained by a group of Georgian physicists.

4.9. Methodical features

We shall now stop on some of the features of nuclear interaction studies in cosmic rays. In these studies, the following factors are very important :

1. Composition of cosmic radiation: In order to study nuclear interactions, it is necessary to know which particles are responsible for the different cases of nuclear interaction. Are the primary particles we are dealing with, for example, nucleons, pions or some other particles ? Therefore, in constructing experiments, we must always consider the necessity for determining the nature of the particles. The situation is simplified to a certain extent by the fact that π-mesons are unstable particles and at not very high energies, when their relativistic life-time prolongation is not large, they have enough time to decay before colliding with nuclei.

2. The investigation of the energy spectrum of cosmic radiation also requires some specific conditions. The differential energy spectrum is usually described by a power law : $N(E_o)dE_o = A\,E_o^{-\gamma}\,dE_o$ (where γ varies from 2.5 at low energies to 3.3 at very high energies). The intensity of nuclear-active cosmic-ray particles is so small, that in Moscow, during a whole year, only a few interactions with an energy 10^{12} eV could be observed by means of an instrument of an area of one square meter and a relative aperture of 0.1 steradian. The number of interactions with an energy 10^{11} eV was already found to be more than 100 interactions per year, but this number was also still too small.

3. The study of high-energy interactions is simplified by the rapid increase of the number of nuclear-active particles with height. For example, at heights of 3 ÷ 4 km, the number of nuclear-active particles increases 15 - 20 times. Therefore, on constructing cosmic-ray experiments, it is desirable to raise the instruments as high as possible and to increase the duration time of the experiment. Special Alpine stations are therefore constructed for the purpose of studying nuclear interactions and other phenomena in cosmic rays.

Several years ago, an Alpine station was constructed on the Pamirs, in the Akbajtal River valley, at a height of 3860 meters above sea level. Another well-known station was built in Armenia on the Aragac mountain (figure 36,a) at a height of approximately 3200 meters. At a similar height, a station was built on the Ala-Tau mountain, 50 kms from Alma-Ata (Figure 36,b). There are other Soviet stations near Tashkend, in Nor-Amberd in Armenia and on the Bakuriani mountain in Georgia. Very well known Alpine stations are found for example on the Jungfran, in the Andes in Bolivia, and on the Norikura mountain in Japan, etc.

When large aircraft were constructed capable of long flights at heights close to 10 km., they were used to carry instruments for studying cosmic radiation. At these heights the intensity of nuclear-active particles is tens of times greater, and approximately 30 flights of 5 - 6 hours each are equivalent to a year's work on a high mountain. There are however severe limitations on the dimension and weight of instruments carried in an aircraft. For this reason aeroplanes can compete with Alpine stations mainly in investigations carried out by using photoemulsion methods, since the dimensions and weights of the

instruments are limited for financial reasons and because of the subsequent difficulties in the examination of large emulsions.

In one of the inevestigations undertaken under the supervision of Perkins, an emulsion chamber was carried by a "Comet", on a regular flight between London and Calcutta. The plates were radiated for a total time of approximately 1800 hours at a height of 11 km. These plates should have been radiated for 54,000 hours on a mountain to obtain the same effect. It is necessary to note that a sensitive emulsion can be preserved for no longer than 1-2 thousand hours. Consequently, one would have to keep changing the emulsion during that long length of time.

Aerostats have a great advantage over aeroplanes. An aerostat made of polyethylene can carry a photo-emulsion chamber to a height equal to 40 km. In this manner, the chamber is radiated by primary particles, which, as known, consist almost entirely of protons and alpha-particles. Aerostats can keep flying for several days. Their flight and place of landing is controlled by means of aeroplanes and radio-locators. Such investigations are usually carried out by a group of states.

Earlier, rubber balloons were used to raise small emulsion chambers. They were applied to raise the instruments to a height of 25 ÷ 35 km in order to investigate nuclear interactions at lower energies ($10^9 \div 10^{11}$ eV). Ionization chambers and counters used for this purpose transmitted all informations by radio to a surface receiving station. The total weight of these instruments reached 100 kg. These, as a matter of fact, are automatic flying laboratories which able to work by a pregiven program and supplied with a chemical energy source with a marginal work time equal to 15 - 20 hours.

The method for transmitting the information by radio was used for the first time by S.N. Vernov in 1936 [17]. These stations were the prototype of the automatic laboratories now widely used for studying cosmic space and cosmic radiation in the earth's vicinity means of rockets and satellites.

In the period between 1947 and the launching of the first satellite, rockets raised to heights reaching 100 ÷ 150 kms and subsequently falling to the ground were used to study cosmic radiation beyond the atmosphere. The measuring time on such a rocket extended for only 10 - 15 minutes. At present investigations by means of satellites are continually gaining ground. The first experiment for studying nuclear interactions in outer space was made in the summer of 1960 with the second Soviet satellite which carried emulsion rouleaus. In 1965, an ionization calorimeter was raised by the satellite "Proton" [18].

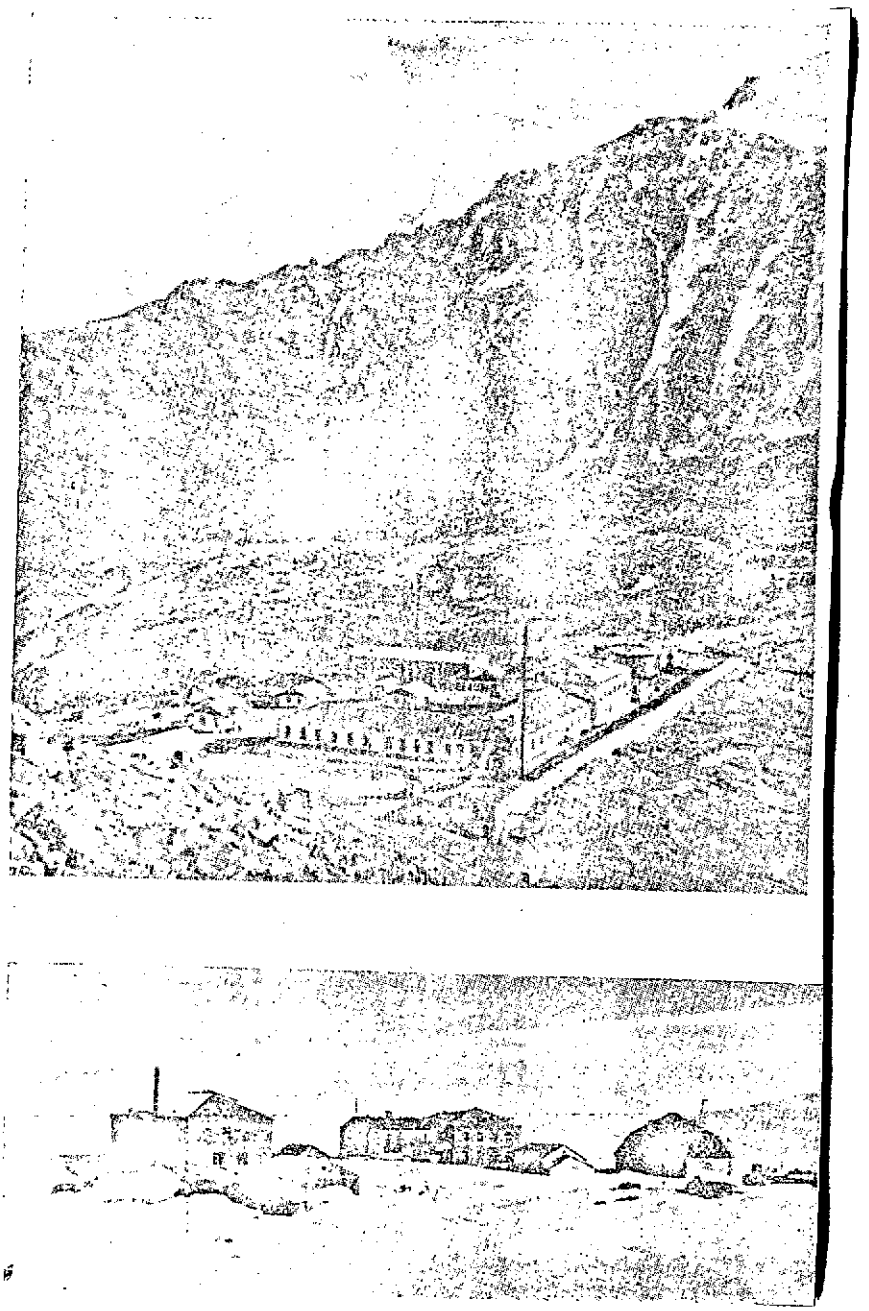

Fig. 36. Alpine stations for studying cosmic rays on (a) Tien Shan and (b) Argac mountain.

REPRODUCIBILITY OF THE
ORIGINAL PAGE IS POOR

5. Investigation of Nuclear Interactions

5.1. Classification

The classification of nuclear interactions observed in emulsions is based on the number of particles and their ionization power. All particle tracks observed in emulsions are divided by their densities into three groups [10] :
(1) thin tracks, $g_{min} \leqslant g \leqslant 1.4\ g_{min}$, caused by rapid particles which are called shower (relativistic) particles, (2) grey tracks, $1.4\ g_{min} \leqslant g \leqslant 6.8\ g_{min}$, and (3) black tracks, $g > 6.8\ g_{min}$. Ionization by $1.4\ g_{min}$ may be induced by mesons of energy > 80 MeV and protons of energy > 500 MeV. Ionization by $6.8\ g_{min}$ corresponds to a proton energy of 25 MeV. Evaporation products of nuclear disintegrations usually have energies less than 25 MeV and therefore cause black tracks. The number of shower particles is denoted by m_s , of grey tracks by N_g and of black tracks by N_b. The total number of highly ionizing particles is equal to $N_h = N_g + N_b$. Nuclear disintegrations observed in an emulsion are characterized by the two numbers which are usually recorded as $(n_s + N_h)_x$, where the index x denotes the nature of the registered particles : $x = p, \alpha, n, \pi$, etc. Stars with $n_s \geqslant 2$ are usually called showers.

5.2. The picture of a nuclear disintegration

In order to analyse the occurrence of a nuclear disintegration, it is useful to have in mind a model representation of the process. The picture of nuclear interaction we are now presenting can be considered as the latest. The primary particle transfers a part of its energy to the other nucleons through the mediation of the δ-nucleons. It is possible to follow and mathematically calculate the evaluation of each δ-nucleon. However, this problem is hard to solve if the nucleus is sufficiently heavy. In this case, one has to develop a statistical formulation for the problem.

Let us assume that all the rapid particles (that formed grey tracks in the emulsion) have already left the nucleus, while the others made a large number of collision such that a statistical equilibrium is already established. If the excitation energy left in the nucleus is equal to U, then the mean excitation energy per nucleon will be equal to U/A. The energy will be distributed around this mean value according to Maxwell's law. In this case, the nucleus will not "remember" how the energy was transformed to it, and the main feature of the collision will not be preserved in it. Such a system very much resembles a heated liquid drop, from which particles are emitted by a process similar to evaporation. The analogy is however not complete since the number of particles in the nucleus is not very large. This will lead to a large fluctuation in the mean value of energy per particle. Moreover, the "evaporation" of a single molecule from a drop will slightly change its temperature whereas the "evaporation" of a nucleon from a nucleus significantly changes the

nuclear "temperature" because the number of its particle is small. The "evaporation" of a second nucleon will take place under conditions quite different from the conditions of evaporation of the first particle. This model leads to the following conclusions :

1. Black tracks in stars are isotropically distributed by angles. In the disintegration of light nuclei having a small nucleon number, the equilibrium may be incomplete. It is therefore necessary to study disintegration of heavy nuclei when one is checking the assumption that an equilibrium of energy distribution is established among the nucleons. This can be done by choosing stars with more than eight rays. Such investigations were carried out by Perkins and his collaborators. By investigating 78 nuclear disintegrations, they found that the distribution of black tracks is spherically symmetrical.

2. Assuming that a thermodynamical equilibrium is established, one can calculate the distribution of nucleon energies around their mean value and consequently find the spectrum of emitted particles. This differential spectrum was calculated by Weisskopf. For neutrons, the spectrum has a form similar to a Msxwell distribution

$$p(E)\,dE = \frac{E}{(kT)^2}\, e^{-\frac{E}{kT}}\, dE. \tag{4.38}$$

For protons, it is necessary to take into account the presence of the potential barrier V :

$$p(E)\,dE = \frac{(E-V)}{(kT)^2}\, e^{-\frac{E-V}{kT}}\, dE, \tag{4.39}$$

where $T = (U/CA)^{\alpha}$, c 0.1, kT is expressed in MeV, and α is a constant.

5.3. Nature of particles appearing in nuclear disintegrations

Most of the particles, emitted from a disintegrating nucleus are protons and neutrons with energies varying between 10 ÷ 30 MeV (black tracks) and ~ 150 MeV (grey tracks). In a nuclear evaporation, a number of alpha particles are emitted together with protons and neutrons. Almost 1/3 of the emitted particles are alpha particles, and their relative number changes weakly with energy.

5.4. Hyperfragments. Hyperon's strong interactions

Among the products of nuclear disintegrations, highly excited fragments which subsequently decay are sometimes found. These fragments were observed for the first time by the Polish physicists Danisz and Pniewski in 1933 [19*]. They were observed in cosmic rays at approximately a frequency of 1 per 10000 stars. They decay in many cases by emitting a π -meson. If such a fragment decayed rapidly in a time comparable to the nuclear time, the decay would then take place at the formation point of the star. Experiment showed however that the fragment decayed after being stopped, i.e. after a large time as compared to

nuclear time. In many cases, the fragments decayed while flying, so that it was possible to determine their life time. It was found to be $\simeq 10^{-10}$ sec. In order to explain this, it was assumed that these fragments had one nucleon replaced by a hyperon. Therefore, such fragments were called hyperfragments or hypernuclei.

The rapid decay of a hypernucleus is forbidden by the strangeness conservation law.
The following two weak reactions are possible :

$$\left.\begin{array}{l}\Lambda^\circ \to p + \pi^- + 37\ Mev \\ \Lambda^\circ + n \to 2n + 175\ Mev\end{array}\right\} \Delta S = 1.$$

Most often, hyperfragments are produced in stars in which pion formation is observed. This proves that the energy of the primary particles $\gtrsim$ 3 - 5 GeV. The energy balance in a mesonic decay is given by

$$Q_{\Lambda^\circ} - B_{\Lambda^\circ} + B_n = 37\ Mev + B_n - B_{\Lambda^\circ},$$

where B_n is the binding energy of the neutron in the nucleus and B_{Λ° is the binding energy of the hyperon. Binding energy B_{Λ° increases with increasing atomic number of the hyperfragment (see table 19).

Table 19

Hypernucleus	H^3	H^4	He^4	He^5	Li^7	Li^9	Be^8	Be^9
B_{Λ°, Mev	0,2±0,5	1,80±0,20	2,0±0,2	2,8±0,2	4,8±0,5	6,7±0,7	6,8±0,6	6,4±0,4

The existence of hyperfragments proves the strong interaction of hyperons with nucleons.

5.5. Energetical properties of nuclear disintegrations

The excitation energy U of the nucleus is exhausted on the evaporation of nucleons from the nucleus. The total energy, transferred by the incident particle is much less than U, since it includes the energy of nucleons knocked out of the nucleus with a large energy ("grey" tracks) and not participating in the evaporation process. The number of black tracks is almost linearly proportional to the number of grey tracks (see figure 37,a). At energies less than a few MeV, the number of grey tracks in stars increases with increase in energy, and consequently, with the increase of excitation energy U. According to the

data obtained by Powell's group, the number of "grey tracks" per star in the emulsion 2 at an incident energy equal to 10^9 eV, and $N_g \approx 4$ at an incident enerty equal to 5×10^9 eV. This means that both excitation energy U and total disintegration energy E_d increased twice. However, in the remaining very large energy interval from 10^3 GeV to at least 10^3 GeV, the disintegration energy remains constant. The number of highly ionizing particles N_h, and the mean energy of protons forming the grey tracks also remain constant (figures 37,b,c).

What about the total energy transferred to the nucleus in a high energy nuclear collision ? It is absolutely clear that this energy E_p will be different from one case to another becauze of fluctuations. It is therefore useful to define the mean energy $\bar{E}_d$ that goes into disintegrating the nucleus. Energy $\bar{E}_d$ must depend on the nuclear volume since a particle makes more collisions in a larger nucleus. This makes the study of the mass number dependence of $\bar{E}_d$ an important problem.

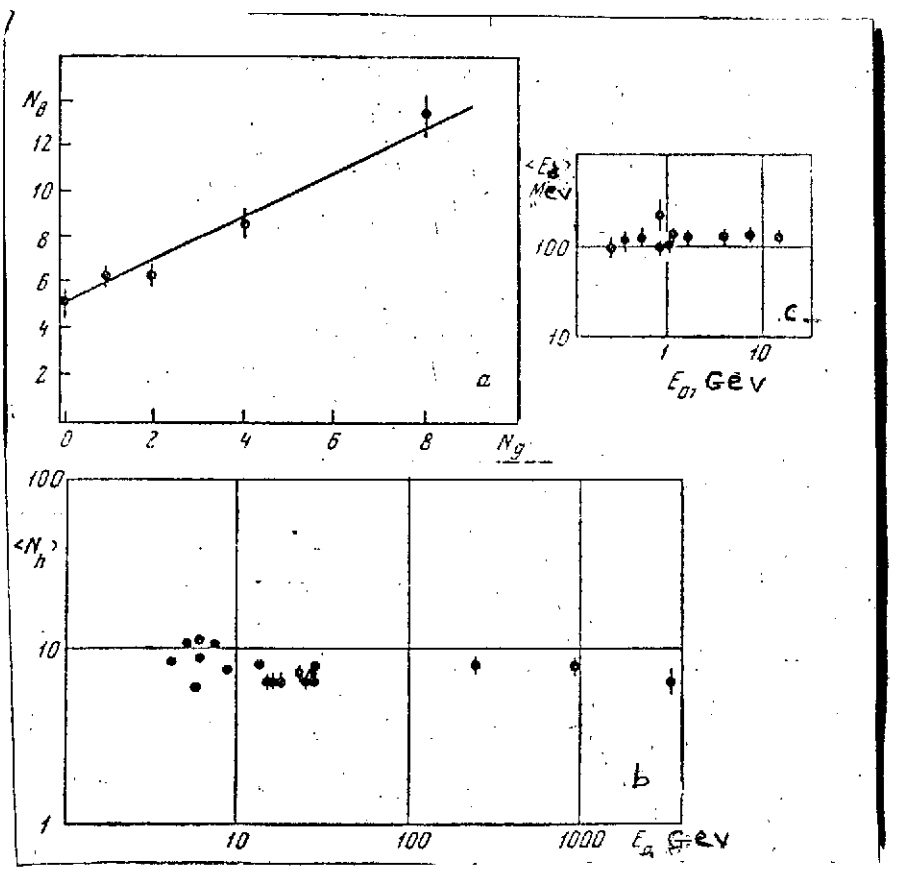

Fig. 37. Properties of nuclear disintegrations.
a) dependence of the number of black tracks on the number of grey ones, b) dependence of the number of highly ionizing particles on the energy of the primary particle, c) dependence of the mean energy of the δ-protons on the energy of the primary particle.

A rough estimate for energy $\bar{E}_d$ of heavy nuclei may be obtained by summing the energies of all the N_h highly ionizing particles, observed in the photo-emulsion, and then adding to the resulting value the energy carried away by the neutrons. It is usually assumed that the relative number of the emitted neutrons is proportional to the relative number of neutrons in the nucleus, i.e. to $\frac{A-Z}{A}$. The energy of neutrons is assumed to be the same as the energy of protons.
Such an estimation was made by Powell's group and led to the following relation:

$$E_d = 37N_h + 4N_h^2.$$

This relation enables us to compute $\bar{E}_d$ when the mean value $\bar{N}_h$ is known; $\bar{N}_h$ is approximately equal to 10 (see figure 37,b) and hence $\bar{E}_d \simeq 800$ MeV.

In order to study the dependence of $\bar{E}_d$ on the nuclear mass number, it is important to study by any means, nuclear disintegrations that occur in a material of a given mass number. Such experiments were carried out in Moscow State University under the supervision of N.L. Grigorov [20*]. In these experiments, photo-plates were screened by absorbers of graphite or lead. The results of these measurements were compared with results obtained with unscreened plates. Measurements were made at heights exceeding 20 kms. The results obtained were the following :

$$\frac{E_d^{Pb}}{E_d^{air}} = 2,1 \pm 0,3; \quad \frac{E_d^{C}}{E_d^{air}} = 0,82 \pm 0,08$$

where $\bar{E}_d^C$ is the disintegration energy of the carbon nucleus.

Consequently, the nuclear disintegration energy depends on mass number A. The dependence is such that the disintegration energy is proportional to $A^{1/3}$. Noting that the volume of the nucleus is proportional to A, so that $A^{1/3}$ determines its linear dimension, we conclude that the disintegration energy is proportional to the geometrical path of the particle in the nucleus.

One can determine E_d in air by means of an ionization chamber. By using an impulsive ionization chamber, one can determine the ionization, produced by highly-ionizing nuclear-disintegration products in a given layer of air, i.e. the quantity :

$$32N \int_{p_1}^{p_2} \bar{N}_T(I_T)\, I_T dI_T .$$

Dividing this quantity by the number of interactions induced by high-energy particles in the given layer, one obtains the energy spent on nuclear disintegration in a single act. It is found that this disintegration energy is approximately equal to 400 MeV and does not depend on the energy of the primary particle when $E_0 > 3$ GeV. This result was obtained by measuring E_d at large heights and at different latitudes. One deals with particles with a mean energy

$\sim$30 GeV at the equator and $\sim$3 GeV at our latitudes. Comparing these results with photo-plate data, we obtain

$$E_{\alpha}^{Pb} \simeq 840\ Mev, \quad E_{\alpha}^{air} \simeq 400\ Mev, \quad E_{p}^{C} \simeq 320\ Mev.$$

Angular distribution of nuclear-disintegration products

Particles, producing black tracks, have a spherically isotropic distribution.

The angular distribution of "grey" particles in the stars of a photo-emulsion is not spherically symmetrical. Particles are emitted as a result of a small number of collisions and are therefore sensitive to the direction of motion of the primary particle. The average flight angle of grey protons from heavy nuclei is in the order of 40°. In the collisions of protons with energy >50 MeV with light nuclei, the difection of motion of the primary particle is even more conserved. The average angle of flight of such protons from light nuclei is less than 30°.

6. Nature of Shower Particles

The nature of shower particles is studied mainly by the photo-emulsion method. The masses of the particles are determined by comparing the grain densities and the multiple scatterings (figure 20). These measurements can be carried out for energies less than 10^9 eV.

The mass distribution of particles with energy $> 10^9$ eV is of great interest. It is difficult to apply the direct method to determine the masses of the particles. One of the possible approaches to the solution of this problem is the following. It follows from most general considerations that, in a nucleon-nucleon collision in the centre-of-mass system, the nature and the other properties of particles emitted in the forward and backward hemispheres must be the same. Particles, emitted in the backward hemisphere in the centre-of-mass system will have a lower energy in the laboratory system. Actually, the energy of a particle in the laboratory system is given by (see equation 4.5)

$$\varepsilon \approx \gamma_c (\tilde{\varepsilon} + \tilde{p}c \cos \tilde{\theta}) \approx \tilde{\varepsilon}\gamma_c (1 + \cos \tilde{\theta}).$$

If the particle is emitted with an angle θ, close to π, then the term in the brackets will be small, and, consequently $\varepsilon \ll \bar{\varepsilon}$. These particles constitute the wide cone of the electronic-nuclear shower, since they fly with large angles in the laboratory system. Due to symmetry, the wide and narrow cones must be similar to each other.

If the energy of the primary particle is known, then the separation of the wide and narrow cones of secondary particles is not difficult. Using equation (4.3) for the angle transformation, and noting that angle $\theta = 90°$ is the limiting angle which separates the wide and narrow cones, in the centre-of-mass system, we find that, when $\vec{v} = v$, the angle which separates the two cones in the laboratory system is given by

$$\operatorname{tg} \theta = \frac{1}{\gamma_c}. \tag{4.40}$$

In practice, however, the energy of the primary particle is often unknown. Equation (4.40) is then applied to estimate the energy of the primary particle. From the symmetry condition, it follows that the number of particles in the forward and backward cones are equal. Measuring angle $\theta_{\frac{1}{2}}$ which divides the particles in the laboratory system into two equal parts, we find

$$\gamma_c = \frac{1}{\operatorname{tg}\theta_{1/2}}. \tag{4.41}$$

Since the energy of the particles in the wide cone is small, then the nature of these particles can be determined by the method of multiple scattering and ionization density. It was concluded from these experiments that about 80% of all the newly created particles were pions, of which about 20% were kaons and protons. This ratio is kept up to the highest energies studied ($\simeq 10^4$ GeV).

It is clear that only charged mesons can be identified by the above method. The ratio of the number of neutral and charged mesons can be obtained by observing electron-positron pairs, appearing in the emulsion near electronic-nuclear showers. In this case, one must take into consideration only the pairs whose angle's bisector passes near the shower's centre (not further than by a few microns), and whose energy exceeds 100 MeV. Only such mesons, being charged, give a shower track.

In the experiments carried out by Daniel and Perkins, the ratio $R = N_{\pi^0}/N_{\pi^\pm}$ was determined using the following assumptions : 1) the angular distributions of π^0 and $\pi^\pm$ concide, and 2) the mean path of a photon, before the creation of an electron-positron pair in the emulsion, has a length equal to the length of the t-unit, $t_0 = 4.45$ mm.

The number of pairs created by photons in the emulsion under consideration, is equal to $N_{pair} = n_\gamma W$, where n_γ is the number of gamma quanta and W the probability of a pair creation: $n_\gamma = 2N_{\pi^0}$; $W = \bar{l}/t_0$; $\bar{l} \ll t_0$; where $\bar{l}$ is the mean path of each gamma quantum in the emulsion. This quantity is much less than t_0 and only depends on the angular distribution of the particles because it is defined by geometrical shape g. Consequently

$$N_{pair} = 2N_{\pi^0}\frac{\bar{l}}{t_0}.$$

and, hence, $N_{\pi^0}\bar{l} = \frac{1}{2} N_{pair} t_0$ whereas $N_{\pi^\pm}\bar{l} = L_{ch}$ which is the total path of the charged π-mesons in the same emulsion. In these experiments, the number of pairs was found to be 19, and the total path of charged π-mesons $L_{ch} \simeq 84$ cm. Then

$$\frac{N_{\pi^0}}{N_{\pi^\pm}} = \frac{19 \cdot 4{,}45}{2 \cdot 84} = \frac{1}{2},$$

i.e., in agreement with the principle of charge independence of nuclear processes,

$$N_{\pi^0} = \frac{1}{2}(N_{\pi^+} + N_{\pi^-}).$$

This result was obtained for showers induced by cosmic-ray particles having an energy $E \simeq 10$ GeV.

The relative number of kaons, at high energies, can be determined by considering the experimentally measured ratio of the number of neutral pions to the number of total charged particles :

$$R = \frac{N_{\pi^0}}{n_s} = \frac{N_{\pi^0}}{N_{\pi^\pm} + N_K}.$$

If $N_{\pi^0} = \frac{1}{2} N_{\pi^\pm}$, then quantity R can easily be used to estimate the relative number of kaons :

$$Q = \frac{N_{K^\pm}}{N_{K^\pm} + N_{\pi^\pm}} = 1 - 2R.$$

Averaging over a large number of experiments, quantity $R = 0.41 \pm 0.03$ in the energy interval $10^2 \div 10^4$ GeV, which gives $Q = 0.20 \pm 0.06$.

7. Number of Shower Particles

Experiments show that the number of shower particles in nuclear interactions increases with the increase of energy. In the energy range, varying from a few GeV to 50 GeV, this increase is described by the relation $n_s \simeq n_s^0 E^{\frac{1}{2}}$, while in the energy range $>50 \div 100$ GeV, the increase with energy becomes slower and becomes proportional to $E^{1/4}$ or even to ln E (see figure 38). The latter dependence ($n_s \sim \ln E/Mc^2$) makes it possible to describe the relation between n_s and E in a wide energy interval.

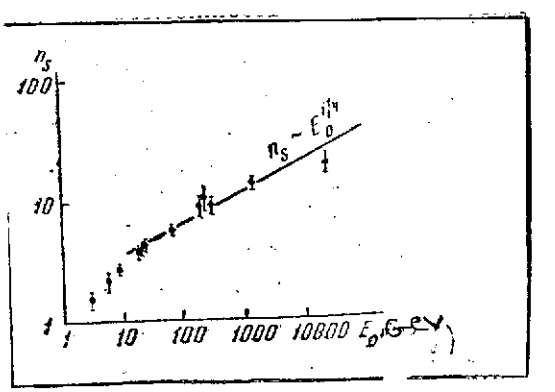

Fig. 38. Dependence of the number of shower particles on the energy of the primary particle.

In emulsions, 5 shower particles are observed on the average in the interaction of 25 GeV protons with nuclei, while at 200 MeV on carbon nuclei, $n_s \approx 10$. The number of shower particles also increases with the dimension of the target nucleus approximately as $A^{1/5}$, where A is the nuclear mass number.

Up till now, we spoke about the mean number. A large fluctuation is observed around this mean number and given in the average by $\Delta n_s = \frac{1}{2} \langle n_s \rangle$. If the collision is between the primary nucleus and the target nucleus, then very large showers are sometimes observed, in which n_s may reach 300. On the average, the number of shower particles in the interaction of nuclei is proportional to A/2, where A is the mass number of the incident nucleus.

8. Angular Distribution of Shower Particles

8.1. Description methods

Shower particles contrary to black tracks are sharply collimated in the forward direction in the laboratory coordinate system. According to the measurements by the Bristol group, at a height of 3860 m, more than half of the particles are emitted in the angular interval from 0 to 5°. This narrow angular distribution is a consequence of the large momentum and energy of the generating particle, which is subsequently transferred to secondary particles. Cases of very high energies are of great interest where the number of secondary particles is large. In these cases it is not possible to study the angular distribution statistically but separately for each individual case. One of the first stars, registered by Schein, had 15 shower particles, 7 of them moving in a narrow cone of an angle $\simeq 0.003$ radians (17°), with the other particles more widely distributed ($\sim 7°$). This star may be considered as the earliest proof for the multiple production of -mesons.

The angular distribution significantly depends on the velocity of the centre of mass (see equation (4.3)). Therefore, in order to analyse angular distribution, a special representation, called lg tg θ - representation or x-representation, is often used. This representation is very convenient in the case of very high energies, where the velocities of particles in the C-system is close to the velocity of light : $\vec{v} \simeq v \simeq c$. The usefulness of this representation immediately follows from equation (4.30) for transformation of angles. Taking the logarithm of both sides of this equation, we obtain

$$x_i = \lg \operatorname{tg} \theta_i = -\lg \gamma_C + \lg \operatorname{tg} \frac{\tilde{\theta}_i}{2}. \tag{4.42}$$

It follows from here that the transformation from one energy to another, is simply done by shifting the coordinate origin by the quantity lg γ_c. A slightly different representation is therefore often used, namely

$$X_i = \lg \gamma_C + \lg \operatorname{tg} \theta_i = \lg (\gamma_C \operatorname{tg} \theta_i). \tag{4.43}$$

In the X-representation, the angular distribution is symmetric with respect to point $X_i = 0$. This can be easily seen by summing equation (4.42) over all emitted particles. We then obtain

$$\sum_{i=1}^{n} \lg \operatorname{tg} \theta_i = -\sum_{i=1}^{n} \lg \gamma_C + \sum_{i=1}^{n} \lg \operatorname{tg} \frac{\theta_i}{2}.$$

It is easy to see that the last term vanishes in the case when the particles are symmetrically emitted in the centre-of-mass system. In this case,

$$\lg \gamma_c = -1/n \sum_{i=1}^{n} \lg \operatorname{tg} \theta_i = \langle \lg \operatorname{tg} \theta_i \rangle . \tag{4.44}$$

Consequently, the mean value $\langle \lg \operatorname{tg} \theta_i \rangle$ is equal to $\lg \gamma_c$, and the angular distribution in the x-representation is symmetric around $\lg \gamma_c$, and in the X-representation around $X_i = 0$.

It is found that a symmetric angular distribution in the C-system may be represented by a Gaussian curve, centered at $\lg (\gamma_c \operatorname{tg} \theta_i)$:

$$\frac{dn}{d(\lg \gamma_c \operatorname{tg} \theta_i)} = \frac{dn}{dx} = \frac{1}{\sqrt{2\pi}\sigma} e^{-x^2/2\sigma^2} . \tag{4.45}$$

The dispersion of the angular distribution, σ is invariant under Lorence transformations[1].

$$\sigma = \frac{[\Sigma (\lg \operatorname{tg} \theta_i - \langle \lg \operatorname{tg} \theta_i \rangle)^2]^{1/2}}{n} . \tag{4.46}$$

In the case of isotropy, $\sigma = 0.38$. If the particles in the C-system are collimated in the direction of motion of the colliding particles, then $\sigma > 0.38$.

8.2. Experimental data

The angular distribution measurements gave a large number of interesting results.

Firstly, by measuing dispersion, it was found that the angular distribution of created particles is slightly anisotropic in the energy region near 100 GeV, and that dispersion increases at higher energies. This means a sharper anisotropy of particle emission in the C-system, where particles start to concentrate themselves near the forward and backward directions.

The second important result is the discovery of the so-called asymmetric showers [21*]. These showers were discovered by means of a Wilson chamber. Factor γ_c was determined by means of an ionization calorimeter. By plotting angular distributions in the X-representation, it was found in some cases that angular distributions were asymmetric with respect to point X = 0. This means that in the C-systems, the numbers of particles emitted in the forward and backward directions, are different. Figure 39 shows the angular distributions of particles in showers, registered in a magnetic field by a Wilson chamber. The

---

1) This is valid only in the very-high-energy approximations considered here, where the velocity of particles in the C-system, v, as well as the velocity of the C-system, v, are close to the velocity of light.

arrow lengths are proportional to the momenta of the corresponding particles. By definition, the sum of the momenta of particles in the C-system is zero.

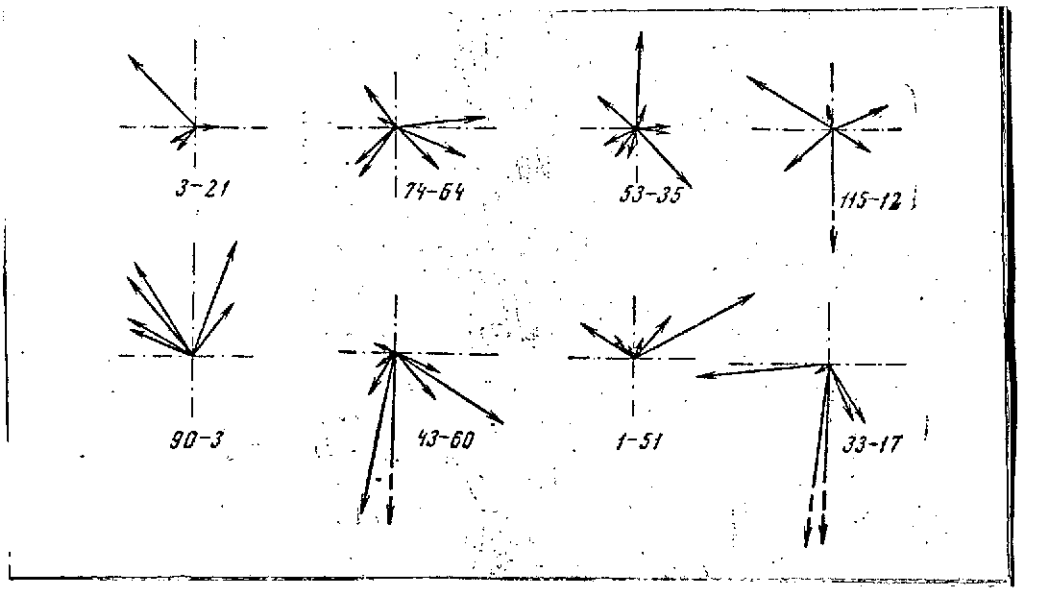

Fig. 39. Angular distributions of particles in the C-system in showers, registered by a Wilson chamber (reference [1*] Chapter 3). The arrow lengths are proportional to the momenta of the corresponding particles (momenta were measured by trajectory curvatures in a magnetic field). Cases of asymmetric showers are easily seen.

The deviation from symmetry therefore means that there exists a particle that compensates the sum of momenta of the newly created mesons. This particle can be a primary nucleon, keeping almost all its energy after interaction whereas another nucleon transfers all its energy to the newly created particles.

In the case of asymmetric showers, quantity $\langle X_i \rangle$ will not be equal to $\lg \gamma_c$, but will define instead a completely different coordinate system, which will be called symmetric or S-system. In the symmetric system, the sum of momenta of the newly created charged pions is equal to zero. Charged pions are namely considered because in a Wilson chamber, only momenta of charged particles are measured.

A third property of angular distributions, is the existence of angular distributions having two maxima in the $\lg \operatorname{tg} \theta_i$ - scale in the high energy region at large values of dispersion σ ($\sigma > 0.6$) (figure 40). These distributions were discovered by a group of Polish physicists headed by Professor M. Ja. Miezovic [22].

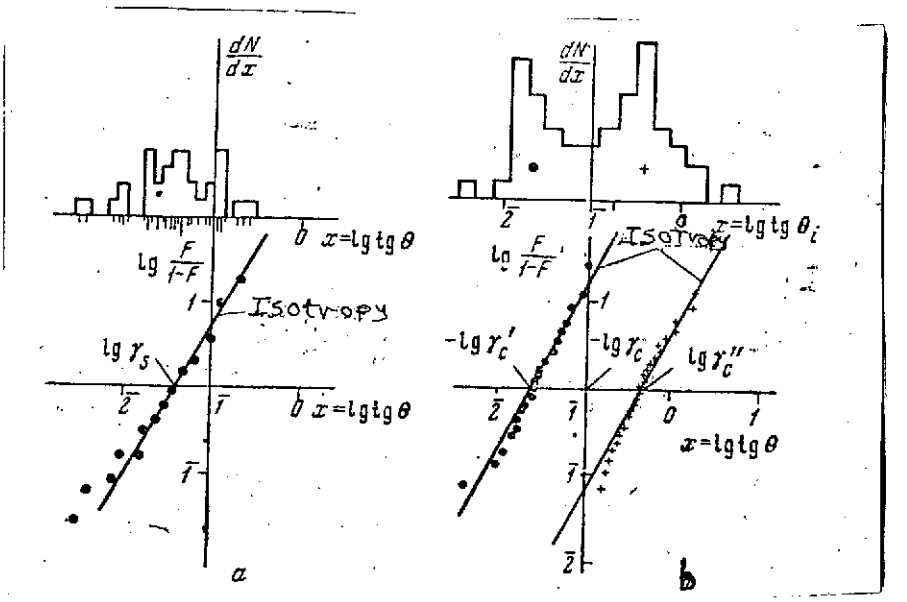

Fig. 40. Angular distributions in the lg tg θ - scale : a) a single-maximum distribution (shower (6 + 36) α), b) a two-maximum distribution.

In favourable cases ($\sigma \gg 0.8$), the maxima are so well separated that one can assume that there are two groups of particles, each emitted independently from its own centre. By considering each group separately, one can obtain the Lorence factor of the S-system for each group. It is found that, in many cases, the particles are isotropically emitted from a centre called emission centre. The emission centres are evidently moving relative to the C-system. If γ'_s and γ''_s are the Lorence factors of the two emission centres respectively, then their motion relative to the centre of mass of the colliding particles will be described by Lorence factor $\bar{\gamma}$:

$$\bar{\gamma}_1 = \frac{1}{2}\left(\frac{\gamma'_s}{\gamma_c} + \frac{\gamma_c}{\gamma'_s}\right); \quad \bar{\gamma}_2 = \frac{1}{2}\left(\frac{\gamma''_s}{\gamma_c} + \frac{\gamma_c}{\gamma''_s}\right). \tag{4.47}$$

These equations are obtained from the Lorence-factor addition formula (equation (4.24)) for the case of γ'_s , γ''_s and $\gamma_c \gg 1$.

The existance of two-maximum angular distributions, served as a starting point for the introduction for a new model of nuclear interactions, known as the fire-ball model. According to this model interacting nucleons form a cloud of excited matter - a fire-ball, which moves relative to the C-system and decays isotropically. From this point of view, it is assumed that an asymmetric shower appears as a result of the formation of a single fire ball, when the energy is not sufficient for the formation of two fire balls. After collision,

nucleons continue their motion, having lost part of their energy. Their Lorence factor in the C-system will be significantly greater than $\bar{\gamma}$ and from this, it is concluded that nucleons do not enter into the constitution of fire balls.

Another interpretation for the two-maximum angular distribution is given by the assumption that, at higher energies, the angular distribution in the C-system can be represented by $\cos^n \tilde{\theta}$. It is possible to prove that in this case, the angular distribution in the x-representation has to maxima if $n \gg 1$ [6].

8.3. Determination of energies of high-energy particles. Castagnoli's method

Equations (4.44) enable us to determine the energy of the colliding particles by the angular distribution of the created mesons. This method is valid in the very-high-energy regions, where $B \approx 1$. It plays an important role in nuclear investigations because the direct methods of measuring energy in a magnetic field or by scattering in emulsions, are not applicable at energies higher than 10^{11} eV. The first measurements of energy by means of this method were carried out by Castagnoli. In order to determine γ, Castagnoli suggested use of relation $\gamma^2 = \frac{E_1}{2mc^2}$, which is valid for the collision of identical particles at energies $E \gg mc^2$, and relation (4.3) :

$$\operatorname{tg}\theta_i = \frac{1}{\gamma} \cdot \frac{\sin\tilde{\theta}_i}{\cos\tilde{\theta}_i + v/\tilde{v}_i}.$$

In order to determine γ and E from these formulae, it is necessary to know velocity v of the C-system in the laboratory coordinate system and velocities $\tilde{v}_i$ of the particles in the C-system. However, since $E_1 > 10^{11} \gg mc^2$ by condition, then one may assume that v c and that the -mesons are produced with energies $E_2 \gg m_\pi c^2$ so that $\tilde{v} \approx c$. In this case, the formula takes the form of equation (4.3a) :

$$\operatorname{tg}\theta_i = \frac{1}{\gamma} \cdot \frac{\sin\tilde{\theta}_i}{\cos\theta_i + 1} = \frac{1}{\gamma} \operatorname{tg}\frac{\tilde{\theta}_i}{2}.$$

In order to determine angle θ_i, we use the fact that, in the C-system, there is a forward-backward symmetry in the particle emission. In other words, for each particle with momentum $\tilde{p}_i$, there is a conjugate particle with momentum $-\tilde{p}_i$ (in the case of production of two secondary particles, this condition follows from the law of the conservation of momentum). In the case of three particles or any other small number of particles, this condition is not fulfilled. However, if the number of particles is very large, the condition will be at least statistically fulfilled.

Taking the logarithm of the previous expression for each of the particles, and summing the results, we obtain

$$\frac{1}{n_s}\sum_{i=1}^{n_s} \ln \operatorname{tg}\theta_i = -\ln\gamma c + \sum_{i=1}^{n_s} \ln \operatorname{tg}\frac{\tilde{\theta}_i}{2}.$$

The last term vanishes because of symmetry. Then

$$\ln \gamma_C = -\frac{1}{n_s}\sum_{i=1}^{n_s} \ln \operatorname{tg}\theta_i = -\langle \ln \operatorname{tg}\theta_i \rangle. \tag{4.48}$$

The statistical error in measuring $\ln \gamma_c$ is evidently defined by the fluctuations of angular distribution. The measure of fluctuations is the dispersion of the angular distribution. Consequently,

$$\delta \ln \gamma_C = \pm \frac{\sigma}{\sqrt{n_s}}.$$

The existence of asymmetric showers violates the condition for the application of Castagnoli's method and makes uncontrolable the error in determining γ_c.

While using the previous formula, one must keep in mind that in real cases, v_i may be less than c[1]. Another source of error is the fact that only charged particles are observed while π^0-mesons are not. Because of fluctuations, the number of π^0-mesons emitted in the forward direction is not equal to those emitted in the reverse direction. The symmetry in charged particle emission will consequently be violated and the equations derived above will not be correct. These formulae are also not valid for asymmetric showers.

In order to visually demonstrate the previous results, the so-called F-method is often used. This method is based on the same previous formulae but enables one to represent the results in a graphic form. In order to apply this model one has to introduce another subsidiary assumptions which may not be in agreement experimentally. This is namely the assumption on the particle-emission symmetry of the C-system. In the case of an isotropic emission, the number of particles emitted in a solid angle $d\Omega$ is equal to

$$dN = N\frac{d\Omega}{4\pi} = N\frac{2\pi \sin\tilde{\theta}\, d\tilde{\theta}}{4\pi} = \frac{1}{2} N \sin\tilde{\theta} d\tilde{\theta}.$$

The fraction of particles emitted in the angular interval $0 - \tilde{\theta}$ is equal to

$$F = \frac{\Delta N(\tilde{\theta})}{N} = \frac{1}{2}\int_0^{\tilde{\theta}} \sin\tilde{\theta} d\tilde{\theta} = \frac{1}{2}(1-\cos\tilde{\theta}) = \sin^2\frac{\tilde{\theta}}{2},$$

Consequently,

---

1) This fact can be taken into account, if the particle distribution by velocities v_i is known. This can be made by introducing into equation (4.8) the additional term lg C (C 1.4 for nucleon-nucleon collisions at energies 100 - 300 GeV).

$$\operatorname{tg}^2\theta_F = \frac{1}{\gamma^2}\operatorname{tg}^2\frac{\tilde{\theta}}{2} = \frac{1}{\gamma^2}\cdot\frac{\sin^2\frac{\tilde{\theta}}{2}}{1-\sin^2\frac{\tilde{\theta}}{2}} = \frac{F}{1-F}\cdot\frac{1}{\gamma^2}.$$

Hence

$$\frac{F}{1-F} = \gamma^2\operatorname{tg}^2\theta_F.$$

Taking the logarithm of this expression, we obtain (figure 40)

$$\lg\frac{F}{1-F} = \lg\gamma^2 + 2\lg\operatorname{tg}\theta_F;$$

$$\lg\frac{F}{1-F} = \lg\frac{E_1}{2mc^2} + 2\lg\operatorname{tg}\theta_F. \qquad (4.49)$$

The slope of this line in the x-representation must be equal to 2 and the portion of the abscissa cut off by this line, determines the energy. This method is only valid for collision of identical particles, and although it suffers from several disadvantages, it is very widely used.

Schein's star, mentioned above, has about half its particles moving in the laboratory system with angles less than $\theta \sim 0.003$ radians. Using equations (4.22) and (4.41), one finds that the energy of this event is equal to $E_1 = 2\times10^{14}$ eV.

In all these methods, only charged particles are considered. One therefore does not obtain the Lorence factor of the C-system but of the symmetric system. Nevertheless, in many cases these two systems coincide.

In practice, the quantity $\lg\frac{F}{1-F} = f(\lg\operatorname{tg}\theta)$ is not always represented graphically by a straight-line. This indicates that the assumptions made are not always valid. If the angular distribution has two maxima in the x-representation, then the line in the integral F-representation is divided into two parts which are usually analysed separately (figure 40), and interpreted on the basis of the fire-ball model.

Opposed to this model, one sometimes uses an alternative model, in which nucleons in collision form a single emission centre, fixed in the C-system and which includes all nucleons (the Fermi-Landau method).

9. Transversal Momentum

The transversal momentum of the i-th particle is by definition, equal to $(p\perp)_i = p_i\cos\theta_i$. It is clear that the sum of the transversal momenta p is equal to zero if angles θ_i are measured from the direction of motion of the colliding particles. The typical property of $p\perp$ is that it does not change on transformation from a moving to a stationary coordinate system. For instance, the value of $p\perp$ is the same in both the C- and laboratory systems.

Various theories for multiple productions predict different magnitudes for $p_\perp$. This question will be discussed later. Experimentally, it was found that the mean value of transversal momentum $\langle p_\perp \rangle$ depends weakly on the energy of the primary particle, the angle of emission and the energy of secondary particles. The mean value $\langle p_\perp \rangle \simeq 0.35$ GeV (different experiments give slightly different results, varying from 0.28 to 0.40 GeV). Nevertheless, large values of transversal momenta, reaching $2 \div 3$ GeV, are also observed because transversal momenta are widely distributed around their mean value. The constancy of $\langle p_\perp \rangle$ is considered as the basis for many experimental analytical methods which will be mentioned below.

The transversal-momentum distribution is often approximated by

$$W(p_\perp) = \frac{2}{p_0^2} p_\perp \exp\left[-\frac{p_\perp^2}{p_0^2}\right], \tag{4.50}$$

where $p_0 = 2\langle p_\perp \rangle \pi^{-1/2}$. Figure 41 shows a typical transversal-momentum distribution. Experiment shows that the transversal momenta depend on the masses of particles, emitted after interaction. Most probably, heavy particles (kaons and barions) have large values of $\langle p_\perp \rangle$ as compared to pions

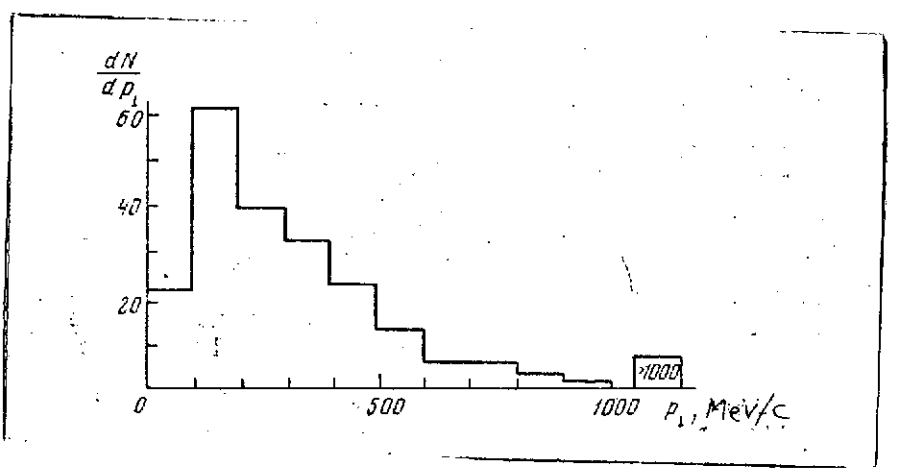

Fig. 41. Transversal-momentum distribution obtained in cosmic rays at an energy $\simeq 1000$ GeV.

10. Inelasticity Coefficient [16]

The inelasticity coefficient is defined as the ratio of the energy transferred to the newly created particles to the energy of the primary particles

$$\varkappa = \frac{\Sigma \varepsilon_i}{E_0}. \tag{4.51}$$

The partial inelasticity coefficient, on the other hand, is given by

$$\alpha_0 = \frac{\Sigma\varepsilon_{\pi^0}}{E_0}; \quad \alpha_K = \frac{\Sigma\varepsilon_K}{E_0} \text{ и др.}, \tag{4.52}$$

where $\Sigma\varepsilon_{\pi^0}$ is the energy transferred to π^0-mesons, $\Sigma\varepsilon_K$ the energy transferred to kaons, etc. Evidently, if ξ is the fraction of energy remaining with the primary nucleon, then

$$\mathcal{K} = (1 - \xi) E_0. \tag{4.53}$$

In the case of a symmetric shower, coefficient K is invariant under Lorence transformations. This can easily be shown by using equation (4.51) and the energy transformation formulae, given by equations (4.12)[1].

It is possible to measure the inelasticity coefficient in the C-system even if the energy of the primary particle is unknown. In the case of a nucleon-nucleon collision, when the energy of all secondary particles are already measured, we obtain

$$\tilde{\mathcal{K}} = \frac{\Sigma\tilde{\varepsilon}_i}{2\gamma_C m_p c^2} = \frac{\Sigma(\varepsilon_i - p_i c\cos\theta_i)}{2m_p c^2}, \tag{4.54}$$

where ε_i and p_i are the energy and momentum of particle i in the L-system, m_p is the proton mass and γ_c is the Lorence factor of the C-system. At high energies, however, measurement of ε_i often becomes impossible.

By measuring the particles of the backward cone, one is able to determine the inelasticity coefficient in the mirror coordinate system, $\mathcal{K}_M$. In this case, the main contribution to $\mathcal{K}_M$ is due to particles, emitted at large angles, since these particles are relatively easy to measure. Actually, $\cos\theta_i \simeq 1$ and $\varepsilon_i \simeq p_i c$ for particles of the front cone and are thus not significant for determining $\mathcal{K}_M$.

It is sometimes possible to identify the recoil nucleon, which often has a small energy and belongs to the group of "grey" tracks. The energy of such a δ-nucleon in the mirror system is equal to

$$E_M = \gamma_0 (E_p - pv\cos\theta_p), \tag{4.55}$$

where γ_0 is the Lorence factor of the primary nucleon, E_p, p and $\cos\theta_p$ are

1) In this case, it is necessary to take into account that in symmetrical collisions, the energies of nucleons after collision are equal.

quantities, related to the recoil nucleon, while v is the velocity of the M-system. Then

$$\mathcal{K}_M = \frac{E_0 - E_M}{E_0} = 1 - \xi_M = 1 - \frac{E_p - pv\cos\theta_p}{m_p c^2}. \tag{4.56}$$

Consequently, it is also unnecessary in this case to know the primary energy of nucleon-nucleon collisions.

One can show a series of properties for the partial inelasticity coefficient. If all the secondary particles are pions, then in the case of their direct generation, the mean value of the fraction of energy transferred to photons

$$\langle \alpha_0 \rangle = \frac{1}{2} \langle \alpha_{\pi^\pm} \rangle, \tag{4.57}$$

where $\langle \alpha_{\pi^\pm} \rangle$ is the mean fraction of energy transferred to charged π-mesons.

By studying this relation, one can discover new photon sources, if these exist. For instance, equation (4.57) would be violated, if a considerable amount of singlet η°-mesons which mainly decay by neutral modes (into π°-mesons and photons), are generated. Up till now, there is no reliable evidence for the validity of relation (4.57).

Experiments :

Quantity $\alpha_\circ$ is mainly measured by means of ionization calorimeters. The photons' energy is determined by the maximum of the electron-photon cascade. The distribution of $\alpha_\circ$ is very wide. One is often met with values of $\alpha_\circ$ close to zero and to unity. Most of the experiments led to a mean value $\langle \alpha_\circ \rangle \approx 0.15$–$0.20$ for the interaction of nucleons with carbon nuclei and other not-very-heavy nuclei.

The total inelasticity coefficient is measured both in cosmic rays and in accelerators. Taking equation (4.57) into consideration, one can determine $\langle \mathcal{K} \rangle$ by the value of $\langle \alpha_\circ \rangle$ or $\langle \alpha_{\pi^\pm} \rangle$. In the later case, one applies a Wilson chambers in a magnetic field, in order to be able to measure the energy of the charged particles. In experiments with emulsions, use is made of the transversal momentum constancy (Section 9) :

$$\varepsilon_i = \langle p_\perp \rangle \operatorname{cosec} \theta_i, \tag{4.58}$$

then

$$\mathcal{K} = \frac{3}{2} \langle p_\perp \rangle \frac{\sum_{i=1}^{n_s} \operatorname{cosec} \theta_i}{\gamma_0 m c^2}. \tag{4.59}$$

Quantity $\gamma_o = 2\gamma_c^2$ (as $\gamma_c \gg 1$). This is often determined by means of Castagnoli's method, though the presence of asymmetric showers makes this determination unreliable. In recent investigations, the Lorence factor γ_o was determined by means of the multiple-scattering method. For this purpose, investigation was undertaken for cases in which the initial nucleus disintegrated into its constituting nucleons after collision. A part of these nucleons interacted with the nucleons of the target nucleus and generated mesons. However, experiment showed that about half the nucleons of the initial nucleus almost received no momentum and were consequently sharply collimated in a very narrow scattering angle.

We shall now investigate the behaviour of these above-mentioned nucleons. Since the energies of all the nucleons in the beam must be the same (a slight difference in energy might occur due to the Fermi momenta), the conditions for applicability of Castagnoli's methods will then be fulfilled in a better way. The accuracy of the method increases by $\sqrt{n_p}$ times, where n_p is the number of nucleons in the beam. The multiple-scattering method gives valid results at energies less than 200 - 300 GeV. Castagnoli's method should be used at higher energies.

Lohrmann et al [24*] measured the energy by the relative scattering of protons in an emulsion rouleau. They found that, in the collisions of nucleons with the light nuclei of the emulsion ($N_h \leqslant 5$), the inelasticity coefficient was nearly 0.5 at $E_o \simeq 250$ GeV (equation (4.59) was used). A similar result was obtained by Koshiba et al [25*] in a higher energy region ($\simeq 1000$ GeV) (figure 42). These authors obtained the distribution of total inelasticity coefficients $\mathcal{K}_M$ in the mirror system, by studying the recoil nucleons (equation (4.56)). The distribution of coefficients $\mathcal{K}_M$ was very wide and involved values from 0.05 to 1.

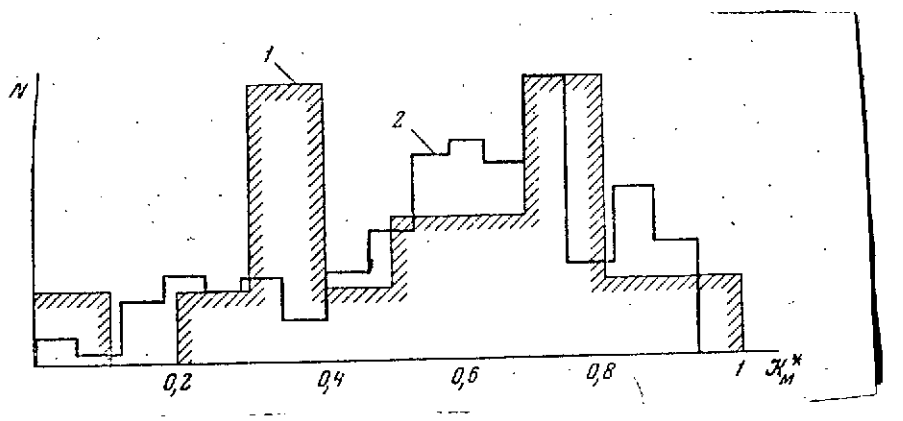

Fig. 42. The distribution of energy fraction, transferred to mesons in nucleon-nucleus collisions: 1- cosmic rays (1000 GeV), 2- acceleration (25 GeV).

The most probable value was apparently near one-half. In accelerators at energies of 10 ÷ 30 GeV, the mean value of the total inelasticity coefficient $\langle K \rangle \simeq 0.5$. Consequently, inelasticity coefficients strongly fluctuate from one case to another but on the average, nucleons after interaction always keep half of the energy. The mean inelasticity coefficient is near to $\langle K \rangle = 0.5$, in a wide energy interval extending from 10 to 10^3 GeV. The study of penetration of cosmic radiation through the atmosphere shows that this situation still holds at much higher energies (see chapter 9).

Accordingly, inelasticity coefficients parallel with the interaction cross sections and the transversal momenta are very stable characteristics. In the mean time, the small value of $\langle K \rangle$ sums to prefer the peripheral nature of the interaction of nucleons. The nucleon apparently does not change its individuality during the collision process and only looses a small part of its energy on the production of new particles.

11. Energy Spectra of the Created Particles

Difficulties in determining the particle energies in the interval of cosmic energies are responsible for the fact that uptil now, we have no extensive information on the energy distribution of secondary particles at different primary energies. Most of the results, obtained in cosmic rays deal with photon spectra.

While studying secondary particle spectra in cosmic rays, it is necessary to take into consideration the wide energy distribution of primary particles, i.e. collision kinematics. Particles having the same energy in the C-system, which result from the interaction of primary particles of different energies, will naturally have different energies in the L-system.

$$\frac{\varepsilon_1}{\varepsilon_2} = \frac{\gamma_{C_1}}{\gamma_{C_2}},$$

where γ_{C_1} and γ_{C_2} are the Lorence factors of the primary particles in the C-system. It is thus necessary to study the energy spectra either in the C-system or after normalizing to the same primary energy in the L-system.

11.1. Form of the energy spectrum in the L-system

The energy distribution of particles may be obtained experimentally in accelerators. The energy differential spectrum has a maximum in the region of small energies of secondary pions. At pion energies $\varepsilon > 0.1\ E_0$, the energy spectrum may be represented by an exponential function. Denoting ε / E_0 by u, we obtain

$$N(u)\,du = \frac{n_s}{u_0} e^{-u/u_0} du. \tag{4.60}$$

The energy spectrum on the particle emission angles. At smalle angles, quantity u_o is large, i.e. the spectrum slopes more gently. Evidently, the integral spectrum $N(>u)$ is described by the same exponential function. Figure 43,a shows a spectrum, obtained with an accelerator, for nucleon nucleon collisions. Averaging over all angles, quantity u_o is near to 0.07.

One can use emulsion chambers or the controlled-emulsion method to study the energy spectrum of photons, produced in a special target located at some distance from the emulsion chamber. The distance is chosen in such a manner, that the π^o-meson-decay photons have enough time to scatter over a large distance so that the cascades they produce in the emulsion-lead "sandwich" could be studied separately. A group of photons, produced in a single interaction, will then form a "photon family".

Showers produced by each photon are observed in the emulsion. The photon

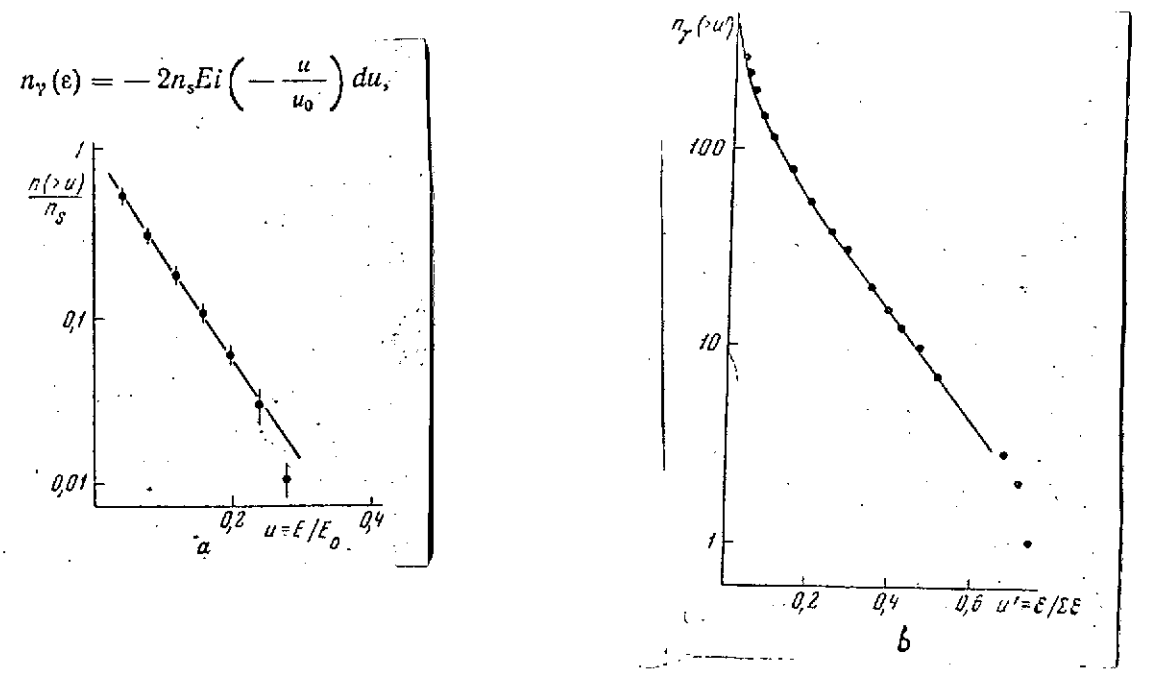

Fig. 43. Integral energy spectra of secondary particles. a- Spectrum of π-mesons obtained on an accelerator at 20 GeV, in nucleon-nucleon collisions. b- Spectrum of photons, appearing in the interaction of cosmic nuclear-active particles with light nuclei (Fowler, 1964). The energy of separate photons is divided by the total energy of the family photons.

energy is determined by using the methods discussed in chapter 2, section 11. If the spectrum of π^o-mesons produced in a single act is exponential, it is then easy to show that the spectrum of the decay photons is given by

while the integral spectrum, obtained by integrating the previous expression, is in the form of

$$n_\gamma(\geq \varepsilon) = 2n_s\left[e^{-u/u_0} + \frac{u}{u_0} Ei\left(-\frac{u}{u_0}\right)\right]. \tag{4.61}$$

where $Ei\left(-\frac{u}{u_0}\right)$ is the integral exponential function.

In most cases, the energy of the primary particle is unknown. Therefore, it is difficult to represent the photon distribution as a function of quantity u. For the purpose of normalization, the energy of each photon of the family is divided by the total energy of the family photons (figure 43,b) :

$$u' = \frac{\varepsilon}{\sum_i \varepsilon_i}.$$

Quantity $\sum \varepsilon_i$ is related with the primary energy by the inelasticity coefficient α_0. If α_0 is the fraction of energy, transferred to photons in a single act, then $\sum_i \varepsilon_i = \alpha_0 E_0$ and

$$u' = \frac{\varepsilon}{\alpha_0 E_0}.$$

This spectrum will evidently be less sharp than when expressed in terms of u. Quantity u'_0 is given by

$$u'_0 = \frac{u_0}{(\alpha_0)_{eff}} \tag{4.62}$$

where $(\alpha_0)_{eff}$ is the effective value of quantity α_0, after taking into account the resolving power of the instrument.

Any instrument, in which the choice of events is made by the value of the energy transferred to photons, will mainly register in cosmic experiments, the cases where the energy transferred to the photons is near its maximal value. This effect is easy to study on the example of impulsive instruments, considered in chapter 4, Section 3. Number N_I of registered impulses with energy transferred to photons $\sum \varepsilon$, is equal to

$$N_I(\Sigma\varepsilon) = (1 - e^{-x/\lambda}) \int_{\Sigma\varepsilon}^{\infty} N(E_0)\, dE_0 W(E_0, \Sigma\varepsilon),$$

where $N(E_0)$ is the cosmic-ray particle spectrum, and W the probability that an energy of $\sum \varepsilon$ is tran ferred to photons. In the first approximation, the cosmic-ray spectrum may be represented by a power function :

$$N(E_0)\, dE_0 = AE_0^{-2,7} dE_0.$$

The probability W apparently has the same value for all energies E_o, i.e.

$$W(E_0, \Sigma\varepsilon)\, d(\Sigma\varepsilon) = W\left(\frac{\Sigma\varepsilon}{E_0}\right) d\left(\frac{\Sigma\varepsilon}{E_0}\right) = W(\alpha_0)\, d\alpha_0.$$

Then, assuming that $N(E_o) = AE_o^{\gamma}$, we obtain

$$N_I(\Sigma\varepsilon)d(\Sigma\varepsilon) = (1 - e^{-x/\lambda}) N(\Sigma\varepsilon) d(\Sigma\varepsilon) \int_0^1 \alpha_0^{\gamma-1} W(\alpha_0)\, d\alpha_0.$$

We see that the number of impulses is decreased by $\int_0^1 \alpha_0^{\gamma-1} W(\alpha_0) d\alpha_0 = \langle \alpha_0^{\gamma-1} \rangle$ times as compared to the number of primary particles. This is equivalent to an energy of $\sqrt[\gamma-1]{\langle \alpha_0^{\gamma-1} \rangle} = (\alpha_0)_{eff}$ times (in the case of a power spectrum). In other words, $\Sigma\varepsilon = (\alpha_0)_{eff} E_0$, from where equation (4.62) follows. Quantity $(\alpha_0)_{eff}$ depends on the form of distribution $W(\alpha_o)$. The main contribution of $(\alpha_o)_{eff}$ is due to the maximal values of α_o.

Figure 43,b shows a normalized photon spectrum, measured by means of emulsion chambers, for quantity $\Sigma\varepsilon \geqslant 3000$ GeV. The energy spectrum may be approximated by formula (4.61) with $u_o \simeq 0.05$. The value of u_o obtained in cosmic rays indicates that the form of the normalized pion spectrum in the L-system changes slightly with the energy.

Mean energy of pions in the C-system

The mean energy of pions in the C-system may be obtained from the values of the inelasticity coefficient and the multipolarity, and also by the direct measurement of energy of separate pions in the L-system with the subsequent calculation of the corresponding energy in the C-system. Many experiments have shown that the mean energy of pions in the C-system increases with the increase of primary particle energy. This increase proceeds in such a manner that the total inelasticity coefficients remains constant (figure 44) :

$$\langle \mathcal{K}_C \rangle = \frac{3}{2} \frac{\langle n_s \rangle \langle \varepsilon \rangle}{2\gamma_C m_p c^2} = \text{const.} \tag{4.63}$$

Assuming that $n_s \simeq E^{1/4}$ (see Section 7), we obtain from equation (4.63) that

$$\langle \varepsilon \rangle \sim \frac{\gamma_C}{\langle n_s \rangle} \sim \gamma_C^{1/2}. \tag{4.64}$$

Spectrum of pions in the C-system

The energy distribution of pions in the C-system was studied by means of ionization calorimeters and Wilson chambers in magnetic fields at primary particle

energies $E_o \sim 200$ GeV. The differential energy spectrum was well described by Planck's formula, with the exception of a small number of particles near the high energy limit (figure 45) :

$$\frac{dn}{d\varepsilon} = \frac{A\varepsilon^2}{\exp(\varepsilon/kT)-1}, \tag{4.65}$$

where $kT \approx \mu c^2$

It is assumed that the most energetic pions are produced in the decay of isobars[1)], which are excited states of a nucleon. Isobars occur as a result of the resonant excitation of nucleous, and depending on the degree of excitation (characterizing the isobar's mass) the isobar decays into a nucleon, a single or a few mesons. The typical property of pions obtained from isobars is their high energy, which is proportional to the energy of the parent isobar in the L-system. According to this point of view, the preserved nucleon must fly in an excited state. Pions, whose energy distribution is described by Planck's formula appear in processes, where the most important role is played by statistical processes in which the excitation energy is uniformly distributed among all degrees of freedom.

The nature of excited states serving as sources of particle emission is not clear. Processes of multiple production of particles are often called

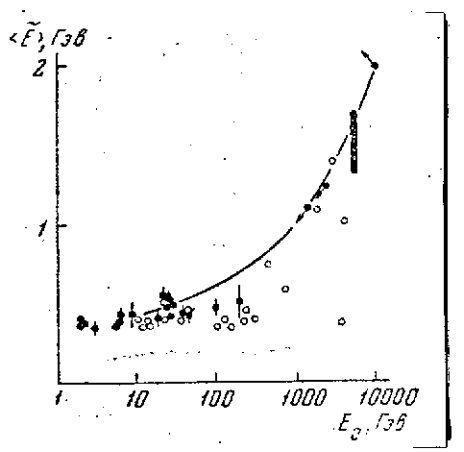

Fig. 44. Mean energy of pions in the C-system. The solid curve shows the expected dependence in the case when $\mathcal{K}$ does not depend on energy and when multipolarity $n_s \sim \ln E_o$.

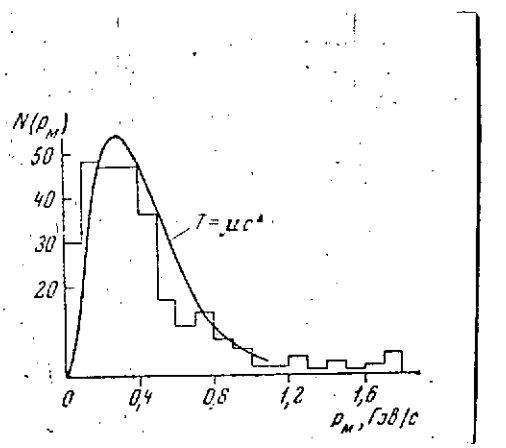

Fig. 45. Differential spectrum of particles in the C-system.

1) Isobaric pions also contribute in the low energy region. When the isobar decays into a pion and a nucleon, the spectrum of the decay mesons will be uniform in a given energy interval, depending on the mass of the isobar.

"pionization" (a term, suggested by Cocconi that has a "hybrid" sound).

12. Interaction of Nuclei at High Energies

In studying the interaction of nuclei, one may ask whether the nucleus interacts as an entity or the process of interaction is reduced to a sum of interactions of individual nucleous.

If we consider the collision of a nucleus with a stationary nucleon, we may then draw a picture for this process by analogy with the "mirror" process of a nucleon colliding with a nucleus. For this purpose, it is necessary to transform the momenta and angles of all particles into the mirror coordinate system.

Let us, for instance, find the mean angle of particle emission in the laboratory system when a primary nucleus interacts with a stationary nucleon. The nucleus distingerates in its coordinate system in such a manner that the disintegration products (protons and alpha particles) are isotropically emitted. Isotropy means that in the M-system, the number of particles emitted with angle θ_M is equal to

$$\frac{d\Omega}{4\pi} = \frac{1}{2}\sin\theta_M d\theta_M = \frac{1}{2} d(\cos\theta_M).$$

The mean value $\langle tg^2\theta \rangle$ is given by

$$\langle tg^2\theta\rangle = \frac{1}{2\gamma_0}\int_0^\pi \frac{\sin^2\theta_M d(\cos\theta_M)}{(\cos\theta_M + \beta_0/\beta_M)^2}.$$

Integrating, we obtain (for $\beta_0 \gg \beta_M$) :

$$\langle tg^2\theta\rangle \simeq \frac{2}{3}\cdot\frac{\beta_M^2}{\beta_0^2}\cdot\frac{1}{\gamma_0^2}.$$

The mean energy of particles producing black tracks in the emulsion is equal to

$$\varepsilon_i = \frac{1}{2} m_i \beta_M^2 c^2,$$

Consequently

$$\langle tg^2\theta\rangle \simeq \frac{4}{3}\cdot\frac{\varepsilon_i}{m_i\beta_0^2c^2\gamma_0^2} \simeq \frac{4}{3}\cdot\frac{\varepsilon_i m_p^2}{E_{0m_i}^2},$$

where E_0 is the energy of each nucleon in the primary nucleus. Since $\varepsilon_i \ll E_0$, then

$$\langle tg^2\theta\rangle \simeq \langle\theta^2\rangle;$$

and

$$\sqrt{\langle\theta^2\rangle} = \sqrt{\frac{4\varepsilon_i}{3m_i}\cdot\frac{m_p}{E_0}}.$$

The mean energy of an alpha particle emitted by the disintegrating nucleus is close to 10 MeV. Substituting into the latter equation the numerical values of $\mathcal{E}_i$ and $m_i = 4\ m_p$, we obtain

$$\sqrt{\langle\theta_\alpha^2\rangle} = \frac{0{,}056}{E_0} \tag{4.66}$$

where E_0 is in GeV. The angle that corresponds to the maximum energy of the alpha particles $(\mathcal{E}_i)_{max} \approx 30$ MeV :

$$\langle\theta_{max}\rangle \sim \frac{0{,}12}{E_0}. \tag{4.67}$$

Therefore, alpha particles produced by the disintegration of the primary nucleus are concentrated in a very narrow angular region. When the energy E_0 of each nucleon in the primary nucleus is for instance equal to 100 GeV (the total energy of the nucleus is equal to 100 A GeV, where A is its mass number), then the value of $\langle\theta_{max}\rangle = 1.2 \times 10^{-3}$ radians, i.e. about 0.07°. The mean angle of proton emission is

$$\sqrt{\langle\theta_p^2\rangle} = \frac{0{,}12}{E_0}. \tag{4.68}$$

This result concerns only protons producing black tracks in the emulsion. The existence of δ-nucleons with energies of several hundreds of MeV (grey tracks) leads to the fact that protons may be emitted at considerably larger angles than given by equation (4.68). Equations (4.66 - 4.67) are used for determining the energy when several alpha particles are found among the disintegration products.

The product of disintegration of the primary nucleus are called fragments and the process itself fragmentation. The number of fragments of a given type per single interaction is called fragmentation parameter. Fragmentation parameters depend on the dimensions of the incident and target nuclei. Nuclei, having atomic numbers (or charges Z) close in magnitude are called, in cosmic experiments, groups. Notations used for each group are given in table 20.

Fragmentation parameter P_{ij} of a nucleus denotes the number of fragments of type j, produced in the fragmentation of a nucleus of type i. Table 21 gives fragmentation parameters P_{ij} for different nuclei in emulsion and in air. Data, given in the table shows that the largest number of disintegration fragments is that of alpha particles which are usually present in a number exceeding unity.

Table 20

z	Notation	Name of group
1	p	Protons
2	α	α-particles
3÷5	L	Light nuclei
6÷9	M	medium nuclei
≥10	H	heavy nuclei
10÷14	H_1	—
15÷19	H_2	—
≥20	H_3, VH	Very heavy nuclei

The study of meson generation by nuclei shows that, in the collision of the primary nuclei with the light nuclei of the emulsion, the multipolarity of the secondary particles increases in proportion with A/Z, where A is the mass number of the primary nucleus. In other words, half of the nucleons of the nucleus take part in the interaction. The other nucleons emerge in the form of an almost monoenergetic beam, keeping their primary energy almost unchanged.

The inelasticity coefficient also indicates that, on the average, only half of the nucleons of the nucleus participate in the reaction. If the energy

Table 21

i	j					Reference
	Material	H	M	L	α	
H	Emulsion air	0,31±0,07 0,17±0,03	0,40±0,09 0,29±0,04	0,10±0,03 0,26±0,04	1,64±0,20 1,34±0,12	[6,8]
M	Emulsion air	— —	0,10±0,03 0,11±0,02	0,35±0,04 0,24±0,03	1,42±0,11 1,00±0,08	
L	air	—	—	0,15±0,05	0,51±0,08	

of each nucleon in the primary nucleus is E_0, so that the energy of the nucleus is AE_0, then the inelasticity coefficient is equal to

$$\mathcal{K}' = \frac{\Sigma \varepsilon_i}{AE_0} \sim 0{,}25.$$

The inelasticity coefficient per interacting nucleus is then equal to

$$\varkappa = \frac{\Sigma \varepsilon_i}{E_0 A/2} \sim 0{,}5.$$

Sometimes, the nucleus remains unchanged after collision. In this case, the multipolarity of secondary particles is almost the same as in nucleon-nucleon collisions (see reference [6] for more details).

13. Theoretical Interpretation of Multiple Production of Particles

13.1. Main assumptions

The most typical features of high-energy nuclear interaction are the large interaction cross sections (approximately equal to the geometrical ones) and the multiple production of mesons. Attempts for the theoretical interpretation of the multiple generation of particles was done nearly a quarter of a century ago by Heisenberg. His model is still being investigated uptill today. It was shown recently that Heisenberg's model is close in idea to a Landau theory on which we shall speak in more detail. Lewis and Oppenheimer suggested a model for particle production analogous to bremsstraalung. They assumed that the nucleon was surrounded by a cloud of mesons exactly as the electron was surrounded by a cloud of virtual photons. During collision, the mesons are "shaken" off the nucleon. Later on, a number of models were suggested amongst which was the model suggested by Fermi and improved later by Landau. It is important to note that this theory, as developed by Landau, is based on the deep knowledge of the structure of matter. Its verification is consequently of great importance for checking our ideas on the behaviour of matter at infinitesimal distances. The most logically developed version of the theory is based on the concept that nuclear matter behaves as a relativistic liquid as well as on the following general hypotheses :

1. Our ideas on space and time are valid up to the smallest distances and time intervals.
2. "Multiple production" means the excitation of a large number of degrees of freedom, so that the system may be considered as a classical system.
3. The interaction is so strong, that the momentum of the incident particle is practically completely transferred during collision.

Further construction of the theory is strictly logical :

A. It is more convenient to consider the nucleon-nucleon collision in the C-system. The energy of the nucleons in the C-system is given by

$$\tilde{E} = \sqrt{\frac{mc^2 E}{2}}; \quad \gamma = \frac{\tilde{E}}{mc^2} = \sqrt{E/2mc^2}. \tag{4.69}$$

Consequently, the nucleons will have in the C-system, the form of discs compressed by $\gamma = \tilde{E}/mc^2$ times in the longitudinal direction. The longitudinal dimension of

the nucleon will then be

$$\Delta = \frac{2r_0}{\gamma} = 2r_0\sqrt{\frac{2mc^2}{E}}. \tag{4.70}$$

while the diameter of the nucleon, equal to $2r_0$ is in an order of magnitude equal to $\hbar/\mu c$, where μ is the meson mass. Accordingly,

$$\Delta \sim \frac{\hbar}{\mu c}\sqrt{\frac{2mc^2}{E}}.$$

At energies $\simeq 10^{12}$ eV, this dimension becomes equal to $\simeq 10^{15}$cm.
B. The system may be considered classical if the action $\delta S \gg \hbar$, i.e. if $\Delta E \Delta t \gg \hbar$,

$$\delta S \approx \mathcal{K}\tilde{E}\frac{\Delta}{c} \sim \frac{\hbar}{\mu c^2}\sqrt{\frac{2mc^2}{E}}\,\mathcal{K}\sqrt{\frac{mc^2E}{2}} \simeq \frac{m}{\mu}\mathcal{K}\hbar, \tag{4.71}$$

where $\mathcal{K}$ is the inelasticity of the nuclear interaction. Consequently, the above condition reduces to the following :

$$\frac{m}{\mu}\mathcal{K} \gg 1; \quad 7\mathcal{K} \gg 1. \tag{4.72}$$

Even if $\mathcal{K} = 1$, condition (4.72) will be sufficiently fulfilled. This means that the hydrodynamical theory can be meaningfully applied even to collisions with inelasticity coefficients equal to unity. These conditions are best of all applied to central, or so called head-on nucleon collisions.

Accordingly, the assumption of the classical character of the interaction is on the border line of its validity. The situation is much better, when collision between two nuclei of mass number A is considered. The condition of the classical nature of the system then becomes

$$\mathcal{K}\frac{m}{\mu}A \gg 1.$$

Therefore, condition (4.72) is well fulfilled for heavy nuclei ($A \gg 1$) even for collisions with $\mathcal{K} < 1$. If we assume that this condition holds true sufficiently well, we then definitely arrive to the hydrodynamical formation of the problem. Indeed, a classical system of an infinite number of degrees of freedom, consisting of strongly interacting particles must be a hydrodynamical system or a liquid. Our system however will not be a usual liquid but a relativistic one.

13.2. Fermi's theory

Fermi made the first attempt to consider multiple production processes using statistical methods. Fermi's hypothesis consisted in the following : The two colliding nucleons form a common system, in which the whole energy of the nucleons will be separated. At the expense of this energy the compound system will be strongly heated to temperature T. Inside the system, extremely strong interactions between particles (the quanta of the nuclear field) will take place and lead to an equilibrium state, which may be considered statistically. The volume in which energy is separated is a relativistically compressed sphere of radius $r \sim \frac{\hbar}{\mu c}$, i.e.

$$\Omega = \Omega_0 \frac{mc^2}{\tilde{E}}; \quad \Omega_0 = \frac{4}{3}\pi r^3 \sim \frac{4}{3}\pi\left(\frac{\hbar}{\mu c}\right)^3. \tag{4.73}$$

After equilibrium is established, the second stage starts, namely the emission of the created particles. Fermi suggested that the particles in the emission state do not interact with each other. This led Fermi to the thermodynamics of an ideal gas and not to hydrodynamics. Using the Stephan-Boltzmann law, according to which the energy density $\mathcal{E}$ is given by $\mathcal{E} \sim (kT)^4$, Fermi obtained

$$\frac{\tilde{E}}{\Omega} \sim (kT)^4; \quad \tilde{E} \sim \frac{mc^2}{E}\Omega_0 (kT)^4; \quad \tilde{E} \sim \sqrt{mc^2\Omega_0}\,(kT)^2. \tag{4.74}$$

The energy of each particle is proportional to kT and hence the particle density is equal to

$$\Delta n \sim \tilde{E}/\Omega kT \sim (kT)^3;$$

The total number of particles is then given by

$$n \simeq \Omega (kT)^3 \sim \Omega \tilde{E}^{3/2} \sim \Omega_0 \frac{mc^2}{\tilde{E}} \tilde{E}^{3/2},$$

i.e. $n \sim \tilde{E}^{1/2}$. Noting that $\tilde{E} \sim E^{\frac{1}{2}}$, we obtain

$$n \sim E^{1/4}. \tag{4.75}$$

Consequently, the multipolarity in Fermi's theory is proportional to the 4-th root of the energy in the laboratory system. Hence, according to Fermi, particles are produced practically at the moment of collision.

13.3. Landau's theory [30*]

Landau strongly criticized Fermi's point of view, described above. Actually, in the presence of a strong interaction between particles, one cannot generally speak about the number of particles. As a result of the strong interactions, the particles are continuously created and annihilated. This will continue as far as interaction between particles takes place. Consequently, the number of particles is well defined, only when they are separated by such distances that their mutual interactions practically vanish. It is natural to assume that the creation of particles ends when the energy of particles falls to a value in the order of the rest energy of a π-meson, i.e.

$$kT_{cR} \sim \mu c^2.$$

This is a very important difference between the Landau and Fermi theories. According to Fermi, particles are produced at a temperature $kT \gg mc^2$. Therefore different particle numbers in Fermi's theory are only determined by the number of states available for the different particles. Consequently, according to Fermi's theory, a large number of nucleon-antinucleon pairs must be produced after collision. The ratio of the number of nucleons and π-mesons will then be equal to

$$\frac{N_p}{N_\pi} = \frac{8}{3},$$

because a nucleon can have 8 states :

$$\left.\begin{array}{l} p\tilde{p}\,(s = +1/2,\ -1/2) \\ n\tilde{n}\,(s = +1/2,\ -1/2) \end{array}\right\} \text{8 states}$$

where s is the spin, while a π-meson can have only three states : π^+, π^- and π^0.

In Landau's theory, on the other hand, the main part of the particles are π-mesons because of the low temperature at the moment of creation of particles; $T_{cr} \sim \mu c^2$. Other particles will be rarely created. In the case of equilibrium, the number of particles of other masses will be proportional to

$$e^{-mc^2/kT_{cR}} \sim e^{-m/\mu}.$$

It is well known that, in photo-emulsion experiments, π-mesons are found to be more than 80% of all particles. This result is in strong disagreement with the predictions of Fermi's theory but consistent with the conclusions of Landau's theory.

a) Multipolarity

Both Fermi's and Landau's theories give identical results as far as one is concerned with the dependence of multipolarity on energy. In both theories, the particle multipolarity is defined in terms of the entropy of the system. Indeed

$$dn \sim \frac{d\mathcal{E}}{kT} \sim \frac{d\widetilde{E}}{k\Omega T} \sim dS, \quad dS = \frac{dQ}{T},$$

Where S is the entropy of the system.

In Fermi's theory, the number of particles is proportional to the entropy at the initial moment, i.e. $n \sim S_i$, while in Landau's theory $n \sim S_f$ at the final moment. Since the liquid is Landau's theory is ideal, with no friction in it, the expansion process proceeds without energy dissipation, i.e. isentropically. Consequently $S_i = S_f$ and

$$n_s \sim E_0^{1/4} \sim \widetilde{E}^{1/2}. \tag{4.76}$$

One can thus conclude that the mean energy of pions in the C-system increases with energy (because of the constancy of the inelasticity coefficient $K \approx 1$) $\langle \varepsilon_c \rangle \sim \gamma_c^{1/2}$. This is in agreement with the corresponding experimental results (see Section 11).

b) Angular distribution

Angular distributions predicted by Fermi's and Landau's theories are different. If the energy is very large, then the angular distributions predicted by Fermi's theory will be isotropic because the particles do not interact with each other at the emission stage, while at the initial stage, equilibrium has been established so that the energy has been uniformly distributed over all degrees of freedom.

In Landau's theory, the presence of a strong interaction makes it necessary to consider the equation of motion for the liquid. Since the volume is strongly compressed at the initial moment, then expansion will have a one-dimensional character at first. Furthermore, when the particles are sufficiently separated, one must take into consideration their divergence in the different directions. By solving the equation of motion of the liquid, Landau showed that the angular distribution would be highly isotropic. Particles would be concentrated on the direction of motion of the primary particles. We have already mentioned that in Schein's star, two sharply defined particle cones were observed. If we make a transformation into the centre-of-mass system, we obtain two cones one in the front and the other in the back direction. This is in complete agreement with Landau's theory. A large number of such showers have now been observed; they are presently called "jets". The angular distributions predicted by Landau's theory are described in x-representations by a Gaussian curve with a dispersion

depending logarithmally on energy. At energies $> 10^3$ GeV, Landau's theory predicts very large values for the dispersion, $\sigma \sim 0.9 \div 1.2$, but only a single maximum for the angular distribution.

c) Transversal momentum

We still have to speak about a very important nuclear interaction characteristic, namely the transversal momentum $p_\perp = p \sin\theta = \tilde{p} \sin\tilde{\theta}$. The transversal momentum depends on the thermal motion of particles inside the volume. In Fermi's theory, this momentum is defined by the initial temperature ($T \sim \sqrt{\tilde{E}}$), and hence increases with energy. In Landau's theory, the energy exchange continues up to $kT_{cr} \sim \mu c^2$. Consequently, the transversal momentum $\tilde{p}_\perp \sim \mu c$ and will not depend on the energy of the interacting particles. This conclusion of the Landau theory is in good agreement with experiment. It is found that the transversal momentum of π-mesons is approximately equal to $2m_\pi c^2$ (0.35 GeV). Consequently, Landau's theory is apparently in better agreement with experiment than Fermi's. The theory however, does not yet give a complete picture for the phenomena. For instance, it does not consider the establishment of statistical equilibrium nor gives the specific conditions for its establishment.

As mentioned above, Landau's theory can only be applied to collisions, with an inelasticity condition $\mathcal{K} = 1$[1].

Theory cannot tell us in which cases the inelasticity coefficient is equal to unity and in which case it is not. Experiment shows that the mean value of the inelasticity coefficient is equal to 0.5, i.e. much less than 1, so that half of the energy is carried away by a single nucleon.

13.4. Other theories

The obvious disagreement between Landau's theory and the experimental facts stimulated a whole series of attempts to improve the theory and make it agree with the experiment. One of these attempts was to consider the initial stage of collision. In the first moment of collision, a shock wave occurs in the nuclear liquid. When the shock wave reaches the nucleon boundary, the emission of particles starts immediately. Calculations show that the shock wave carries a considerable fraction of the energy while most of the particles are behind the front of the shock wave. This means that the front of the shock wave involves a small number of particles having a large energy. Quantitative estimates are not in disagreement with the assumption that there is only one particle at the front of the shock wave and that this particle carries an energy of 0.5 E.

---

1) It follows from Landau's theory that $\mathcal{K} \approx 1$ since in the initial moment, the nucleons completely fuse into each other, i.e. the collision is completely inelastic. Experimental measurement of $\mathcal{K}$ with subsequent application of equation (4.53) yields $\mathcal{K} < 1$ because the nucleon may by regenerated and this case cannot be distinguished experimentally from the case in which the nucleon is conserved.

It might appear that this approach will lead to a good agreement with the experiment. However, it was experimentally found that these fast particles were protons (in p.p. collisions), whereas most of the particles in Landau's theory were π-mesons. Consequently, the front of the shock wave will be predominated by π-mesons and not nucleous. This indicates that we are still as far from agreeing between Landau's theory and the experimental facts, as we were before speaking about shock waves.

It is possible[2] in the cases when the inelasticity coefficient $K \sim 1$ (this holds in collisions of heavy nuclei) that a considerable part of the energy is carried away by a single pion. There remains however, a wide range of phenomena, where the inelasticity coefficient is less than 1 and the main fraction of the energy is carried away by a nucleon. Such a conservation of the nucleon energy may be understood by assuming that nucleons do not loose their individuality during collision. In other words, the two nucleons do not form a common system, as postulated in the Fermi-Landau model, but interact through their pionic clouds. Particularly simple is the process, in which only one pion cloud participates in the interaction. Such an interaction is called a one-pion interaction.

All cases of interactions between pionic clouds are called peripheral collisions, in contrast with central collisions, considered earlier. One should not, however, give the term "peripheral collision" its literal geometrical meaning; the interaction process in this case also has a quantum-mechanical nature.

Following Weizsacker and Williams, we can imagine the pionic clouds of the colliding nucleons as beams of virtual mesons with a mean momentum q and an energy $\tilde{E}$

$$\vec{q} \sim \frac{\mu}{m} \vec{\tilde{p}}, \quad E = \frac{\mu}{m} \tilde{E}_0;$$

where $\vec{\tilde{p}}$ and $\tilde{E}_0$ are the momentum and energy of the nucleous in the C-system, respectively. We further use the general methods of relativistic quantum-mechanics to consider the collision of one of these relativistic π-mesons with the nucleon or the other mesons.

The common system appearing in the collision of pions may be considered a fire ball. Experiment shows that the mean energy of mesons in the coordinate system fixed with the mesonic mass does not depend on the energy of the incident particle and is in all cases approximately equal to 0.5 GeV. Consequently, there is enough time for equilibrium energy distribution to be established between particles in the mass. As a consequence of the constancy of the mean energy of means, the mass m of the fireball will be proportional to the multipolarity.

The anisotropy of particle emission in the centre of mass system of high-energy colliding nucleous is thus explained as a result of the motion of the fire ball in the C-system. If the Lorence factor γ of this motion increases with

---

2) As shown by I.L. Rozental', Landau's theory, under certain conditions, can predict a generation of a nucleon with a considerable part of the energy, so that the measured value of K will be reduced.

energy, then the particles resulting from the decay of the fire ball will be emitted with smaller angles in the C-system (see equation 4.3).

In order to explain the symmetric showers in the C-system, one has to postulate the formation of two fire-balls, moving in opposite directions in the C-system. This is required by the experiments made for the study of angular distributions, in which two peaks in the lg tg θ scale are obser ed.

G.T. Zacepin suggested that two interacting virtual pions can fuse into each other and form a common system only if their momenta is less than a given limiting momentum, q_o. If the momenta are greater than q_o, then they can only exchange an amount of momentum equal to q_o. In this case, two fire-balls can occur in the centre-of-mass system of the pions.

In order to keep the inelasticity coefficient independent of energy in the fire-ball model, it is necessary to impose a restriction on the dependence of on γ_s . Indeed, if the energy of pions in the fire-ball system is $\mathcal{E}_s$ and in the C-system $\mathcal{E}_c$, then $\mathcal{E}_c = \overline{\gamma}\, \mathcal{E}_s$. According to equation (4.65), The condition that $\mathcal{E}_s$ = constant then leads to the relation $\overline{\gamma} \cong \gamma_c^{1/2}$. Uptil now, there are no reliable experimental data on the dependence of $\overline{\gamma}$ on γ_c .

This brief review of the theoretical ideas and models available and the outcome of their comparison with experimental data shows that probably none of these models can satisfactorily explain all the experimental results.

We are more frequently met with peripheral collisions. They can be more easily described by the fire-ball model, which involves many parameters yet to be determined by fitting the data. Nevertheless, uptill now, no one is sure that some of the collisions are not central collisions.

Questions and Problems

1. Use the curve given in figure 31 to obtain the cross section and the interaction path of pions in carbon. Compare the resulting values with the corresponding values for protons. Do you expect a large difference in the cross sections of pion- and nucleon interactions with lead nuclei ?
2. Derive the Lorence-factor addition formula (equation 4.24) from the velocity addition formula.
3. Compare the Lorence factors of the C-system for the following two cases :
a) A 100-GeV proton collides with a stationary proton.
b) A 100-GeV proton collides with the nucleons of a stationary nucleus. (Take energy of the Fermi motion of the nucleons into account, $(E_f)_{max} \simeq 30$ MeV).
4. Compare the Lorence factors of the C-system for the collision of a 100 GeV proton (mass m_p) with a pion (mass 0.15 m_p) and a proton.
5. Find energy E_{cr} at which pions effectively participate in nuclear interactions at heights of 5 and 10 kms in the atmosphere. (Use table 25).
6. The same for kaons.
7. Calculate the minimum energy required by a nucleon to create a pion in a collision with a nucleus.

8. Find the Lorence factor of the symmetric system for an electronic-nuclear shower, produced as a result of a nucleon-nucleon collision, using Castagnoli's method. In the shower, there are 7 particles moving in the L-system with angles:

1. 12° ,	5. 3° ,
2. $7^\circ\ 30'$,	6. 14° ,
3. 2° ,	7. 31° .
4. $1^\circ\ 30'$,	

Calculate the accuracy of the energy determination.

9. Find the dispersion of the angular distribution for the shower, described in problem No. 8.

10. Find the energies of particles 1-3, 5-7 in problem No. 8 by the mean transversal momenta. (Assume that the particles are pions).

11. Assuming that the shower described in problem No. 8 is symmetric, calculate the energy of particle 7 in the mirror coordinate system.

12. Compute the inelasticity coefficient in the shower described in problem No. 8.

13. At which energy will the probability of decay of a π-meson in water be equal to the probability of nuclear interaction ? By how much does this energy change in lead and air at atmospheric pressures.

PART TWO

INTERACTION OF PRIMARY RADIATION WITH MAGNETIC FIELDS AND MATTER

CHAPTER 5

PRIMARY COSMIC RADIATION

1. Basic Definitions

According to the definition given in the introduction, cosmic rays are a flux of atomic nuclei, most of which are protons, created and accelerated in cosmic objects or in cosmic space. In practice, cosmic rays after understood as being particles having energies higher than several hundreds of millions of electron-volts. A close relation, however, exists between these particles and particles with much lower energies (subcosmic particles) as well as electrons, X-rays and γ-rays.

At the present time, numerous characteristics of primary cosmic rays are well established. Most of them are obtained by observing the interaction of primary radiation with the atmosphere, dense materials and the earth's magnetic field. Recently, it became possible to study cosmic rays in cosmic space by means of instruments carried by rockets and cosmic stations flying to the moon, Mars and Venus. Thanks to the progress in radio astronomy, it became possible to observe cosmic rays at their source.

The quantitative analysis of cosmic-ray properties is based on the introduction of the following definitions.

1. The intensity of cosmic radiation $J(\theta)$ in the direction θ is defined as the number of particles passing through a unit area perpendicular to direction θ in a unit solid angle per unit time. Intensity $J(\theta)$ has dimension $[J(\theta)] = [cm^{-2}\ sec^{-1}\ ster.^{-1}]$. A particular case of this directional intensity is vertical intensity.
2. The particle flux, J_s, is defined as the number of particles passing through a horizontal area of 1 cm^2 per unit time. Flux J_s is related to directional intensity by the following relation

$$J_s = \iint J(\theta)\cos\theta\, d\Omega,$$

where $d\Omega$ is the element of solid angle.
3. The integral (global) intensity, I, is defined as the number of particles passing through a sphere of a section of 1 cm^2 from all directions per unit time :

$$I = \iint J(\theta)\, d\Omega.$$

The difference between the directional and global intensities is related to the different methods of measuring cosmic radiation.

The directional intensity is measured by instruments which separate a given direction, namely telescopic instruments ("telescopes"). A "telescope" consists of two or more counters located in one plane and switched on in a coincidence scheme. The line that connects the centres of the counters is called the telescope axis. The telescope is characterized by its relative aperture S. The larger the relative aperture, the faster the counting rate. In the simplest case of two small counters, the relative aperture is defined by the following simple relation

$$dS = \frac{d\sigma_1 d\sigma_2}{R^2},$$

where $d\sigma_1$ and $d\sigma_2$ are the areas of the two detectors constituting the telescope. The number of counts will then be given by

$$dN(\theta) = \frac{d\sigma_1 d\sigma_2}{R^2} \mathcal{J}(\theta). \tag{5.1}$$

The counters are not usually separated by a large distance and have considerable extension in a given direction. In this case, the quality of reigstration will be affected (even in the vertical position of the telescope) not only by the value of the relative aperture but also by the angular distribution of the cosmic-ray particles (figure 46,a). The number of particles registered by such an elementary telescope will then be equal to

$$dN = \frac{\mathcal{J}(\theta)\, d\sigma_1 \cos\theta\, d\sigma_2 \cos\theta}{R^2}. \tag{5.2}$$

At sea level, the angular distribution of cosmic radiation is in the form of $J(0) = J_o \cos^2 \theta$. Substituting this expression into equation (5.2) and integrating over $d\sigma_1$ and $d\sigma_2$, we obtain

$$N = \frac{1}{4} \mathcal{J}_0 a^2 \left[\frac{l^2}{l^2 + d^2} + \frac{3l}{d} \operatorname{arctg} \frac{l}{d} \right]. \tag{5.3}$$

At the atmosphere's border, cosmic rays have an isotropic angular distribution in the whole upper atmosphere, i.e. $J(\theta) = J_o$ = constant. In this case, the equation becomes

$$N = \mathcal{J}_0 \frac{a^2 l}{d} \operatorname{arctg} \frac{l}{d}. \tag{5.4}$$

By using these equation and measuring the number of coincidences, one can calculate the vertical intensity J_o.

The global intensity is measured by means of an ionization chamber or a single counter. In this case, an important role is played by the intrinsic background of the counter or the chamber. The background can be eliminated by using the so-called circular instrument (figure 46,b) which consists of counters switched on in a coincidence scheme.

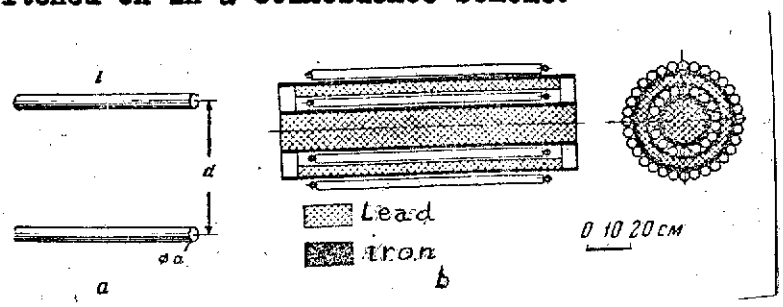

Figure 46. A telescopic instrument (a), and a circular instrument (b).

In order to measure the intensity of the hard-component, a filter is placed between the counters.

Cosmic-ray particles have an energy distribution. The number of particles with energy in the interval between E and E + dE is characterized by the differential intensity N(E)dE. Function N(E) is called differential energy spectrum and is measured in units of "particle/cm^2, sec. ster. GeV".

Very often, cosmic radiation is characterized by the integral spectrum

$$N(>E) = \int_E^{\infty} N(E)\,dE,$$

which defines the number of particles having an energy larger than a given vlaue. (Its dimension $[N] = [cm^{-2}\ sec^{-1}\ ster^{-1}]$.

2. Basic Properties of Primary Cosmic Rays

2.1. Intensity of cosmic radiation

The intensity of cosmic rays is only measured uptill now to within the limits of our solar system. The activity of the sun in these conditions has a great influence on intensity. In 1959, in a period close to a maximum in solar activity, the intensity of cosmic rays measured on a Soviet cosmic rocket, was equal to $J_o = 0.18 \pm 0.8$ $cm.^{-2}$ $sec.^{-1}$ $ster^{-1}$. Such an intensity is observed far from the earth in any direction because cosmic radiation is isotropic. Near the boundary of the terrestrial atmosphere, the integral intensity I is two times less than it values far from the earth because all the lower hemisphere is screened by the body of the earth. During the period of minimum solar activity, cosmic rays penetrate more easily in the solar system and their intensity on the earth increases. Therefore, the intrinsic intensity

of cosmic rays should be measured during the period of minimum solar activity. Measurements yield $J \simeq 0.23$ cm.$^{-2}$ sec.$^{-1}$ ster.$^{-1}$

2.2. Composition of the primary radiation

The above-mentioned intensity is generally related to cosmic particles. In fact, the composition of primary radiation is very complex, although the major part of all particles are protons.

The first experiments for the investigation of the composition of primary radiation were carried out by Bradt, Peterson and others in 1948. By means of photo-emulsions, these authors observed a large number helium and heavier nuclei. They utilized the quadratic dependence of ionization on charge in order to identify these nuclei. Figure 47 shows the tracks caused in an emulsion by nuclei of different charges [2*]. Further investigation of the nuclear composition of cosmic rays were made by means of photo-emulsions, Cerenkov counters and proportional counters. A large amount of investigations was made during the past few years on board Soviet sateelites and automatic stations. "Luna-2" and "Luna-3" stations (1959) carried Cerenkov counters switched on in coincidence with gas-discharge counters. The results obtained are given in table 22.

Table 22

Nucleus	Intensity (cm^{-2} sec^{-1} ster^{-1})
$z = 1$	0,18
$z = 2$	$150 \cdot 10^{-4}$
$z \geqslant 5$	$10,6 \cdot 10^{-4}$
$z \geqslant 15$	$0,4—0,5 \cdot 10^{-4}$
$z \geqslant 30—40$	$1,5 \cdot 10^{-8}$

The comparison of intensities of different nuclei at a given energy is of particular interest. There are two ways to compare the energies. In the first case one compares the intensities of nuclei for a given energy per nucleus while in the second case, the comparison is made for a given energy per nucleon (in units of GeV/nucleon). The two definitions evidently coincide for a proton but differ for atomic nuclei with different mass numbers A, and concide only when the nuclei have different energies each proportional to the mass number A of the nucleus.

Measurements of intensities for nuclei with different energies was made on satellites of the "Proton", type [3*]. The energy was measured by using an ionization calorimeter and the nuclear charge by using a proportional counter.

In the low-energy region, the method used is based on the analysis of charged-particle motion in the earth's magnetic field (the latitude-effect method, see chapter 6). In this case, the nuclear charge is determined by means of photo-emulsions and Cerenkov counters. The results of measuring the

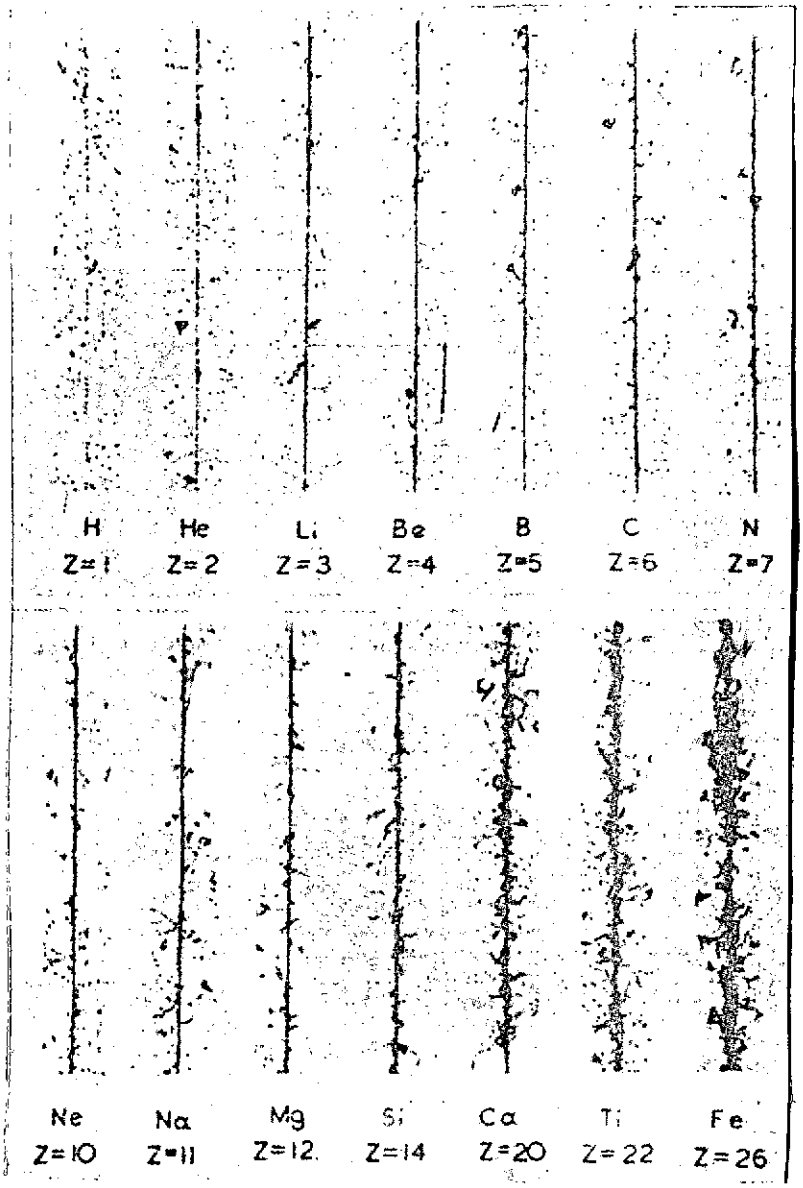

Fig. 47 - Tracks of different particles having relativistic energies in an emulsion.

intensities of nuclei with energies higher than 2.5 GeV/nucleon near the atmospheric boundary and outisde the atmosphere's limits by means of satellites are given in table 23.

The composition of primary radiation is of vital importance for understanding the origin of cosmic rays. It must in some way reflect the prevalence of elements in cosmic rays and in the universe as a function of their atomic numbers. The redundancy of heavy elements, seen in figure 48, [4*] indicates that these elements are more effectively produced. Quite interesting also is the redundancy of nuclei of group L (Li, Be and B). Nuclei of this group

are very rare in the chemical composition of the Galaxy's stars, plantes, etc. One therefore expects to find these nuclei more rarely than nuclei of

Table 23

Nuclear group	z	Intensity (m^{-2} sec.$^{-1}$ ster.$^{-1}$)
p	1	1300±100
α	2	94±4
L	3—5	2,0±0,3
M	6—9	6,7±0,3
H	≥10	2,0±0,3
H_1	10—14	1,4±0,4
H_2	15—19	0,1±0,1
H_3	≥20	0,5±0,2

group Z 5 (C, N, and O). The ratio of the numbers of nuclei in cosmic radiation is found to be equal to

$$\frac{N_L}{N_M + N_H} \simeq 0{,}23 \pm 0{,}05.$$

On the other hand, the prevalency of nuclei of group L in nature is 10^5 times less and the ratio of these groups in nature is equal to 3×10^{-6}. The existance of such nuclei in cosmic radiation may be due to their production as a result of the decay of heavy elements after their interaction with the interstar gas. By knowing the density of the inter-star gas and the probability of formation of nuclei of group L in the disintegration (fragmentation) of heavy nuclei (see table 17), one can estimate the path and consequently the roaming time of nuclei in cosmic space. Calculation shows that the path covered by nuclei must be as long as 5 g/cm^2 in order to explain the large number of nuclei of group L observed.

2.3. Electrons in primary radiation

The intensity of cosmic-ray electrons in primary radiation is 100 times less than that of nucleons. The number of electrons is measured by means of instruments, involving lead plates where electron-photon cascades are produced by incident electrons. Scintillating counters register the number of particles under the lead plates. This enables us to evaluate the energy of the incident electrons.

Subsidiary instruments and special measuring programs made at the atmospheric boundary enables us to eliminate the background from the the nuclear interaction of proton [5*]. The resulting energy spectrum of electrons having energies greater than 2 GeV may be represented in the form of [6*] :

$$N_e(>E) \simeq 1{,}3 \cdot 10^{-2} E^{-2{,}6 \pm 0{,}1} \text{ см}^{-2}\text{сек}^{-1}\text{стер}^{-1}\text{Гэв}^{-1}.$$

A number of authors determined fraction of positrons in primary radiation. They separated positrons from electrons either by means of a magnetic field and a system of spark counters raised to the atmosperic boundary, or by using the east-west asymmetry effect (see chapter 6). For this purpose, they had to take into consideration the contribution due to secondary electrons, created in the atmosphere, since there still remained a few grams of matter above the instrument. This increased the uncertainty of the results. Recent measurements (1966) showed that in the energy region $E > 0.5$ Gev, the ratio of the number of positrons to the total number of particles (electrons and positrons) is not large:

$$\frac{N_{e^+}}{N_{e^+} + N_{e^-}} < 0.2$$

In the energy interval from 200 to 500 MeV, a small position flux is observed:

$$\frac{N_{e^+}}{N_{e^+} + N_{e^-}} \simeq 0.35 \pm 0.10$$

2.4. Energy distribution of cosmic particles

The main feature of the energy distribution of cosmic rays is the sharp decrease of intensity with increasing energy. The range of energies studied covers almost 12 orders of magnitude ($0.1 - 10^{11}$ GeV). In the energy region of $10 - 10^6$ GeV, an increase of energy by one order of magnitude decreases the intensity 50 times. At energies higher than 10^6 GeV, the decrease of intensity with energy is much faster (about 200 times per oder of magnitude). These numbers can be analytically expressed in terms of an exponential law: $N(E_0)\, DE_0 = AE_0^{\gamma}\, DE_0$, where γ slowly varies with energy. The value of γ is approximately equal to 2.7 in a wide energy interval (up to $E_0 \simeq 10^6$ GeV).

Methods for obtaining the form of the spectrum are numerous and require the consideration of a number of new phenomena. At energies below 20 GeV, the energy of the spectrum is determined by analyzing the motion of particles in the magnetic field of the earth (Chapter 6). Measuring the energy spectrum by means of geomagnetic fields is only possible up to energies of a few tens of GeV. The form of spectrum at energies higher than 50 GeV is obtained either by studying the interactions of the nuclear-active particles in the atmosphere or by a direct method by means of an ionization calorimeter located in a satellite. Such an experiment was carried out in the Soviety Union under the supervision of N.L. Grigorov in 1965-1966 in the cosmic station "Proton" weighing 12 tons and which was set in orbit. An instrument of a calorimetric type (figure 27) made it possible to obtain the shape of the spectrum. Results of the measuring are illustrated in figure 49, a [7*]. It was found that the cosmic-particle spectrum in the energy range from 60 to 10^5 GeV could be approximated by the above-mentioned power function with apower $\gamma = 2.74 \pm 0.06$. Data obtained by indirect methods give very similar results. Consequently, at energies $E_0 > 100$ GeV, the spectrum decays with energy more sharply than it does at lower energies.

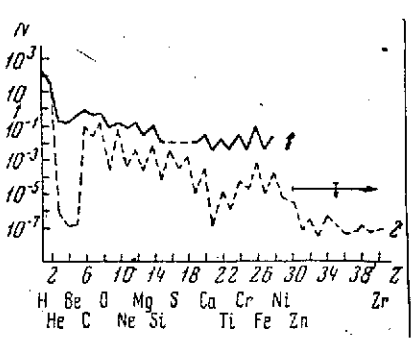

Fig. 48- Distribution of different elements in cosmic rays (1) and in the space (2).

Measurements in the energy range of $E_o > 10^5$ GeV are only possible by studying the interaction of particles in the atmosphere. Wide atmospheric showers appearing at these energies have longitudinal dimensions reaching twenty kilometers and with transversal dimensions in hundreds of meters. The energy of such particles is determined by a method very similar to the calorimetric method. However, in view of the gigantic dimensions of the showers, the whole terrestrial atmosphere is used as an "absorbing calorimeter". The measurement of the form of the spectrum in this energy region is made by means of very complicated instruments. The method used to determine the energy will be discussed later.

The latest data shows that the energy spectrum in the energy interval of $10^5 - 10^8$ GeV varies rapidly and that the exponential power γ is around 3.2. In the highest energy range ($10^8 \div 10^{10}$ GeV), the decay of intensity seems to be slower ($\gamma \approx 2.7$) as it might be concluded from certain data.

Figure 49,b shows the behaviour of the energy spectrum of cosmic rays in the total energy interval studied from 1 to 10^{10} GeV. The highest energies measured up to these days are close to 10^{11} GeV.

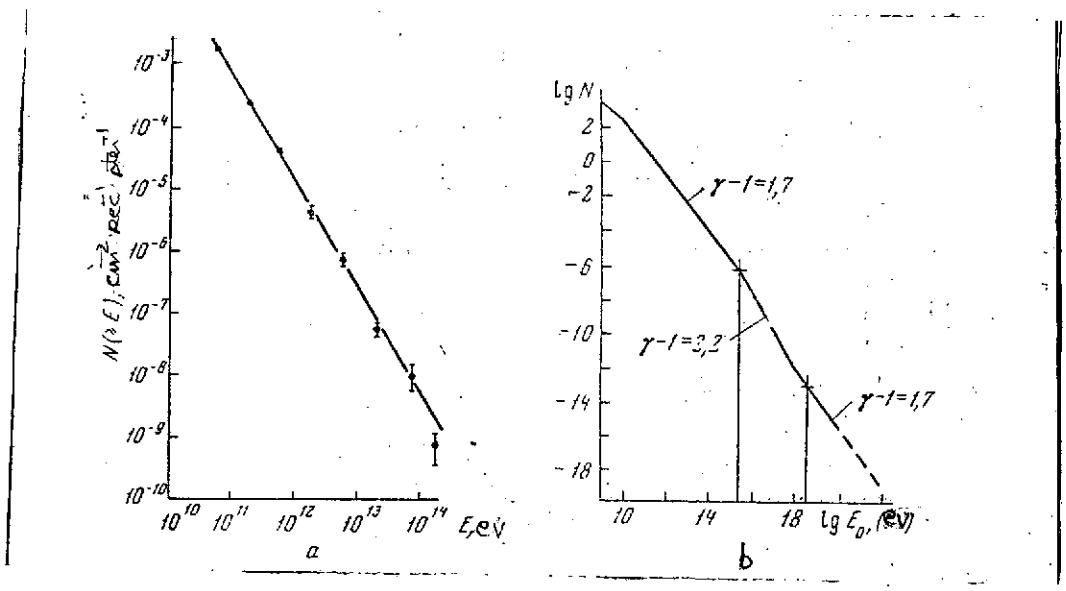

Fig. 49. The integral energy-spectrum of the primary cosmic radiation : (a) by data obtained by the "Proton" satellite, (b) summary of data obtained by different methods.

2.5. The upper limit of the cosmic-ray energy spectrum

Several years ago, an assumption was made that the Universe was full of cosmic radiation produced in an early stage of evolution of the Universe, when matter was in a highly condensed state and had a high temperature. In addition, an electromagnetic radiation was present in equilibrium with the heated

matter. The radiation was cooled as the Universe expanded and should now have a maximum in the micro-wave radio band. Such a radiation was recently observed at wave-lengths of 3.2 and 7.35 cm. Its spectrum was well described by a Planck distribution with a temperature close to 3°K. This corresponds to a mean energy of $kT \sim 2.5 \times 10^{-4}$ eV. The radiation density reached the value : $n \approx 550$ photons/cm^3.

Greisen as well as G.T. Zacepin and B.A. Kux'min /8*/ suggested that the existence of such a radiation would lead to an end of the spectrum of the primary radiation at energies higher than $5 \times 10^{19} - 10^{20}$ eV.

At sufficiently high proton energies, a photo-production of pions will occur as a result of the interaction of protons with photons. A proton will then loose in the average about 20% of its energy. Calculations showed that if the cross section of photon-proton interaction in the high-energy region was taken as a constant equal in order of magnitude to 10^{-28} cm^2/nucleon (as obtained from experiments on accelerators with GeV-protons), then the collision of protons with photons in the Galaxy would occur relatively often; the time between two successive collisions $\sim 10^7$ years. If the time of accumulation of cosmic rays in the Galaxy is sufficiently large ($\sim 10^8$ years, see chapter 10), then during this time the high-energy protons will completely loose their energy and the spectrum will be cut off starting with an energy of $5 \times 10^{19} - 10^{20}$ eV. At lower energies, the spectrum of primary nuclei may start to become poorer. As a result of interaction of nuclei with older radiation, nuclei will be photo-disintegrated and the process will continue till they finally disintegrate into nucleons.

Questions and Problems

1. Prove the validity of equation (5.3) by direct calculation.
2. How many times does the intensity of primary radiation decrease when energy increases from 20 to 2000 GeV ?
3. Find the energy at which creation of pions starts as a result of collision of protons with the older photons.

CHAPTER 6

INTERACTION OF PRIMARY RADIATION WITH THE EARTH'S MAGNETIC FIELD

1. Geomagnetic Effects

1.1. The earth's magnetic field

Cosmic radiation falling on the earth involves charged particles. The magnetic field of the earth must have a considerable influence on these particles. Low-energy particles are deviated by magnetic field and hence, do not reach the

earth. The discovery of a dependence of the intensity of cosmic rays on latitude, gave the first indication that cosmic rays consist of charged particles.

In a first approximation, the earth can be represented by a magnit with a magnetic moment of 8.1×10^{25} gauss. cm^3, located at a distance of 343 km from the earth's centre in such a way, that the dipole axis crosses the earth's surface at points: latitude 80.1°N, longitude 82.7°W and latitude 76.3°S, longitude 121.2° E. These points are called geomagnetic poles.

In practice, the dipole is often assumed to be in the earth's centre and the shift is considered as a peturbation. Since the geomagnetic and geographic poles do not coincide, a separate geometric set is developed. In the eastern hemisphere, the geomagnetic equator passes north of the mean geographic equator. Assuming a dipole field, Moscow is located at a geomagnetic latitude 51° S (its geographic latitude is 56° N). It is known that the magnetic field of a dipole decays with distance as $1/R^3$.

Recent investigations by means of satellites showed that the geomagnetic field can be only roughly considered as a dipole field. Better agreement with experimental facts was obtained by considering the quadrupole and octupole (parallel with the dipole) terms of the expansion of the actual earth's field in spherical harmonics. Several local anomalies of terrestrial magnetic fields are observed up to heights reaching 300 kms. One of these anomalies is observed over the southern part of the Atlantic Ocean. In this region, the magnetic lines of force approach the earth's surface. At large distances from the earth, the role of anomalies and non-dipole terms is reduced.

The interval between the earth's magnetic field and the interplanetary field is called a magnetopause. The form of the magnetosphere is determined by the interplanetary space conditions. Recent investigations showed that a flux of ionized gas, called solar wind, propagates from the sun. The variation of the density or velocity of the solar wind changes the pressure of the ionized gas in the magnetosphere and at its boundary.

1.2. Magnetic hardness

The force acting on a particle of charge Ze in a magnetic field is equal to (Ze/c) v x H and is always perpendicular to velocity v. If the particle velocity does not change in magnitude, then the particle will move on a circle of radius R, which can easily be obtained using the following relations

$$\frac{mv^2}{R} = \frac{Ze}{c} vH; \quad \frac{pc}{Ze} = HR.$$

If the magnetic field depends on coordinates r and φ, then

$$R(r; \varphi) = \left(\frac{pc}{Ze}\right) \frac{1}{H(r, \varphi)}.$$

Consequently, the velocity of a particle moving in a magnetic field is determined by the quantity $pc/Ze = \mathcal{E}_\theta$, where $\mathcal{E}_\theta$ is the energy per unit charge. The particle motion proceeds in such a manner that quantities E,v,p and $\mathcal{E}$ remain constant. Quantity $\mathcal{E}$ is called by a specific name: "magnetic hardness" of the particle. Particles with the same magnetic hardness will move along the same trajectories in a magnetic field. Hardness is measured in volts. At equal hardness, the energies per nucleon for all nuclei are equal, whereas the energy of a proton is twice as large (in the relativistic energy region and for nuclei with $A \times 2Z$).

Not all particles can fall on the earth. If the particle momentum is small, the particle will be deviated by the magnetic field of the earth at a large distance from its surface and will not fall on the earth. With increasing the magnetic harndess, particles penetrate deeper and deeper into the terrestrial magnetic field and finally, at a given magnetic hardness, particles will be able to reach the earth's surface (or the atmosphere's surface) and can be instrumentally registered. If telescopic instruments are used which are capable of separating any given direction, in order to register a particle with momentum p_{min}, the telescope must then be set in such a direction that particles with a hardness $\mathcal{E}_m$ can arrive from this direction.

The theory of geomagnetic effects deals with the problems of determining limiting momenta and permitted directions. This problem was considered for the first time by Stermer in connection with the appearance of the northern lights, and later on in works by Lemaitre and Vallarta /1/.

2. Motion of a Charged Particle in a Magnetic Dipole Field

2.1. Equation of motion and measuring units

The motion of a particle in a magnetic field proceeds under the action of the Lorence force. The equation of motion is of the form of

$$m\frac{d\vec{v}}{dt} = \frac{e}{c}[\vec{v}\vec{B}]. \tag{6.1}$$

Let us now introduce a polar coordinate system (figure 50) and consider the particle motion in the meridional plane and the motion of the meridional plane itself. Expanding the field intensity B into two components: a polar B_r (along radius-vector r) and a tangential B_t, we obtain that the force acting on the particle is perpendicular to the meridional plane and equal to

$$F_\varphi = \frac{e}{c}(v_t B_r - v_r B_t), \tag{6.2}$$

where v_r and v_t are the radial and tangential components of velocity

$$v_r = \frac{dr}{dt}; \quad v_t = r\frac{d\psi}{dt};$$
$$B_r = \frac{2M\cos\psi}{r^3}; \quad B_t = \frac{M\sin\psi}{r^3}. \tag{6.3}$$

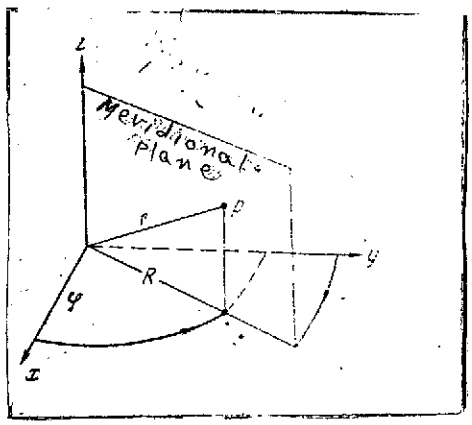

Figure 50. The polar coordinate system (ψ = $\angle$ zr). The z-axis is in the direction of the northern geographic pole.

The moment of force relative to the z-axis is equal to RF_φ where R is the projection of the radius-vector on the xy-plane. Combining equations (6.2) and (6.3) together, we obtain

$$RF_\varphi = \frac{eM}{c}\cdot\frac{d\left(\frac{R^2}{r^3}\right)}{dt}. \tag{6.4}$$

The moment of force is known to be equal to the time derivative of the angular momentum. The angular momentum with respect to the z-axis is equal to $R^2 m\, d\varphi/dt$. Noting that (relativistic) mass m remains constant during the motion, we arrive to the following equation

$$\frac{eM}{c}\cdot\frac{d\left(\frac{R^2}{r^3}\right)}{dt} = m\frac{d}{dt}\left(R^2\frac{d\varphi}{dt}\right)$$

and

$$R^2\frac{d\varphi}{dt} = \frac{eM}{cm}\cdot\frac{R^2}{r^3} + a, \tag{6.5}$$

where a is an integration constant. Since velocity v is constant, we replace

time t by a geometrical variable, namely the path length s = vt. Equation (6.5) then becomes

$$R^2 \frac{d\varphi}{ds} = \frac{eM}{cmv} \cdot \frac{R^2}{r^3} + b.$$

Quantity $\sqrt{/eM/cmv/} = S$ has a dimension of length. Choosing the length scale to be such that S = 1, we obtain a universal equation which neither depends on the masses nor velocities of the particles. The length unit S is called a störmer.

The importance of the length unit störmer in the theory of geomagnetic effects is explained by a quite solid reason. Particles in a dipole field can move along periodic orbits. The radius of such an orbit, R_o, can be obtained by equating the centrifugal force to the Lorence force

$$\frac{mv^2}{R_0} = \frac{e}{c} \cdot \frac{M}{R_0^3} v.$$

Then

$$R_0^2 = \frac{eM}{cmv}. \tag{6.6}$$

Comparing the expressions obtained for R_o^2 and S^2, we find that $S = R_o$. Consequently, the radius of a circular periodic motion in a dipole field has a length of 1 stermer. In this manner, the unit of length chosen in the geomagnetic theory comes from the radius of the central orbit. Naturally this scale is different from particles of different masses and momenta.

We shall now consider the physical meaning of integration constant b. Putting $r \to \infty$, we see that b becomes equal to the angular momentum, $\vec{m}$, with respect to the z-axis outside the range of the magnetic field.

By setting $m/_{r=\infty} = -2\gamma$, we finally obtain the equation of motion of the meridional plane, where the particle is located,

$$R^2 \frac{d\varphi}{ds} = \pm \frac{R^2}{r^3} - 2\gamma. \tag{6.7}$$

where the upper sign in this formula is to be used for describing the motion of positively charged particles.

2.2. The particle energy. Motion in the meridional plane

The kinetic energy of a particle, $T = \frac{1}{2} mv^2$ is a constant quantity. Expressing T in terms of coordinates and using a system of units in which m = v = 1, we obtain

$$T = \frac{1}{2}\left[R^2\left(\frac{d\varphi}{ds}\right)^2 + \left(\frac{dr}{ds}\right)^2 + r^2\left(\frac{d\psi}{ds}\right)^2\right] = \frac{1}{2}. \tag{6.8}$$

We now expand the motion into two components, one parallel and one perpendicular to the meridional plane (plane Rz in figure 50). The kinetic energy, Q', in the Rz-plane is given by

$$Q' = \frac{1}{2}\left[\left(\frac{dr}{ds}\right)^2 + r^2\left(\frac{d\psi}{ds}\right)^2\right].$$

Using equations (6.8) and (6.7), we obtain

$$Q' = \frac{1}{2}\left[1 - \left(\pm\frac{R}{r^3} - \frac{2\gamma}{R}\right)^2\right]. \tag{6.9}$$

By analyzing equation (6.9), we arrive to the two following conclusions :

1. The motion in the meridional plane does not depend on the rotation of the plane itself around the dipole axis since Q' does not depend on .

2. For a given γ , kinetic energy Q' is only a function of the coordinates. Consequently, the dipole field is a potential field. The force in this field is a force of attraction since energy Q' decreases as the distance to the dipole increases.

Usually, instead of Q', quantity Q = 2Q' is considered. Quantity Q has the following two typical properties :

i) The maximal value of Q is equal to 2T = 1. In this moment, the particle moves in the meridional plane.

ii) The minimal value of Q is equal to zero. When Q = 0, the particle moves perpendicular to the meridional plane and the projection of velocity into the Rz-plane changes sign, i.e. the particle turns backwards when it reaches line Q = 0. Consequently, line Q = 0 in the Rz-plane gives the limit of a region, inaccessible to the particles.

Equation (6.9) defines a system of exponential lines. Among these lines, line Q = 0 is of most particular interest. Rotating line Q = 0 around the z-axis, we obtain a surface of revolutions, giving the boundary of the space region in which the particles cannot penetrate. The form and dimension of this evidently depend on γ .

2.3. Permitted regions

In the chosen system of units of m = v = 1, quantity Q is nothing else but the square of velocity in the meridional plane. Consequently, quantity $\pm\sqrt{1 - Q}$ is equal to the normal component of velocity. Let us denote by w the angle between the geomagnetic parallel and the direction of trajectory, which coincides with the direction of measuring φ , i.e. from west to east (see figure 50). Evidently, angle w is the angle between the trajectory and the normal to the plane, so that

$$v_n^2 = v^2\cos^2\omega = \cos^2\omega = 1 - Q.$$

Using equation (6.9), we find that for a positively charged particle

$$\cos\omega = \frac{R}{r^3} - \frac{2\gamma}{R}. \tag{6.10}$$

Noting that the ratio $R/r = \cos\lambda$, where λ is the geomagnetic latitude, we obtain

$$\cos\omega = \frac{\cos\lambda}{r^2} - \frac{2\gamma}{r\cos\lambda} \tag{6.11}$$

Consequently, for a given value of angular momentum γ at infinity, the trajectories passing through the chosen point with coordinates λ and r will form a cone with an axis tangent to the geomagnetic parallel and an appex angle equal to w.

By solving equation (6.11) relative to r, we obtain

$$r = \frac{\cos^2\lambda}{\gamma \pm \sqrt{\gamma^2 + \cos\omega\cos^3\lambda}}. \tag{6.12}$$

At the boundary surface $Q = 0$, $\cos w = \pm 1$ and

$$r = \frac{\cos^2\lambda}{\gamma \pm \sqrt{\gamma^2 \pm \cos^3\lambda}}. \tag{6.13}$$

Consequently, there are several possible values for r. For $\gamma^2 > \cos^2\lambda$, the equation has three roots :

$$\left.\begin{aligned} r_1 &= \frac{\cos^2\lambda}{\gamma + \sqrt{\gamma^2 + \cos^3\lambda}}; \\ r_2 &= \frac{\cos^2\lambda}{\gamma + \sqrt{\gamma^2 - \cos^3\lambda}}; \\ r_3 &= \frac{\cos^2\lambda}{\gamma - \sqrt{\gamma^2 - \cos^3\lambda}}; \end{aligned}\right\} \tag{6.14}$$

If $\gamma^2 < \cos^3\lambda$, only one root (r_1) is possible. Therefore, if $\gamma^2 > \cos^3\lambda$, the radius-vector crosses surface $Q = 0$ three times. This means that the region of permitted trajectories ($Q > 0$) consists of two separate regions. When $\gamma^2 < \cos^3\lambda$, the region of permitted trajectories is a single region. Since the maximum value of $\cos^3\theta$ is unity, one may then conclude that, if $\gamma > 1$, there are two regions of permitted trajectories. The internal region, which is nearest to the dipole, is isolated from the external region and forms a toroid involving bound trajectories that cannot go to infinity. The internal region thus forms a trap for particles, from which they cannot escape . It is however impossible to fall into this region from the outside, because a

particle coming from infinity cannot pass through the surface Q = 0 of the external region. The configuration of areas, forbidden for particles at $\gamma > 1$ is shown in figure 51,a.

It was previously considered that the internal region was not full of particles. However, recent investigations on satellites and rockets showed that there are a large number of particles in this region. These particles move along the toroid axis (rotation of the meridional axis) as well as along the meridian between the northern and southern reflection points (Q = 0).

Details on the motion of particles in the internal region will be given in chapter 7. We shall now study the regions, accessible to particles coming from outerspace. Figure 51 shows that the internal region is located at $r < 1$.

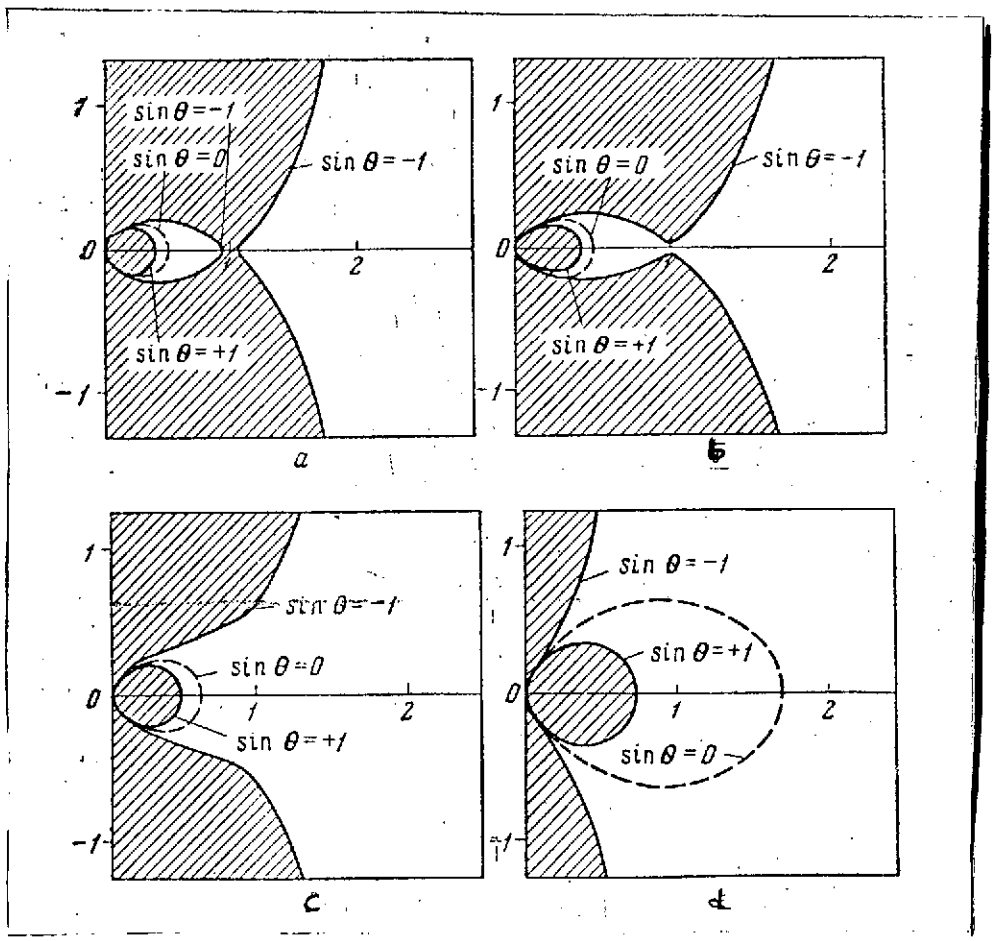

Figure 51. Regions, forbidden to particles, in a magnetic dipole field (dashed) at different values of γ : a) $\gamma_1 = 1.001$, b) $\gamma_1 = 0.999$ c) $\gamma_1 = 0.8$, d) $\gamma_1 = 0.3$ (the coordinate axes are λ and r; $\theta = \pi/2 - w$).

It also shows lines Q = 0 and the forbidden regions for $\gamma < 1$. In this case, the shell covering the internal region is divided into two parts and the internal and external region become unified.

2.4. Permitted and forbidden directions. Azimuthal asymmetry

When $\gamma > 1$, particles cannot penetrate into the region $r > 1$. We shall now determine the interval of angles w_o, within which the forbidden directions exist. The forbidden directions are defined by the values of γ, and hence, according to equation (6.11), they fill a circular cone confined by a surface defined by[1] :

$$\cos \omega_0 = \frac{\cos \lambda}{r^2} - \frac{2\gamma}{r \cos \lambda} \quad (r < 1). \tag{6.15}$$

This cone is opened for positively charged particles from the east and is called the Stormer cone ($\pi > w > w_o$). Directions lying outside this cone are permitted.

Consequently, positively charged particles cannot come from the east and negatively charged particles cannot come from the west. For these latter particles, all the directions are opposite and the Stormer cone is opened from the west. Negatively charged particles therefore cannot come from the west when r satisfies condition (6.15). This phenomenon is called the azimuthal effect and is usually used to determine the charge sign of primary particles.

2.5. Limiting momenta

The boundary of the permitted zone nearest to the dipole is described by the radius vector r_1 (see equation (6.14)) at $\gamma = 1$, and hence equation (6.14) gives

$$r = \frac{\cos^2 \lambda}{\sqrt{1 - \cos \omega \cos^3 \lambda} + 1}. \tag{6.16}$$

In our system of units, r is a function of momentum p. We can thus use equation (6.16) to obtain the minimum value of momentum, required by a particle to reach point r at latitude λ along direction w (see item 2.7).

---

1) We did not consider the possibility that particle, on its way from infinity to a given point, crosses the earth and become absorbed (the shadow effect). Taking this effect into account will no longer keep the cone as given by equation (6.15) in a circular shape. It is clear that the permitted particle trajectory will be only in upper hemisphere. Due to the complicated shapes of many trajectories, it is difficult to take into account the shadow effect.

2.6. Equatorial plane

We consider the method of calculating the limiting momenta in the particular case of an equatorial plane [2]. Coordinates r and λ at the equatorial plane take the values r = R and $\lambda = 0$. Equation (6.7) then becomes

$$R^2 \frac{d\varphi}{ds} = -2\gamma + \frac{1}{R}$$

and

$$\gamma = \frac{1 - R^2 \cos\omega}{2R}. \tag{6.17}$$

The area of permitted directions is defined by the values $-1 < \cos w < 1$. Equation (6.17) then gives the equation for the boundary lines corresponding to Q = 0 (see equation (6.9)). These are the two lines :

$$\begin{aligned} &\text{I.} \quad \cos\omega = -1; \quad \gamma = \frac{1 + R^2}{2R}. \\ &\text{II.} \quad \cos\omega = 1; \quad \gamma = \frac{1 - R^2}{2R}. \end{aligned} \tag{6.18}$$

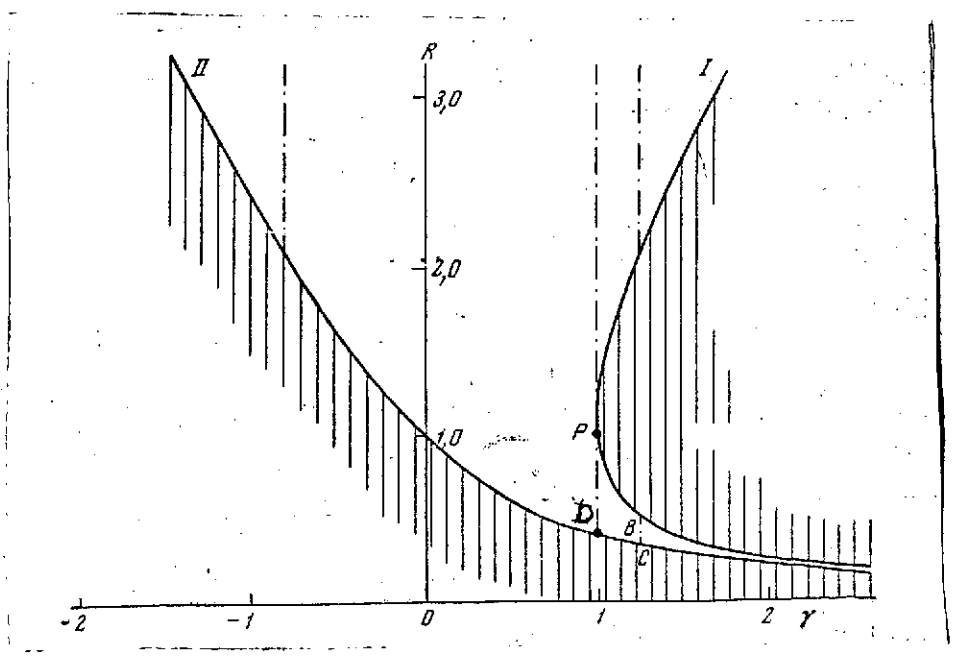

Figure 52. Permitted and forbidden (dashed) regions in the equatorial plane.

These lines are shown on the R γ-plane (figure 52). The dashed part corresponds to the forbidden regions. Each of the particle trajectories correspond to a given value of γ and hence represented by a vertical line in the R γ-plane. Point R = 1 and γ - 1 corresponds to a periodic orbit. The region where particles coming from cosmic space cannot fall into, is located at R $<$ 1 and $\gamma >$ 1. All orbits in this region are closed and the particles vibrate between points of curve I and those of curve II (trajectory BC).

When $\gamma < 1$, the particles are free to move up to the reflection point where they turn around and move in the reverse direction. These trajectories lie at $\gamma > 1$ and R $>$ 1 (reflection from curve I). Figure 51 shows that no particles coming from the outside can approach the dipole at a distance less than that indicated by point D on curve II (γ = 1).

Substituting γ = 1 into equation (6.18-II), we obtain

$$R_{min} = 0{,}414. \tag{6.19}$$

When R = R_{min} , only trajectory cos w = +1 is permitted. When R $>R_{min}$, all trajectories are permitted (-1 $<$ cos w $<$ 1° while all directions are forbidden when R 0.414. Quantity R is here expressed in stormers, i.e. in multiples of the value of the periodic orbit's radius.

The particle momentum (energy) at the circular orbit (in electron volts) is given by

$$E_0 = p_0 c = 300\,BS = 300\,\frac{M}{S^2},$$

where M is the magnetic dipole moment. If the radius of the earth, R_E , is measured in stormers, then

$$R = \frac{R_E}{S}; \quad S = \frac{R_E}{R}; \quad p_0 c = 300\,\frac{M}{R_E^2}\,R^2.$$

Thus, p_o is the momentum of a particle whose circular orbit has a radius equal to the radius of the earth. Since, for R$>$1, all the directions are different, particles with momentum p $>$ p_o may fall on the earth from any direction. Substituting the numerical values of R_E and M into the previous equation, we find that p_o = 59.3 GeV/c (R_E = 6.371 x 10^8 cm).

Distance R_{min} = 0.414 (equation 6.19) corresponds to the momentum, with which a positively-charged particle can reach the surface of the earth while moving from the west along the horizontal.

$$p_{min} = p_0 R_{min}^2 \approx 10 \text{ GeV/c}.$$

When $p < p_{min}$, the particle cannot reach the earth at its equator.

2.7. The general case

In the general case when $\lambda \neq 0$, we must replace the substitution $r = R$ by substituting the value of the radius vector, given by equation (6.16). The limiting value of the momentum will then be equal to

$$p_{min}(\lambda, \omega) = p_0 \frac{\cos^4 \lambda}{(\sqrt{1 - \cos\omega \cos^3 \lambda} + 1)^2}.$$

In particular,

$$p_{min}(\lambda, 0) = p_0 \frac{\cos^4 \lambda}{(\sqrt{1 - \cos^3 \lambda} + 1)^2};$$

$$p_{min}(\lambda, \pi) = p_0 \frac{\cos^4 \lambda}{(\sqrt{1 + \cos^3 \lambda} + 1)^2}.$$

For $p > p_{min}(\lambda, 0)$ all directions are permitted and for $p < p_{min}(\lambda, \pi)$ all are forbidden. In the vertical direction ($w = \pi/2$)

$$p_{\perp}\left(\lambda, \frac{\pi}{2}\right) = \frac{p_0}{4} \cos^4 \lambda = p_{\perp}\left(0, \frac{\pi}{2}\right) \cos^4 \lambda. \tag{6.20}$$

It follows from the latter equation that the limiting momentum along the vertical direction decrease as λ increases (figure 53). This corresponds to the increasing opening of the permitted cone.

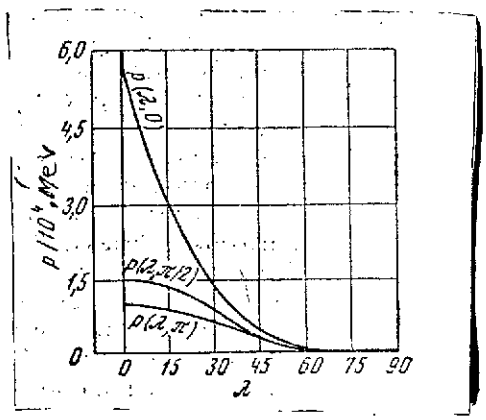

Figure 53. The limiting momenta as functions of angle θ and latitude λ.

2.8. On Liouville's theorem

If the particle density in a given region of space is such that the

particles do not interact then the number of particles in the phase-space volume element remains unchanged. If the volume element is $d\Omega = dVdp$ and the particle number is dN, then the particle phase density is equal to

$$D = \frac{dN}{d\Omega}. \tag{6.21}$$

Liouville's theorem states that the particles' motion in a magnetic field proceeds in such a manner, that $dD/dt = 0$. In order to find the particle intensity

$$I = \frac{\delta N}{\delta s \delta \omega \delta p \delta t}, \tag{6.22}$$

where δS is the area element and δw the solid-angle element, we must integrate equation (6.21) over the phase space $\delta N = \int D dp_z dp_y dp_z dx dy dz$. It is clear that

$$dxdydz = ds\frac{pdt}{m};$$
$$dp_x dp_y dp_z = p^2 dp d\omega;$$

so that

$$\delta N = \int D \frac{p^3}{m} ds dt dp d\omega = \langle D \rangle \frac{p^3}{m} \delta s \delta t \delta p \delta \omega.$$

Consequently

$$I = \frac{p}{m}\langle D \rangle.$$

In the particular case we are interested in, p and m = constant and this I is proportional to D so that $dI/dt = 0$. Consequently, the particle intensity along the whole trajectory does not change.

We thus arrive to an extremely important conclusion, namely, that the influence of the earth's magnetic field reduces the restriction of some definite trajectories and that the intensity of particles in the permitted directions is the same as that outside the range of the earth's magnetic field.

3. Practical Application of the Theory

3.1. Geomagnetic equator

It follows from the data available on the magnitudes of the limiting momenta that the intensity of cosmic radiation must be minimum at the equator. This makes it possible to find the position of the geomagnetic equator by measuring cosmic rays at different geographic latitudes. The dependence of

the cosmic-ray intensity on latitude is called the latitudinal effect.

By means of satellites, it became possible to study the radiation intensity distribution over the whole surface of the earth. Figure 54 shows the results of investigating the cosmic-ray equator by means of data obtained by Soviet satellites [3*].

3.2. Longitudinal effect

The lack of coincidence between the dipole centre and the earth's centre and the influence of the non-dipole terms, make the limiting momenta at the same geomagnetic latitude and at an equal distance from the earth's surface, have different values in the western and eastern hemispheres. Accordingly, the cosmic-ray intensity varies with the variation of not only latitudes but also longitudes. This phenomenon is called the longitudinal effect.

Limiting momenta are uniquely related with hardness $\xi = pc/Ze$. Table 24 gives the dependence of the magnetic hardness (in GV) on geographic coordinates [4]. In the calculation, contributions from nondipole components of the field are taken into account.

3.3. Limiting momenta

Much information on the properties of primary radiation can be obtained by studying limiting momenta. Examples in the use of limiting momenta for the study cosmic rays are given below.

In the forties, a serious question on the composition of the primary cosmic radiation was raised. Are primary particles light particles like electrons, or heavy ones ? The answer to this question was obtained in 1940 by the American physicist Schein and his collaborators. In experiments carried out at a height of 25 ÷ 35 kms, these authors found that primary particles were not subject to a cascade multiplication and were hence heavy particles. In the post-war years, this result was confirmed in the Soviet Union by means of experiments carried out under the supervision of S.N. Vernov [5]. Instruments consisting of small thin-walled counters were raised to a height approximately equal to 30 kms. During the flight, the counters were moved alternatively into and out of a lead sphere (Figure 55,a). The lead thickness in different flights was different. Using this method, the cosmic-particle intensity at different lead thicknesses (0, 1, 2, 4 and 8 cm Pb) was measured. The curves obtained have the typical cascade curve forms (Figure 55,b). The energy of the electrons was determined by measuring the number of particles at their maximum and at the position of the maximum. It was found that this energy is approximately 10^8 eV, i.e. much less than the minimal energy of primary particles at latitude 56°, which is equal to 1.5 GeV. This means that the electrons observed are secondary particles and that most of the primary particles are heavy.

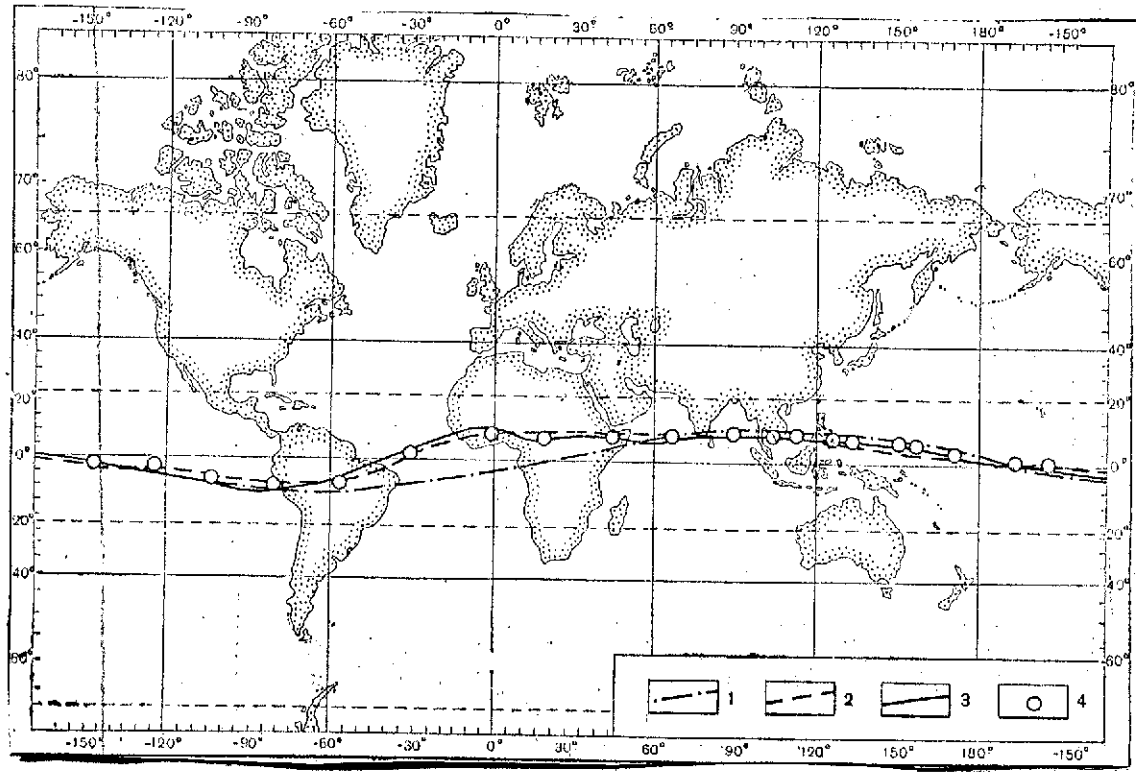

Fig. The cosmic-ray equator. 1- The dipole approximation, 2- Taking into account quadrupole term, 3- Taking into account of octupole terms, 4 - data obtained by the 2nd cosmic vessel.

Table 24

Geographic latitude		Eastern longitude									
			0°	20°	40°	60°	80°	100°	120°	140°	160°
Northern		70°	0,274	0,376	0,453	0,505	0,54	0,55	0,56	0,57	0,512
		60°	1,12	1,28	1,42	1,54	1,70	1,82	1,87	1,90	1,76
		50°	3,06	3,60	3,81	3,77	3,84	3,98	4,15	4,26	4,37
		40°	6,7	7,20	7,60	7,80	8,2	9,4	9,6	9,0	8,5
		30°	11,2	11,6	12,6	13,5	14,3	14,5	14,5	13,9	13,1
		20°	14,4	14,9	15,5	16,1	16,5	16,8	16,4	16,0	14,8
		10°	15,1	15,6	16,4	17,0	17,6	17,7	17,1	16,5	16,0
		0°	14,4	14,9	15,7	16,3	16,8	17,2	17,0	16,5	16,2
Southern		10°	12,5	12,4	13,4	14,4	14,9	15,0	15,1	15,2	15,2
		20°	10,5	10,2	10,7	10,5	10,8	10,9	10,5	11,1	12,1
		30°	8,9	7,9	6,8	5,9	5,01	4,62	4,70	5,2	6,2
		40°	6,3	4,59	3,77	3,18	2,48	2,03	1,98	2,28	3,01
		50°	3,76	2,65	1,81	1,34	0,90	0,63	0,55	0,63	1,02
		60°	1,90	1,24	0,77	0,512	0,281	0,136	0,096	0,086	0,194
		70°	0,82	0,512	0,294	0,136	0,055	0,0136	0,0033	0,0024	0,256

Geographic latitude		Western longitude									
			20°	40°	60°	80°	100°	120°	140°	160°	180°
Northern		70°	0,151	0,061	0,0177	0,082	0,152	0,056	0,161	0,288	0,421
		60°	0,72	0,365	0,181	0,125	0,174	0,381	0,75	1,20	1,55
		50°	2,24	1,28	0,73	0,63	0,85	1,44	2,23	3,22	4,09
		40°	4,94	3,01	2,06	1,97	2,52	3,83	4,99	6,2	7,7
		30°	8,8	5,8	4,48	4,45	5,6	7,3	8,9	10,4	12,3
		20°	12,8	10,1	8,5	8,3	9,8	12,0	13,2	13,7	14,2
		10°	14,6	13,6	12,4	11,8	13,3	14,5	14,7	15,0	15,4
		0°	14,2	14,1	13,6	13,5	14,6	15,1	15,4	15,6	15,9
Southern		10°	13,1	13,4	13,6	14,0	14,6	14,8	14,8	15,2	15,3
		20°	11,4	12,2	12,8	13,6	14,0	14,0	13,8	13,3	12,6
		30°	9,9	11,1	11,6	12,6	13,1	12,6	11,7	9,5	7,7
		40°	8,0	9,3	10,2	10,4	9,7	8,3	6,7	5,2	4,03
		50°	5,1	6,7	7,3	6,8	5,6	4,50	3,39	2,29	1,45
		60°	2,81	3,85	4,15	3,89	3,05	2,19	1,42	0,82	0,458
		70°	1,24	1,61	1,69	1,57	1,27	0,85	0,512	0,269	0,109

3.4. Experimental study of the azimuthal effect

The charge sign of the primary particle can be determined by the azimuthal effect. We already know that positively charged particles must come from the west and negatively charged particles from the east. Comparing the intensities of particles, coming from different directions, one obtains the charge sign of cosmic particles.

In 1949, S.N. Vernov and I.L. Grigorov measured the east-west effect at the equator by means of an instrument consisting of a telescope, inclined at an angle of 60° and with an orienting system (figure 56). By means of a photo-element and an electric motor, the telescope was constantly directed in the west-east plane. Orientation was made by the sun which moves almost in the east-west plane at the equator. After a number of minutes, the direction

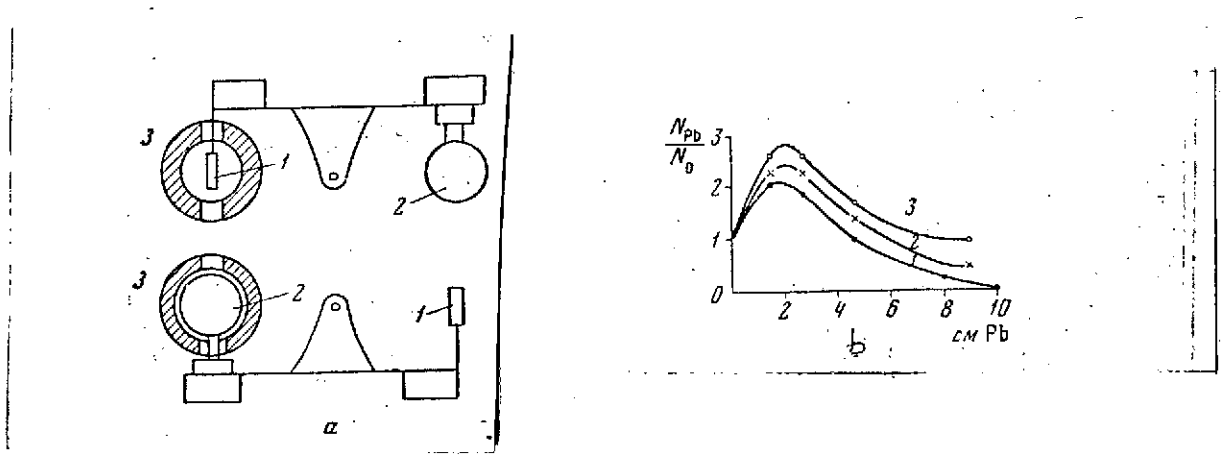

Figure 55. Experimental determination of the nature of primary particles. a- The system of the instrument (a view from above): 1. the counter, 2. the ionization chamber, 3. a lead filter; b- Tansitional curves air-lead for the soft component at latitude 51°. During the flight the counter and chamber changed places. The comparison of the ionization and the number of particles proved that the observed particles were relativistic.

of the telescope's axis was switched from east to west. It was found in this experiment that the asymmetry of heavy particles was equal to

$$2\frac{\mathcal{J}_\omega - \mathcal{J}_e}{\mathcal{J}_\omega + \mathcal{J}_e} \simeq 0{,}7 \pm 0{,}1. \qquad (6.22)$$

where J_w and J_e are the intensity of particles coming from the west and east respectively. This shows that primary particles are mainly positively charged.

3.5. Determination of the form of the energy spectrum

In the experiment on the determination of the form of the cosmic rays energy spectrum, the earth's magnetic field is used as an analyzer. The scale of the phenomenon under investigation requires an "instrument" of a suitable scale. It follows from Liouville's theorem that measurements at particle momenta $p > p_{min}(\lambda)$ yields correctly the intensity of particles outside the range of the terrestrial magnetic field. Consequently, the intensity at a given latitude λ is uniquely related to the intensity of particles with momenta greater than p_{min} (equation (6.20)) :

$$\mathcal{J}(\lambda) = \mathcal{J}\left(> \frac{p_0}{4}\cos^4\lambda\right).$$

In 1949, S.N. Vernov and A.N. Carahc'jan carried out a series of experiments for measuring the energy spectrum of cosmic radiation. They raised in the statosphere an instrument consisting of telescopic counters separated by lead layers of a thickness of x = 10 cm. The number of particles passing without interaction through 10 cm of lead was determined. This number satisfies the relation

$$N(\lambda) = N_0(\lambda)\, e^{-x/L_{Pb}},$$

where L_{Pb} is the interaction path of the particle in lead. Since the interaction cross section does not depend on energy, then $N(\lambda) \sim N_0(\lambda) \sim N_0(> p_{min})$.

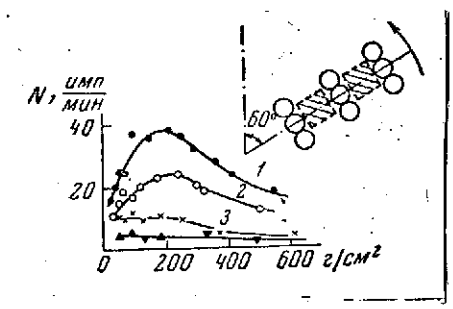

Fig. 56. Azimuthal assymetry at the equator: 1. Number of counts N in the telescopic instrument, when directed to the west, 2. The same but with the instrument directed to the east. 3. The hard component; particles coming from the west. 4. The same but with particles coming from the east.

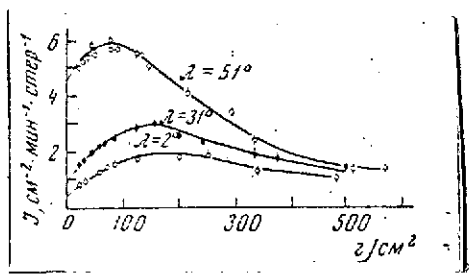

Fig. 57. The latitudinal effect for verticle particles of cosmic rays at different latitudes and different depths inside the atmosphere.

The kinetic energy of the vertical particles at the equator was found to be approximately equal to 15 GeV and at latitude 51° to 2.5 GeV. The latitudinal effect of the particle number between these two latitudes was approximately 10.

Figure 57 shows the dependence of the cosmic ray intensity on latitude, which follows from measurements at different distances from the earth's surface. By using this data on the latitudinal effect, one can reconstruct the primary-particle energy spectrum. It is found that the energy spectrum of protons in the energy interval from 4 to 20 GeV follows the power relation

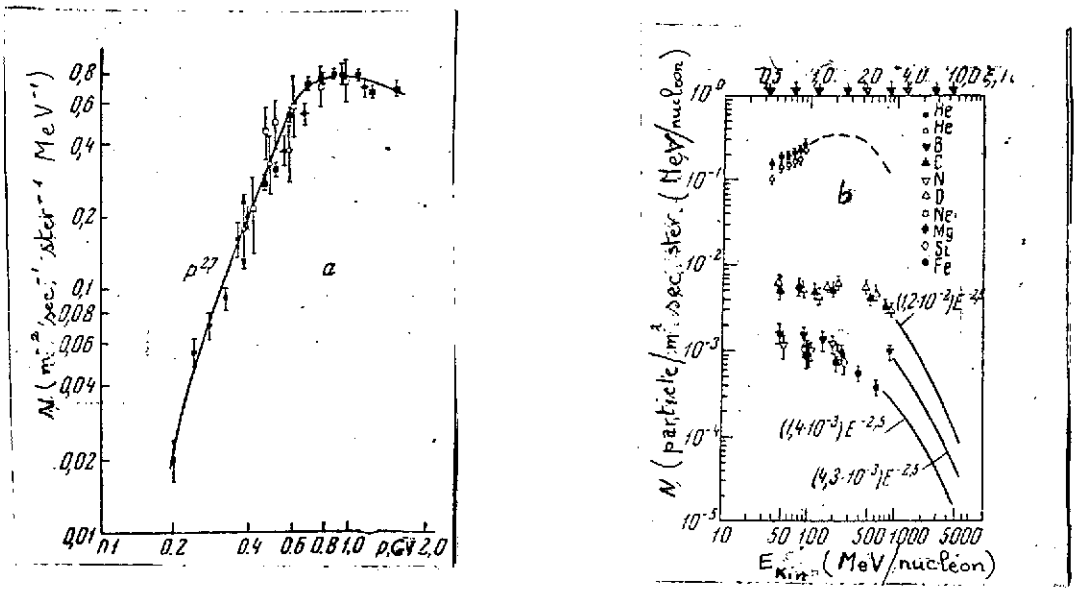

Figure 58. The energy spectrum of primary particles in the range of small hardnesses : a- protons, b- nuclei.

$$\frac{dN}{dE_0} = \frac{A}{E_0^{\gamma}}, \qquad (6.23)$$

where $\gamma \approx 2.5$. In the lower-energy range however, the proton intensity starts to decrease sharply as energy decreases. Figure 58 shows the spectrum of proton hardnesses $\mathcal{E}$ (1963 [8*]). The observed decrease in intensity in the low-hardness region is called high-latitudinal spectrum cut-off. It takes place at latitudes near 55° and is observed for protons as well as for nuclei.

The reason for the high-latitudinal cut-off has already been discussed for many years. It was suggested that during the years of maximum solar activity, a plasma carrying a regular magnetic rield and magnetic inhomogeneity (the so called "solar wind") was emitted from the sun. This plasma resists the penetration of low-energy cosmic particles from the Galaxy into the solar system. The fact that high-latitudinal cut-off is also observed during years of minimum solar activity when the solar wind is weak, may suggest particles with a hardness less than 1 Gv (proton energy less than 0.4 GeV) do not exist in the Galactic cosmic rays. However, even during the years of minimum solar activity, there is a relatively weak solar wind. L.I. Dorman showed that this weak solar wind has a sufficient effect to modify the primary-radiation spectrum in the energy range lower than 0.4 GeV.

We can thus conclude that the high-latitudinal cut-off is a result of the modulation of the galactic cosmic rays in the solar system. However, the problem of cosmic-ray spectra outside the boundaries of the solar system is not finally resolved.

3.6. Cosmic-radiation energy

The cosmic-radiation energy can be estimated by integrating the spectrum, illustrated in figure 50. There is, however, an alternative calorimetric method for measuring the cosmic-ray energy. The terrestrial atmosphere in this method serves as an ionization calorimeter, and ionization chambers raised on an aerostat to the atmospheric boundary, are used as ionization detectors. It is assumed that all the cosmic-ray energy is exhausted by heating the atmosphere and the earth's crust. This effect is small, however, and is not easily measured.

Prior to the transformation of cosmic-ray energy into heat, it is first exhausted by the ionization of the atmosphere. It is known that a charged particle looses 32.5 eV on producing a pair of ions in air (table 3). If we measure the total ionization produced by cosmic rays in the atmosphere, we will be able to estimate the energy carried by cosmic rays. Extensive measurements by means of ionization chambers raised on balloons were carried out by Millikan in 1940 /4*/. The dependence of ionization on height obtained at different latitudes is shown in Figure 59.

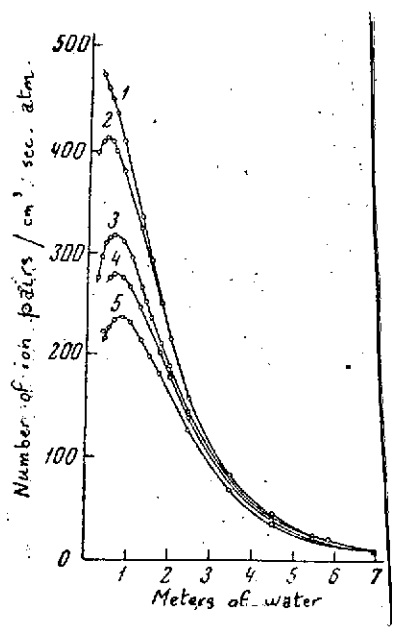

Figure 59. Dependence of ionization on height at different latitudes (Millikan's experiment). 1- latitude 56.0°N, 2- latitude 51.3°N, 3- latitude 44.8°N, 4- latitude 41.7°N, 5- latitude 38.5° N.

Let us assume that at height h, i(h) ions were measured in 1 cm^3 during 1 sec. Consequently in a layer of thickness dh, i(h)dh pairs of ion were produced, and $n = \int_0^\infty i(h)dh$ ion pair/sec were produced in an air column of 1 cm^2 cross section. This integral is equal to the area enclosed by the experimental curve. By means of this method, the energy carried by cosmic rays was determined and found to be equal to $E = 2.4 \times 10^9$ eV/cm^2 sec. One must add to this energy, the energy lost on the earth's crust and that carried away by neutrinos.

The energy brought to earth by cosmic radiation is 300 million times less than the energy coming from the sun and is almost equal to the energy of the visible light coming from the stars.

Let us now find the mean energy of cosmic rays. For this purpose, we divide the value obtained for the energy by the flux of cosmic-radiation particles, $E/J_s = \langle E \rangle$. As

$$J_s = 2\pi \int_0^{\pi/2} J(\theta) \cos\theta \sin\theta d\theta.$$

At the atmospheric boundary, the radiation is isotropic. Consequently

$$\mathcal{J}_s = 2\pi\mathcal{J}(0)\int_0^{\pi/2}\cos\theta\sin\theta d\theta = \pi\mathcal{J}(0).$$

The vertical cosmic-ray intensity $J(0) = 0.20$ cm^{-2} sec^{-1} $ster^{-1}$. Thus, the particle flux $J_s \approx 3 \times 0.20 = 0.60$ cm^{-2} sec^{-1}. The mean energy of cosmic rays at Moscow's latitude is then equal to

$$\langle E\rangle = \frac{2{,}4\cdot 10^9}{0{,}60} \simeq 4\cdot 10^9 \text{ ev}$$

Using data on the cosmic-ray intensity and cosmic-ray spectrum, one can estimate the energy density of cosmic rays in the space near the sun. Assuming that the radiation is isotropic, the density of particles having an energy higher than E will be given by

$$n(>E) = 4\pi\int_E^\infty \frac{\mathcal{J}(E)\,dE}{c\sqrt{1-\left(\frac{Mc^2}{E}\right)^2}},$$

where

$$\text{где } \sqrt{1-\left(\frac{Mc^2}{E}\right)^2} = \frac{v}{c} = \beta.$$

In the case of relativistic particles ($E > Mc^2$),

$$n(>E) = 4\pi\frac{\mathcal{J}(>E)}{c}.$$

The energy density will evidently be equal to

$$\mathcal{E} = \frac{4\pi}{c}\int_E^\infty \frac{E\mathcal{J}(E)\,dE}{\sqrt{1-\left(\frac{Mc^2}{E}\right)^2}}. \qquad (6.24)$$

Using data on the cosmic-ray intensity during the period of minimum solar activity (p.140) and integrating equation (6.24) after substituting the values of the actual cosmic-ray spectrum, one obtains [10]

$$\mathcal{E} = 0{,}9 \text{ эв/см}^3.$$

However, if one assumes that the high-latitudinal cut-off is due to the modulation of cosmic-rays by the solar wind inside the solar system, then the energy density of cosmic rays in the Galaxy will be several times greater.

Questions and Problems

1. Evaluate the azimuthal asymmetry at the equator at an angle of 60° t with the vertical direction, assuming 30% of the primary radiation are negatively charged particles.
2. Find the limiting momentum at geomagnetic latitude 51° (at Moscow) along the vertical direction.
3.a) Evaluate the latitudinal effect for vertically incident particles with energies higher than 7 GeV between latitude 51° and the equator.
b) Evaluate the latitudinal effect for vertically incident particles with energies higher than 15 GeV between the equator and latitude 51°.
4. Find the radius of the periodic orbits for protons with energy 60 GeV.

CHAPTER 7

MOTION OF PARTICLES IN THE INTERNAL PERMITTED REGION (CAPTURE REGION)

1. Geometry of the Capture Region

It was shown in chapter 2, section 6 that there exists a class of solutions for the equation of motion of particles in a magnetic dipole field, which correspond to bound trajectories. The boundary of the region of bound trajectories (the capture region) is a surface of revolutions, described by equation (6.14). In the capture region, $r_1 \leqslant r \leqslant r_2$ and $\gamma > 1$. The dimension of the capture region at the equator, is defined by the maximal distance between the region's boundary and the dipole centre /1/. The dimensions of the internal permitted region for different values of proton- and electron hardness, calculated by means of equation (6.14), are given in table 25.

Table 25

r_{max} $R_0=1$	r_{min} $R_0=1$	$\frac{pc}{ze} = \xi$ (GV)	Energy (GV)	
			proton	electron
1,00	0,41	59,5	58,6	59,5
2,00	0,83	14,9	14,0	14,9
4,00	1,66	3,72	2,90	3,72
6,00	2,49	1,65	0,96	1,65
10,00	4,14	0,60	0,173	0,60
15,00	6,21	0,264	0,036	0,264

It is clear that particle capture is only possible if r_{min} R_o, where R_o is the earth's radius.

The boundary of the permitted zone corresponds to a value of the particle's kinetic energy in the meridional plane, equal to Q = 0 and to a change of sign of the particle-velocity projection in the meridional plane. In other words, the particle will always be reflected by the boundary of the zone it cannot penetrate. The particle viluates between the boundaries of the permitted region in the Rz - plane (figure 50). The particle, together with the Rz - plane drifts with a velocity r φ' around the earth. Positively charged particles will drift to the west and negatively charged particles to the east.

2. Particle Sources in the Capture Region

It follows from the results obtained in chapter 6, that although a charged particle can have a stable motion in the capture region, it cannot yet penetrate from the outside into this region whatever its initial angular momentum γ . For a long time, it was assumed that the internal permitted region, is void of cosmic-ray particles. One may wonder whether there are any mechanisms which may lead to the appearance of particles in the trap, created by the internal permitted regions. Actually there are at least three such mechanisms :

1. The density variation of the solar wind and the penetration of the ionized gas coming from the sun into the atmosphere can for some time destruct the peripheral part of the earth's magnetic field. Magnetic waves will then start to propagate in the earth's magnetosphere and accelerate the particles. This will lead to the appearance of temporary channels and through these, particles will be able to penetrate into the trap.
2. Charged particles can be injected into the trap by means of neutral unstable primary particles. Neutrons originating from the sun or produced in the atmosphere, decay into protons and electrons in the trap zone and thus populate the trap by these particles.
3. Nuclear reaction products of nuclear explosions at large heights are captured by the field, becoming in this manner an artificial source of particles in the internal permitted zone.

Accordingly, there are several possible reasons for the occurence of particles in the internal zone. The particles are stored there, being unable to leave. Alongside the filling of the capture region by means of the above-mentioned sources, a reduction in the particle number of the region due to energy loss or scattering, takes place.

The density of particles in the zone will be thus defined by the dynamical equilibrium between the entrance and escape of particles. The intensity of the captured particles will be evidently defined as the product of the power source by the particle life time.

Figure 60 shows an example of a trajectory in a magnetic trap. This trajectory was calculated by Stormer in 1907 for a particle capture in the solar corona (not in the magnetic field of the earth).

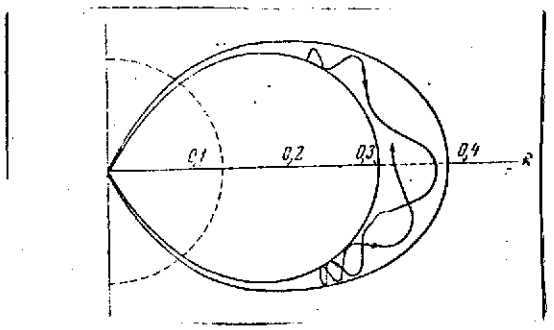

Figure 60. A particle trajectory in a magnetic trap, drawn according to Stormer's calculations.

In summary, it was recognized during the last half-century that the geomagnetic field forms a trap for charged particles. However, it was believed that the internal permitted region was void of particles, until experiments on satellites gave their first result.

3. Radiation Belts of the Earth

3.1. Discovery of terrestrial cospuscular radiation (radiation belts of the earth)

One of the most important discoveries of our time is the observation of a highly intensive radiation at a distance of a few terrestrial radii. The intensity of this radiation is millions of times greater than the intensity of the cosmic rays observed up till now in the terrestrial atmosphere.

First indications as to the existance of a very-high-intensity region were obtained while measuring cosmic rays by means of the second Soviet satellite, launched into orbit in November 1957 [2*]. The satellite flew at heights varying from 225 to 700 kms and measured the altitudinal behaviour of cosmic rays in this height interval. The cosmic-ray intensity was measured by means of two Geiger counters, working independently. A considerable increase of intensity (roughly twice) was systematically observed in the polar zone (see figure 61). No particular variation of cosmic radiation was observed on earth during that time. This suggested that the observed increase in cosmic-ray intensity was caused by an extremely soft radiation which did not reach the surface of the earth.

At the beginning of 1958, Van Allen and collaborators [3*] started a series of experiments on the study of cosmic radiation with the American satellites "Alpha" and "Gamma".

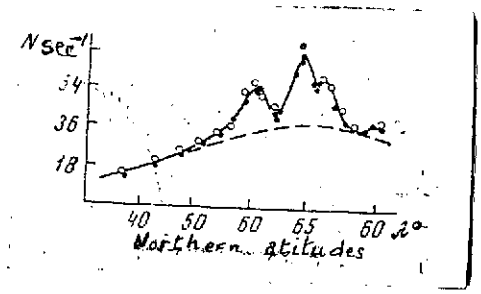

Figure 61. Cosmic-ray intensity, measured in 1957 by the second Soviet satellite, Sputnik-II.

The orbits of these satellites passed near the equatorial plane. The satellites carried a number of Geiger counters and at heights higher than 1000 kms in the equatorial zone the satellites passed by regions where the number of Geiger counts were so large that the counters reached their saturation limit.

In preliminary surface experiments, intensity levels saturating the counters were determined. Assuming that the radiation consisted of penetrating particles, it was concluded that the rate of counting would exceed the cosmic radiation intensity thousands of times. If the radiation consisted of soft electrons with an energy $\sim 1 - 0.1$ MeV, then these electrons would not be able to penetrate through the satellite's skin. They would be registered at the expense of the bremsstraalung x-rays which were produced as a result of electron deceleration in matter. Since the effectiveness of measuring X-rays by Geiger counters was small, it was necessary to assume that the intensity of these electrons were 10^{11} cm^{-2} sec^{-1}. Further investigations showed however, that the major contribution was due higher-energy particles having a lower intensity ($\sim 10^{8}$ cm^{-2} sec^{-1}).

The region where the radiation intensity strongly varies, is located at heights in the region from 700 to 1000 kms (figure 62). The dnesity of air at these heights is very small and the quantity of matter there is too small to explain the sharp variations in radiation intensity. However the radiation is soft there. Consequently, the observed radiation is retained in the region under consideration by some external effects. Since these particles are charged, it is natural to assume that they are held by the terrestrial magnetic field. In the following, we shall call the zone, in which particles are captured by the terrestrial magnetic field, a radiation belt.

In May 1958, the third Soviet satellite Sputnik-3 was launched into orbit [2]. On this satellite, a systematic measuring of intensity was carried out not only in the equatorial region, but also at large latitudes (till 67°). A scintillation counter, registering cases of energy release in the crystal higher than 35 MeV was used for registering cosmic radiation. It was un-

expectadly found that the equatorial high-intensity zone terminated abruptly at a latitude approximately equal to 40°. At a latitude 60°, the satellite again entered a region of a rapidly increasing intensity. A.E. Cydakov suggested that this observation might be explained by assuming the existence of a second radiation belt, which was observed at heights 200 - 300 kms and at latitudes $\geqslant$ 60°.

The theoretical interpretation of this phenomenon was published almost

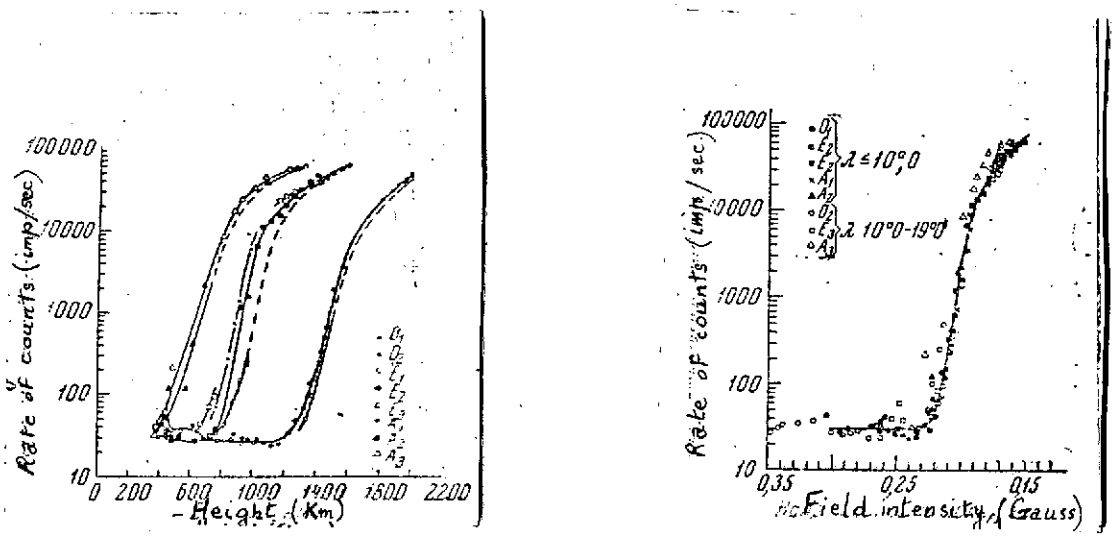

Figure 62. Count rates by the gas-discharge counter on the American satellite "Explorer", a- as a function of altitude at various latitudes (left curve over the Atlantic, right curve: over Singapore), b- as a function of the magnetic-field intensity. Points O, E and A represent the results of different measurements.

simultaneously by S.N. Vernov and A.I. Lebedinskij in USSR and by Cristofilos, Van Allen and others in the USA /3*,4*/.

3.2. Alfven's approximation /5/

The calculation of particle trajectories in the terrestrial magnetic field is extremely complicated. For particles of not-very-high energies, Alfven suggested to solve the problem by using adiabatic-invariance considerations. The radius of that surface, along which a particle in a magnetic field of flux-density B moves, is equal to

$$R_L = \frac{mvc \sin\theta}{eB},$$

where v is the particle velocity and R_L the rotation radius, or the Larmor radius. The condition for the applicability of Alfven's approximation is that the magnetic field does not change over lengths in the order of the Larmor radius. Moreover, field B must be constant with respect to time, i.e.

does not vary during a time in the order of the Larmor period :

$$T_L = \frac{2\pi R_L}{v_\perp} = \frac{2\pi mc}{eB},$$

Accordingly

$$R_L \left| \frac{\partial B}{\partial r} \right| \ll B; \tag{7.1}$$

$$T_L \left| \frac{\partial B}{\partial t} \right| \ll B. \tag{7.2}$$

The characteristic dimension of the magnetic field is the earth's radius R_o and hence the first condition may be written as

$$R_L \ll R_0 = 6 \cdot 10^3 \text{ Km}$$

Table 26 gives the Larmor radii at a distance of $2R_o$ from the earth's centre ($\sin \Theta = 1$). It follows from the table that condition (7.1) is fulfilled

energy (KeV)	R, км	
	electrons	protons
10	0,087	3,71
10^2	0,287	11,70
10^3	1,22	37,10
10^4	12,2	118,0
10^5	122	381,0
10^6	—	1451

for particles with energies less than 100 MeV. For particles, whose motion satisfies equation (7.1), the motion may be divided into three independent components :

1. The particle moves along a circle of radius equal to the Larmor radius. The circle's centre is called the leading centre.
2. The leading centre moves with velocity v in a direction making an angle of Θ with the line of force. The particle reaches the maximal height at the reflection point and the minimal height at the equator.
3. The leading centre of the particle moves around the earth along the surface of revolution of the line of force (in a dipole field). Let us consider this motion in the more detail.

a) <u>First adiabatic invariant</u>.

An electron, moving along a circle of radius R can be represented by a current loop having a magnetic moment

$$\mu = \pi R^2 j, \tag{7.3}$$

where j is a current equal to $j = ew_c$, and w_c is the cyclic (Larmor) frequency of the electron's rotation along the orbit :

$$\omega_c = v(\sin\theta)/R. \tag{7.4}$$

Since $R = \frac{mvc \sin\theta}{eB}$, then $w_c = \frac{e}{c} \cdot \frac{B}{m}$.

The period of the electron's Larmor vibration is measured in microseconds while that of the proton in milliseconds. Therefore

$$\mu = \pi R^2 e\omega_c = \frac{\pi m v^2 \sin^2\theta}{eB} \tag{7.5}$$

or

$$\mu \sim \frac{v_0^2 \sin^2\theta}{B}. \tag{7.6}$$

Since velocity v_o in the magnetic field is constant, then

$$\mu \sim \frac{\sin^2\theta}{B}. \tag{7.7}$$

Alfven proved that if nothing resists the electron motion, then quantity u remains constant. In other words, u is an adiabatic invaraint (first adiabatic invariant).

The magnetic moment vector is perpendicular to the current loop, and hence is along the line of force. In analogy with a magnetic needle, the vector will follow the line of force. Assuming that at a given line of force at the equator, the particle velocity makes an angle θ_o with the direction of the line of force, and that the particle magnetic moment is equal to

$$\mu_0 = \frac{\sin^2\theta_0}{B_0}. \tag{7.8}$$

then, at latitude λ where the magnetic flux density is equal to $B(\lambda)$,

$$\mu_0 = \frac{\sin^2\theta_\lambda}{B(\lambda)}, \tag{7.9}$$

where θ_λ is the angle between the direction of the particle velocity and the line of force at latitude λ (the pitch angle). The terrestrial magnetic field is an inhomogeneous field. The line of force of a dipole is described by the equation :

$$R = R_e \cos^2\lambda, \tag{7.10}$$

where λ is the geomagnetic latitude. The flux density of the geomagnetic field at a given line of force is given by

$$B(\lambda) = \frac{B_0\sqrt{4-3\cos^2\lambda}}{\cos^6\lambda}; \quad B_0 = M/R_e^3 \tag{7.11}$$

Here, M is the magnetic moment of the terrestrial dipole and R_e the distance from the earth in the equatorial plane. With increasing , the magnetic flux density $B(\lambda)$ increases. Consequently, the necessity for increasing the angle follows from the constancy of u .

When sin θ_o reaches its maximum value, equal to unity, and the particle motion becomes perpendicular to the line of force, further motion of the particle along the line of force becomes impossible. Each value of angle θ_o at the equator has its own latitude λ_{max} where it reaches its maximum value /2. At this latitude the particle is reflected and starts its motion in the inverse direction. Such a behaviour of the particle is understood from simple qualitative arguments. Let us assume that the particle is moving in the direction of increasing magnetic field. The particle velocity can be expanded into two components, v_{11} along the line of force along which the particle is moving and v_1, related to the particle motion along a circle around the line of force. Let the radial component of the flux density B, be B_r. The interaction of component B_r with velocity component v_1 leads to the occurence of a force of $f = \frac{e}{c} v_1 B_r$ in the direction of the decreasing magnetic field. This force will decrease the parallel velocity component and consequently increase v_1. At the reflection point, $v_{/\!/} = 0$, $v_1 = v$ and $F_{/\!/}$ is maximum. Consequently, when the particle reaches the reflection point, it returns back and starts to move towards the equator. The longitudinal velocity component will then increase and the transversal component decreases as a result of the action of force F . If velocity v makes an angle θ_o with the line of force at the moment it passes the equator, then the angle becomes equal to $\pi - \theta_o$ in the inverse direction. The trajectory along which the particle moves between the reflection points is shown in figure 63.

Accordingly, the particle makes an infinite number of vibrations between latitudes λ_{max} and $-\lambda_{max}$ if it does not loose energy or is not scattered from collision with the atoms of the air.

According to the general theory, all the directions within the permitted zone are allowed. It might therefore seem that the angular distribution of particles in the permitted zone would be isotropic. However, if the energy loss of particles due to atomic collisions is taken into account, the situation will be different. In fact, all particles whose reflection points are located at a distance less than 100 kms from the earth's surface, loose a considerable part of their energy on ionization and die in the atmosphere. Consequently, there exists a cone of directions with an apex angle $\theta_{o\,min}$, which encloses all the directions forbidden by the violation of the first adiabatic invariant.

The height h of the reflection point is determined by the equation of the line of force (equation 7.10)

$$h = R - R_0 = R_e \cos^2 \lambda - R_0.$$

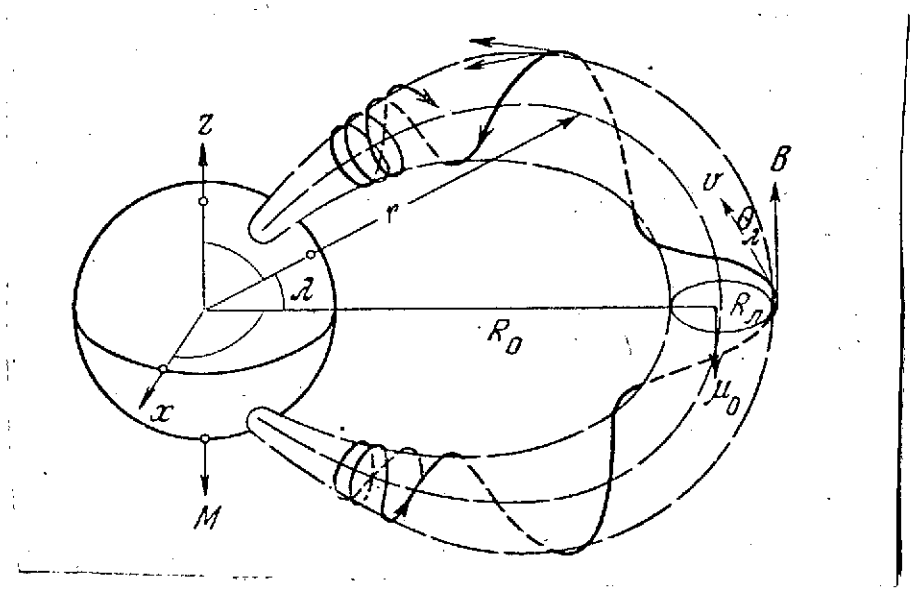

Figure 63. The trajectory by which a particle moves between the reflection points.

Quantity $\cos^2 \lambda_{max}$ is related to angle θ_o by means of equations (7.9) and (7.11). The condition that limits the value of θ_o is such that $h(R_e, \theta_o)$ 100 kms. Angles less than θ_o are forbidden.

The vibration period of a particle between reflection points is in the region of 0.1 ÷ 1 second for electrons and 1 - 50 secs. for protons on orbits located at a distance $R_e \sim 2R_o$. The velocity of a particle along a line of force will be maximum at the equator and very small near the reflection points.

Other forces, for instance a force proportional to B X grad B will act alongside the Lorentz force, $\frac{e}{c}$ v x B , on a particle in a magnetic field. The gradient of the terrestrial magnetic field is directed along the normal from the earth's centre, since in this direction the field namely decreases. Since the vector product is a vector perpendicular to both B and grad B, this force will then act on the particles in such a manner that it makes them move around the magnetic dipole. In other words, the force will drift the particle around the earth.

b) Second adiabatic invariant

The second adiabatic invariant is often called the longitudinal adiabatic invariant. It is equal to the integral of the action of vibrational motion of particles along the line of force between reflection points M and M* (figure 64) :

$$\mathcal{J} = \int_M^{M^*} p_{\parallel} ds = p_0 \int_M^{M^*} \cos\theta ds = p_0 \int_M^{M^*} \sqrt{1-\sin^2\theta}\, ds. \tag{7.12}$$

Quantity p_o = constant, since neither the mass nor the velocity of the particle,

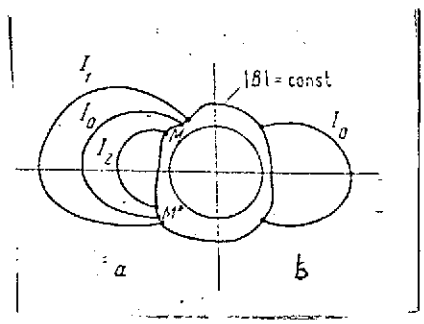

Figure 64. The second adiabatic invariant (explained in the text).

change along the line of force. It follows from equation (7.9) that

$$\frac{\sin^2\theta}{B} = \frac{\sin^2\theta_M}{B_M} = \frac{1}{B_M}, \tag{7.13}$$

where θ_M is the angle at the reflection point, equal to $\pi/2$ and $\vec{B}_M$ the magnetic flux density at the reflection point. Therefore

$$\mathcal{J} = p_0 \int_M^{M^*} \sqrt{1-B/B_M}\, ds; \quad I = \frac{\mathcal{J}}{p_0} \int_M^{M^*} \sqrt{1-B/B_M}\, ds. \tag{7.14}$$

Why is this adiabatic invariant called longitudinal ? The reason is that the conservation of quantity I enables us to predict, in which of the infinitely large number of lines of forces will the particle move after being drifted by the latitude (due to the action of force B x grad B).

The first invariant predicts that the reflection points lie in a plane with definite values of B_M and B_{M^*}. The conservation of the second invariant implies that if at moment t the particle moved along a line of force with

$I = I_o$ (figure 64,a), then at moment t_2, it would move along another line of force for which $I = I_o$ also (figure 64,b).

The existance of the first and second adiabatic invariants indicate that there exists a given cloud around the earth, at which there is always a particle having given values of B_M and I_M at the initial moment.

3.3. The coordinate system

In the theory of geomagnetic effects, the coordinate system (r, λ) was used, r being the radius vector and λ the geomagnetic latitude. In an ideal dipole field, the line of force that passes by point (r, λ) crosses the equator at point $R_e = r/\cos^2 \lambda$. Therefore, the coordinate system (R_e, λ) is sometimes considered instead of the coordinate system (r, λ). In the actual terrestrial field, different anomalies of the magnetic field are observed at small heights. Systems (R_e, λ) and $(r\ \lambda)$ are also inconvenient at distances greater than $6R_o$ where the field is modified by the solar wind. The above mentioned systems are accurate for the regions at distances enclosed between 3 and $6R_o$.

Mac Ilvein [6,12] introduced a coordinate system, in which one of the coordinates of point F is defined by the distance L from the centre of the earth to the point where the line of force passing by point F crosses the equator. Point L is expressed in earth radii, i.e.

$$L = \frac{R_e}{R_o}. \tag{7.15}$$

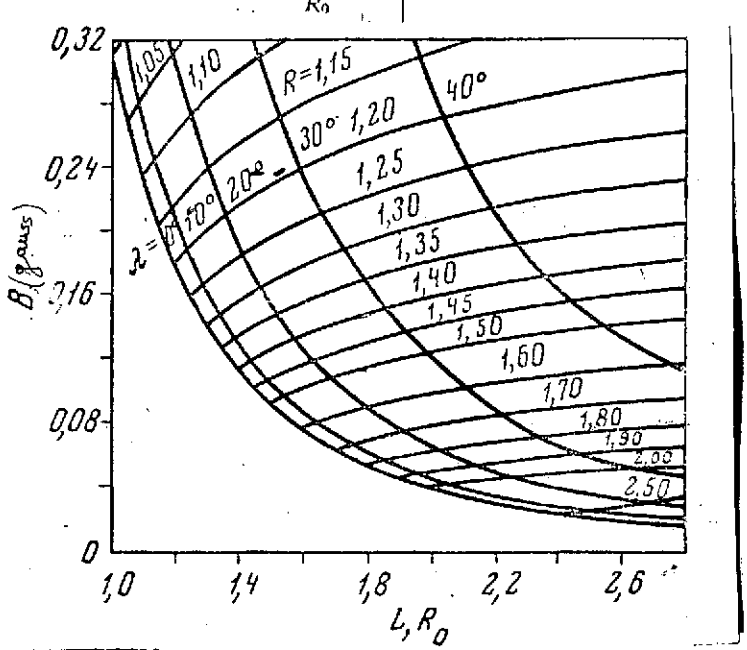

Fig. 65 – Relation of the systems of coordinates (R.λ) and (B,L) for the field of dipole.

Flux density B at point F is calculated taking into account the actual terrestrial magnetic field and considered as the second coordinate. Consequently, the coordinate set in this "natural" (B,L) coordinate system is obtained by the crossing of the lines of surfaces L = constant and B = constant. Its relation with the "classical" (r, λ) coordinate system is given in figure 65. System (B,L) is accurate for distances up to L = 6. Representation of the results by this system requires the use of a computer.

The relation between the "natural" system and the (r, λ) system takes the following simple form in the case of a dipole field :

$$\cos^2\lambda = \frac{r}{L} \text{ и } B = \frac{M}{r^3}\left(4 - 3\frac{r}{L}\right)^{1/2}. \qquad (7.16)$$

4. Instruments for Studying Radiation Belts

a) Measurement of particle intensity and density

Different problems appear while studying the trapped cosmic rays. Aside from the determination of radiation intensity, it is necessary to determine the energy spectrum of particles and identify their nature, i.e. their charge and mass distribution, etc. The instruments used must be compact and economic. The large particle intensity in the radiation belts makes it possible to use instruments of a small size. The second Soviet satellite Sputnik-II (November 3, 1957) carried two gas discharge counters. Sputnik-III (May 15, 1957) registered the radiation by means of a scintillation counter [2]. A cylindrical sodium-iodide crystal of radius approximately equal to 40 mm was used as a scintillator. The crystal was creened by 1 g/cm^2 of aluminium. A similar instrument was also carried by cosmic rockets. Threshold instruments were used to measure the number of cases in which energies 45 keV, 450 keV and 4.5 MeV were separated. Furthermore, total ionization was measured in a scintillator covered by a foil thickness of only 1.9 mg/cm^2. In other experiments, semiconductor detectors, ionization chambers, photo-emulsions and magnetic spectrometers were used [7, 8].

The typical equipment of American satellites consisted of scintillators, crystal and gas-discharge counters (a cylinder of dimensions 7 x 9 mm) of the "Anton-302", type. For instance, the "Explorer-4" satellite carried a counter with a lead screen thickness of 1.6 g/cm^2. This counter could determine the intensity of protons having an energy E 40 MeV, electrons having an energy E 3 MeV and X-rays with an E 80 keV. When the screen of this counter is removed, the counter could register electrons with an energy E 1.6 MeV and protons with an energy E 23 MeV. Scintillators with a diameter of 0.76 cm, made of caesium iodide and having a protecting foil of thickness 1.0 mg/cm^2, could register protons with an energy E 20 keV and protons with an energy E 400 keV. In this manner, by applying different screens, different parts of the spectrum could be studied separately.

On board the second Soviet satellite, the estimation of particle energy was done by using a scintillating crystal with a photo-multiplier [2]. The current of each intermediate dynode of the photo-multiplier is proportional to the ionization occuring in the crystal. The current impulse at the anode increases with increasing energy till the latter becomes equal to 2 MeV, and then reaches the saturation point. A relativistic particle loosing an energy of 20 MeV while passing through the crystal, gives a full contribution to the dynode current but contributes by 10% to the anode current. Hence, the difference in the measured values of anode current I_A and dynode current I_D can be used to estimate the contribution of relativistic particles to the ionization produced. For instance, when primary cosmic rays pass through a scintillator, the ratio $I_A/I_D \sim 6$. In the internal radiation zone, quite different values for I_A and I_D are observed. This means that ionization in the counter is caused by particles having energies higher than 10 MeV.

The energy spectrum of protons in the internal belt was measured by means of photo-emulsions raised by rockets. The energy interval carried by the measurements extended from 75 to 750 MeV [8].

b) Identification of particles

The second Soviet satellite helped in making the first conclusions on the nature of particles in the internal radiation belt. It was noted that even when the satellite left the trapping region, an increased number of counts was still observed. This was explained to be due to an induced radioactivity in the crystal of the scintillator. By measuring the half-life times and the energy lost by particles for inducing an artificial radio-activity into the crystal, it was concluded that the crystal was subject to the action of protons with an energy approximately equal to 100 MeV.

The American satellite "Explorer-12" carried magnetic spectrometers which measured electrons with energies of 45 to 60 keV (SpL-channel) and from 80 to 110 keV (SpH-channel). Electrons of corresponding energies were registered by a counter of the "Anton-213" type, with mica covered windows of approximately 1.2 mg/cm^2 thickness. The penetrating-particle background was measured by another spectrometer. A combination of detectors, as described above, and a total-energy detector (a CdS-TE crystal) made it possible to establish the electron spectrum.

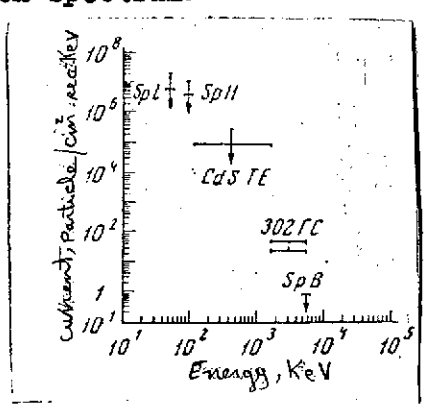

Fig. 66. Efficiency of different detectors in different energy regions. Sp-spectrometers, Cds-crystalline counters, GC- Geiger counters.

Figure 66 shows the energy intervals measured by different currents as well as the differential fluxes of electrons in the centre of the external radiation belt.

The analysis of the data, obtained by the above mentioned methods enables us to determine the energy and composition of particles in the radiation belts.

5. Experimental Investigation of Radiation Belts

5.1. General picture

In the first experiments made with rockets and satellites, high-energy particles were mainly registered. The intensity of this penetrating radiation has two maxima at distances of 1.5 and 3.5 - 5 earth radii respectively (in the geomagnetic equator plane). These two high-intensity zones are called internal and external belts.

Particles of the internal belt are held on lines of force, reaching the earth's surface (the atmosphere) at latitudes less than 40 - 45°. There is no high-energy trapped radiation on lines of force meeting the atmosphere in the latitude region 45 - 60°. Lines of force at higher latitudes are again populated with penetrating particles. At the equator, they disappear up to a distance of 5 - 7 earth radii. Accordingly, the internal and external belts are separated by a slit located in the region between 2 and 3 earth radii. The particle flux is greater in the external belt than in the internal one. The particle composition is also different; the internal belt involves protons and the external one electrons.

The application of unscreened detectors significantly increased our knowledge on radiation belts. Electrons with energies of a few tens of kiloelectron volts and protons of several hundreds of kiloelectron volts were observed. These particles have essentially different spatial distributions in comparison to penetrating particles. The intensity of the low-energy protons has a maximum at a distance approximately $3R_o$ from the earth. Low-energy electrons occupy the whole caputre region. For these electrons, the division into external and internal belts has no meaning. Particles with energies of tens of kiloelectron volts are hard to be related to "cosmic rays". A radiation belt however, is a unit phenomenon and should be studied as a complicated entity with all its particles, whatever their energies are.

2. Lower boundary of the radiation belt

The altitudinal dependence of the trapped-radiation intensity at the equator, was first studied by Van Allen in 1958 [3*]. Figure 62,a shows the results of the experimental measurement made by a single Geiger counter at the equator. Curves, related to different latitudes are distinguished by the region of heights where a sharp increase in intensity occurs (400 kms over the centre of the Atlantic Ocean and 1300 kms in the region of Singapore). Such a discrepancy is easily understood in terms of the eccentricity of the terrestrial dipole. Figure 62,b shows the same results in the natural coordinate

system. These curves shows that the intensity is indeed a function of the magnetic flux density and in this manner illustrates the advantage of using the natural coordinate system.

5.3. Nuclear component of the radiation belt

Photon-emulsion experiments [8] made it possible to study the composition of the captured radiation. It was found that at energies higher than 30 MeV, 99% of the nuclear component consisted of protons, and the rest deuterons and tritons. Recently, alpha particles, trapped by the terrestrial magnetic field were observed by means of semiconductor detectors at a height of L 3.

5.4. Spatial distribution of protons and their flux

The spatial distribution of various energy protons (the equi-intensity lines) is shown in figure 67 [9]. This data shows that (a) the intensity of high-energy protons has a maximum located nearer to the earth's surface than the intensity of low-energy protons, (b) the flux of protons with energies greater than 35 MeV is 3 - 4 times less than the low-energy proton flux, and (c) the maximum of the high-energy proton intensity corresponds to the internal radiation belt (L = 1.5 R_o). Low energy protons occupy the external belt (L 4). The flux of protons with an energy $0.1 < E < 4.5$ MeV exceeds 10^8 cm^{-2} sec^{-1}. At E 35 MeV, the flux is equal to 3×10^4 cm^{-2} sec^{-1}.

5.5. Proton energy spectrum

The spectrum of high-energy protons in the internal region can be represented by a power function, $J_p(E)dE \sim E^{-1.8}$ dE ($75 < E < 700$ MeV). As the distance from the internal belt's centre increases ($L > 1.5 - 8$), the mean proton energy decreases. With increasing L, the spectrum becomes softer and softer. In the energy interval 10 - 50 MeV at a distance L = 1.79, the spectrum becomes

$$\boxed{\mathcal{J}_p(E)\,dE \sim E^{-4.5\pm0.5}dE.}$$

At lower energies, the spectrum is well approximated by an exponential function :

$$\boxed{\mathcal{J}_p(E)\,dE \sim e^{-E/E_0}dE,}$$

where $E_o = (306 \pm 0.28)\ L^{-5.2 \pm 0.2}$ MeV, ($1.2 \leqslant L \leqslant 8$). Future experiments should give more accurate results.

5.6. Stability of the proton flux

The proton flux in the internal belt is quite stable relative to time. Measurements have been carried out at distances $L > 2R_o$. In September 1963,

after a strong magnetic storm, the intensity of protons with an energy $E > 35$ MeV at a distance $L = 2.4$ changed 5 times whereas at a distance $L = 2.1$, the flux remained unchanged. Apparently, the intensity of protons in the external zone also remained unchanged.

5.7. Electrons in the radiation belt. Particles of natural origin

Earlier experiments showed that high-energy electrons ($E > 1 \div 1.5$ MeV) were concentrated in the external belt. At a distance $L \sim 4.5\ R_o$, the flux of electrons with an energy $E > 1.1$ MeV reaches $5.5 \times 10^5\ cm^{-2}\ sec^{-1}$. Electrons with an energy $E > 5$ MeV in the radiation belt are quite few. According to measurements on the Soviet station "Luna-2", the flux of these latter electrons does not exceed $10^3\ cm^{-2}\ sec^{-1}$. As the electron energy increases, their spectrum becomes sharper. In the energy interval $350 \div 650$ keV, the exponent of the power energy spectrum $\gamma = -2$, while $\gamma = -7$ in the energy interval $1 \div 5$ MeV.

Electrons with an energy less than 1 MeV occupy almost all the magnetosphere. They however show several characteristic features. At a height of 1000 kms, the flux of electrons with an energy greater than 40 keV is approximately invariable up to a latitude $\lambda = 69°$ at midnight (local time) and up to a latitude $\lambda = 75°$ at midday, and then ends abruptly. Lines of force corresponding to these latitudes cross the equator at distances of $8R_o$ and $15R_o$ respectively. This indicates that the capture region is different in the day-time and at night. In order to explain this effect, the influence

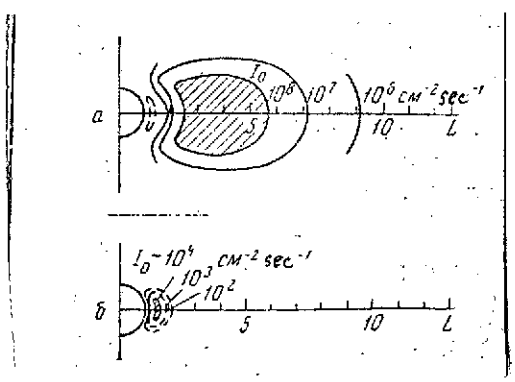

Fig. 67. Spatial distribution of protons of different energies in the radiation belt a- proton energy $0.1 < E_p < 5$ MeV, b- $E_p > 30$ MeV.

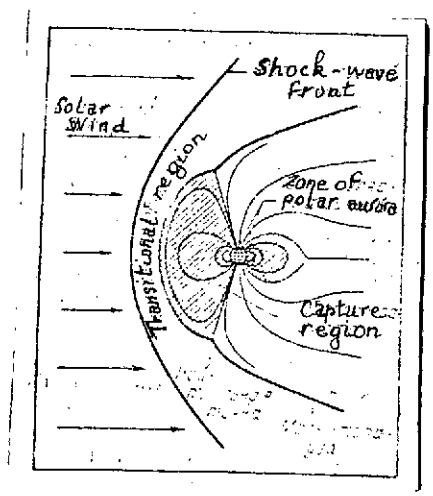

Fig. 68. Variation of the magnetoscope by the influence of solar wind. The dashed area represents the region of particle capture.

of solar wind on the magnetosphere has been considered /10/. The solar plasma (solar wind) collides with the magnetosphere of the earth and starts to flow round it. According to the conclusions in chapter 6, the positively charged particles are deviated eastwards and the negatively charged particles westwards. The resulting polarization of the flux can be described by an equivalent current, J, directed anticlockwise if one looks from the northern pole side of the earth. As a result of interaction with the terrestrial magnetic field, current J produces a force parallel to the vector product J x B. This force is antiparallel to the pressure force of the plasma and the two forces counterbalance one another. Consequently, in the day side, the terrestrial magnetic field is compressed and the flux-density of the field near the boundary of the atmosphere increases. In the night-side, the magnetosphere is stretched and the magnetic flux density is reduced. Accordingly, the capture region extends approximately to the atmosphere's boundary at midday in the day-side and only occupies a small part of the atmosphere in the night side. Figure 68 illustrates the deformation of the terrestrial magnetosphere by the influence of the solar wind and the capture region for low-energy electrons (the dashed area).

Electron fluxes in the radiation belt at distances $L \geqslant 2R_o$ are subject to strong time vibrations, related to the magnetic perturbations. At distances of $L \geqslant 3\ R_o$, the variations may be as large as two orders in magnitude. The number of low-energy electrons increases particularly during strong magnetic storms. The number of high-energy particles first decreases and then increases. These variations may last for a whole twenty-four hours. During the calm periods, the electron intensity reaches a value $J_e \sim 10^8\ cm^{-2}\ sec^{-1}$. Figure 69 shows the spatial distribution of electrons of different energies in the day side /10/. The study of electrons coming from natural sources in the internal radiation belt is now impossible. They are mixed with electrons of an artificial origin coming from American nuclear explosions (see item 58). This situation will continue during at least the next decade.

5.8. "Argus" and "Starfish" Experiments /12/

A considerable amount of electrons were injected in the internal zone by the large explosions of American atomic bombs. These explosions were devoted to the study of several aspects of the radiation belts. These experiments also had military objectives besides their scientific nature.

The first experiment was made in 1958 and called operation "Argus". The scientific purpose of the experiment was to experimentally prove the existence of the magnetic trap and to measure the life-time of particles in the radiation belt.

The idea of the experiment was suggested by the American physicist, Christofilos. It consisted in introducing a quantity of electrons into the terrestrial magnetic field in order to observe the high intensity belts they formed and the subsequent resolution of this zone. The electron source they used was three atomic bombs which were exploded one after the other in 1958

at a height of 450 kms and at a latitude 50°S, i.e. in the space region where the natural belts form a slit between the upper and lower zones. "Explorer-4" satellite was simultaneously launched and it had to cross the artificial zone several times a day and give information on its intensity.

At the moment of the explosion, an intensive sky luminescence was observed at the end of the lines of forces, both in the southern and in the northern hemispheres near the Azores where the ships of the US Navy were stationed. Due to the electron drift round the earth (due to force HXgrad H), the electrons formed a thin cloud around the whole earth. At the equator, this cloud was located at a height of 6500 kms ($L \simeq 2R_o$), i.e. in the slit between the internal and external radiation belts. This position remained unchanged for several weeks, as long as the observations were continued. A month after the explosion, the electron intensity was almost the same as the natural background intensity.

The second series of experiments of this type was made in 1962 and called operation "Starfish". An artificial radiation belt was produced in the region of the internal radiation belt. Electrons of an artificial origin, having energies of several megaelectronvolts will continue to exist at a distance approximately equal to 1.5 R_o for several decades. The intensity of the injected electrons with an energy $E > 5$ MeV reaches 1.5×10^7 cm^{-2} sec^{-1}. The analysis of the results shows that the particles die at distances $L < 1.4$ R_o because of the energy loss and scattering in the atmosphere.

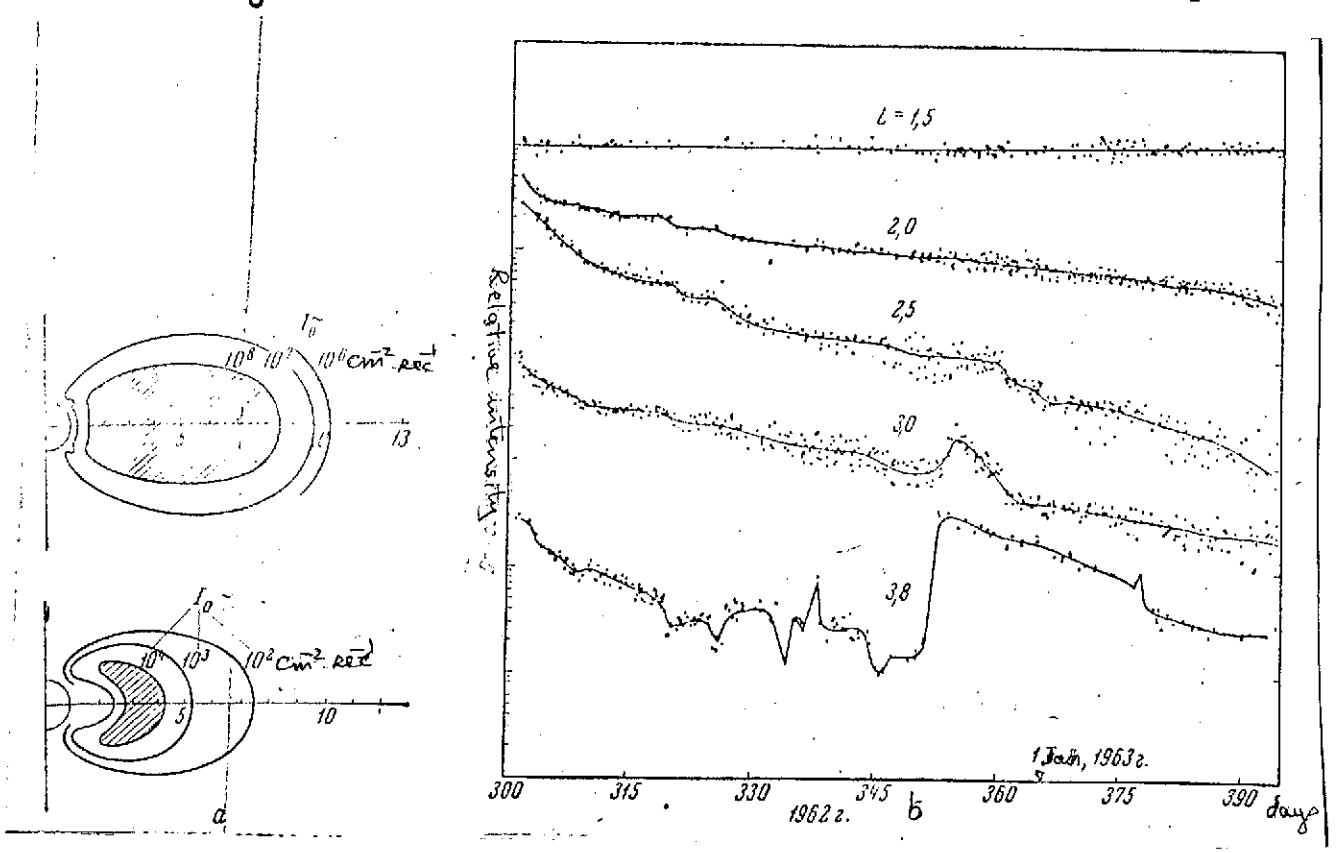

Fig. 69. Properties of electrons in the radiation belt: a– Spatial distribution of electrons having different energies in the day-side; in the upper figure E_e 40 KeV, and in the lower E_e 1.6 MeV. b– Time variation of electrons intensity.

The investigation of radiation belts during the magnetic storm periods is of particular interest. The behaviour of the belts in these periods is extremely complicated. The intensity of the low-energy component increases during the period of a strong magnetic storm while the intensity of the high-energy particles ($E_e > 1.5$ MeV) decreases. During the period of the inverse phase of a magnetic storm, the intensity increases and sometimes exceeds several times over the intensity in the period before the storm. Later, after several weeks, the intensity returns back to its initial value. These results suggest that there is a mechanism responsible for accelerating the electrons during the period of magnetic perturbations.

Parallel with intensity variations, the geometry of the radiation belt also changes. The intensity maximum is displaced towards the interior of the magnetic field during the first phase of the storm. The variation in distance reaches 10% of the initial value. In the case of weak magnetic perturbations the intensity of particles with an energy $E_e > 5$ MeV at $L < 3.8$ decreases. This effect was observed by the American satellite "Explorer-15".

It is possible that the particles are decelerated during small magnetic perturbations while their number in the trapping region remains unchanged. During strong storms, an inverse acceleration takes place.

5.9. Sources of particles injected into the capture region

The above-mentioned intensity variations of particles in radiation belts show that in many cases, the adiatic invariants are violated. The reflection points are then displaced and may fall into the atmosphere. The change of the pitch-angle as a result of scattering and the energy loss by particles due to collisions with atoms, may remove the particles outside the capture region. Energy loss by particles occurs at the reflection points, where particles spend the greatest time.

Table 27 gives the life-time of particles in the atmosphere and the energy losses on collision at different L's and energies [13]. Life-times given in table 17 are not actually realized.

Magnetic perturbations also remove particles from the belts by moving the reflection points to lower heights. In particular, it was considered earlier that polar auroras were caused by the falling of charged particles from the belts. It is already now known that the particle flux in a radiation belt is not sufficient for maintaining polar auroras for the lengths of time observed. By direct investigation, it was found that polar auroras were induced by very-low-energy particles (with $E < 10$ keV).

Accordingly, particle capture into the belts is not absolute. If there were no permanently acting sources compensating the particle loss, the existance of these belts would have been impossible. The existance of several possible sources was proposed :

Table 27

Particles	Energy (Mev)	Lifetimes		
		$L=1,2\ R_0$	$L=1,6\ R_0$	$L=3\ R_0$
Proton . .	10 100	2 months 5 years	30 years 1000 »	100 years most captured
Electron .	0,3 2	10 days 3 months	6 » 60 »	20 years 200 »

1. Albedo neutrons

The neutron mechanism was suggested by S.N. Vernov, A.I. Lebedinskij and Singer [4, 14]. The capture of charged particles by the magnetic field is possible if these are carried by any artificial means in such a way as to avoid the limitations imposed by the conservation law of magnetic-moments. The first point that comes to mind is that these particles are transported in the form of neutral particles, namely neutrons. It is well known that neutrons decay into electrons and protons. These particles have small energies and are thus captured by the earth's magnetic field. The origin of neutrons, capable of injecting charged particles into the magnetic trap could be various. A small part of such neutrons could be of solar origin. The sum is a huge nuclear reactor. The neutrons produced can reach the earth and decay there. However, due to the large distance between the sun and the earth, only a small fraction of these neutrons will be able to arrive to the earth.

Another source of neutrons could be the terrestrial atmosphere. In atmospheric nuclear disintegrations, a large number of neutrons are produced. These neutrons are isotropically distributed. A large part of them may escape from the atmosphere's range and decay in the region of the magnetic trap (the so called "albedo" neutrons). In decaying, the neutrons produce protons which carry the major part of the neutrons' energy. This leads to the occurence of protons with energies up to 100 MeV.

Low-energy protons ($E_p \geqslant 10$ MeV) could occur as decay products of neutrons produced by the bombardment of the atmosphere by low-energy particles of solar origin. These particles could only penetrate the terrestrial magnetic field in regions close to the poles. Neutrons, emerging from the polar zones decay in the trapping region and inject it with protons. Calculation shows that the injection only occurs at $L > 1.6$. Figure 70 shows the calculated and measured proton spectrum at $L = 1.7$.

We know very little on protons having energies less than 10 MeV. It is assumed that the loss of these protons must be so large that the neutron mechanism might be insufficient. The neutron source is very weak. The albedo neutrons could only fill the belt with particles after a time period of approximately 30 - 50 years. In that region of heights, where intensity fluctuation is considerable, the neutron source cannot have a decisive role.

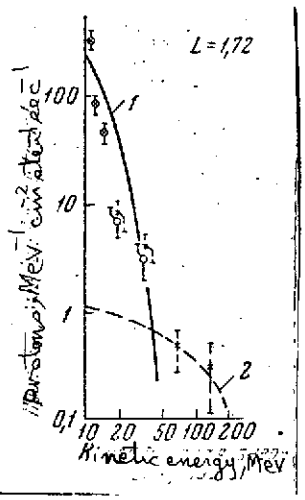

Figure 70. Energy spectra of protons in the radiation belt. The solid and dashed curves are theoretical. 1-Protons from neutrons of the polar caps.
2- Protons from cosmic neutrons.

2. Interaction of plasma with the magnetic field /15, 16/

The failure for explaining the existance of low-energy particles in the belts by the neutron mechanism, as well as the sharp variation in particle intensities at $L > 2$, require the introduction of sources more effective than the neutron. A possible explanation could be achieved by the various mechanisms of particle acceleration by the variable magnetic field in the terrestrial magnetosphere. Density and velocity fluctuations of the solar wind at the boundary of the magnetosphere produces magneto-hydrodynamic waves, which propagate from the atmosphere's boundary to the earth's centre. Such a moving magnetic field could accelerate charged particles (see chapter 10). The waves are however damped as they start to penetrate into the region of strong magnetic fields (at distances $L > 4 \div 5$). Consequently, deeper zones are less affected by this mechanism.

The ionized cloud encircling the earth might serve as a source of particles. This cloud was discovered by Soviet physicists under the supervision of K.I. Gringauz. This zone is partially located with the limits of the terrestrial magnetosphere (in the night side) so that its particles can be captured by the magnetic field (i.e. move along the lines of force). In

the day-side however, the ionized cloud is outside the limits of the magnetosphere. The energy of the particles of the cloud is not more than a few electron-volts.

Questions and Problems

1. Find the Larmor radius for a proton moving with an energy of 100 keV at a distance of $6R_o$ from the dipole's centre.

2. Find the coordinates of the reflection point of a captured particle making an angle of 60° with the direction of the line of force at the equator at a distance of $3R_o$ from the dipole's centre. Repeat the problem for particles making angles of 0° and 90°.

3. Find the natural coordinates for a particle at $R = 3R_o$ and $\lambda = 30°$.

4. At what height from the earth's surface does the reflection point of a particle make an angle $\theta_o = 45°$ (at the equator) at $L = 10$?

CHAPTER 8

STABILITY AND VARIATION OF COSMIC RADIATION

1. Conservation of Mean Intensity

1.1. Formulation of the problem

Up to this moment, we were considering the mean intensity of cosmic radiation. At energies higher than 5 GeV, the intensity, averaged over a period of one year, did not change during the past few decades. At lower energies, significant variations of the mean intensity occur and are related with the cyclic solar activity. During the period of maximum activity, the total intensity of cosmic rays at the earth's surface decreases by a half. One may wonder on how radiation intensity changes during periods of a thousand, a million or a billion years. This question is of great importance, not only for Cosmogony, but also for the problem of the origin of cosmic rays. The answer to this question is also important for archaeologists who use radioactive-carbon methods for measuring the age of archaeological objects.

The genetic action of cosmic rays raises a question on the role of cosmic rays in the formation of species. From this point of view, it is important to know the intensity of cosmic rays during ancient times. It was even suggested that the sudden extinction of giant pangolins at the end of the Cretaceous Period ($\sim$70 million years ago) was due to a strong outburst of cosmic radiation.

It is well known that the systematic observation of the cosmic-radiation intensity has only been made during the past 3-4 decades. It might seem

impossible to solve the problem formulated above and often known as the "history of cosmic rays". However, several methods have been recently developed to determine the mean intensity of cosmic rays in epoch several billion years ago. The main contribution in the investigation of this problem is due to Libbi, Honda, Arnold and Geiss [1-4].

1.2. Methods for determining the cosmic-radiation intensity in ancient epochs

Radioactivity is induced to various objects by the action of cosmic rays. The isotopic composition of the resulting elements is quite complicated. Many of these elements have very large half-life times, which are rarely met within normal conditions. Some stable nuclei are also formed.

Denoting the probability of production of an isotope with mass number A by p^A, we find that the probability of occurence of N^A atoms of type A is given by

$$N^A = \int p^A I(t)\, dt,$$

where I is the cosmic-radiation intensity. Probability p^A depends on the probability of formation of the isotope and on the irradiation conditions. For instance, if the irradiated object is put under a layer of absorbing material, then the number of occuring atoms will depend on the thickness and other properties of the absorber.

For constant values of p^A and I,

$$N^A = p^A I T, \tag{8.1}$$

where T is the exposure time. If stable isotopes are being considered, their concentration will be proportional to N^A. The quantity of radio-active isotopes will evidently vary with time in accordance with the intrinsic half-life time T_0 of the isotope. If the half-life time is much less than T, then an equilibrium between the modes of formation and decay will be established. Simple calculation shows that, when an equilibrium is established,

$$N^A = T_0 p^A I. \tag{8.2}$$

It then follows that, by studying the ratio of the number stable and radio-active nuclei, it is possible to determine the age T of the object. Assuming that the probability of forming a radioactive isotope is equal to p' and a stable isotope to p" (these probabilities could be measured on an accelerator), we obtain

$$\frac{N'}{N''} = \frac{p'}{p''} \cdot \frac{T_0}{T}. \tag{8.3}$$

Thus, by measuring N' and N" we can obtain T provided that we know p', p" and T_o. Moreover, equation (8.1) could be used to obtain the mean intensity I, averaged over the whole period of irradiation. Equation (8.3) shows that it is necessary to choose isotopes having long life times in order to study ancient periods of time.

In order to apply the method described above, it is necessary to have in hand a number of objects of a known age which have been irradiated for a long time by cosmic rays. The most suitable objects for this purpose are meteorites which have wandered in space for a long time. Many of the meteorites have an age that exceed 4 billion years. This age is counted from the instant of their formation inside a larger body, say a planet, and corresponds to the time of eixtence of the solar system. As long as a meteorite exists inside the material of a planet, the meteorite is screened from irradiation by cosmic rays. We therefore have to know the time that each meteorite spends as a free body in space. In order to determine this time T, the ratio of the content of the two potasium isotopes K^{40} (radioactive with half-life time T_o 1.2×10^9 years) and K^{41} (stable) which are rarely met with in a normal situation, could be used.

In the simplified description of the method given here, we did not mention a number of the difficult problem involved, such as the destruction of the surface layer of the meteorite when it penetrates the atmosphere, the erosion of its surface during its motion for hundreds of millions of years, etc. The exact calculation of all the possible details of these processes is extremely difficult.

Investigations have shown that the time of the independent existance of stone meteorites reached 10^7 years, and of iron meteorites about $10^8 - 10^9$ years. Accordingly, meteorites could be considered as an integrating counter of cosmic radiation, capable of measuring cosmic-ray intensities during the periods $10^7 - 10^9$ years.

Side by side with integrating detectors, there are differentiating detectors which measure the cosmic-radiation intensity during narrow periods of time. In order to study such differential detectors, let us now leave the cosmos and return back to earth.

1.3. Radio-active-carbon method

The interaction of cosmic rays with the terrestrial atmosphere leads to the production of neutrons. These neutrons are sooner or later absorbed in the reaction

$$N^{14} + n^1 = C^{14} + p^1.$$

Nucleus C^{14} is unstable and is transformed into a nitrogen nucleus by a B-decay of a half-life time of 5700 years :

$$C^{14} \rightarrow \beta^- + N^{14}.$$

Carbon is an important part of all organisms living on earth. It participates in the intensive matter exchange between the animate and inanimate nature. Hence, radio-active carbon C^{14} enters the composition of all living organisms in a given ratio with normal carbon. Two C^{14} nuclei are produced (and consequently decay) in each second in a volume occupying 1 cm^2 of the earth's surface. On each 1 cm^2 of the earth's surface, there are approximately 8.5 g/cm^2 of carbon. Therefore, about 15 C^{14} decays occur each minute in each gram of carbon included in a living object. When a living organism dies, it no longer remains in equilibrium with the surrounding nature, and the quantity of C^{14} it includes starts to decay with a half-life time of 5700 years. The cosmic-ray intensity at time T before our time is then defined by

$$\frac{I(T)}{I_0} = \frac{N}{N_0} e^{T/T_0}, \tag{8.4}$$

where T is the organic material, investigated by the C^{14} content, N the number of decays per minute in one gram of material, $N_0 = 15$, I_0 the radiation intensity at present and $T_0 = 5700$ years.

The main difficulty in applying the radio-active-carbon method for measuring I(T) is the dating of the organic samples. Various objects found in the Egyptian pyramids and the ruins of Pompei and other places have been used. It was found that the trunk cores of old trees were not renewed by rings. The oldest samples are pieces of wood found in the pharaonic underground tombs of Set and the vizier Hemaka (the age of these tombs is 4900 ± 200 Years). A wooden funeral ship was found in the tomb of the Pharaoh Senusert III (about 3900 years ago). Figure 71 shows the number of C^{14}-decays as a function of the sample ages. The solid curve shows the expected dependence for the case when the cosmic-radiation intensity does not vary with

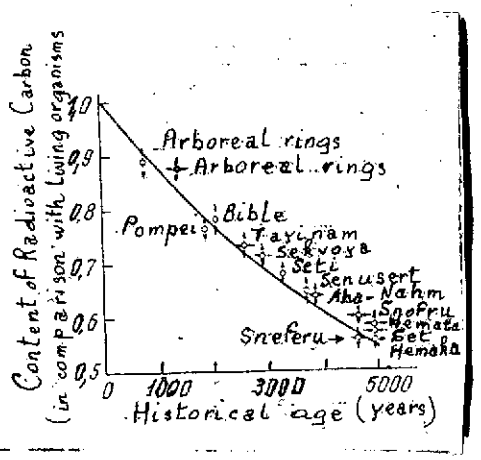

Figure 71. Dependence of the number of decays (concentration of the radio-active carbon) on the sample ages. The solid curve is calculated in assumption of a constant cosmic-ray intensity.

time. Near the experimental points, the names of the samples studied are written.

In agreement with theory we conclude that the cosmic-ray intensity did not vary during the past 5000 years. By studying the organic silt at the ocean bottoms, it was concluded that cosmic-ray intensity remained constant, up to within 20% during the past 35000 years. The ages of the silt layers were dated by calculations based on the assumption that the speed of accumulation of the silt was always the same. The recently accuracy achieved is sufficiently high when one is speaking of thousands of years. For instance in 1964 the Japanese physicist Higashi studied the C^{14} content in the annual rings of an 1820 cryptomerium and found that the intensity of cosmic radiation 700 years ago was less than the present intensity by 1.5 ÷ 2%.

The proved constancy of cosmic radiation, within the above mentioned accuracy, justifies the application of the radio-active-carbon method in Archaeology. By using this method, considerable success has been achieved.

1.4. Investigation of meteorites

Iron and stone meteorites were used to determine the age of cosmic rays. The calculation of several meteoritic trajectories before their fall on earth shows that they move in the solar system at a distance of about 5 astronomic units. Apparantly, they are fragments of larger bodies, namely planets that previously existed in the solar system. One of the best studied meteorites is the iron meteorite "Arus" which fell in 1959 in Azerbaijan and has a weight of approximately 150 kgs.

The list of nuclei which could be used for the determination of meteorite ages and cosmic radiation intensity is quite large (Table 28).

In order to use the nuclei mentioned in table 28 in cosmic-ray investigations, it is necessary to know the cross section of their formation when iron

Table 28

Stable nuclei	Unstable nuclei (half-life times given in brackets)		
	Short-lived	Internediate	long-lived
Cr^{53}, Cr^{54} V^{50}, Cr^{50} Sc^{45}, Ca^{48}, Ca^{46} K^{41}, Ca^{42} Ar^{38}, Ar^{36}, S^{36} Ne^{20}, Ne^{21}, Ne^{22} He^{3}, He^{4}	Mn^{52} (5,7 days) V^{48} (16 days) Sc^{46} (84 days) Ar^{37} (35 days) Be^{7} (53 days)	Mn^{57} (300 days) V^{49} (330 ») Ca^{45} (165 ») Ca^{41} ($8\cdot10^{4}$ years) Ar^{39} (260 ») Na^{22} (2,6 years) C^{14} ($5,7\cdot10^{3}$ years) H^{3} (12,3 years)	Mn^{53} ($2\cdot10^{6}$ years) Ti^{44} (48 ») K^{40} ($1,3\cdot10^{9}$ ») Cl^{36} ($3\cdot10^{5}$ ») Al^{26} ($7,4\cdot10^{5}$ ») Be^{10} ($2,5\cdot10^{6}$ »)

is exposed to cosmic rays. Experiments made on accelerators at proton energies E varying from 150 MeV to 5.7 GeV showed that the cross section of formation of nucleus with mass number A is a function of the difference between A and the mass number of the iron nucleus, A = 56. Denoting this difference by ΔA, the cross section of formation of a nucleus with mass number A in the form of

$$\sigma(\Delta A, E) = \sigma_0 A_0^{2/3} c E^{-2/3} \exp\{-cE^{-2/3}\Delta A\}, \tag{8.5}$$

where $A_o = 56$, $\sigma_o = 60$ mb, $C = 0.11\ (\mathrm{GeV})^{2/3}$ and ΔA in the interval $6 < \Delta A < A_o - 20$.

It is clear that the number of the produced nuclei is given by

$$\mathfrak{N}(\Delta A) = \int_0^\infty \frac{dN}{dE}\, dE\, \sigma(\Delta A, E), \tag{8.6}$$

where $\frac{dN}{dE} = f_o E^{-\gamma}$ is the differential energy spectrum of the cosmic radiation. After integrating, we obtain

$$\mathfrak{N}(\Delta A) = R \Delta A^{-k_2}. \tag{8.7}$$

Quantity k_2 is a function of exponent γ of the cosmic radiation spectrum[1]:

$$k_2 = \frac{1}{2}(3\gamma - 1), \tag{8.8}$$

and R is a function of the cosmic-radiation intensity and exponent γ:

$$R = \frac{3}{2} f_0 A_0^{2/3} \sigma_0 c^{1-\gamma} \Gamma(\gamma). \tag{8.9}$$

The number of radio-active nuclei with half-life time T_o is sensitive to the properties of the cosmic radiation in a period of time of the same order of magnitude as T_o (see equation (8.2)), whereas the number of stable nuclei is an integral of the intensity over time period T (equation (8.1)). It follows from equations (8.8) and (8.9) that constants R and k_2 must have the same value for all nuclei, whether they are stable or unstable, if the cosmic radiation remains unchanged. Comparing R and k_2 for stable and unstable nuclei with half-life time T_o, would therefore establish whether the cosmic radiation changed or not during that period of time. A change in quantity k_2 would mean

1) Quantity k_2 also depends on the conditions of irradiation, since higher-energy particles are produced deep inside the meteorite.

that the power exponent of the spectrum changed. If k_2 remained constant while R changed, then one could assume that the intensity had changed.

Figure 72 shows the dependence of the concentration of various stable nuclei in the iron meteorite "Arus" on ΔA. The slope of the curve in a double logarithmic scale defines k_2. Quantity k_2 was found to be the same for both stable and unstable nuclei, and was approximately equal to 2.4. This suggests that radiation during the past 100 million years remained constant, to within 30 - 40%.

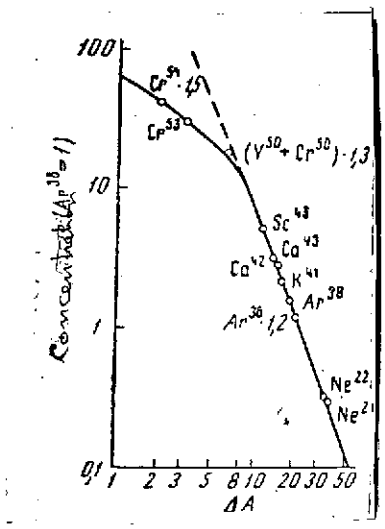

Figure 72. Concentration of various nuclei in meteorites as a function of A.

This conclusion is illustrated in figure 73, which shows the time dependence of intensity, determined by the contents of nuclei having different half-life times.

In the billion-year region, a further progress could be achieved by studying the ratio of concentrations of K^{40} and K^{41}. Having obtained the life time T of the meteorite by measuing the ratio of numbers of nuclei Ar^{36}/Cl^{36} Ne^{21}/Al^{26} (equation (8.3)), one searches for the dependence of the concentration ratio of $K^{40}:K^{41}$ on T, assuming that the time dependence of cosmic-ray intensity is well represented by an exponential function :

$$I = I_0 e^{-\alpha t}.$$

Figure 74 shows the dependence of the concentration ratio of K^{40}/K^{41} on T /1/. The solid lines are obtained with the assumption that $\alpha = 0$ or $\pm$ 1/700 (million year)$^{-1}$. The figure shows that there is no evidence for a considerable variation in the intensity of cosmic radiation during the past billion years.

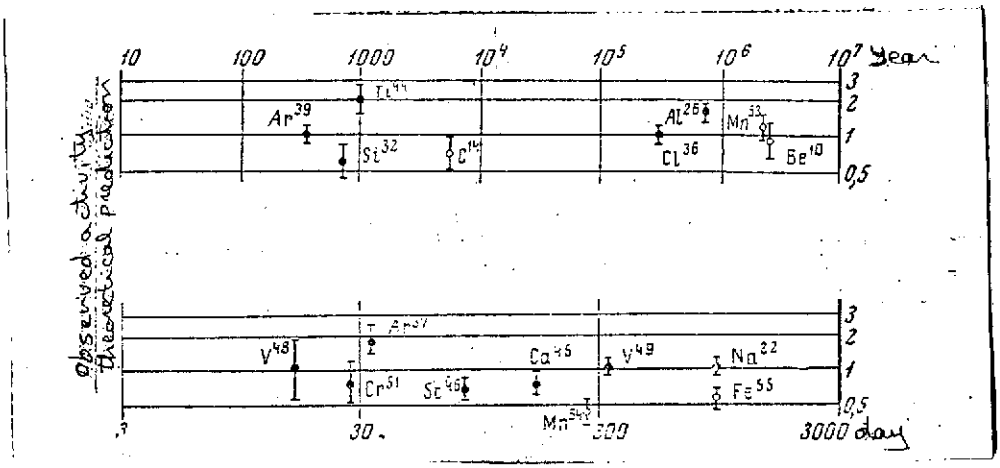

Figure 73. Time dependence of cosmic-ray intensity. The abscissa defines time and the ordinate defines the ratio of the observed activity in meteorites to the theoretical values, calculated with the assumption of a constant cosmic-radiation intensity.

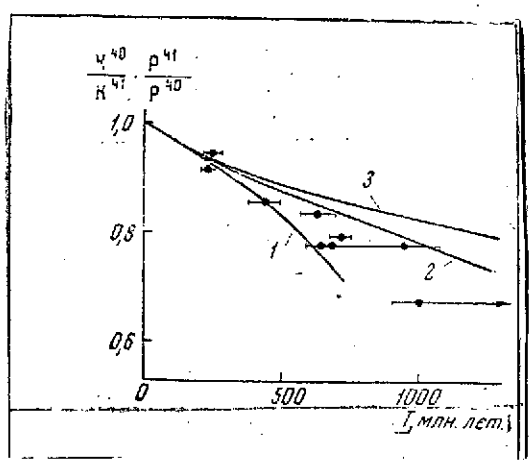

Figure 74. Dependence of the K^{40}/K^{41} concentration ratio on the age of the sample for different time-depending cosmic ray laws. 1- The intensity increases, 2- The intensity is constant, 3- The intensity decreases.

2. Variations of Cosmic Rays [5-9]

2.1. Historical information

The mean cosmic-ray intensity is relatively stable against time change. Each moment of time is characterized however, by its own radiation intensity. In other words, variations in cosmic-ray intensity are observed. Some of these variations have small periods and amplitudes, others appear suddenly, and still others continue for decades.

The cosmic-radiation variations occur as a result of changes in atmospheric conditions, in the interplanetary medium, on the sun and in the Galaxy. They could also be produced by the asymmetry of the distribution of cosmic rays in the Galaxy or by the discreteness of the cosmic-ray sources.

The first investigation of cosmic-ray variations was carried out in 1926 by L.B. Mysovskij and L. Tuwin. They discovered that the cosmic-ray intensity at sea level depends on atmospheric pressure (0.345% per 1 mm Hg). During the few following years, several attempts were made to establish a relation between cosmic-ray intensity and the Sun's position in the horizon as well as the distribution of the stars in the Galaxy. These attempts did not lead to the required relationship.

At the beginning of the 1930's, Compton developed an ionization chamber for the continuous registration of the global intensity of hard components. He carried out long-term measurements of hard-component intensities by means of counters and telescopes. Most of these measurements were performed at sea level and thus were concerned with muons. During this period however, no success had been achieved in explaining the mechanism of cosmic-radiation variations although major variation types were discovered: the 11-year variations, the seasonal variations, the 27-day variation, and the solar-twenty four hour variations, as well as the effects of magnetic storms and solar outbursts. During solar outbursts, the intensity variation may be as large as 10%. In other cases, for example, in half-day variations, the variation reaches only a few hundredths of one percent. Most of the variations have amplitudes equal to a few fractions of one percent or a few percent.

2.2. Instruments for measuring variations

The smallness of the variation amplitude imposes a severe restriction on the instruments used to register the cosmic ray variations. In order to register small vibrations, a very high statistical accuracy must be obtained.

Accordingly, the major requirements for instruments used in the study of cosmic ray variations are : 1) a sufficiently high statistical accuracy (which is usually achieved by increasing the effective dimensions) and 2) a highly stable working system (which is necessary for studying vibrations of long periods such as the 27-day variations, the 11-year variations, the seasonal variations, etc.).

A typical feature of present-day investigations on cosmic-ray variations is the continuous registration of the various components of cosmic radiation in different parts of our planet, at various heights in the atmosphere and also underground. At the present time, there are more than 100 stations for the continuous registration of cosmic rays. In these stations, the global intensity of the hard component of cosmic radiation is observed. Ionization impulses are registered by means of ionization chambers of large dimensions of large pressures. The variation of cosmic-ray intensity in the vertical and other different directions are measured by using telescopes and Geiger-Müller counters. The continuous measurement of neutrons is made by using neutron counters. All these measurements are carried out at sea level and

on hill tops. Similar measurements are carried out in balloons, aeroplanes and satellites, though the instruments used in these cases are of smaller dimensions.

For the purpose of studying cosmic-ray radiations, the following instruments are used :

The large ionization chamber :

The large ionization chamber for the continuous registration of cosmic radiation was developed in the USSR under the supervision of N.L. Grigorov and Ju. G. Šafer. This chamber (figure 75,a) has a diameter of 1.5 m and is filled with argon at a 10 atmosphere pressure. The counting accuracy is increased by using a compensational method. An auxiliary chamber with a uranium B-source is placed inside the principal chamber. This source emits electrons and consequently produces an ionization current in the compensational chamber. One of the compensational chamber electrodes simultaneously serves as an electrode for the principal chamber. The other electrodes in both chambers are kept at positive potentials. Consequently, the currents in the principal and compensational chambers are in opposite directions. By adjusting the position of the β-compound, one can vary the compensating current and make it equal to the current in the principal chamber. The currents will then completely compensate each other and the current-registering electrometer needle will not deviate. If the pressure in the chamber or the feeding voltage are changed, both the principal and compensational chambers will be equally affected. The instrument is thus sensitive only to cosmic-radiation variations and not to the alteration of the instrument. This method could measure the hard-component intensity to within 0.7% during a one-hour measurement.

The cubic telescope (figure 75,b)

During the International Geographical Year, (1957 - 1958), counters called cubic telescopes became widely recognized. The cubic telescope consists of two identical telescopes, capable of registering the intensities of the hard soft components. The axis of one of the instruments is oriented from east to west and the other from north to south. The hard component is separated by means of a lead layer, shielding the lower counter row.

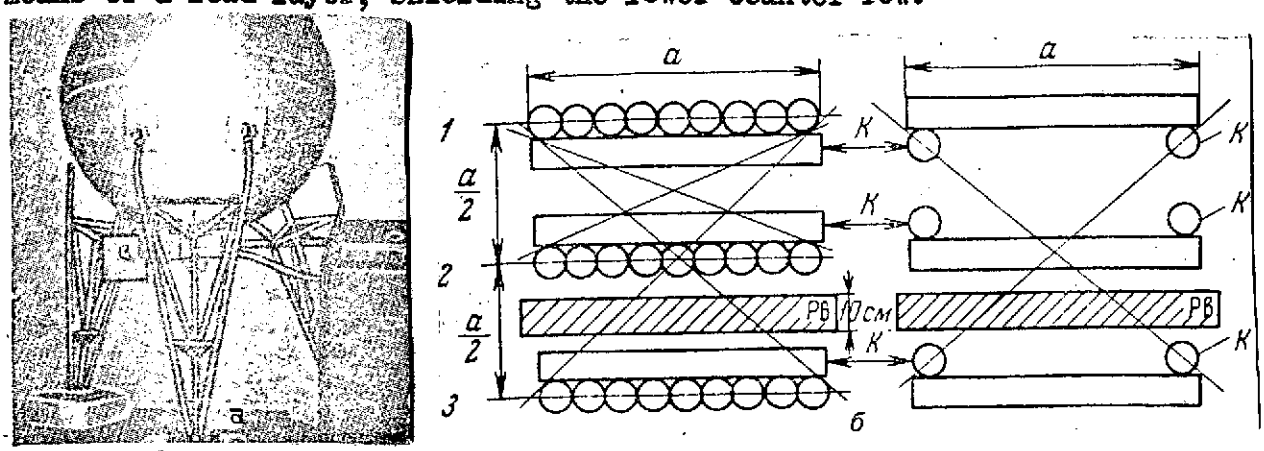

Fig. 75. Instruments for studying cosmic-ray variations: a-The ionization chamber b-The cubic telescope; K-counters for decreasing the end effect.

The neutron detector (neutron monitor)

Neutrons are produced by low-energy primary particles. The study of the neutron variation will therefore make it possible to investigate the low-energy part of the spectrum. Moreover, neutrons are rapidly absorbed in the atmosphere so that their intensity at sea level is small. Consequently, the statistical accuracy of neutron registrations is not high. Neutrons are registered by local generation detectors. These consist of lead blocks, in which neutrons are generated, delay elements made of paraffin and neutron counters filled with BF_3. Neutrons are absorbed by B^{10}-nuclei with a subsequent emission of 2.5-MeV alpha particles :

$$B_5^{10} + n_0 \rightarrow Li_3^7 + He_2^4 + 2{,}5 \text{ Мэв.}$$

Sometimes, the lead is covered by cadmium and paraffin in order to absorb neutrons coming from the air.

Other methods

By carrying out the measurements at large heights, one can use counters to study the variation of very low energy primary particles. Particularly interesting are the balloon carrying counter flights made during large solar outbursts. In the Soviet Union, regular measurements of the cosmic-radiation intensity near the atmospheric border are made at various latitudes, starting from Murmansk to the Crimea. Systematic flights are made also over the Antarctic Continent.

2.3. Classification of the variations /1/

Measurements deep in the atmosphere always deal with secondary cosmic-radiation components. Three factors govern the observed intensity of these secondary components :

1. The geomagnetic threshold, i.e. the minimum energy of particles admitted to the earth by the magnetic field. Any change in this threshold would lead to a change in the intensity. The magnetic field changes during magnetic storms, etc.
2. The instrument integral multiplicity, i.e. the number of secondary particles registered by the instrument per single primary particle. This quantity is denoted by $m^i(\mathcal{E}, h)$ where $\mathcal{E}$ is the energy, h the height and index i denotes which cosmic-radiation component is measured. If any change occurs in the atmosphere, such as changes in pressure, temperature, etc, then changes will subsequently occur in the meson-decay processes, so that the number of muons will be altered. In this manner, the integral multiplicity will vary at the expense of meteorological effects and the corresponding variations will have a terrestrial atmospheric origin.

3. The energy spectrum $D(\varepsilon)$. The variation of the primary-particle spectrum which occurs at the expense of processes occuring outside the earth also causes intensity variations. These variations could be due to cosmic-ray formation processes and hence are of a most particular interest. A part of these variations is related with the generation of a fraction of cosmic rays from the sun. Another part is caused by modulational effects, i.e. with a solar activity not related with the direct generation of cosmic rays but with the varying conditions of cosmic-ray penetration through the solar system. It is assumed that the variations in the condition of cosmic-ray propagation through the solar system is due to the fact that the sun emits fluxes of ionized gas. These fluxes carry a magnetic field and in this manner affect cosmic ray propagation.

Variations caused by processes occuring in the Galaxy or outside its limits might also exist. The observation of such variations could give many useful informations on the origin of cosmic rays. It is now established that if these variations exist, then, in the energy region $<10^{15}$ eV, they will be $\sim 0.1\%$ (the so called sidereal-daily variations). The sidereal-daily variations are caused by the anisotropy of cosmic ray motion in the Galaxy. The above-mentioned variation in amplitude 0 % with a maximum of about 20 hours sidereal time could be caused by the flux of particles, captured in the spiral branch of the Galaxy where the solar system is located.

The mathematical problem of separating the different types of variations could be formulated in the following manner. The intensity of particles of the i-th kind at an observation depth h_o and a geomagnetic threshold g is given by

$$N_g^i(h_0) = \int_g^\infty D(\varepsilon)\, m^i(\varepsilon, h_0)\, d\varepsilon. \tag{8.10}$$

Varying this relation with respect to all parameters, we obtain

$$\delta N_g^i(h_0) = -\delta g D(g)\, m^i(g, h_0) + \int_g^\infty D(\varepsilon)\, \delta m^i(\varepsilon, h_0)\, d\varepsilon + \int_g^\infty \delta D(\varepsilon)\, m^i(\varepsilon, h_0)\, d\varepsilon. \tag{8.11}$$

Introducing functions $W_g^i(\varepsilon, h_o)$:

$$W_g^i(\varepsilon, h) = \frac{D(\varepsilon)\, m^i(\varepsilon, h_0)}{N_g^i(h_0)}; \tag{8.12}$$

$$W_g^i(\varepsilon, h) = -\frac{1}{N_g} \cdot \frac{\partial N_g}{\partial g}. \tag{8.13}$$

we obtain

$$\frac{\delta N_g^i(h_0)}{N_g^i(h_0)} = \int_g^\infty \frac{\delta m^i(\varepsilon, h_0)}{m^i(\varepsilon, h_0)} W_g^i(\varepsilon, h_0)\, d\varepsilon - \delta g W_g^i(g, h_0) + \int_g^\infty \frac{\delta D(\varepsilon)}{D(\varepsilon)} W_g^i(\varepsilon, h_0)\, d\varepsilon. \tag{8.14}$$

The terms in the right-hand side of equation (8.14) describe three classes of variations: first, I-class variation (of atmospheric origin); second II-class variations (of geomagnetic origin) and third, III-class variations (of non-terrestrial origin). The third-class variations are divided into three subclasses : the IIIa-class caused by the modulational effects in the inter-planetary space, the IIIb-class caused by the solar cosmic rays and the IIIc-class which are variations of Galaxial and non-Galaxial origin (sidereal-daily variations).

3. Variations of Various Origins

3.1. Atmospheric variations

In order to bring to light the second- and third-class variations, we must learn how to eliminate variations of atmospheric origin. What is the mechanism of these atmospheric variations? The basic role in this mechanism is played by the spontaneous decay of muons. Assuming that muons are most effectively produced in a given atmospheric layer h g/cm^2, then an increase in atmospheric pressure will raise this layer higher. This will lead, on one hand, to an increase of the meson absorption in the lower atmospheric layers due to the increased quantity of matter and on the other hand, to the enhancement of the decay rate as a result of increasing the geometrical paths. Both these factors lead to the fact that if the pressure increases by 1 mm, the muon intensity falls by 0.345% (the barometric effect).

An analogous explanation could be given to the dependence of intensity on temperature. If temperature increases, the atmosphere expands and the effective generation layer is raised. This leads to an enhancement of the decay rate and an increase of the temperature coefficient by 0.18% 1°C. The effect depends not only on the temperature of the observation level, but mainly on the temperatures of all the atmospheric layers (temperature effect). The distribution of temperature in the atmosphere is different in summer and in winter. This could be the reason for the seasonal variations, i.e. the difference in the atmospheric variations in winter and in summer.

The alteration of the atmospheric conditions also leads to the alteration of the intensity of the cosmic-radiation neutron component. In contrast to muons, neutrons are generated and absorbed independently of the geometrical

paths in the atmosphere. Their intensity mainly depends on the total quantity of matter above the observation point, which is proportional to the atmospheric pressure. The most decisive factor for neutrons will thus be the barometric effect; the temperature effect will be small. In the period preceeding the International Geophysical Year (1957-1958) L.I. Dorman in the USSR developed a method for accounting for the corrections due to the meteorological effects. By means of this method, the meteorological effects could be completely eliminated.

3.2. Variations of goemagnetic origin

The terrestrial magnetic field is a superposition of two fields, one produced by terrestrial magnetism, and another induced by electric currents in the upper atmospheric layers and outside the atmospheric range. The value of these currents depends on many factors, such as the tidal motion in the atmosphere induced by the interaction with the moon, the arrival of corpuscular currents to the earth, and the deformation of the magnetosphere by influence of the solar wind. All these factors have an influence on the geomagnetic cut-off threshold and are responsible for second class variations.

3.3. Variations of a solar origin

Recently, a large class of variations related to the sun was discovered. Many of these variations are caused by modulation effects, i.e. changes in the conditions of cosmic-particle penetration through the interplanetary space. Others are related with the direct generation of particles on the sun.

1. Eleven-year variations

It is well known that solar activity has a time period of 11 years. This suggests that the 11-year variations of cosmic rays are directly related to the sun. According to measurements by Forbush, the intensity of muons at the maximum of the solar cycle in 1957 was 6% less than its value at the minimum. According to Simpson's data, the intensity of neutrons during the same period was decreased by 25%. Consequently, it was concluded that there existed a negative correlation between cosmic ray intensity and solar activity.

Measuring the intensity during the solar cycle period from 1958 to 1966 by means of neutron monitors on the earth, counters in the stratosphere and Soviet cosmic stations flying to the Moon, Mars and Venus showed that the radiation intensity in space changed by more than 2.5 times during the 11-year cycle period. The variations registered by the neutron monitors were not significant. This suggests that the variations are induced by particles with energies less than $3 \div 5$ GeV, which do not reach the earth (figure 76).

2. Twenty-seven-day variations (figure 77)

Another type of cosmic-ray variations is the 27-day variation. It is well-known that the period of the sun's rotation about its own axis is equal

to 27 days for the equatorial regions of the sun. The coincidence between the periods of the 27-day variations and the rotation of the sun about its own axis suggests that there is an active zone on the sun, located on a given solar meridian. The 27-day variations appear equally clear at all latitudes and hence, must be induced by sufficiently-high-energy particles. Another interesting property of these variations is that they sometimes almost completely disappear and then appear again and remain stable for long periods of time (months or years). In the period of high solar activity the 27-day variations have the best recurrence and maximum amplitude 0.7 ÷ 1%.

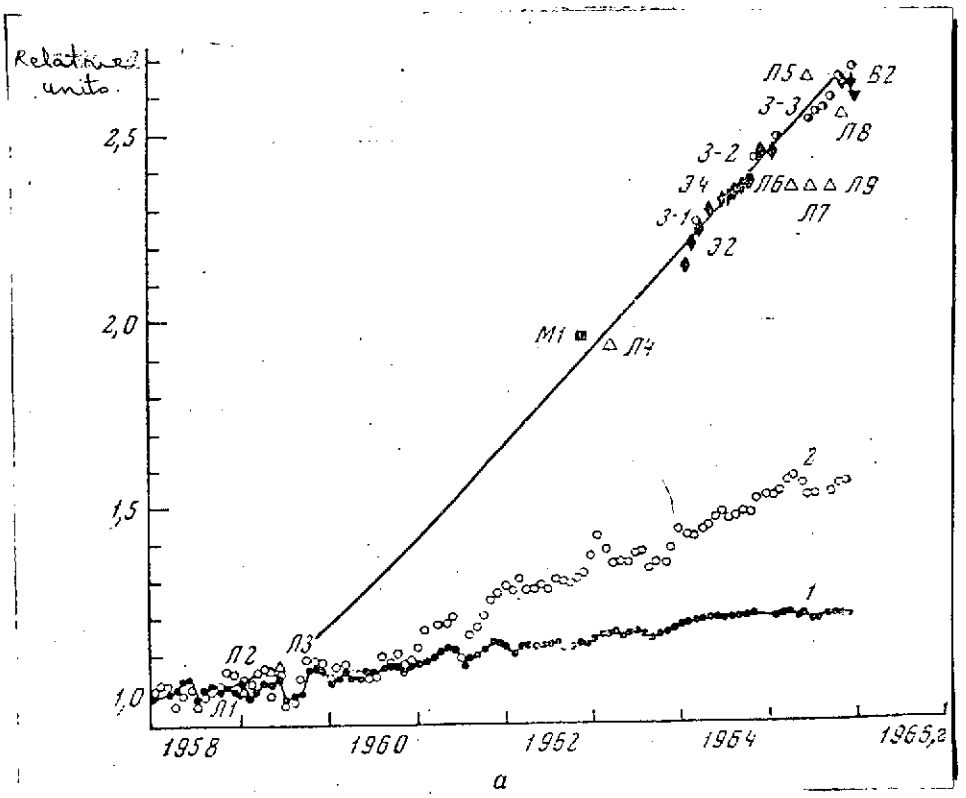

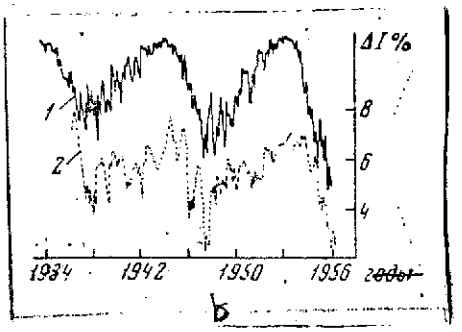

Figure 76. The 11-year variations. a) Measurements by means of a neutron manometer: (1) stratospheric instruments, (2) cosmic instruments, (3) Л-"Moon", В-"Venus", М-"Mars", Э-"Electron" satellite, -"Zond" satellite b) Terrestrial measurements: 1- solar spots, 2- cosmic rays.

3. Solar-daily variations

The solar-daily variations are another type of variations having a short period equal to a terrestrial day. These variations have an amplitude of

approximately 0.15 ÷ 0.20%. They are connected with the 27-day variations since their amplitude has a 27-day recurrence.

All the previous facts indicate the close relation between the variations considered and the sun.

4. Effects due to magnetic storms (Forbush effect)

The study of magnetic storms causing an alteration of the terrestrial magnetic field, is of great practical interest. It is clear that any alteration of the terrestrial magnetic field is accompanied by a cosmic ray variation.

The alteration of the cosmic-ray intensity during a magnetic strom is usually reduced to a rapid decrease of the intensity with a speed of 1.5 ÷ 2% per hour followed by a slow increase with a speed of 0.02 ÷ 0.05% per hour continuing till the normal value is reached. Storms occur with a high frequency during periods of high solar activity in such a manner that the cosmic radiation has not enough time to be restored. This leads to a decrease in the mean cosmic-radiation intensity. In some cases, a slight increase in intensity with an amplitude of 1.5% preceeds the rapid decrease of intensity. The manners of intensity time dependence can be divided into types: first, a rapid decrease followed by a smooth increase and, second, a smooth decrease followed by a smooth increase.

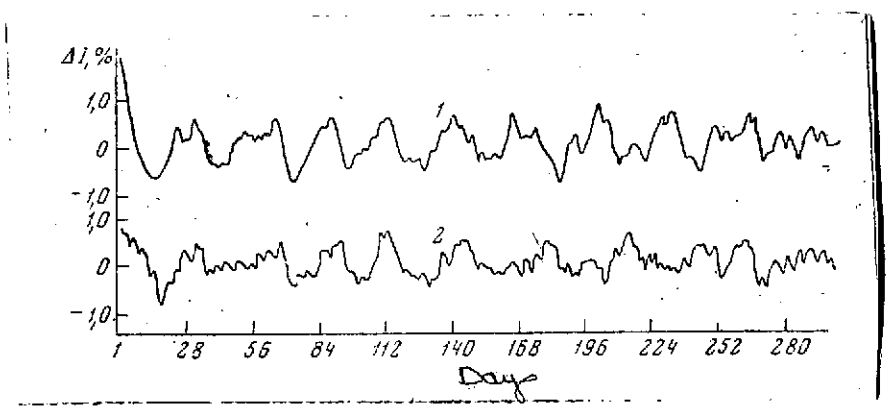

Figure 77. The 27-day variation (Yukutsk). 1- without temperature correction; 2- with temperature correction (the correction reduces the effect).

3.4. Solar outbursts

During the periods of high solar activity, large solar outbursts are sometimes observed. These are huge eruptions or explosions occuring on the sun. These pheomena lead to a sudden increase in cosmic-radiation intensity. For instance, the intensity of neutrons observed in several stations was increased

50 fold, and that of primary particles with an energy of 3 GeV was increased 300 times during the great outburst that occured on February 23, 1956. The outburst was registered by many stations. This made it possible to study the distribution of the variation amplitude over the earth. The largest increase was observed at high latitudes. The intensity increase was investigated at latitudes reaching $\sim 80^{\circ}$. The investigation showed that there were particles with an energy up to 1 GeV among the particles that reached the earth after the outburst. Accordingly, particles responsible for the variation had energies less than 15 GeV (the energy threshold at the equator).

During the past 27 years, only 12 solar outbursts were registered on the earth. Half an hour after great solar outbursts, protons and nuclei of energies >200 MeV and electrons of energies >100 MeV are observed at the earth's polar regions. The normal intensity is restored after 2-3 days. The nuclear constitution of the particles is close to the distribution of the corresponding elements on the sun. In particular, helium nuclei constitute 10% of the flux.

4. Mechanism of Solar-Connected Variations

4.1. Corpuscular fluxes from the sun and the solar wind

What is the mechanism that governs solar-connected variations ?

Today, one could consider it well established that a plasma is continuously, though not homogeneously, flowing out of the surface of the sun. Parker suggested to call this phenomenon a "solar wind". The inhomogenous distribution of the sources of solar wind over the solar surface is responsible for the occurrence of "jets" or "tubes" of plasma in the space surrounding the sun. The outflowing plasma carries with it, a magnetic field. The rotation of the sun and consequently the sources of the solar wind, makes the tubes twist into an Archimedes type screw. The magnetic field enclosed in the tubes will be stretched along the tubes' axes creating in the space surrounding the sun, an interplanetary magnetic field with lines of force directed along the Archimedes' spirals. This induces an anisotropy of the magnetic field and accordingly an anisotropy of the cosmic radiation and can thus be a reason for cosmic-ray variations. The pressure of the wind will depend on the solar activity and for reason will have an 11-year variation cycle. The speed of the solar wind in calm days reaches 300 km/sec and its density has a value of $10 \div 20$ particles/cm^3. The flux of solar-wind particles is of an order of magnetic equal to $10^8 \div 10^9$ particles/cm^2 sec.

Together with the solar wind, other short-lived fluxes must be present. These fluxes are responsible for the great magnetic storms.

In order to explain the sufficiently large amplitude of cosmic-radiation variations, it is necessary to assume the existence of a magnetic field in the fluxes. This so-called "frozen" magnetic field is a result of the ordered motion of particles in the flux. If the particles after being ejected from the sun pass through a zone having a magnetic field, the particles will start to move in this field along cyclic paths. Since the plasma is a superconductor, the electric resistance in the flux will be small and once the induced circular

motion is conserved, it will itself produce a magnetic field. A particularly strong magnetic field occurs at the forward front of the travelling flux. As a consequence of the presence of a magnetic field in the flux, the flux will scatter the cosmic-ray particles. Even a weak magnetic field is capable of scattering cosmic-ray particles due to the great extension of the flux. Low-energy particles will generally be reflected by the magnetic field of the flux. Accordingly, cosmic-radiation density inside the flux will generally be less than in the free space. Since the magnetic field at the forward front of the flux is particularly strong, this front will effectively reflect the particle. A wave of reflected particles will thus propagate before the front end of the flux. This wave causes an increase in cosmic-radiation intensity before the magnetic storm that starts the moment the magnetised front of the flux enters the terrestrial magnetic field. Immediately beyond the front of the flux, the cosmic-ray intensity sharply decreases which leads to a sharp decay in intensity (figure 78). As the flux propagates, it becomes more dilute and the magnetic field inside it decreases and is gradually filled by cosmic rays. If the earth enters such a flux from its lateral side, then neither an increase nor a sharp decrease in intensity will be observed. The intensity will smoothly decrease and then smoothly increase (alteration of the second type). High energy particles are less affected by the magnetic field of the flux.

Therefore, the magnetic-storm effect will be stronger at high latitudes where low energy particles are found.

With large solar activities, the cosmic ray intensity after a storm does not have enough time to restore itself before a second storm arrives. This leads to a decrease in cosmic-ray intensity during the period of maximum solar activity, i.e. with the 11-year period. However, quantitative estimates of the phenomenon show that magnetic storms alone are not sufficient to explain the 11-year variations. One must take into consideration other phenomena such as the deceleration of cosmic rays by the "solar wind". The difference between the intensity decrease at the expense of the Forbush effect and the 11-year variations starts, in particular, when particles responsible for

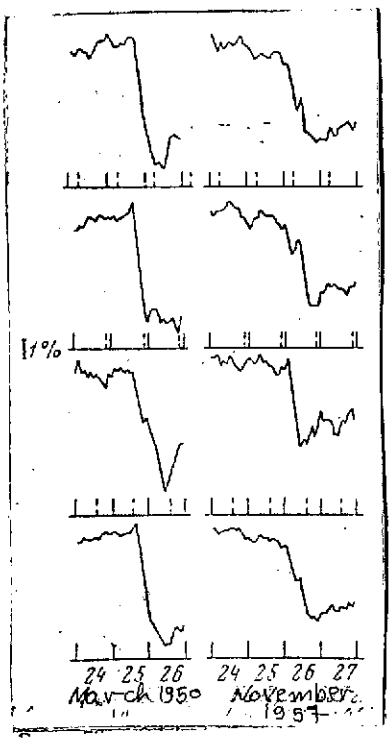

Figure 78. The magnetic storm effect (Forbush effect) at various longitudes.

the 11-year cycle have a softer spectrum than the particles whose intensity varies during magnetic storms.

4.2. 11-year cosmic-ray variations

The inhomogeneous character of the magnetic field in a solar wind, propagating in the solar system, could be used to interpret the 11-year cosmic-ray variations. We shall qualitatively consider a possible mechanism for decreasing the cosmic-ray intensity during the period of maximum solar activity.

Particles falling from the Galaxy into the range of the solar system (more precisely, in the region occupied by the solar wind[1]) occupy a space which involves travelling inhomogeneities of the magnetic field. These are formations like plasma "clouds", more strongly magnetized than the surrounding space. Collision of particles with such travelling magnetized clouds increases the particle energy in the case of the particles meeting each other and decreases the particle energy on collision of the particles with one another during their pursuit (compare with the change in kinetic energy of a ball when it hits a moving wall, or with the change of temperature of a gas during an adiabatic compression and expansion, see chapter 10).

During the radial motion of magnetic inhomogeneities away from the sun, the distances between them continuously increases. V.L. Ginzburg, S.B. Pikel'ner and I.S. Sklovskij showed that under these conditions, the pursuit collisions predominate. The energy E of a particle will be decreased by quantity $\Delta \overline{E} = \frac{E}{c^2} v \Delta u$ in each collision. Here, v is the velocity of the particle and Δu is the speed of separation of two neighbouring clouds.

In the periods of maximum solar activity, the number of inhomogeneities increases, and thus the energy of the particles decreases more strongly than in the calm years. This leads to a stronger decrease of the cosmic-ray intensity during the years of maximum solar activity.

It is important to note that the ascribed mechanism for the 11-year variations predicts a delay in the change in cosmic-ray intensity as compared to the start of the solar activity. The delay time depends on the velocity of propagation of the solar wind from the sun to the boundary of the area that takes part in the cosmic-ray modulation. The experimental determination of this delay time enables us to estimate the dimensions of the region, in which the cosmic rays are modulated by the solar wind. It is found that this region has dimensions 100 a.e.

4.3. 27-day variations

The active zones of the solar surface which are responsible for inhomogeneity of the solar wind, are inhomogeneously distributed over the longitudes. This leads to the longitudinal asymmetry of the solar wind. Due to the

---

1) This region has dimensions 100 a.e., where a.e. is the astronomic unit (radius of the terrestrial orbit).

rotation of the sun, the longitudinal asymmetry produces the 27-day periodicity of the magnetic fields in the vicinity of the earth and the modulation of cosmic rays with a 27-day period. The 27-day variations are found to be delayed from the phenomena causing them on the sun. This means that the dimensions of the region in which the conditions for propagation of cosmic rays change are quite large (tens of a.e.)

4.4. Solar-daily variations

The interplanetary magnetic field, twisted into an Archimedes spiral, induces a significant anisotropy of the magnetic field (figure 79). Under

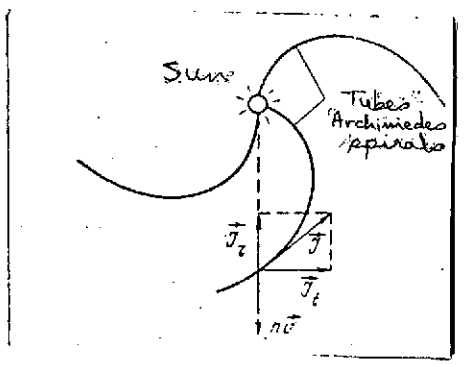

Figure 79. Interpretation of the solar-daily variations. The form of solar-wind tubes (Archimedes spirals) is shown : $r = \left(\frac{vT}{2\pi}\right)\varphi$, v is the velocity of the plasma, T the period of solar rotation (27 days) and φ the heliocentric angle.

these conditions, the cosmic ray distribution becomes anisotropic especially for low-energy particles. Cosmic rays will propagate mainly along the tubes of the magnetic field.

The particle flux J is divided into two components: a radial and an azimuthal with respect to their direction to the sun. The radial component of the flux to the sun is compensated by the inverse convectional ejection of the particles from the solar system produced by the action of the solar wind. The absence of such a compensation would lead either to the devastation of the near-solar space or to the gradual increase of the cosmic-ray intensity in the vicinity of the sun. Only the azimuthal component of the flux will remain uncompensated. Due to the rotation of the earth, the azimuthal component will produce an intensity variation with a period equal to a terrestrial day with a m ximum at about 6 p.m. local time. Calculation shows that the maximum amplitude of the solar-daily variations at a distance of 1 a.e. from the sun is nearly 0.5 %.

It is important to note that the compensation of the radial component of the flux occurs only as an average. In separate periods, an uncompensated

radial flux might appear and cause a variation in intensity with a maximum at midday or midnight.

A detailed considerations of the different hypotheses for the explanation of the solar-daily variations is given in reference [6].

4.5. The effect of solar outbursts

In the preceeding subsections, we considered cosmic ray variations produced by the changes in the conditions of particle propagation through interplanetary space (modulational effects). However, during the periods of maximum solar activity, outbursts occur on the sun from time to time. During these solar outbursts, particles of high energies are generated. If the energy

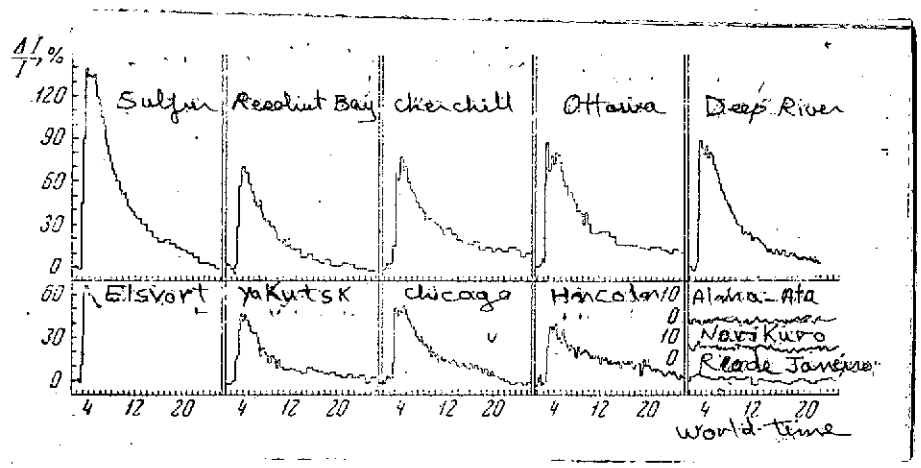

Figure 80. Variation in the number of counts of a neutron monitor during the solar outburst on November 15, 1960 at different stations: Sulfur-51°N, 115°W, 200m above sea level; Resolute Bay-74°N, 94°W, sea level. Churchill-58°N, 94°W, sea level; Ottawa- 45°N, 75°W, sea level; Deep River- 46°N, 77°W, sea level; Elsvort- 77°S, 41°W, sea level; Yakutsk- 62°N, 129°E, sea level; Chicago- 41°N, 87°W, sea level; Lincoln- 40°N, 96°W, sea level; Alma-Ata- 43°N, 76°E, sea level; Norikura- 36°N, 137°E, 2900m above sea level, Rio de Janeiro-22°S, 43°W, sea level.

of the particles produced is less than 1 ÷ 1.5 GeV, then due to absorption in the atmosphere, neither the particles nor their decendants arrive to the earth. The existance of outbursts, after which a change in intensity is observed on the earth up to relatively low latitudes, shows that particles with energies up to 10 GeV are sometimes generated on the sun.

During 27 years (1937 - 1964) only 12 outbursts leading to a clear effect on the terrestrial surface occured. In cosmic space, the intensity of particles

with an energy > 3 GeV increases by several hundreds of times. Together with protons, nuclei of helium, carbon, nitrogen and neon as well as electrons are accelerated.

Figure 80 shows the variation in the number of counts of neutron monitors during a solar outburst. The existance of a series of registering stations enables us to follow the dynamics of the development of an outburst and to determine the energy spectrum of particles reaching the earth. Data obtained by 37 stations of continuous registration located at the latitude intervals from 83°N to 73°S during the outburst on February 23, 1956, were accurately

Table 29

Reason for cosmic-ray variation	Nature of the variation	Amplitude%		
		muons	neutrons	Outside the atmosphere
Change of the integral multiplicity (change of atmospheric condition	seasonal temperature Barometric	⩽ 5 0,1—0,2%/degree 0,1—0,2%/mbar	— — 0,7	— — —
Change of the geomagnetic threshold.	Some effects occuring during magnetic storms and solar-daily variations, related with the deformation of the magnetosphere.	⩽ 5	⩽ 10	—
Modulations	11 year 27-day solar- daily Forbush effect	⩽ 6 ⩽ 0,5 0,2—0,3 ⩽ 10	⩽ 30 ⩽ 1—2 0,5 ⩽ 30	~ 200 ⩽ 10 ⩽ 2 ⩽ 50
Generation of particles on the sun	Effect of solar outbursts	⩽ 400	⩽ 5000	Hundreds and thousands of times greater than the normal level
Anisotropy of Galactic Cosmic rays	Sidereal-daily variations	~ 0,2	~ 0,5	—

analyzed. The observation of the outburst started at 3.50 a.m. and continued till 8.00 p.m. world time. It was found that at the first moment, there was a flux of particles coming from the sun which was shown by the difference in the value of intensity increase on the day- and night-sides. Half an hour after the start of the outburst the particle flux became isotropic.

The distribution of variation amplitudes over various latitudes made it possible to establish the energy spectrum of the outburst particles at different moments of time. Approximating the spectrum by a power law, the exponent γ was found to be approximately equal to 5. The most energetic particles arrived to the earth from the first moment after the outburst.

From the above picture, we conclude that the general picture of the outburst is the following. At the first moment, a number of high-energy particles are generated at a given "point" source on the sun. Most of these particles reach the earth and only a few of them are scattered in the magnetic fields near the sun. This period lasts for about 30 minutes. Later on, particles scattered by the magnetic fields in the solar system fall on the earth.

Alongside high energy particles, lower energy particles ($E < 1$ GeV) are generated during solar outbursts. Effects due to these outbursts are only observed in the statosphere or outside its limits.

4.6. Comparison of the different types of variations

Table 29 gives data on the amplitude of different types of variations [6].

Questions and Problems

1. Which measurements have to be made in order to estimate the intensity of cosmic rays 100 million years ago by means of a soil sample, brought from the surface of the moon ? Has this method an advantage over the investigation of meteorites ?

2. What can you say about the origin of a variation that has the same phase at 6 p.m. (local time) at the end of March and at 6 a.m. at the end of September ?

CHAPTER 9

INTERACTION OF COSMIC RAYS WITH THE TERRESTRIAL ATMOSPHERE

1. The atmosphere

Most of the interesting cosmic-ray phenomena occur in the atmosphere. The atmosphere consists mainly of oxygen and nitrogen. Usually, with the exception of special cases, one takes these two gases into consideration. Their atomic numbers are Z = 7 (78.1%) and Z = 8 (21%).

The density of air at the earth's surface is equal to 0.00123 g/cm^3. The total quantity of matter in an air column extending from the surface of the earth to the boundary limit of the atmosphere is equal to 1030 g/cm^2. The thickness of the atmosphere is negligibly small as compared to the earth's radius (200 times), and for this reason the atmosphere is usually considered as flat.

The atmospheric pressure changes with altitude. In a standard atmosphere, having a constant temperature gradient in the troposphere (Δt =-6.5 degree/km) and a constant temperature in the stratosphere (-56.5° at heights greater than 11 km), the pressure varies according to the barometric formula.

Height h is related to pressure p by the relation

$$h = 44\,308\,[1 - (p/p_0)^{0.1903}], \quad h \leqslant 11 \text{ км};$$
$$h = 11\,000 + 6340 \ln (p_{11}/p), \quad 30 > h > 11 \text{ км}.$$

Table 30 presents the distribution of pressure in a standard atmosphere, and also at large heights, obtained by rockets and by the deceleration of satellites;

Table 30

Height, km	pressure m bar	Height km	pressure m bar	Height km	Pressure m bar
0	1013	5	540	30	11,3
1	914	10	280	40	3,1
2	808	15	120	50	0,9
3	712	20	55	100	$5 \cdot 10^{-4}$
4	626	25	25	200	$3,3 \cdot 10^{-7}$

What is the atmospheric boundary? If the atmospheric boundary is defined as the region where cosmic-ray intensity significantly increases with increasing depth, global intensity for the atmospheric boundary is then at a height

of 50 kms (1 g/cm^2 of matter). For the vertical intensity, the atmospheric boundary is at a height of 40 km (3 g/cm^2).

2. Cosmic-Ray Penetration Through the Atmosphere

The hypothesis on the existence of nuclear-cascade processes proposed in 1949 by G.T. Zacepin /1/ is one of the bases of the penetration theory of cosmic radiation through the atmosphere.

In chapter 4, experimental data proving that a primary nucleon interacting with nuclei looses only part of its energy on the production of secondary particles, are given. Nearly half the energy remains with the secondary nucleon. Due to the weak dependence of the interaction characteristics on energy, the second interaction of a nucleon does not differ practically from the first. Pions produced at high energies do not have enough time to decay so that they also participate in the nuclear process. The thickness of the atmosphere is enough for tens of successive "primary" particle collisions to collision take place in it. Low-energy charged pions will decay giving a start for themuonic component. Neutron pions decay into photons and in this manner initiate electronic-photonic cascades. Consequently, if a primary particle of a sufficiently high energy is "unlucky" to penetrate the earth's magnetic screen and fall into the atmosphere, the particle will create in the atmosphere a whole series of processes, schematically illustrated in figure 81.

The main feature of a nuclear-cascade process in the atmosphere is the weak coupling between various components of the secondary cosmic radiation. Indeed, only nucleons contribute to all types of radiation. Pions have almost no contribution to the production of high energy nucleons. The electron-photon component does not generate any new type of radiation (except the Čerenkov and radio-frequency radiation) and is supported by nucleons, pions and muons (in the atmospheric depths and underground).

In most cases, the observation of cosmic rays in the atmospheric depths does not make it possible to determine which particles have been produced by the same primary particle. At moderate (< 100 GeV) and high ($10^2 \div 10^4$ GeV) energies, the cascade processes by the particles cover such a large area that the available detectors cannot collect them. In this energy interval, various radiation components are thus statistically studied separately. At ultra-high energies ($E > 10^5$ GeV), however, an extremely large number of particles are produced in the cascade (from tens of thousands to hundreds of millions or more particles). In this case, separate primary interactions can be registered by means of small detectors distributed over a large area. All components are simultaneously studied in such a "coherent" shower, known as an extensive atmospheric shower.

Muon production in extensive showers is a typical feature resulting from the existance of the atmosphere. The number of muons in the moon's soil at a depth of a few meters will be one thousand times less than the corresponding number at the same depth in the earth.

As a result of the strong absorption of the nuclear-active particles in the atmosphere, cosmic radiation at sea level consists mainly of muons (the

hard component), electrons and photons (the soft component) and neutri .
The intensity of charged particles at sea level is expressed in terms of the following quantities :

$$J(0) = 0.82 \times 10^{-3}\ cm^{-2}\ sec^{-1}\ ster^{-1},$$
$$J_s(0) = 0.31 \times 10^{-3}\ cm^{-2}\ sec^{-1}\ ster^{-1},$$
$$I_h = 1.68 \times 10^{-2}\ cm^{-2}\ sec^{-1},$$
$$I_s = 0.73 \times 10^{-2}\ cm^{-2}\ sec^{-1}$$

where J_h, J_s, I_h and I_s are the vertical and global intensities of the hard and soft components respectively. The total intensity

$$J(0) = 1.13 \times 10^{-2}\ cm^{-2}\ sec^{-1}\ ster^{-1}$$
$$I = 2.41 \times 10^{-2}\ cm^{-2}\ sec^{-1}.$$

The intensity of the hard component decreases 18 times on moving from the edge of the atmosphere to sea level. If the nature of the hard component at the edge of the atmosphere and at sea level was the same, one would then expect that if a layer of matter, equal to the atmospheric height was added to it, (being equal to 1000 g/cm^2), the cosmic-ray intensity would be decreased by another 18 times. To see whether this correct or not, we measure the intensity of the hard component somewhwere in a mine. In order to obtain an additional

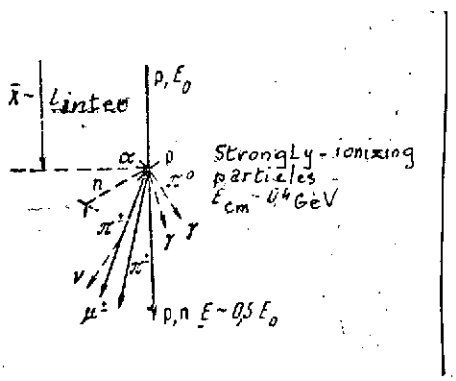

Figure 81. Development of a nuclear-cascade process in the atmosphere.

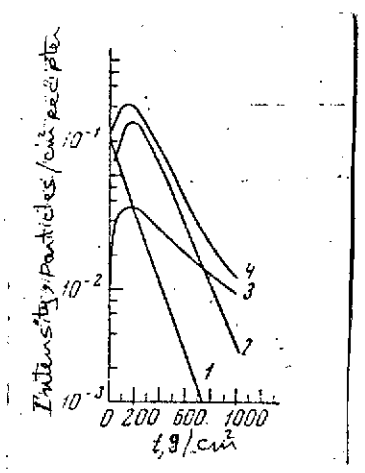

Figure 82. Latitudinal dependence.
1. protons and alpha-particles, 2. the soft component, 3. muons (the hard component), 4. the total intensity.

layer of matter with a thickness of 1000 g/cm^2, it is sufficient to carry out the measurements at a depth of 5m. It is found that such an experiment shows

that the cosmic-radiation intensity decreases to a half. This means that the absorption coefficient of the hard component at sea level is 10 times less than at greater heights. In this manner, it was proved long ago, that the hard component had a different nature at large heights and at sea level.

The hard component at sea level consists of muons which mainly losse their energy on ionization. The energy loss in a layer of 100 g/cm^2 thickness is equal to only 200 MeV, i.e. 6% of the mean energy of muons at sea level of $\sim$3000 MeV. At the atmospheric boundary, the hard component mainly consists of protons and alpha particles. These particles loose in 100 g/cm^2 of matter, approximately half of their energy and are therefore rapidly absorbed (figure 82).

The soft component consists of electrons and photons which are rapidly absorbed at the expense of bremsstraalung. However, even at a depth of 6000 g/cm^2 (30 m of soil) the soft component constitutes about 15% of the total intensity. This means that the soft component could be generated inside the earth by the particles of the hard component (muons).

At large atmospheric heights the charged component of the cosmic radiation mainly consists of electrons. The vertical intensity of electrons has a maximum at a height of 15 kms and the global intensity at a height of 20 kms. In previous years, this relation was used to prove two important facts : the isotropy of the primary radiation and the weak scattering of the secondaries in the interactions.

2.1. Gross scaling

There exists a well-defined relationship between vertical intensity and global intensity. This relationship is known as the Gross scaling.

Gross' formula was obtained under the following assumptions: 1) radiation outside the atmospheric range is isotropic, 2) secondary particles keep the direction of the primaries, and 3) cosmic-ray intensity only depends on the quantity of matter penetrated.

Let us assume that we measure the intensity at a depth x g/cm^2. A particle coming with an angle θ penetrates through a layer of matter of thickness $x/\cos\theta$. Assuming that $J(x)$ particles come in the vertical direction to a depth x, we find that the number of particles coming with an angle θ is equal to $J(x/\cos\theta)$. The global intensity is by definition equal to

$$I(x) = \int_0^\theta \mathcal{J}(x/\cos\theta)\, d\omega = 2\pi \int_0^\theta \mathcal{J}(x/\cos\theta) \sin\theta d\theta.$$

Here, the upper limit of integration must be $\pi/2$, however, we leave it undefined for the time being. Introducing the variable $\xi = x/\cos\theta$, we obtain

$$I(x) = 2\pi x \int_x^{x/\cos\theta} \mathcal{J}(\xi)\, d\xi/\xi^2.$$

Differentiating with respect to x, we obtain

$$\frac{dI(x)}{dx} = 2\pi \int_{x}^{x/\cos\theta} \mathcal{J}(\xi)\, d\xi/\xi^2 + 2\pi x \left\{ \frac{1}{\cos\theta} \mathcal{J}\left(\frac{x}{\cos\theta}\right) \frac{\cos^2\theta}{x^2} - \frac{\mathcal{J}(x)}{x^2} \right\}.$$

Consequently, when $\theta = \pi/2$,

$$2\pi\mathcal{J}(x) = I(x) - x\frac{dI(x)}{dx}.$$

This equation gives the relationship between vertical and global intensities.

From the previous relation these follows a very important property: The maximum of the vertical intensity occurs where the global intensity has an inflection point. This result agrees with the experimental data, when the above-mentioned assumptions are satisfied. By measuring the global intensity by means of a aingle counter, a maximum was found at a height of 20 kms and an inflection point at a height of 15 kms. This agreement justified the assumptions which lead to the Gross scaling and proved the isotropy of the primary radiation. At present, this is proved by means of direct measurements.

The difference between the latitudinal dependence if the vertical and global intensities has a clear practical meaning. In measuring global intensity, most of the particles were found to move with an inclination, so that they made a longer path in the atmosphere and reached the maximum intensity earlier than the vertical particles.

3. Nuclear-Cascade Processes in the Atmosphere

3.1. Equation for the nuclear-cascade process

The general picture of penetration of cosmic radiation through the atmosphere, described in the preceeding section, could be mathematically formulated. The calculation of the nuclear-cascade process in the atmosphere was carried out by several authors [2-6].

A general solution for the equation of a nuclear-cascade process is not possible. We thus consider a simplified model which clarifies the mean features of the process and illustrates the problems that occur.

We shall assume that the primary particles are nucleons which interact in the atmosphere and produce pions. We shall neglect kaon generation since kaons are less frequently produced than pions and the characteristics of their interaction are apparantly but slightly different from those of pions. We assume that pions do not produce high-energy nucleons (only nucleons of energies less than 1 GeV in nuclear disintegrations). A series of simplifying assumptions will be made in the process of solving the problem.

In the first approximation, the kinetics of a nuclear-cascade process is reduced to the production of nucleons by nucleons and of pions by nucleons and pions. It is therefore sufficient to start with the two following basic equations

$$\left.\begin{aligned}
&\frac{\partial N(E,x)}{\partial x}\,dE = -\frac{1}{\lambda_p}N(E,x)\,dE + \frac{1}{\lambda_p}\int_E^\infty N(E',x)\,dE'\,n_p(E',E)\,dE;\\
&\frac{\partial \Pi(E,x)}{\partial x}\,dE = -\frac{1}{\lambda_\pi}\Pi(E,x)\,dE + \frac{1}{\lambda_\pi}\int_E^\infty \Pi(E',x)\,dE'\,n_2(E',E)\,dE +\\
&\qquad + \frac{1}{\lambda_p}\int_E^\infty N(E',x)\,dE'\,n_1(E',E)\,dE - \frac{C}{Ex}\Pi(x,E)\,dE.
\end{aligned}\right\} \qquad (9.1)$$

Here $N(E,x)$ is the summed energy spectrum of protons and neutrons at depth x, $\Pi(E,x)$ the energy spectrum of pions, λ_p and λ_π are the interaction paths of nucleons and pions, respectively, $n_p(E',E)$ the spectrum of nucleons produced by nucleons of energy E', $n_1(E',E)$ the spectrum of pions produced by nucleons of energy E', $n_2(E',E)$ the spectrum of pions produced by pions of energy E' and constant C characterizes the decay of pions. The last term in equation (9.1) determines the number of pions that have decayed in a path of 1 g/cm^2 (if x is expressed in g/cm^2). Denoting the decay threshold by L_p, we obtain

$$L_p = \frac{c\tau_0 E}{mc^2}\ \text{cm}$$

where τ_0 and m are the life-time and mass of a stationary pion. This threshold, expressed in g/cm^2, is equal to

$$L_p' = L_p\rho,$$

where ρ is the density of air, changing in an isothermal atmosphere according to the relation $\rho \approx \rho_0\, x/x_0$ (see table 5 on page 22). Here ρ_0 is the density of air at normal pressure and x_0 the pressure of the "standard" atmosphere in g/cm^2. Accordingly

$$\frac{1}{L_p'} = \frac{mc^2}{c\tau_0 E}\cdot\frac{x_0}{\rho_0 x} = \frac{C}{Ex};\quad C = 116\ \text{GeV} \qquad (9.2)$$

3.2. Solution of the equation for nucleons. The absorption threshold

The first term in equation (9.1) for nucleons describes the decrease of the number of nucleons of a given energy due to interactions (λ is the inelastic path). The second term shows that some of the nucleons having an

energy $E_o > E$ before the interaction will fall after interaction in the energy interval under investigation, with a probability equal to $n_p(E,E_o)dE$. We can easily predict some of the properties of function $n(E,E_o)dE$. Firstly, the number of nucleons, preserving a significant energy is equal to 1. Consequently, $n_p(E,E_o)$ could be considered as the probability of formation of a secondary nucleon with energy E. Therefore

$$\int n_p(E, E_0)\, dE = 1.$$

Furthermore, the quantity

$$\int \frac{E}{E_0} n_p(E, E_0)\, dE = 1 - \bar{K}$$

where $\bar{K}$ is the mean inelasticity coefficient, does not depend on energy E_o (see Chapter 4, Section 10). This is possible in the case when function $n_p(E,E_o)dE$ is homogeneous, i.e. depends only on the ratio $E/E_o = \beta$ (β is the fraction of energy, kept by the nucleon after the interaction):

$$n_p = W\left(\frac{E}{E_0}\right)\frac{dE}{E_0}. \tag{9.3}$$

Noting that the energy spectrum is in the form of

$$N(E_0)\, dE_0 = \frac{A dE_0}{E_0^{\gamma}},$$

we transform the second term into the following form

$$\int_E^{\infty} N(E_0)\, dE_0 W\left(\frac{E}{E_0}\right)\frac{dE}{E_0} = \frac{A dE}{E^{\gamma}} \int_1^0 \beta^{\gamma} \frac{\beta}{\beta^2} W(\beta)\, d\beta = N(E)\, dE \int_1^0 \beta^{\gamma-1} W(\beta)\, d\beta. \tag{9.4}$$

The solution of equation (3.8) could be written as

$$N(E, x)\, dE = N(E, 0)\, e^{-x(1-\overline{\beta^{\gamma-1}})/\lambda} dE. \tag{9.5}$$

This formula was obtained for the first time by G.T. Zacepin.

Function $N(E,0)dE$ describes the energy spectrum of cosmic-ray protons at the atmospheric boundary. The fact that the exponent of the exponential function does not depend on energy leads to the important conclusion that,

in this case, the form of the energy spectrum of protons does not depend on the depth in the atmosphere. From the formula, it also follows that the number of nucleons changes with depth by an exponential law, with exponent not being equal to the interaction path. In the present case, the number of protons decreases by e times after a distance of

$$L = \frac{\lambda}{1-\beta^{\gamma-1}}. \tag{9.6}$$

Quantity L is called the absorption path. It follows from the above discussion that the introduction of the definition "absorption path" is closely related to the power behaviour of the primary spectrum. Actually, exponent γ varies with energy, which leads to the conclusion that L also will depend on energy.

3.3. Experiments

The experimental determination of the absorption path enables us to estimate the value of quantity $\beta^{\gamma-1}$. The nucleon intensity at different depths is usually measured by observing the interaction of the nucleons, i.e. by the number of electronic-nuclear showers or electromagnetic cascades occuring from the decay of π°-mesons. In both cases, one can apply photo-emulsions and electronic instruments.

The so-called "impulsive" instruments have obtained wide recognition. They consist of targets (often made of graphite) and ionization chambers screened by thin layers of lead (figure 33). The lead thickness is chosen in a manner that the electron-photon cascade maximum (when $E_o \sim 100$ GeV the thickness is $5 \div 6$ t units) is observed inside the chamber. In nuclear interactions occuring in carbon, π°-mesons are produced, which give photons after decaying.

Photons mainly begin to multiply in lead. By measuring the number of particles at the maximum, one defines energy E transferred by the π°-mesons. By adjusting the registration threshold of phenomena in the ionization chambers such that $E_\gamma \gg \xi$, one is able to select particles with an energy $E > \mathcal{E}_o$. The number of events, N_T, registered by the instrument will be

$$N_T(E_\gamma)\,dE_\gamma \approx (1-e^{-x_C/\lambda_C}) \int_{E_\gamma}^{\infty} N(E_0)\,dE_0 f(E_\gamma, E_0)\,dE_\gamma,$$

where x_c and λ_c are the thickness of the graphite target and interaction threshold in carbon respectively. Function $f(E_\gamma, E)$ defines the probability that a primary particle with energy E_o forms photons with total a energy E_γ in the target.

Again assuming that function $f(E_\gamma, E_o)dE_\gamma$ is homogeneous and denoting E_γ/E_o by α, we obtain

$$N_T(>E) = (1 - e^{-x_C/\lambda_C})\, N(>E)\, \langle \alpha^{\gamma-1} \rangle, \qquad (9.7)$$

where $(\gamma - 1)$ is the exponent of the integral spectrum. The bromogeneity of function f means that the energy fraction $\alpha = E_\gamma / E_0$, transferred to the target by photons, does not depend on the energy of the primary particle. Here $N(>E)$ is the integral energy spectrum of nucleons, which $N_T(>E)$ is the number of "pulses" in the ionization chamber with an ionization greater than I, corresponding to energy E_γ. Consequently, if quantities λ_c and $\langle \alpha^{\gamma-1} \rangle$ are constants, the number of pulses in the chamber will be proportional to the number of the nuclear-active particles.

An alternative method for determining the absorption threshold is based on the application of "photo-emulsion chambers" (see chapter 4, section 4). The performance of these experiments does not differ principally from experiments with ionization chambers. The only difference is that photo-emulsions are used as detectors rather than ionization chambers.

In the latter experiments, the surface of the photoemulsion is made almost perpendicular to the direction of the particles' motion. Therefore, each particle will have a track in the emulsion in the form of a short dash. In the case of a shower, the tracks will be a collection of dashes, almost all in the same direction.

When the energy of photons is higher than $\sim 5 \times 10^{12}$ eV, the collection of dashes will be seen by the nacked eye. Showers produced by lower-energy photons will be searched for by means of a miscroscope. In order to simplify the search for showers in the emulsion, emulsions are recently made covered with X-ray films. In X-ray films, showers produce spots of different diameters and with considerable blackening in their centre.

Measurements with emulsion chambers were made at different heights, and the absorption threshold of nuclear active particles produced by photons were determined. Recently, chambers with an area of several square meters were used. This makes it possible to register photons with an energy up to 10^{14} eV. Chambers of smaller dimensions are used for measurements made near the atmospheric boundaries (by aerostats° or at a height ~ 12 kms (by aeroplanes).

All the above mentioned methods give good values for the absorption coefficient of the nuclear-active particles, in the interval of 110 - 120 g/cm^2 for the energy region of $E > 100$ GeV. As energy increases, the absorption path of nucleons apparantly decreases. This is possibly related to the change of the form of the primary spectrum.

The variation of the number of high-energy nucleons with height is shown in figure 83 /7/. In the region of energies sensitive to the terrestrial magnetic field, i.e. when $E \lesssim 15$ GeV, the absorption path could be determined by comparing data on the absolute value of the particle flux at the atmospheric boundary with the directly measured proton intensity on mountains and at sea level. These measurements were carried out by N.M. Kočarjan in the USSR and

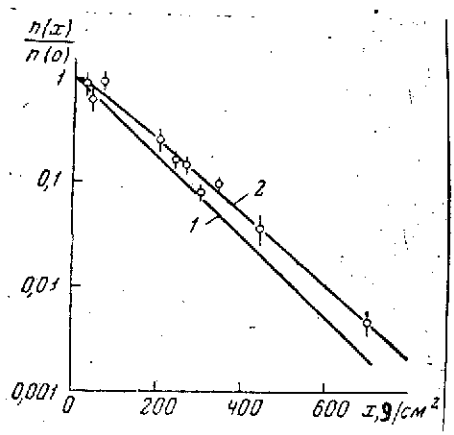

Figure 83. Latitudinal dependence of the number of nuclear-active particles: 1- for nucleons $L \sim 110$ g/cm^2, 2- for all the nuclear-active particles $L \sim 120$ g/cm^2.

Wolfendail in England using magnetic spectrometers [8-10]. As a result of these experiments, the nucleon absorption path was found to be equal to ~ 125 g/cm^2.

3.4. Lower-energy nucleons in the atmosphere and nuclear disintegrations

The principal process occuring in the atmosphere is the production of an electronic-nuclear shower by primary particles. The investigation of the latitudinal effect of showers having a small number of particles by means of hodoscopic counter systems (figure 32) showed that the latitudinal effect produced by electronic-nuclear showers at the atmospheric boundary is less than the latitudinal effect of primary particles. This shows that not all of the primary particles produce electronic-nuclear showers at large heights.

Experiments by A.N. Čarahč'jan and C.N. Vernov showed that electronic-nuclear showers, in which mesons with energies $> 10^8$ eV are generated, can be produced only by particles having energy $> 10^9$ eV, as the latitudinal effect of these showers is found to be half than for primary particles.

Let us now consider the behaviour of low-energy nucleons, namely the products of nuclear disintegrations and the δ-nucleons. Low-energy protons [1] are rapidly slowed down in the atmosphere at the expense of the ionization loss, whereas neutrons, colliding with nuclei can cause nuclear disintegrations up to energies of 20 ÷ 30 MeV. All primary particles are capable of producing

1) At an energy of about 500 MeV, the nuclear path is approximately equal to the ionization path. Hence, protons of lower energies do not participate in nuclear interactions.

nuclear disintegrations. For this reason, the latitudinal effect of the nuclear disintegrations at the atmospheric boundary is equal to the latitudinal effect of the primary particles.

The most typical feature of the dependence of the number of nuclear disintegrations on altitude is the existence of a maximum in intensity. This indicates to a multiplication of the component that generates nuclear disintegrations in the atmosphere. At heights less than 15 ÷ 20 ms, the number of nuclear disintegrations starts to fall exponentially such that $N \sim e^{-x/x_0}$ where x_0 increases with a decrease in the latitude of the observation point (table 31). This means that primary particles with energies ~ 15 GeV are capable of producing much more disintegrations than nucleons with energy > 20 GeV. The total number of nuclear disintegrations occuring during 1 sec $N_{n.d}$ in a column of cross-section 1 cm, can easily be obtained by integrating over the high-altitude motion :

$$N^0_{n.d} = \int_0^\infty N^\lambda_{n.d}(x)\,dx. \qquad (9.8)$$

The number of nuclear disintegrations, generated at different latitude, is given in table 31.

Once the flux of primary particles at each latitude is known, the average number of nuclear disintegrations induced by one primary particle of arbitrary energy can be calculated. The results of such calculations are given in the second row from bottom of table 31.

We can see that that the number of disintegrations increases as energy increases. According to measurements made by means of neutron counters [11], 7 low-energy neutrons are produced in an air column of cross section i cm at latitude 51°. This means that three such neutrons occur on the average in each disintegration.

Table 31

λ	51°	31°	0°
E_0, GeV	>1,5	>7	>15
$N_{n.d}$, cm² sec⁻¹	2,5	0,9	0,6
$N_{n.d}/N_p$	5	10	12
x_0, g/cm²	145	180	240

Low-energy nuclear disintegrations are mainly produced by neutrons. Stars with a number of rays $N_h > 16$ are produced equally by both charged and neutral particles. The reason is that small stars are produced by particles with an energy less than 500 MeV. The ability of primary particles of different energies to produce nuclear disintegrations can be illustrated by the fraction of energy that protons of different energies transfer to strongly ionizing particles in the atmosphere in all the interactions (figure 84).

3.5. Neutrons

Low-energy neutrons are closely related to nuclear disintegrations. Neutrons having an energy tens of millions of electron-volts and higher,

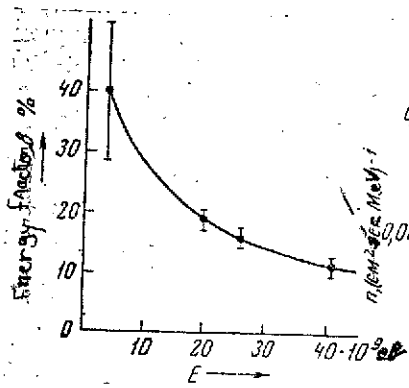

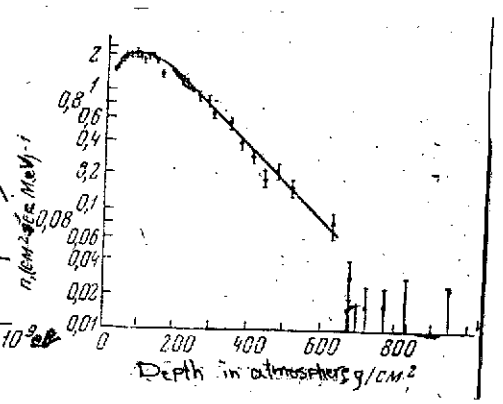

Figure 84. Energy fraction, as per cent, transferred to strongly ionizing particles in the whole atmosphere by primary particles of different energies.

Figure 85. Dependence of the number of neutrons, n, on depth in the atmosphere at latitude $\lambda = 53°$.

will produce nuclear disintegrations in the atmosphere. The variation of their intensity with height coincides with the latitudinal dependence of nuclear disintegrations. Low-energy neutrons in the final stage are captured by the nitrogen nuclei.

The number of neutrons in the atmosphere is measured by means of proportional counters or ionization chambers filled with BF_3. As a result of capturing thermal neutrons by B^{10} nuclei, alpha particles are emitted and these are easily registered. In order to register neutrons with an energy 50 keV - 20 MeV, counters involving hydronge-containing molecules are used. The recoil protons are then registered by means of scintillators. Figure 85 shows the absolute intensity of fast neutrons as a function of altitude at latitude 53°N. The curve has a sharp maximum which gives evidence for the cascade multiplication of neutrons in the atmosphere. The depth corresponding to the maximum depends on the geomagnetic latitude of the observation point. At the equator, the maximum is located at a depth of 125 g/cm^2 whereas at latitude 7° it is found at a depth of 90 g/cm^2. Figute 86 shows the latitudinal effect of neutrons at the depth of the atmosphere.

4. Pions in the Atmosphere

4.1. Solution of the nuclear-cascade equation for pions

We shall now consider the equation that describes the development of a pion cascade. It is clear from general considerations that the pion flux at the atmospheric boundary is equal to zero. The boundary condition to be implied on the solution of equation (9.1) is then

$$\Pi\ (0,\ E)\,dE = 0.$$

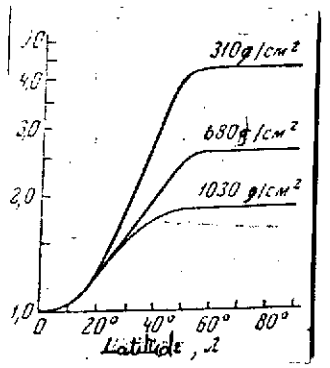

Figure 86. Latitudinal effect for slow neutrons in the atmosphere.

The decaly term has the greatest influence in the region of small energies and large altitudes. This term is, however, negligible when $E \gg 116$ GeV. At energies much less than 116 GeV, the pion flux is small because of decay.

The solution of equation (9.1) can be obtained by using the method of successive approximations [4]. For this purpose, we expand function Π (E,x) in a series

$$\Pi(E,\ x) = \sum_{i=1}^{\infty} \Pi_i(E,\ x); \tag{9.9}$$

$$\Pi_i(E,\ 0) = 0 \tag{9.10}$$

Putting $x/\lambda_p = y$, we obtain the following system of equations

$$\begin{aligned} &\frac{\partial \Pi_1}{\partial y} + \left(\frac{\lambda_p}{\lambda_\pi} + \frac{C}{Ey}\right)\Pi_1 = \int_E^\infty N(y,\ E_0)\, n_1(E,\ E_0)\, dE_0; \\ &\frac{\partial \Pi_i}{\partial y} - \left(\frac{\lambda_p}{\lambda_\pi} + \frac{C}{Ey}\right)\Pi_i = \int_E^\infty \Pi_{i-1}(y,\ E_0)\, n_2(E,\ E_0)\, dE_0. \end{aligned} \tag{9.11}$$

These equations express each of functions $\Pi_i(y, E)$ in terms of Π_{i-1}. Consequently, function $\Pi_i(y, E)$ could be considered as the distribution of pions of the i-th generation descended from the (i-1)-th. Integrating, we obtain

$$\Pi_i(x,\ E) = y^{-\frac{C}{E}} e^{-\frac{\lambda_p}{\lambda_\pi} y} \left[\int_E^\infty \int_0^y N(E,\ 0)\, n_1(E,\ E_0)\, dE\, e^{-\frac{\lambda_p}{\lambda_p} z} e^{\frac{\lambda_p}{\lambda_\pi} z} z^{\frac{C}{E}}\, dz.\right. \tag{9.12}$$

In chapter 4, we pointed out that the pion interaction threshold is close to 120 g/cm^2, i.e. approximately equal to the nucleon absorption path: $\lambda_\pi \approx L_p$. Assuming that $n_1(E,E_0)$ is a homogeneous function, we then obtain

$$\Pi_1(y, E) = N(y, E)\frac{y}{\frac{C}{E}+1}\int_E^\infty \left(\frac{E}{E_0}\right)^{\gamma-1} n_1\left(\frac{E}{E_0}\right)\frac{dE}{E_0} = N(0, E)\, n_1 \langle u^{\gamma-1}\rangle \frac{y}{\frac{C}{E}+1} e^{-\frac{\lambda_p y}{L}}, \tag{9.13}$$

where n_1 is the pion multiplicity in a single act and $u = E/E_0$. Quantity $\langle u \rangle$ is interpreted as the mean energy fraction carried away by pions. Then $\sqrt[\gamma-1]{\langle u^{\gamma-1}\rangle}$ is the mean effective energy fraction of pions in a single act. It is clear that the effective energy depends on the form of the pion spectrum in a nucleon-nucleus collision.

Equation (9.13) shows that the first generation of pions has a maximum in the depth distribution. The energy spectrum in the energy region of $E \gg C$ coincides with the nucleon spectrum at the atmospheric boundary, whereas in the energy region of $E \ll C$, the spectrum decays more gently.

$$\Pi(E)\,dE \sim AE^{-\gamma}EdE = AE^{-\gamma+1}dE,$$

where γ is the exponent of the initial spectrum. In order to calculate the spectra of the next generation, it is necessary to know the spectrum of generating pions by pions. The contribution of large i's is particularly large in the depth of the atmosphere.

Unfortunately, the shape of spectrum $n_2(E,E_0)$ is almost unknown, so that it is impossible to obtain a reliable solution. Many scientists made calculations based on various assumptions on the form of function $n_2(E,E_0)$ [4-6]. It is found that the intensity maximum is displaced to a greater value when the generation number i is increased; $\Pi_i(x) \sim x^i e^{-x/L}$. The mean particle energy decreases with the increase of the generation number. Summing over all the generations, we find that the number of pions decreases almost exponentially with the increase in depth, though absorption takes place more slowly than in the case of nucleons. The measured absorption path L is usually related to the nuclear component. The nucleon absorption path is thus less than the value 120 g/cm^2, obtained experimentally.

Calculations show that pions constitute a considerable part of the nuclear components at heights of 3 - 4 km above sea level (up to 30 - 50%). At a height of 12 km however, this fraction becomes smaller ($\lesssim$ 10%).

4.2. Experimental investigations of high-energy pions in the atmosphere

Direct measurement of particle masses at energies higher than 50 GeV is

almost impossible. Indirect methods are used for this purpose. One of these methods is to determine the ratio of the number of neutral and charged particles responsible for the high-energy phenomena, for instance, electronic-nuclear showers in a Wilson chamber.

On high mountains, the number of high-energy protons is slightly more than the number of neutrons. The excess of charged particles is due to pions. One can also determine the ratio of the number of charged particles to that of neutral particles, which cause high-energy pulses in ionization chambers. In these experiments, the presence of a charge is registered by hodoscopic counters.

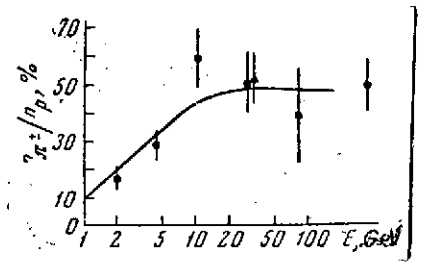

Figure 87. The ratio of the number of pions to that of protons in the depth of the atmosphere as a function of particle energy.

In the energy region of 10^{10} eV, direct measurements of particle masses could be made by means of a magnetic mass-spectrometer. Such measurements showed that the fraction of π-mesons reaches 20% at an energy of 2×10^{10} eV (on high mountains). In the energy region of $10^{10} \div 4 \times 10^{10}$, the composition of the nuclear component can be determined by means of a direct method. For this purpose, a group of Indian scientists used a Čerenkov gas counter. It is well known that Cerenkov radiation occurs when the particle velocity exceeds a certain limit, given by the refractive index of the medium. For instance, in air, at a pressure approximately equal to atmospheric pressure, pions reach the velocity necessary for radiation to commence at an energy of approximately 6 GeV, and protons at an energy of $\sim$ 40 GeV. This makes it possible for us to distinguish between pions and nucleons in the energy range of $6 \div 40$ GeV. In this experiment, particle energies were measured by means of an ionization calorimeter. The Čerenkov counter had a height of more than one meter. It was found that on mountains, the number of pions was about 30 - 40% that of protons. At higher energies, up to 500 GeV, this ratio increases to 50% (25% of the total nucleons) (see figure 87).

5. Muons

5.1. General consideration

The study of muons is of particular interest from many points of view. Firstly, muons are the only penetrating component that can easily be detected even at large underground depths. Secondly, the intensity and energy spectrum of muons are related in terms of well known decay constants with particles directly created in nuclear processes. The number of π-meson decays in the depth interval from the atmospheric boundary to the observation level x_o is given by :

$$N_\pi(x_0, E)\,dE = dE\int_0^{x_0} \Pi(x, E)\,\frac{Cdy}{Ey}.$$

Substituting the expression for Π (x,E), given in equation (9.13) into this equation, we obtain [1] :

$$N_\pi(x_0, E)\,dE = \frac{N(E, 0)\,dE\,\langle nu^{\gamma-1}\rangle C}{E\left(\frac{C}{E}+1\right)} \cdot \frac{L}{\lambda_p}(1 - e^{-x_0/L}).$$

In order to obtain the muon spectrum, it is necessary to note that in the decay of pions, muons are given on the average, 3/4 of the pions energy. Therefore, $E = (4/3)E_\mu \approx 1.3\ E_\mu$, and the muon intensity is equal to

$$N_\mu(x_0, E_\mu)\,dE_\mu = \frac{N(E_\mu, 0)\,dE_\mu\,\langle nu^{\gamma-1}\rangle}{E_\mu\left(\frac{C}{1{,}3E_\mu}+1\right)1{,}3^\gamma} \cdot \frac{L}{\lambda_p}(1 - e^{-x_0/L}). \qquad (9.14)$$

The life-time of a muon is 100 times greater than for a pion. Consequently, muons with energies higher than 100 GeV almost do not decay in the atmosphere. The slowing down of muons is only due to electromagnetic losses, mainly ionization losses, if one is speaking of low wnergy muons. At higher energies, bremsstraalung, pair production and nuclear processes are responsible for the energy loss. Muons are very slowly absorbed in the atmosphere. From the top of mountains to sea level, the total intensity of muons only changes 2 - 2.5 times; (the nuclear component changes in this interval by a factor of 20). Consequently, muons are the major constituents of cosmic rays at sea level.

5.2. Methods for studying muons in cosmic rays Definition of measuring units

Muons are investigated on the earth's surface (often at sea level), under water and deep underground. In order to reduce the measurements to standard conditions, the depths at which the measurements are made are expressed in terms of water-equivalent meters (w. - e. m). This unit is defined as the thickness of layer in meters, multiplied by the density in g/cm^2. Recently, Menon and Ramana Murti, suggested a new unit [13]: 1 standard-soil hectogram = 1 ssh = 100 g/cm^2 = 100 g/cm^2. A standard soil is understood as matter with a mean density of 2.65 g/cm^2, mean value of ration Z/A = 0.5 and mean value of Z^2/A = 5.5. The necessity for such a definition comes from the fact that the absorption rate of muons depends on Z/A (ionization loss) and on Z^2/A

---

1) One can show that the major contribution to the muon intensity is due to first-generation π-mesons.

(pair production and bremsstraalung). The transformation to water-equivalent meters does not take into consideration the chemical composition of the soil.

Energy loss of muons[1)]

In the analysis of the bremsstraalung of muons, electromagnetic losses only are taken into consideration. Electromagnetic losses are divided into ionization losses, loss on bremsstraalung showers, on electron-position pair production and on photo-nuclear processes (Maass-Kessler showers).

Ionization losses depend weakly on energy, while other types of losses are almost proportional to energy. Therefore, the specific energy loss of muons could be represented in the form of

$$\left\langle \frac{dE}{dx} \right\rangle = A(E) + B(E)\,E. \tag{9.15}$$

In a soil of a standard composition,

$$A(E) = \left(\frac{dE}{dx}\right)_{ion} = 1{,}888 + 0{,}0768 \ln \frac{E}{mc^2} \ \text{Mev/g cm}^{-2}.$$

Coefficient B(E) is a linear superposition of coefficients B_e characterizing the energy loss on bremsstraalung, B_β characterizing the loss on pair production and B_n characterizing the nuclear losses.

The calculation of partial loss B_n is based on representing the muon field in terms of a photon spectral distribution using the Weizsacker-Williams method. Taking into consideration the cross sections of photo-nuclear processes, Fowler and Wolfendeil [14] obtained the following approximate expression :

$$B_n = 0{,}28 \cdot 10^{-6} \ \text{cm}^2/\text{g}.$$

In fact, quantity B_n changes slightly its value from 0.26×10^{-6} at an energy of 10 GeV to 0.32×10^{-6} at 70 TeV. In different studies, slightly different values for the B_e coefficient were obtained, depending on the introduction of the various corrections. At energies higher than 2.5 TeV, coefficient B_e varies weakly

$$B_e \approx 1{,}66 \cdot 10^{-6} \ \text{cm}^2/\text{g}.$$

At lower energies, coefficient B_e decreases to 1.33×10^{-6} (E = 1 GeV).

---

1) A detailed discussion on this subject is given by I.L. Rozental' (U.F.N., 94, 91, 1968) and in a dissertation by Ju. D. Kotov (MIFI, 1968).

Quantity B_p increases from 1.6×10^{-6} cm^2/g at 100 GeV to 2.4×10^{-6} cm^2/g at energies higher than 10^4 GeV. Accordingly, at the highest energies, quantity B(E) reaches a value of 4.4×10^{-6} cm^2/g. The behaviour of various types of energy losses is represented in figure 88.

Integrating equation (9.15) leads to a relation between the mean muon path and energy. The dependence of the muon path, R (in g/cm^2) on energy is represented in table 32 for two values of the absorber's atomic number Z.

The above-derived formulae are related to mean values. In fact, losses represented by the second term of equation (9.15) fluctuates strongly. The relation between energy and path might then not be unique; a given path could be given to a whole set of energies at sea level. Consequently, a given

Table 32

E, GeV	R, g/cm²	
	Z=10	Z=12
20	$1{,}04 \cdot 10^{-4}$	$1{,}04 \cdot 10^{4}$
50	$2{,}30 \cdot 10^{4}$	$2{,}30 \cdot 10^{4}$
$1 \cdot 10^{2}$	$4{,}24 \cdot 10^{4}$	$4{,}23 \cdot 10^{4}$
$2 \cdot 10^{2}$	$7{,}70 \cdot 10^{4}$	$7{,}59 \cdot 10^{4}$
$5 \cdot 10^{2}$	$1{,}59 \cdot 10^{5}$	$1{,}54 \cdot 10^{5}$
$1 \cdot 10^{3}$	$2{,}53 \cdot 10^{5}$	$2{,}41 \cdot 10^{5}$
$2 \cdot 10^{3}$	$3{,}74 \cdot 10^{5}$	$3{,}50 \cdot 10^{5}$
$5 \cdot 10^{3}$	$5{,}61 \cdot 10^{5}$	$5{,}14 \cdot 10^{5}$
$1 \cdot 10^{4}$	$7{,}14 \cdot 10^{5}$	$6{,}48 \cdot 10^{5}$
$5 \cdot 10^{4}$	$1{,}09 \cdot 10^{6}$	$9{,}71 \cdot 10^{5}$

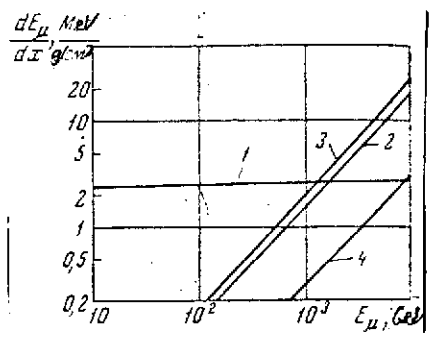

Figure 88. Energy loss of muons: 1- on ionization, 2- on radiation, 3- on pair production, 4- on nuclear processes.

threshold corresponds to an effective energy, which depends not only on the fluctuation of the losses, but also on the shape of the muon spectrum. Actually, the energy will as a result of fluctuations, be sometimes larger and sometimes smaller than the mean energy. The number of muons sharply decreases with the increase in energy. When energy is therefore calculated by means of a formula derived from mean values, one increases the energy more often (corresponding to raising the particle from the low-energy region where the intensity is less) than decreases it. The sharper is the muon spectrum, the stronger is the effect. This effect could be taken into account by a corrective energy-dependent factor, since the contribution of the fluctuating part depends on energy. The corrective factor varies from ~ 0.9 (for measurements at a depth of $\sim$ 2000 ssh) to $\sim$ 0.27 (at 10000 ssh) [15].

5.3. Experimental instruments and methods

In order to study the muon spectrum in the high-energy region (up to a few

tens of GeV) magnetic spectrometers are used (figure 19) located at sea level or on hills.

In underground experiments, systems of hodoscopic counters or scintillators are applied. Studying the angular distribution of muons at a given depth, makes it possible to determine the intensity below thick layers of matter. Actually, the path made by muons penetrating to a depth x with an angle θ with respect to the vertical direction is equal to $x/\cos\theta$. For this reason, in order to investigate muons, circular hodoscopic instruments are used to be able to determine the direction. An example of such instruments is shown in figure 46.

The spectrum of pulses produced by muons in ionization chambers has been studied in a series of investigations. Pulses are mainly produced in the case of a pair production by a muon or a bremsstraalung shower in the filter below the ionization chambers. Using the pair production and the bremsstraalung shower cross sections as well as the cascade theory, one can determine the spectrum of muons by knowing the spectrum of the pulses. Instruments of a calorimetric type, made of several rows of ionization chambers under an absorber make it possible to follow the whole cascade curve. By comparing the pulse spectrum and the muon spectrum obtained by an independent method, one can obtain information on the non-electromagnetic interactions of muons.

5.4. Experimental results

We have seen that the intensity and spectrum of muons can be obtained by measurements with magnetic spectrometers at sea level (in the energy range of $E < 100$ GeV), by the curve describing the dependence of intensity on depth in the soil and also by an indirect method based on equation (9.14) if the spectrum of muons in the atmosphere is known.

In order to measure the muon absorption curve under thick layers of matter, instruments are sent down to the bottoms of lakes or inside deep mines. Muons were investigated for instance, in the south of India in the Kolar Gold Mine, at a depth exceeding 3 kms. At this spot, rocks mainly consist of quartz. Similar measurements have been carried out in tunnels, in highlands, in salt mines, etc.

Figure 89,a shows the dependence of intensity on depth, obtained in various measurements. Figure 89,b shows the energy spectrum of muons at sea level obtained by different experiments, including magnetic spectrometric data [13].

5.5. Muon energy spectrum at large zenith angles

It is clear that the intensity of muons is maximum in the vertical direction and decreases when the zenith angle is increased. By considering muons, coming from directions close to the horizontal, one can easily see that the spectrum will be enriched with high energy muons. Indeed, pions moving with large angles will travel a much longer path in a dilute medium than vertical pions, and therefore have a greater probability to decay and produce high-energy muons. The intensity of muons having an energy of $\sim$100 GeV is the same at the

vertical direction and with an angle of 80°. At higher energies, the intensity of muons with large angles must be greater than that of vertical muons.

The study of muons is rapidly progressing with respect to the problem of weak interactions at high energies and also with the problems described in chapter 3.

5.6. Excess of positive muons : μ^+/μ^-

The ratio of the numbers of positively and negatively charged muons depends on the charge composition of the primary cosmic rays and on the mechanism of muon production. The observed excess of positively charged muons is generally

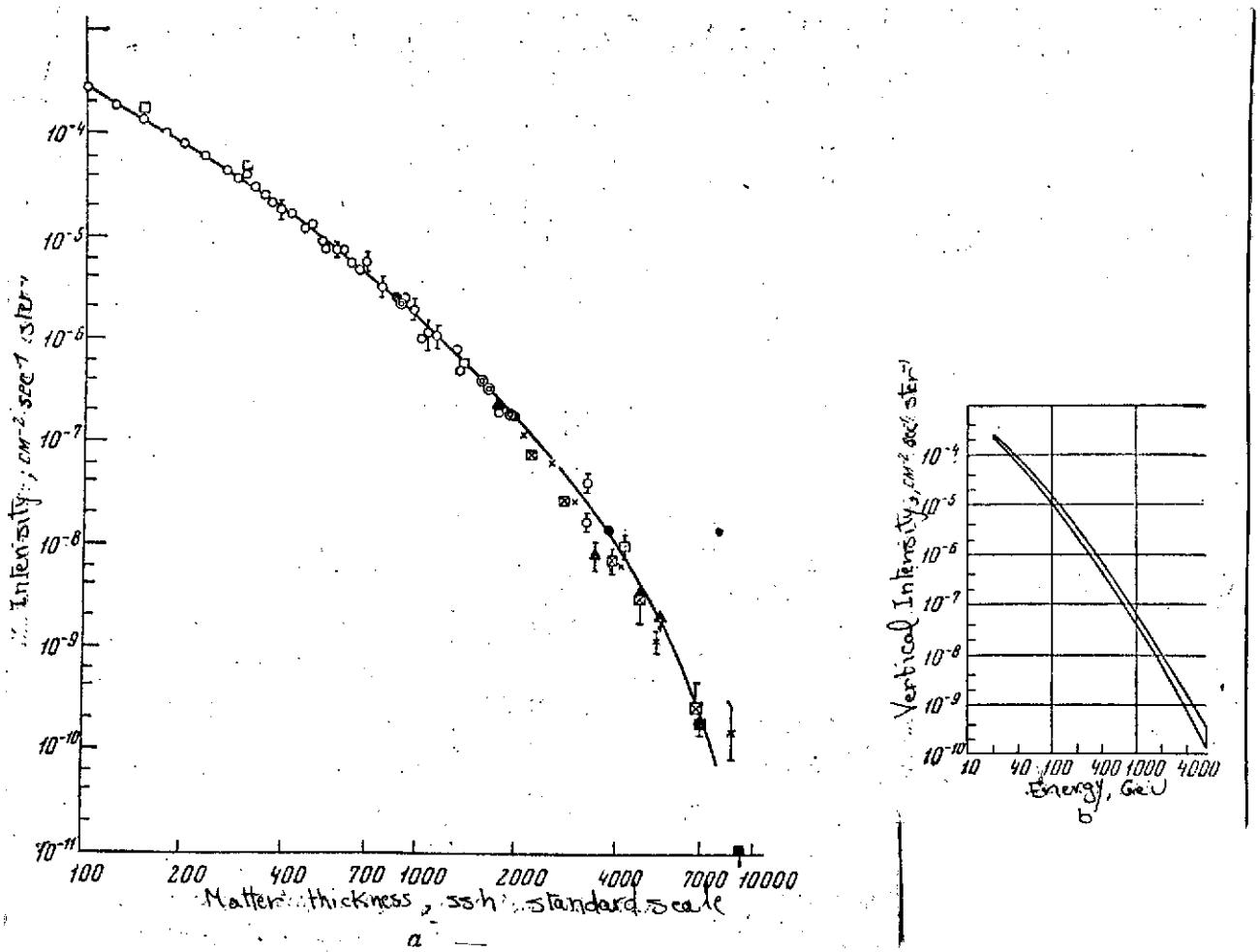

Figure 89. Dependence of muon intensity on depth (a), and on energy (energy spectrum of muons at sea level) (b).

interpreted as being due to the positive charge of the primary radiation. Quantitatively, quantity μ^+/μ^- depends on the fraction of protons in the primary radiation, the multiplicity of pions in the first interaction acts on the primary particles and on the mechanism of their production. In a multiple production of pions of a statistical ttpe, the positive charge excess must decrease with the increase of energy due to an increase in pion multiplicity. If an isobaric mechanism is acting, the magnitude of the excess will be given by the charge distribution of pions occuring in the decay of the isobar. In this case, the magnitude of the positive excess may not vary with energy.

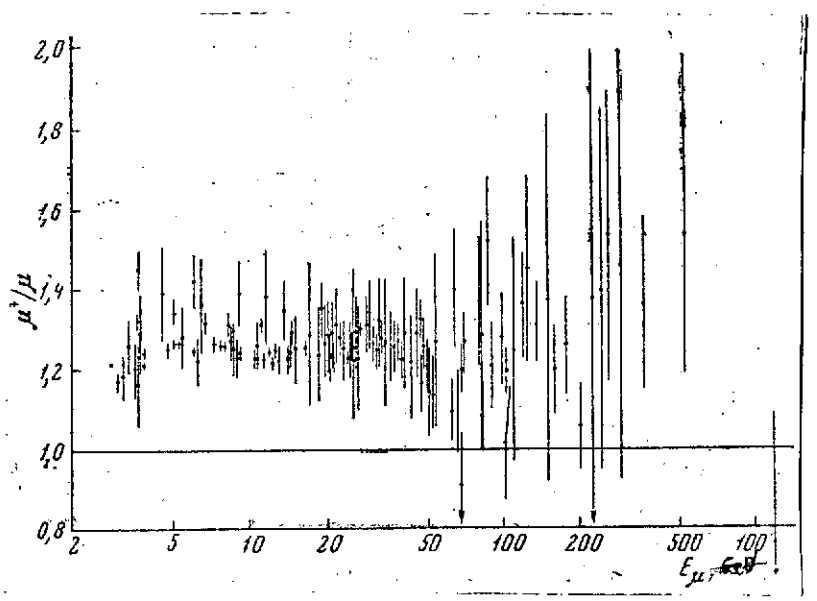

Figure 90. The excess of positively charged pions (a collection of results of various investigation) [10*].

A similar picture will also be observed in other interaction mechanisms if the produced pion will carry a major fraction of the primary energy. In the region of very low energies (E < 1 GeV), the ratio μ^+/μ^- must decrease, because pions created in the depth of the atmosphere, start to play an important role. Here, the generated component has a positive excess, less than at the atmospheric boundary. At high energies, an important contribution to the ratio μ^+/μ^- will be given by kaons, whose decay plays an important role up to higher energies as compared to that of pions.

Consequently, the study of the value of μ^+/μ^- could give information on the mechanism of high-energy nuclear interactions. Experimental data on the value of μ^+/μ^- is shown in figure 90 [10*].

6. The Electron-Photon Component

The electron-photon component has two possible origins. First, photons occuring as a result of the decay of π°-mesons, and second, electrons and photons produced by muons as a result of the δ-processes, bremsstraalung and decay.

At sea level, the electron-photon component is solely due to muons. The energy of this component is proportional to the energy of muons. Such electrons are in equilibrium with the muons and hence are called the equilibrium soft component. At large heights, the electron-photon component is almost entirely of a nuclear origin, and is often called the non-equilibrium component.

The discovery and investigation of the non-equilibrium component initiated the discovery of electronic-nuclear showers by Soviet physicists. The electron-photon component accordingly has a secondary origin and must have an intensity maximum. The energy spectrum and the dependence of the number of electrons on height will depend on two factors: the generation of photons by nuclear-active particles (mainly through the decay of π°-mesons) and the development of electromagnetic cascades in the atmosphere. The total number of electrons will depend on the depth in the atmosphere in the following manner :

$$n_e(x_0) = \int_0^{x_0}\int_0^{\infty} N_{n.a}(x', E)\,\frac{dx}{\lambda}\cdot\frac{\alpha_\gamma E}{n_\gamma}\,n_\gamma\left\{\mathcal{P}\left(x_0 - x', \frac{\alpha_\gamma E}{n_\gamma}\right)\right\}dE, \tag{9.16}$$

where $N_{n.a}(x',E)$ is the number of the nuclear-active particles and $P(x_0 - x', \frac{\alpha_\gamma E}{n_\gamma})$ the cascade curve in air for primary photons having an energy of $\alpha_\gamma E/n_\gamma$. This integral could be calculated if the altitudinal dependence and energy spectrum of the nuclear-active particles as well as the properties of the nuclear-interaction act were known.

It is easy to calculate the energy of the equilibrium soft component. For this, one makes use of the equilibrium condition which consists in the following: the energy transferred by the decay electrons during a path equal to 1 t-unit is equal to the energy lost in this layer on ionization. This condition is satisfied because the path of electrons is much shorter than the path of muons.

$$n_e\varepsilon = \frac{\mu c^2}{\tau_e c E_\mu}\,t E_\mu\,\frac{1}{3} = \frac{1}{3}\,\frac{\mu c t}{\tau_0}, \quad n_e = \frac{\mu c t}{3\tau_0 \varepsilon}, \tag{9.17}$$

where ε is the critical energy and μ the muon mass. Since the length of the t-unit increases with height, the number of decay electrons per muon also increases. At sea level, $n_e \simeq 0.2$ i.e. 20% of the number of muons.

Noting that another 15% of the electrons are created by the δ-processes, one can see that the whole electron-photon component at sea level has an equilibrium origin. The non-equilibrium electron-photon component is closely

related with pions because it mainly originates from the decay of π°-mesons. The photon spectrum is related by a simple relation with the spectrum of π°-mesons. In the high-energy region, for a power spectrum,

$$\frac{\partial \Gamma(E)}{\partial E} = \frac{2}{\gamma} \cdot \frac{\partial \pi^{\circ}}{\partial E}, \tag{9.18}$$

where $\frac{\partial \pi^{\circ}}{\partial E}$ is the generation spectrum of π°-mesons.

The experimental investigations of the photon spectrum were mainly carried out by means of emulsion chambers (figure 16) or impulsive instruments (figure 33). The photon energy is determined by the spatial distribution of electrons crossing the nuclear emulsion or by the maximum of the cascade.

Measurements were carried out near the atmospheric boundary on aeroplanes and on mountain tops. Instruments of large dimensions were used to observe the sufficiently high-energy photons coming from the atmosphere. The first of the emulsion chambers for the investigation of photons was built on the Norikura mountain in Japan and has a dimension of 3 m^2. Emulsion chambers make it possible to study photons separately even if they are only separated by distances not exceeding a tenth of a micron. Ionization chambers sum the energies of several photons if the distance between them is smaller than the dimensions of the chamber. At large heights, where the density of the atmosphere is small, photons have enough time to be dispersed over considerable distances and the conditions for the applicability of ionization chambers for registering separate photons is better.

The shape of the photon energy spectrum is the subject of many scientific debates. In studies by Japanese scientists and in the joint research between Japanese and Brazilian scientists on mountains, it was found that the photon spectrum could be described by a power law (figure 91):

$$n_{\gamma}(>E) = AE^{-\beta}, \tag{9.19}$$

where B = 2.2 ± 0.1 at energies higher than 1000 GeV and B ≈ 1.9 ± 0.1 at E < 1000 GeV. Experiments undertaken by Indian and English scientists with emulsion chambers near the atmospheric boundary also indicated towards the change in the slope of the photon spectrum. The interpretation of this result is not unique.[1] The change in the slope of the spectrum could be produced either by changes in the elementary acts or by a change in the primary nucleon spectrum at energies approximately 50 - 100 times higher than the energy corresponding to the break point of the spectrum measured on high mountains. In the first case, one assumes that the energy fraction, transferred to photons during the interaction with nucleons with energy $E > 10^3$ GeV with nuclei, decreases or suggests the occurence of other changes in the interaction act.

If the energy corresponding to the break region changes with altitude, then the break is more probably due to a change in the primary spectrum. Photons having an energy of 10^3 GeV are on the average, produced by nucleons

having a much higher energy, in the order of $(2 \div 3) \times 10^4$ GeV. They are collected from distances of 1 - 2 t-units, i.e. occur near the registering instrument. Protons with energies of $(2 \div 3) \times 10^4$ GeV on mountains are produced by protons with energies of $(2 \div 3) \times 10^5$ GeV or nuclei with energies of $\sim 10^6$ GeV [16]. The whole problem is quite interesting and still requires further investigations.

Along side single photons, photon families, i.e. groups of photons simultaneously falling on the instrument, are registered by emulsion chambers or by the method of correlated emulsion. The study of these photon families may answer a number of interesting questions. Photon families could occur either directly or indirectly as a result of a decay of π^0-mesons, or as a result of a cascade multiplication of photons in the atmosphere. These two cases could be distinguished by studying the angular distribution of the particles. The distance between photons occuring from the decay of π^0-mesons is approximately given by

$$L \simeq t\left(\frac{m_{\pi^0} c^2}{\sqrt{E_1 E_2}}\right), \qquad (9.20)$$

where E_1 and E_2 are the energies of the decay photons, while t is the distance from the point of creation of the π-meson to the detector. The mean dimension of the shower produced by the cascade multiplication is equal to

$$\langle R \rangle \simeq A \frac{E_s}{E},$$

where E is the minimum energy of the registered photons and $E_s \approx 21$ MeV. Quantity A depends on the age of the shower and is approximately equal to 0.1 for small values of t. In many cases L and

$$\langle R \rangle = \frac{\Sigma E_i R_i}{\Sigma E_i}$$

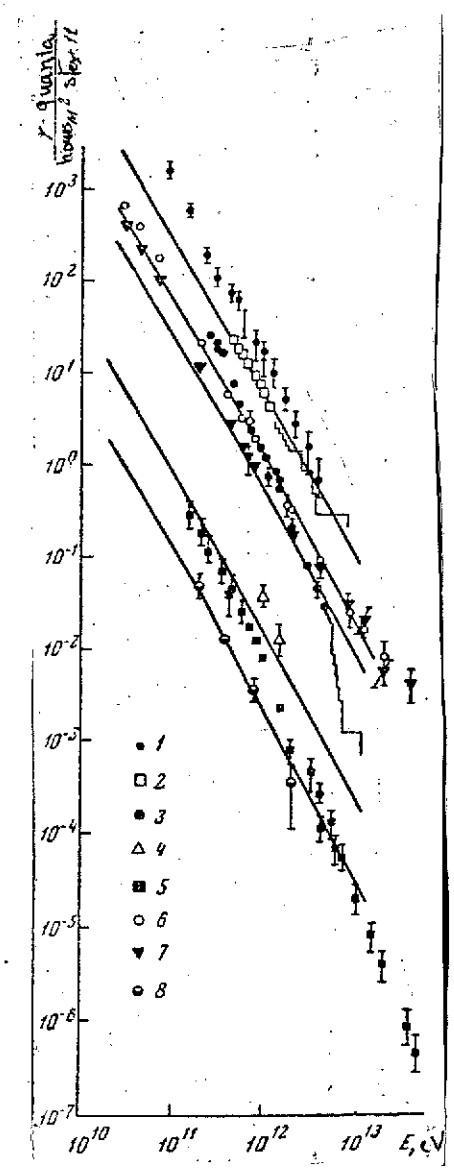

Figure 91. Energy spectrum of photons at different depths. Photoemulsions 1-6.5 g/cm^2, 2-0 g/cm^2 3- 220 g/cm^2, 4- 540 g/cm^2 5- 750 g/cm^2. Impulsive instruments: 197 g/cm^2, 7.310 g/cm^2, 8.1000 g/cm^2.

where E_i is the energy of a photon in the family and R_i the distance from the centre of the family, are different. This enables us to separate the cases of the direct registration of decay photons.

The distance between separate photons and the centre of the family makes it possible to estimate the transversal momenta of π^0-mesons producing the photons. Experiments show that the transversal momenta account for a few hundred MeV at $E > 10^3$ GeV, which is in consistence with lower-energy measurements.

By studying the spectrum of photon families, i.e. the distribution of quantities $\sum_i E_{\gamma i}$, and comparint it with the spectrum of separate photons in the same families, it was found that the spectrum $n(>\sum_i E_{\gamma i})$ was more gentle than the spectrum of separate photons, $n(>E_\gamma)$[1]. The difference of the exìpmemts of the two spectra may reach the value $\Delta B \simeq 0.2 - 0.3$. This disagreement between spectra is easily understood in the light of the increase of multiplicity of π^0-mesons with increasing energy. It is clear that if $n_{\pi^0} \sim E_0^{1/4}$ while $\sum E_\gamma \sim E$, then the energy of separate photons will be proportional to $\sum E_\gamma / E$ so that $\Delta B = 0.25$.

7. The Neutrinos

Neutrinos present in the atmosphere and underground come from various sources. The largest intensity is from low-energy neutrinos coming from the sun. A part of high-energy neutrinos occur in the decay of mesons, produced during the nuclear interaction of primary cosmic rays with the intergalaxial gas. However, the main part of the high-energy neutrinos are produced in the atmosphere at the expense of the following two processes :

$$\left.\begin{array}{l} \pi^\pm \to \mu^\pm + \nu_\mu(\tilde{\nu}_\mu); \\ \mu^\pm - e^\pm + \nu_e(\tilde{\nu}_e) + \tilde{\nu}_\mu(\nu_\mu). \end{array}\right| \qquad (9.21)$$

The neutrino fluxes occuring from the decay of pions and muons are respectively given by [17]

$$\left.\begin{array}{l} \mathcal{J}_{\pi\nu}(E_\nu)\,dE_\nu = \begin{cases} 1{,}85 \cdot 10^{-2}(0{,}08 + E_\nu)^{-2{,}8} dE_\nu & (1 \div 10 \text{ GeV}); \\ 6{,}65 \cdot 10^{-2}(1{,}1 + E_\nu)^{-3{,}2} dE_\nu & (10 \div 300 \text{ GeV}); \end{cases} \\ \mathcal{J}_{\mu\nu}(E_\nu)\,dE_\nu = \begin{cases} 7{,}65 \cdot 10^{-2}(0{,}37 + E_\nu)^{-3{,}75} dE_\nu & (1 \div 10 \text{ GeV}); \\ 1{,}48 \cdot 10^{-2}(3{,}5 + E_\nu)^{-4{,}5} dE_\nu & (10 \div 100 \text{ GeV}). \end{cases} \end{array}\right|$$

The intensity of neutrinos from muons increases with the increase of the angle from the vertical, more rapidly than the intensity of neutrinos from pions. The total flux of high-energy neutrinos reaches $\frac{1}{10}$ of the flux of the primary

radiation.

The investigation of neutrinos is made by using the following weak-interaction reactions :

$$\nu_\mu + n \rightarrow p + \mu^-, \quad \sigma = 1{,}5 \cdot 10^{-38} E_\nu \ cm^2;$$
$$\tilde{\nu}_\mu + p \rightarrow n + \mu^+, \quad \sigma = 0{,}5 \cdot 10^{-38} E_\nu \ cm^2.$$

Experiments are carried out deep underground. The effectiveness of the registration depends on the thickness of the layer in which the neutrinos are collected (the interaction of the neutrinos takes place in the soil). The layer thickness is equal to the muon path which is in the first approximation proportional to E_ν. Taking the neutrino flux and interaction cross section into consideration, one finds that an instrument having an area of 100 m^2 registers 0.3 neutrinos in a month. In order to reduce the background caused by outside phenomena, neutrinos coming from the lower hemisphere, i.e. passing through the whole earth's thickness, are investigated. These events are selected by switching on two or three rows of scintillation counters in a delay coincidence circuit with a delay time equal to the time of flight of a muon. The registration of electronic neutrinos by this method is not effective because the path of electrons is much shorter than the path of muons and the thickness of the effective layer is small.

8. Extensive Atmospheric Showers
Synonyms: air showers, Auger showers

8.1. Occurrence of extensive showers and problems of their investigation

It is apparantly impossible to study the interactions of particles with energies higher than 10^{15} GeV by means of photo-emulsions because of the very low intensity of these particles. For example, the total intensity of particles having energy $E \geqslant 10^6$ at the atmospheric boundary is equal to $J \cong 3 \times 10^{-6}$ m^{-2} sec^{-1} $ster^{-1}$. Emulsion rouleaus usually have an area of 0.01 m^2 and a solid angle in the order of π. By means of this method, only one particle having an energy greater than 10^6 GeV could be registered in a satellite during a time equal to 120 days of continuous measurement. Only a single particle with an energy $\gtrsim 10^7$ GeV could fall once on our rouleau during 19 years of measurement. The situation is however simplified by the fact that the interaction of such particles with nuclei leads to the transfer of a considerable part of the energy to the soft component. At an energy $\gtrsim 10^7$ GeV, an electron-photon cascade is developed. The area containing half of the cascade's particle (at sea level) will have a radius equal to 70 m. Its dimension, i.e. the distance along which the number of particles exceed unity many times over, is equal to hundreds of meters. The trajectory of a primary particle could pass at a distance of 100 m from the detector and the particle would nevertheless be

registered if our instrument were able to register electrons. Accordingly, the effective area of the instrument will be in an order of magnitude equal to

$$S = \pi R^2 \approx \pi \cdot 100^2 \approx 3 \cdot 10^4 m^2.$$

Consequently, particles with energies $\gtrsim 10^7$ GeV could be registered with a frequency of 2.2×10^{-2} sec^{-1}, i.e. 15 particles could be registered in a period of one hour. The study of showers may thus give the possibility of investigating particles with energies $\gtrsim 10^{15}$ eV. In doin this, three basic problems appear, namely 1) study of the properties of the most extensive showers, 2) study of the particle interactions at energies hiehr than 10^{15} eV, and 3) astrophysical problems.

The study of properties of the showers themselves must lie on the basis of all the other problems. The properties of showers since the time of their discovery have been studied by means of instruments of progressively increasing complexity.

The elementary processes that produce showers are still not sufficiently well studied. They are only investigated by indirect methods in which the behaviour of the different components of the extensive atmospheric showers are studied. Apparantly, one could estimate a number of important interaction parameters at super-high energies, such as the inelastic collision cross sections or the inelasticity coefficients. For instance, it can already be considered as established the fact that the nucleon-nucleus interaction cross section does not decrease with increasing energy up to 10^6 eV. The possibility of a more detailed study of the interaction processes at $E_0 > 10^{16}$ GeV in terms of the properties of the secondary shower components is not yet settled.

The conventional approach is to start by some interaction model and calculate the properties of the secondary cómponent on the basis of this model. This approach enables us to reject a number of possible models. However, this approach did not yet lead to many positive results. This creates some kind of pessimism on the possibility of using the properties of extensive atmospheric showers for understanding the nuclear aspects of cosmic rays. Several scientists do not generally accept the validity of the use of such information on extensive atmospheric showers. Japanese physicists. Fujimoto and Hayakawa claim that the study of nuclear interaction through atmospheric showers is as useless as "scratching one's boots". One should not however accept this immoderate point of views. Because of the tremendous variety of particle energies producing showers, even rough data would have considerable value.

One can hardly overestimate the importance of studying extensive atmospheric showers in astrophysics. The composition and shape of energy spectra of cosmic particles up to the highest energies is of great value for solving the problem on the origin of cosmic rays. It could be established by the study of extensive showers that primary radiation involves particles with

energies higher than 10^{11} GeV. One of the important remaining problems is to find the upper limit of the energy spectrum of cosmic radiation.

Although the properties of elementary processes that produce extensive atmospheric showers are still not finally established, many of the characteristics of the showers could nevertheless be qualitatively and sometimes quantitatively explained if one assumes that the act of interaction at ultra-high energies proceeds in the same manner as in the 10^3 GeV energy range. In other words, extensive atmospheric showers occur as a result of a nuclear-cascade process produced by primary gigantic electronic nuclear showers. In this shower, all the three components, available at medium energies in the atmosphere flourished, namely 1) the electron-photon component, 2) the nucleon and π-meson component, and 3) the muon component.

Nucleons and π-mesons constitute the nuclear-active component, whereas muons form the nuclear-passive penetrating component, which almost without alteration penetrates through the atmosphere and can be registered at large depths underground. Electrons and photons have the property of rapid multiplication and therefore constitute the main part of the shower. In the central part of the shower, 95 - 98% of the particles are all electrons. Far from the centre of the shower, the share of muons increases and that of the electrons decreases but even their electrons constitute the major part of all the particles. Accordingly, the simplest and most popular method for observing extensive atmospheric showers is to register their electron-photon component.

8.2. Historical information

Showers in the atmosphere were observed for the first time in 1927 - 1929 by D.V. Skobel'cyn (see chapter 1). Schmeiser and Bothe [21] in 1937 also observed showers in the atmosphere while studying the electron-photon component. Studying Rossi's curve, i.e. the number of coincidences of three counters, they noted that when there was no lead over the counters, showers were still observed.

In 1938, Auger studied the dependence of the number of coincidences on the distance between the counters. He observed showers extending upto a distance of 300 m. He could not separate the counters even further because the number of true coincidences approached the number of occasional ones. At the same time, showers with widths up to 75 m were observed by Kolhörster. This was the extent of the discovery of atmospheric showers. They were known for a long time as Auger showers.

In order to make a step further in the investigation of extensive showers, D.V. Skobel'cyn suggested to complicate the system for selecting the showers. Two groups of counters, switched on in coincidence, were separated by a significant distance. Each group consisted of two subgroups also switched on in coincidence. In this manner, a fourfold coincidence circuit was used. This reduced the number of occasional coincidences and made it possible to measure the extension curve up to a distance of 1 km. On the Pamir, showers of a diameter approximately equal to 1 km were registered 8 times per day. In

such large showers, the number of particles could reach hundreds of millions and even billions.

8. The dimension of a shower

The behaviour of electrons and photons in matter is well described by the electromagnetic cascade theory (see chapter 8, section 6). This theory predicts the occurrence of a maximum number of cascade particles at a given depth. In the cascade theory, parameter S which has the meaning of the exponent of the particles' integral spectrum in the shower, is introduced. At the maximum of the shower $S = 1$, before the maximum $S < 1$ and after the maximum $S > 1$. Consequently, parameter S also characterises the "age" of the shower. In this sense, one may speak of "old" ($S > 1$) and young ($S < 1$) showers. Figure 92 shows the dependence of the total number of electrons on the thickness of air and on parameter S, as calculated by Snyder. These calculations were made by using a conventional method of the cascade theory, which was called approximation B and accounted for the ionization loss. The calculation of the spatial distribution of particles in the shower shows that parameter S also defines the spatial distribution function of particles in the shower, i.e. the particle density in a horizontal plane as a function of the distance from the center of the shower. The problem of the longitudinal and transversal development of a shower could be separately studied since the longitudinal dimension of a shower is ~10 km while the transversal is 100 m. The main mechanism for the transversal development of the electron component of a shower is the Coulomb scattering of the particles. At large distances, the contribution of multiple scattering is important. The dimension of the electronic part of the shower is almost independent of the nuclear processes. The mean square angle of a multiple Coulomb scattering of a particle of energy E is given by equation (2.34) :

$$\sqrt{\langle\theta^2\rangle} \sim E_s\sqrt{t/E},$$

where $E_s \approx 20$ MeV.

If we consider all particles with $E > 0$ in a shower, we then have to take the ionization losses into consideration. In this case the mean square radius of shower with $S = 1$ is according to a calculation by S.Z. Belenkij equal to

$$\sqrt{\langle R^2\rangle} \simeq 0{,}9E_s t_0/\varepsilon, \tag{9.22}$$

where t_0 is the length of the t-unit.

In the theory of extensive atmospheric showers, it is conventional to express distances and angles in the so-called Molière units :

$$r_1 = \frac{E_s}{\varepsilon} t_0; \quad \theta_1 = \frac{E_s}{\varepsilon}.$$

In air $r_1 = 9.5$ g/cm^2 and $\theta_1 \sim 1/4$ radians.

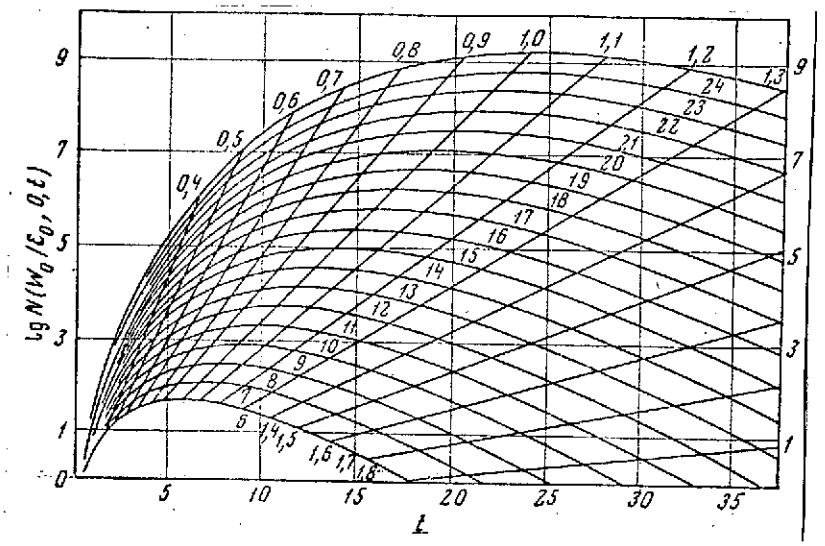

Figure 92. The dependence of the total number of electrons on the thickness of air for different energies. The straight lines corresponds to different values of parameter S.

Equation (9.22) shows that the "shower dimension", measured in Molière units, is almost constant in different materials although the Molière unit itself changes with height. Since the t-unit increases when pressure decreases, the "dimension" of a separate shower will decrease (at S = 1) with increasing depth in the atmosphere.

It might seem that the shower dimension, at S = 1, does not depend on the initial energy. In fact, only the mean dimension, i.e. the radius of the region that includes almost half of the particles, does not depend on the initial energy. If the shower dimension is taken as the distance at which the particle density exceeds a given value ρ_o, then such a dimension will increase with the increase of the initial energy. Particles of an extensive atmospheric shower move with a velocity very close to the velocity of light. This leads to the fact that in each moment, the extensive atmospheric shower has a small extension in the longitudinal direction.

Rossi suggested a simple picture for extensive atmospheric showers. He regarded the shower as a plane disc consisting of particles passing through the atmosphere with a velocity close to the velocity of light (figure 93). American scientist Clark proved this picture by measuring the time of flight of shower particles through a detector. He found that all the particles passed through a plane scintillation counter during a time measured in nanoseconds. Consequently, the instantaneous longitudinal shower dimension Δ was

very small and equal by order of magnitude to

$$\Delta \sim c\Delta t \approx 3 \cdot 10^8 \ m/sec \ 10^{-9} \ sec = 0{,}3 m$$

It is well known that the transversal dimensions of the shower are much larger.

If the showers fall with an angle relative to the vertical, then particle detectors located in a horizontal plane will work with a relative delay from one another, depending on the angle of incidence. By measuring the delay time, one obtains the angle of incidence of the shower.

8.4. Spatial distribution of the particles

In order to solve the problem of the spatial distribution of particles in a shower, it is necessary to start with the kinetic equations of the cascade theory and introduce the characteristics of electron scattering (the taking into account of ionization losses is indispensible). In Molière units, the

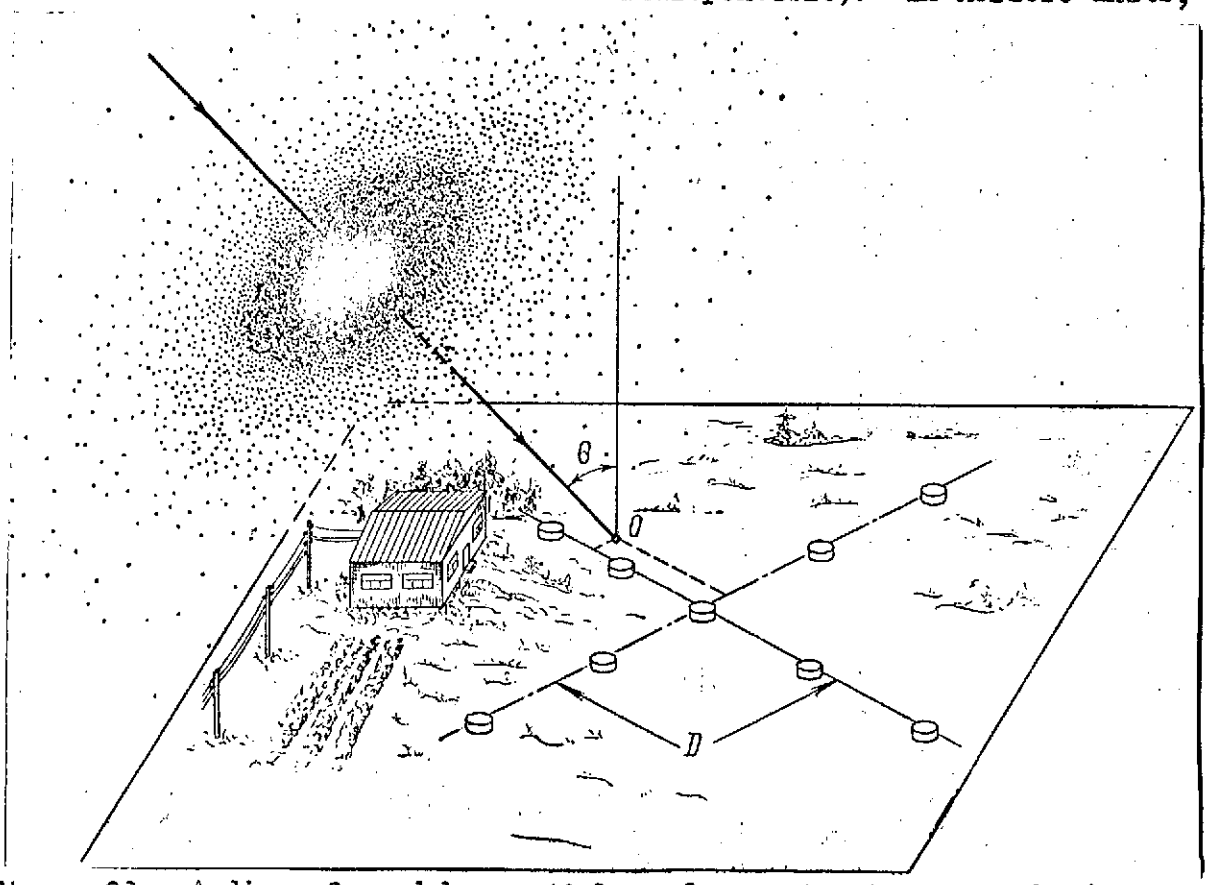

Figure 93. A disc, formed by particles of an extensive atmospheric shower approaching detectors D with an angle θ relative to the vertical.

mean square radius of the extensive atmospheric shower changes slightly with changing heights and is very close to unity.

Let us denote the density of shower particles at distance r from the shower axis by $\rho(r/r_1)$. This function is conveniently normalized in such a way that it will not depend on the total number of particles in the shower. For this purpose, we represent $\rho(r/r_1)$ in the form of

$$\rho(r/r_1) = Af(r/r_1) = Af(x), \quad x = r/r_1,$$

Here f(x) is the normalized spatial distribution function. Constant A could be determined in the following manner. Let us consider the following integral

$$\int_0^\infty \rho(r/r_1)\, 2\pi r dr = N,$$

where N is the total number of particles in the shower at the observation level. Then

$$N = Ar_1^2 \int 2\pi f(x)\, x dx.$$

Requiring that

$$\int 2\pi f(x)\, x dx = 1,$$

we obtain

$$A = N/r_1^2 \text{ и } \rho(r/r_1) = \frac{N}{r_1^2} f(x).$$

In a theoretical investigation of the spatial development of a shower, one usually assumes that the shower has a symmetry centre at each level. The line that connects the symmetry centres at different levels, i.e. the symmetry axis, is then called the shower axis. It is quite true that the symmetry axis lies in the direction of motion of the primary particle that initiated the shower. All spatial characteristics of a shower are studied as functions of the distance from its axis.

At a small distance from the shower axis, the divergence of the shower particles is mainly defined by multiple scattering. At a large distance, it is recommended to consider single and double scattering. Kinetic equations which take scattering into consideration have been constructed by Landau (see equations (2.58)).

The problem of spatial distribution of shower particles was solved for the first time by Molière. The solution was valid for only high-energy particles.

In 1950, Japanese physicists Nishimura and Kamata published an analytical solution of Landau's equation for the total number of particles in the shower in approximation B, for widths corresponding to S = 0.6, 1.0, 1.4, 2.0 [22]. For practical applications, however, it is more useful to have a simple approximation than these complicated analytical expressions. Such an approximation was suggested Greisen [18] and had the form of

$$f(x) = C(s)\, x^{s-2} (x+1)^{s-4,5} \tag{9.23}$$

or

$$\rho\left(\frac{r}{r_1}\right) = \frac{N}{r_1^2} C(s)\, x^{s-2} (x+1)^{s-4,5} \tag{9.24}$$

where normalization function C(s) varies from 0.16 at S = 0.5 to 0.4 at S = 1.5.

Near the shower axis, where $x \ll 1$, $\rho \sim x^{s-2}$ for $S < 2$ and $\rho \approx$ const. for S 2 [1]. A similar expression was obtained in 1944 by I. Ja. Pomerancuk by means of an approximate method.

Expression (9.24) is not valid at distances much greater than r_1 because of the influence of double and single scattering, Figure 94 shows the results obtained by Kamata and Nishimura and the approximation suggested by Greisen. It is necessary to note that Nishimura and Kamata in calculating function f(x), defined parameter S in a manner slightly different from what was given in chapter 2, namely by

$$\lambda_1'(s)\, t + \ln \frac{E_0}{\varepsilon} + \ln x = 0. \tag{9.25}$$

In this case, parameter S depends not only on t and E_0, but also on r_1. Moreover, S increases when r decreases. This reflects the simple fact that for high-energy particles (slightly scattered and moving nearer to the shower axis), the particle number reaches its maximum earlier (see equation (2.50)). Since photons are not scattered by Coulomb forces, they will be more strongly concentrated at the shower axis than electrons. At $r \ll 1$, the spatial distribution of photons will be given by

$$\begin{aligned} \rho_\gamma(r) &\simeq r^{s-2} \ln(1/r), \quad s < 2; \\ \rho_\gamma(r) &\simeq \text{const}, \quad s > 2. \end{aligned} \tag{9.26}$$

Since, according to equation (9.25), parameter S increases when r decreases, then sooner or later there will be a moment, when s becomes close to 2 and the densities of the electrons and photons will be constant. Thid distance

1) More exact calculations yield a dependence of $x^{s-2.15}$ rathern than x^{s-2}.

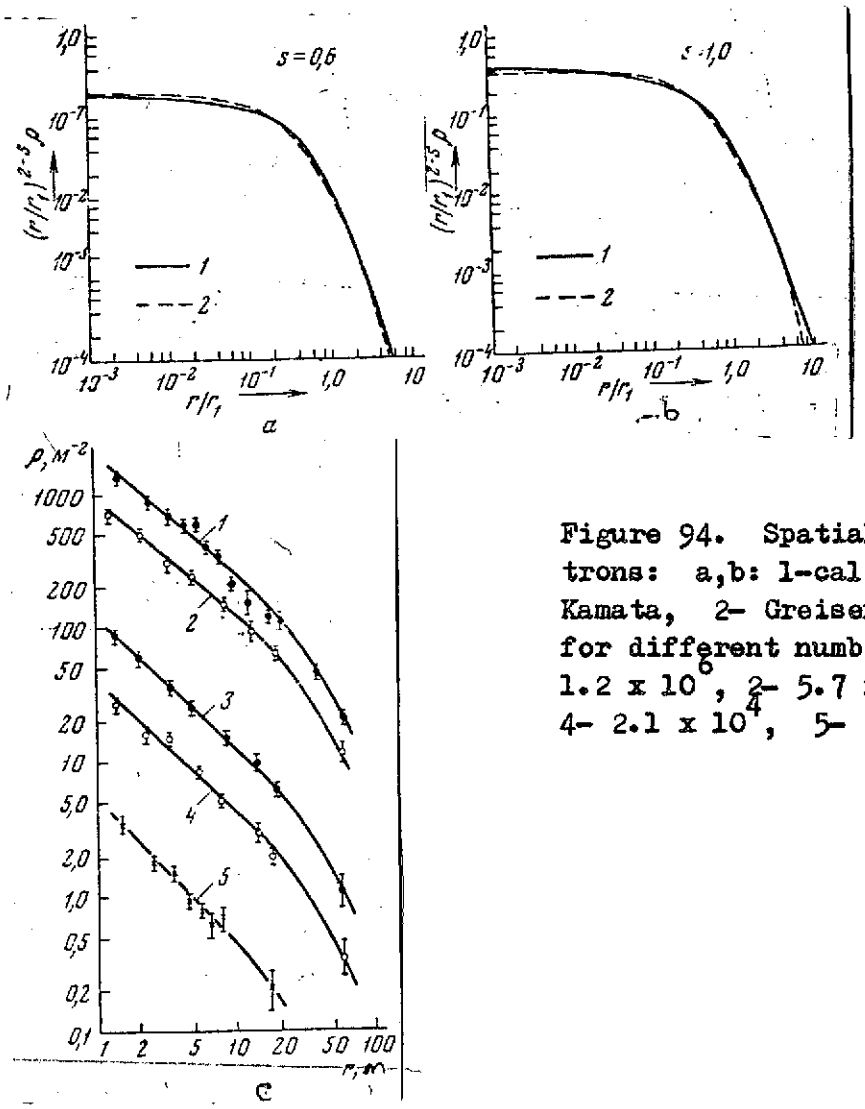

Figure 94. Spatial distribution of electrons: a,b: 1-calculated by Nishimura and Kamata, 2- Greisen's approximation; c: Data for different numbers of particles ; 1- N = 1.2×10^6, 2- 5.7×10^6 3- 6.3×10^4, 4- 2.1×10^4, 5- 2.5×10^3.

defines the electronic body of the shower[1].

8.5. The experiments

In order to experimentally investigate the spatial distribution of the electron number density, it is necessary to use instruments capable of determining the position of the shower axis and the particle number density at various distances from the axis. For this reason, the experimental devices must involve a system of particle-number detectors switched on in coincidence.

An example of the devices used for studying the spatial distribution of particles is the instrument shown in figure 95. It consists of a large number of hodoscopic counter groups. In other cases, scintillation counters of a diameter reaching 1 m are used for this purpose.

The dimensions of the detector are usually small as compared to the

1) Near the shower axis, an important role is played by the nuclear scattering of the particles, which leads to an increase in the dimensions of the shower body.

dimensions of the showers. In this case particle density $\rho(x)$ could be regarded as a constant within the limits of the area occupied by the detector.

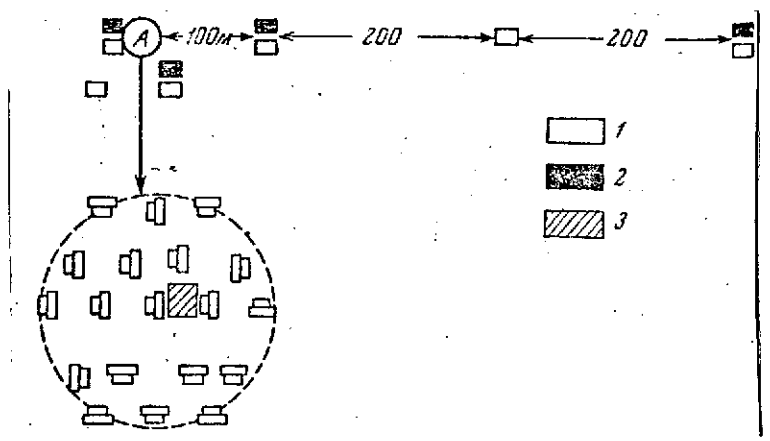

Figure 95. An instrument for studying extensive atmospheric showers: 1- detectors for studying the electrons, 2- detectors for the penetrating particles, 3- detectors for the nuclear-active particles (impulsive instruments or ionization calorimeters).

When scintillators are used, density $\rho(x)$ is determined directly. In measurements by means of hodoscopic counters, it is necessary to consider the possibility that several particles simultaneously enter one of the counters. If the detector involves n counters of which m counters function at the moment of the passing of the shower, the particle density can then be calculated by means of the following formula

$$\rho(x) = \frac{1}{\sigma_0} \ln \frac{n}{n-m}, \tag{9.27}$$

where σ is the area of a single counter.

8.6. Selection of showers

The total number of particles falling on a detector is equal to $\rho\sigma$, where σ is the area of the detector. If the particles fall independently, then the probability that neither of these particles fall on the detector will be equal to $\exp(-\rho\sigma)$. The probability that at least one particle will fall on the area of the nth detector will be equal to $1-\exp(-\rho\sigma)$. If the system registering the shower consists of n detectors in such a manner that it is required that they all function simultaneously, the corresponding

probability of the particles falling on all n detectors is then given

$$P_n = (1 - e^{-\rho\sigma})^n. \tag{9.28}$$

The total number of showers, registered by the instrument will be

$$C_n(\sigma) = \int_0^\infty F(\rho)(1 - e^{-\rho\sigma})^n d\rho, \tag{9.29}$$

Where $F(\rho)$ is the density distribution of the showers. If $\rho\sigma$ is small, then $\exp(-\rho\sigma)$ will be close to unity and the integrand will be close to zero. For large values of $\rho\sigma$, the quantity $1-\exp(-\rho\sigma)$ will be close to unity and in this case, the number of coincidences will be defined by the density spectrum of the showers, $F(\rho)$.

Accordingly, the instrument will select these or those showers depending on the area of the detectors, σ, and the number of coincidences. As the area increases, a smaller number of shower particles will be registered. In this manner, the instrument selects a narrow interval of shower densities, depending on the area of the detectors, on the number of coincidences in the case of small showers, and on the number of showers with a given density, $F(\rho)$, in the case of large showers. Distribution $F(\rho)$ falls with ρ as

$$F(\rho) \sim \frac{1}{\rho^{1.5 \div 2.0}}. \tag{9.30}$$

The leading detector groups could also be switched on in pairs in the coincidence circuit. If two groups are put a large distance apart from each other, the circuit wil select very powerful showers because of the sharp decrease of $\rho(r/r_1)$ with distance. Geiger and Cerenkov counters as well as scintillators may be used as counters that lead the field of instruments used for the registration of showers.

For example, in the quite unique instrument found at Moscow State University, a sixfold coincidence of six counter groups each of an area of 0.132 m^2, is used for the leading, together with a fourfold coincidence of two counter groups (each group consists of two counters), separated by a distance of 300 m.

An alternative type of detector is used in Massachusets University by a group headed by Rossi. There, plastic scintillation disks are used in scintillators 1 m in diameter. The luminescence of the scintillators, whose intensity is proportional to the number of particles, are registered by means of photomultipliers. One of the American groups, working on Volcano Ranch Mountain has 19 scintillation counters, each of an area of 3.3 m^2. In many instruments, there are devices for determining the delay time of particle arrival in different counters. This makes it possible to calculate the angle of incidence of the shower. Such a device exists for instance, in the extensive shower laboratory of Moscow State University.

One of the basic elements is the electror detector. Electron detectors consist of different numbers of counters and have various areas. The position of the detectors is chosen in such a manner that the position of the shower axis, i.e. the symmetry centre of the shower, could be determined. To find the shower axis is a difficult task because the number of particles in the detectors fluctuates strongly. The axis is usually determined by means of calculations carried out on electronic computers.

8.7. Particle number density

Once the position of the shower axis is determined, function ρ (r) can easily be obtained. The results of the experiments are given in figure 94. The comparison between these experimental data and the calculations made by Nishimura and Kamata shows that, whatever the total number of particles in the shower, the spatial distribution ρ (r) coincides with the results of these calculations, if one puts S = 1.3 - 1.2. Such a value of parameter S is obtained at sea level and also on mountains. The spatial distribution fluctuates strongly from one case to another. Sometimes, showers with more than one maximum of electron intensity are observed. The fluctuations are particularly large at $r \lesssim 3$ m.

The above facts reaffirm the complicated behaviour of extensive atmospheric showers, in which secondary interactions of high-energy particles and secondary showers occur. The constancy of the mean values of quantity S at different altitudes (S = 1.3 - 1.2) also suggests that a continuous renewal of the particles is taking place in the shower.

The spatial distribution of shower particles at small distances from the axis is studied by means of Wilson chambers or neon hodoscopic systems. In the latter case, the detectors are small boxes ($\sim$ cm) filled with neon, placed in a strong impulsive electric field (tens of kilovolt pulses). When a charged particle falls on one of them, the box lights up.

Approximating the mean distribution by a power function, ρ (r) $\sim r^n$, one finds that $n \sim 0.6$ as $0.05 < r \leqslant 0.3$ m. Comparing this with the function given by equation (9.24), one obtains $S \approx 1.4$.

8.8. Shower density spectrum and spectrum of showers with respect to the number of particles

The spectrum of extensive-atmospheric-shower densities is defined as the frequency of shower occurrence, for which the particle density in a given place lies in the interval between ρ and $\rho + d\rho$. Experimentally, this quantity is determined independently of the dimensions of the shower and of the distance from its axis. Experiment shows that [1)]

$$F(>\rho) = F_0 \rho^{-\varkappa}. \tag{9.31}$$

1) F($>\rho$) is the integral density spectrum $F(>\rho) = \int_\rho^\infty F(\rho)\,d\rho$

It is expected that $\varkappa$ depends weakly on ρ.

The shower spectrum with respect to the particle number is defined as the number of showers having a total number of particles in the interval between N and N + dN, and whose axes cross a unit element of area in a unit time : k(N)dN. The spectrum with respect to the particle number is, in the first approximation, simply related to the density spectrum. Let us assume that the integral spectrum of showers with respect to the particle number is described by a power function :

$$K(>N) = \int_0^\infty k(N)\,dN = K_0 N^{-\varkappa_1}, \tag{9.32}$$

where $\varkappa_1$ is a constant. As shown previously, $\rho = Nf(x)/r_1^2$, or $N = r_1^2\rho/f(x)$. The frequency of showers having density ρ and particle number N is then given by

$$F(\rho) = F_0\rho^{-\varkappa} = \int_0^\infty 2\pi r dr k\left(\frac{r_1^2\rho}{f(x)}\right) = \tag{9.33}$$

or

$$= 2\pi r_1^{-2(\varkappa_1-1)}\rho^{-\varkappa_1}K_0\int_0^\infty [f(x)]^{\varkappa_1}x dx$$

$$F(\rho) \sim \rho^{-\varkappa_1}. \tag{9.34}$$

Consequently, if $\varkappa$ = constant, then $\varkappa_1 = \varkappa$ and the shower density spectrum coincides with the spectrum with respect to the particle number.

8.9. Total number of particles in the shower

The knowledge of the spatial distribution function makes it possible to calculate the total number of particles in the shower

$$N = \int_0^\infty \rho(r)\,2\pi r dr. \tag{9.35}$$

After determining the total number of particles in each shower, one can determine the spectrum of showers with respect to the particle number, K = K(N). The differential spectrum of showers with respect to the particle number, K(N) was studied by several authors by means of various methods.

Experiments carried out in Moscow University under the supervision of S. N. Vernov and G.B. Hristiansen [23] showed that it was not possible to represent the spectrum in terms of a power function with a single exponent at sea level. It was found that $\varkappa_1 \simeq 1.5$ when the number of particles in the shower was less than 10^6 and $\varkappa_1 = 2.0$ when $N > 10^6$ (figure 96). According to some data, the spectrum again became more gentle at large particle number values ($N \geqslant 10^9$).

The analytical approximate form of the shower spectrum with respect to

the particle number was given in [24] and had the form of (at sea level)

$$\left.\begin{aligned} 10^{10}K(>N) &= (2{,}0 \pm 0{,}1)\left(\frac{N}{10^5}\right)^{-1{,}5\pm0{,}08} \ cm^{-2}\,sec^{-1}\,ster^{-1}; \\ &\qquad (10^4 < N < 10^6); \\ 10^{12}K(>N) &= (5{,}0 \pm 0{,}25)\left(\frac{N}{10^6}\right)^{-2{,}0\pm0{,}07} \ cm^{-2}\,sec^{-1}\,ster^{-1}; \\ &\qquad (10^6 < N < 10^7). \end{aligned}\right| \qquad (9.36)$$

Experiments undertaken in the USA by Clark [25] showed that there was a break in the spectrum measured on mountains. Experiments made in Japan by Fukuju et al [26] confirmed the same property for the spectrum at sea level.

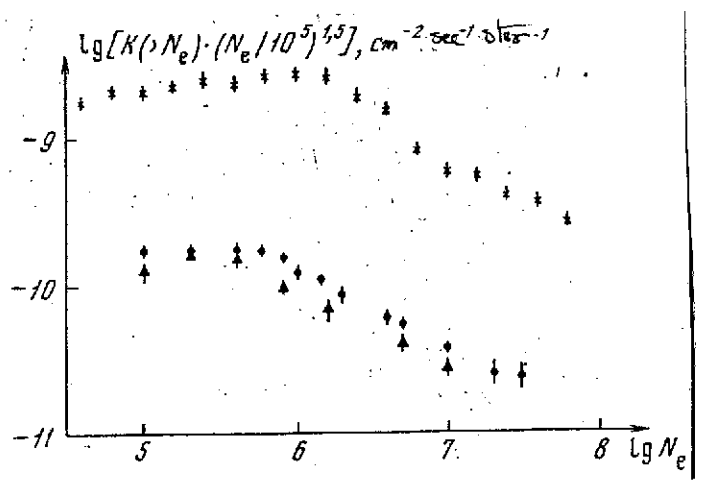

Figure 96. The spectrum of showers with respect to particle number. Thr ordinate axis represents the particle number, multiplied by $N_e^{1.5}$ (for illustrating the change of the spectrum's at $N \gtrsim 10^6$). The higher points are those obtained on mountains [25] and the lower ones at sea level [26].

8.10. Variation of the number of showers with depth

The dependence of the number of showers having a given number of particles on depth (figure 97), i.e. the absorption law of these showers, is well represented by an exponential function in the lower part of the atmosphere. This law could be obtained by measurements carried out at a given level in showers coming at different angles Θ were registered. Assuming that the number of showers coming in the vertical direction is equal to k_o at a depth of x_o, then for $x = x_o/\cos\Theta$, we have $k(N, x) = k_0 e^{-(x-x_0)/\Lambda}$,

where Λ is the absorption path of showers having the given number of particles. Experiment shows that quantity Λ remains almost constant and equal to 140 g/cm^2, in a wide range of particle numbers.

The absorption of showers is closely related with the change of the particle number in a separate shower. Indeed, if $k(>N) \sim N^{-x}$ and N varies according to the relation $N \sim e^{-x/\lambda}$, then

$$\ln N = -x/\lambda_0; \quad -\frac{\partial \ln N}{\partial x} = \frac{1}{\lambda_0}.$$

On the other hand, the variation of the number of showers having a given particle number N with the variation of depth (for constant x) is given by

$$-\frac{\partial \ln K(>N)}{\partial x} = \varkappa \frac{\partial \ln N}{\partial x} = \frac{\varkappa}{\lambda_0}; \qquad -\frac{\partial \ln K(>N)}{\partial x} = \frac{1}{\Lambda}. \tag{9.37}$$

Consequently,

$$\lambda_0 = -\Lambda\varkappa. \tag{9.38}$$

Since exponent $\varkappa = -1.5$ for $N < 10^6$, then $\lambda_0 = 200$ g/cm^2.

Obtaining such a large value for λ_0, independent of the number of particles in the shower in a wide range for N, leads us to conclude that the properties of wide atmospheric showers are different from those of electromagnetic cascades. In the latter case, the absorption path of particles in the shower must depend on N and be much less than 200 g/cm^2 for $S \geqslant 1,2$.

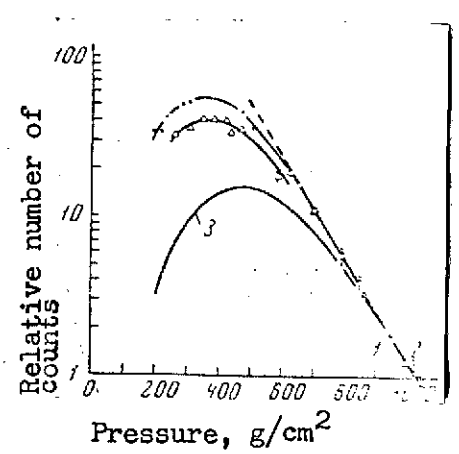

Figure 97. Dependence of the relative number of extensive atmospheric showers on altitude according to measurements by different authors: 1,2- normalization points, 3- vertical intensity of showers obtained by means of Gross scaling.

8.11. Energy flux of electrons

The particle-number distribution in showers is not sufficient for drawing a complete picture for the electron-photon component, even at the observation level. Additional information could be obtained by studying the energy flux density of the electron-photon component at different distances from the shower axis, $\rho_E(r)$.

In order to measure the energy flux of the electron-photon component, it is necessary to place special detectors at different points of the instrument in such a manner that they would function in coincidence with the particle-number detectors, selecting the extensive atmospheric shower. As a detector of shower-electron and photon energies, impulsive ionization chambers covered with layers of lead of a thickness t = 1, 2, 4, 6 cm are used. Combining together data concerning different showers, one can determine the energy of the electron-photon components at various distances from the shower axis. This energy is well-known to be equal to (see equation 2.54)

$$E(r) = \varepsilon \int_0^\infty N(t, r)\, dt. \tag{9.39}$$

Knowing N below various lead thicknesses, one can obtain E(r) and energy flux density $\rho_E(r) = E(r)\,\sigma$, where σ is the area of the detector.

The cascade theory enables one to make definite predictions on the value of the energy flux at various distances from the axis. According to equation (2.55), electrons with energy E have an effective distance from the shower axis equal to $r \sim E_s/E$.
Accordingly,

$$E \sim E_s/r.$$

The energy flux density is then

$$\rho_E(r) \sim E\rho(r) \sim \rho(r)\, E_s/r. \tag{9.40}$$

In other words, the energy flux density must decrease with distance r times faster than the particle number density. Consequently, at small distances from the axis

$$\rho_E(r) \sim r^{s-3} \sim r^{-1,6} \tag{9.41}$$

At large distances, the dependence must be sharper. If we approximate the experimental data by a power function, $\rho_E \sim r^{-n}$, we will find that $n = 1.2 \pm 0.2$ for $0.1 \leqslant r \leqslant 1$ and will increase up to $n = 2.6$ for $r > 100$ m. This affirms the stronger dependence of the energy flux on r as compared with

the particle flux. Such a mean energy flux distribution, as shown experimentally, is apparently independent of the number of particles in the shower. In each separate case however, this distribution is subject to strong fluctuations. At distances $r < 1.5$ m, these fluctuations are particularly sharp and n may fluctuate within the limits of 1.0 to 2.5. Knowing the energy flux distribution and the particle number distribution, one can now calculate the mean energy of electrons in the shower at various distances from the axis

$$\langle E(r)\rangle = \frac{\rho_E(r)}{\rho(r)}.$$

Measurements show that the highest-energy electrons pass near the axis, where the mean energy of the electrons reaches 5×10^9 eV. At $r > 60$ m, the mean energy falls to a value $\sim 10^8$ eV.

8.12. The total energy of the electrons

Once the spatial distribution of the energy flux is known, the total energy $E_{e.p}$ of the electron-photon component at a given level can be calculated.

$$E_{e.p} = \int_0^\infty \rho_E(r)\, 2\pi r dr.$$

The corresponding calculation shows that

$$E_{e.p} \approx K\varepsilon N, \tag{9.42}$$

where ε is the critical energy in air. Because of uncertainties in the spatial distribution functions as well as errors in measuring the energy of the electrons, coefficient K has a value in the range $2.5 \div 3$.

8.13. The electron-shower "make-up"

We have already seen that electrons in a shower are absorbed more slowly than what the cascade theory predicts. This means that the electron-photon cascade consumes for its own maintenance, energy taken from some other source. It is often said that there exists a shower energy "make-up". The source of such a make-up could be nuclear-active particles which penetrate through the depth of the atmosphere. They can transfer their energy to the electron-photon component through π-mesons while interacting with nuclei. Unfortunately, we are now unable to determine exactly the value of this make-up. One can easily see however, that its existance leads to an increase in the absorption path of the electrons. In fact, the increment of the electron-photon component energy is equal to

$$dE_{e.p} = -\varepsilon N dt + \alpha E_{n.a} dt/\lambda, \tag{9.43}$$

where α is the energy fraction, transferred to photons during the interaction of the nuclear-active particles $E_{n.a}$ the energy of the nuclear-active particles and λ their interaction path.

Introducing the mean energy $\bar{E} = E_{e.p}/N$, we obtain

$$\frac{dN}{N} = -\frac{\varepsilon}{\bar{E}} dt + \frac{\alpha}{\lambda} \cdot \frac{E_{n.a}}{E_{e.p}} dt. \tag{9.44}$$

The absorption coefficient of the electrons, $\mu_e = 1/\lambda_e$, is then equal to

$$\frac{d \ln N}{dt} = -\mu_e = -\mu_{0e} + \frac{\alpha}{\lambda} \cdot \frac{E_{n.a}}{E_{e.p}}, \tag{9.45}$$

where μ_{0e} is the absorption coefficient in the absence of the make-up. Putting $E_{n.a} \sim E_{e.p}$, $\alpha = 0.2$ and $\lambda = 80$ g/cm^2, we obtain $\lambda_e = 210$ g/cm^2 (compare with subsection 8.8).

Accordingly, in order to obtain the value of the make-up, it is necessary to know the values of α, $E_{n.a}$ and $E_{e.p}$. From the formula obtained for λ_e, it follows that the particle absorption decreases with increasing $E_{n.a}$.

8.14. The nuclear-active component

We shall now consider the methods for investigating the nuclear-active component in showers. Studying nuclear-active particles could be done by means of impulsive instruments or ionization chambers.

The impulsive instrument does not allow the reliable determination of the energy of the nuclear-active particles. Actually, the coefficient describing the transition from the "pulse energy" to the nuclear-active-particle energy depends on the nature of the particles and is defined by the inelasticity-coefficient distribution (see the description of the work on impulsive instruments in chapter 9). Accordingly, the energy of the nuclear-active particles could be determined up to within a factor of 2 - 3. The energy flux density of the nuclear-active particles could be also defined to the same accuracy. Once the number of nuclear-active particles with different energies at different distances from the shower axis is defined, within the above-mentioned limitations, one can easily obtain the spatial distribution of the energy flux density of the nuclear-active particles :

$$\rho_E(r) = \frac{\Sigma E_i(r)}{N_s(r)\sigma},$$

Here, $E_i(r)$ is the energy of particles, registered in the showers (the shower axis passes at a distance r from the detector) while $N_s(r)$ is the total number of showers with axes at a distance r, and σ is the detector's area. This distribution is found to be independent of the particle number in the shower and is given by

$$(\rho_E)_{n.a} \sim 1/r^n; \; n = \begin{cases} 1{,}5 \pm 0{,}2. & 0{,}22 < r < 1{,}5 \text{ m} \\ 2{,}0 \pm 0{,}2. & 1{,}5 < r < 30 \text{ m.} \end{cases} \qquad (9.46)$$

High-energy nuclear-active particles having an energy $E > 10^{12}$ eV are concentrated about the shower axis at distances $\leqslant 1 - 2$ m. The total energy of the nuclear-active component in showers is obtained from the spatial distribution of the energy fluxes of the nuclear-active component by means of the following formula

$$E_{n.a} = \int_0^\infty (\rho_E)_{n.a}(r)\, 2\pi r dr.$$

The spatial distribution function, $\rho_{n.a}(r)$, is defined to within small distances. The contribution of large distances is not clear. It depends on the sharpness of the decay of distribution $(\rho_E^{(r)})_{n.a.}$ The calculation of this energy shows that, at distances $r \leqslant 2$m, the total energy of the nuclear-active particles is in an order-of-magnitude close to the energy of the electron-photon component.

From the above discussion, it is clear that nuclear processes play an important role in the evolution of showers.

8.15. Properties of showers at different heights

The comparison between showers at different heights could be of a great importance for the furhter study of extensive atmospheric showers. The comparison of spatial distribution of particles in showers shows that small showers with a particle number $N \leqslant 10^6$ have the same values for parameter S at sea level and on mountains.

We have seen earlier that the absorption path of the particle number is very large and cannot be explained within the context of the electron-photon cascade theory. These facts could however be explained by assuming that the shower was constantly being renewed, taking energy from the high-energy nuclear components passing through the body of the shower. This means that the electrons are in equilibrium with the high-energy nuclear-active particles and are gathered at the observation level from a relatively thin atmospheric layer. This was the picture of a shower as visualized by G.T. Zacepin [28].

It was shown in chapter 4 that during the interaction of a nucleon with nuclei nearly half its energy was transferred to pions, whereas a secondary nucleon carried a considerable part of the energy. This could induce considerable fluctuations in the evolution of the shower because of the scattering

of the points of the first and subsequent interactions of a nucleon. The second reason for the fluctuations is the extended distribution of inelasticity coefficients.

The presence of fluctuations leads to the fact that shower particles, registered at the observation level, can be produced relatively near the detector and hence have an equal age S on mountains and at sea level.

It is well known that the absorption of nuclear-active particles with an energy $\lesssim 10^{12}$ eV in the atmosphere proceeds by an exponential law with the exponential factor λ close to 120 g/cm^2 (see chapter 9, section 3). The absorption of showers proceeds more slowly ($\Lambda \simeq 140$ g/cm^2). This result could be explained by the decay of the particles of the nuclear component [28]. Actually, since the nuclear-active component involves mesons, the energy fraction transferred to photons will increase with the increase in atmospheric depth because the probability of pion decay will decrease with increasing atmospheric density. This leads to the slowing of the absorption of the number of showers with a given particle number N.

8.16. The muon component

Further information on extensive atmospheric showers could be obtained by studying the muon component. The energy of muons is determined by measuring their paths. For this purpose lead absorbers and soil layers are used. In the latter case, muon detectors are placed underground. The comparison between the spatial distributions of muons and electrons is conveniently made by introducing the ratio

$$R_\mu = N_\mu(r)/N_e(r).$$

Figure 98 illustrates the dependence of R_μ on the distance from the shower axis. Quantity R_μ is found to have the same value at sea level and on mountains. Experimentally, one does not usually measure the number of muons at a given distance from the shower axis, but the number of penetrating particles. Since nuclear-active particles are concentrated near the shower axis, all the penetrating particles found at large distances from the axis will then be muons.

Consequently, the spatial distribution of muons is more smoothly decaying than for electrons. Detectors placed underground make it possible to select muons having an energy $E_\mu > 10$ GeV. It is found that the spatial distribution of these muons has the form of $1/r^n$, where n 0.8 at distances up to 10 m and n = 1 up to 100 m. This means that muons are sufficiently well separated from the shower axis.

The slow decay of the muon number with the distance from the axis is explained by their occurrence at the greater heights where the probability of decay of π -mesons is relatively high. At an enrgy near 10 GeV, the flight

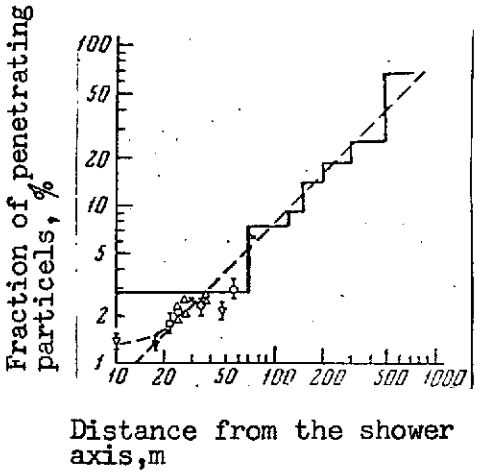

Figure 98. Dependence of the number of penetrating particles, divided by the number of electrons, on the distance from the shower axis (data obtained by various authors).

angle of pions is on the average equal to 0.02 radians. This corresponds to a separation of the muon from the shower axis $\sim$30 - 40 m at the observation level. The mean spatial distribution of muons is in the form of [29]

$$\rho_\mu(r) = N_\mu\, 1{,}6 \cdot 10^{-4} r^{-0.4} e^{-r/80}\, m^{-2}.$$

The number of muons in showers increases more slowly than the total number of particles: $N_\mu \sim N^{0.8}$. This is explained by the fact that a large number of electrons occur in the shower during the interaction of particles having on the average very high energies, so that their decay probability is reduced. In this case, the maximum of the cascade is displaced deeper in the atmosphere and hence the number of electrons at the observation level becomes relatively larger.

On high mountains, the energy of muons reaches half the energy of the nuclear component, whereas the former energy exceeds the latter at sea level. The muon spectrum in extensive atmospheric showers, measured up to an energy of 10^3 GeV, has the form of

$$N_\mu(>E) \simeq (a + E)^{-1/2},$$

where a is an approximately constant quantity. The number of muons is quite

closely related to the multiplicity of pions in the primary acts of the interaction.

Since the multiplicity of pions is closely related to the mass number of the primary nucleus, A, the number of muons in the shower must then be proportional to A, in the first approximation. Consequently, the study of the number of pions in separate showers enables us to obtain information on the composition of the primary component of the cosmic radiation in the high-energy region. Detailed investigations carried out in Moscow University in the Soviet Union and in the Physics Institute of the Academy of Sciences of the USSR, show that at very high energies primary radiation apparently involves nuclei and protons.

On the other hand, showers poor in muons could give information on the number of primary high-energy photons. In showers induced by photons, muons could only be produced at the expense of the low-probability photo-production processes. The number of meson-absent showers is small and, according to data obtained by different physicist groups interested in this subject: the flux of primary photons with energies higher than 10^6 GeV is a thousand times less than the flux of nuclei and protons.

9. Determination of the Energy of Particles, Generating Showers

A very important problem is to determine the energy of a primary particle by observing the number of particles at the observation level. If the showers were pure electron showers, then the problem would have been solved in a quite simple manner. Once the shower age S at a given level and the total number of electrons are known, the cascade theory could be used to construct the cascade curve and hence find E_0. We have seen however, that an important role in extensive atmospheric showers is played by the nuclear-active component and the fluctuations in cascade evolution. Consequently, the relation between the energy of the primary particle and the number of particles at the observation level is a statistical relation, due to the presence of fluctuations.

A more direct relation exists between the energy of the primary particle and the total path of electrons in the atmosphere. Electrons moving in the atmosphere generate a Cerenkov radiation. Registering the total flux of the Cerenkov radiation by means of photomultipliers directed to the sky and switched on in coincidence with an instrument for measuring the number of particles in the shower at the observation level, one can obtain relation between

$$E_0 = \varepsilon \int_0^\infty N_e(t)\,dt$$

and N [30] :

$$E_0 = 10^5 \left(\frac{N}{1{,}7 \cdot 10^5}\right)^{0{,}8 \pm 0{,}05} \text{ GeV} \qquad (9.47)$$

The outbreak of the Cerenkov radiation during the penetration of a shower through the atmosphere is very weak. They can only be observed on clear dark nights. The instrument applied by A.E. Cudakov and collaborators on the Pamirs [30] involved 10 photo-multipliers separated by distances up to 200 m. The intensity of light at sea level is found to be in 7 - 10 times greater than on mountains [31].

An interesting attempt for registering extensive atmospheric showers by means of image converters was made by a group of Australian physicists. These instruments make it possible to estimate not only the light intensity but also the position of the luminous regions in space, i.e. to determine the height at which the shower is started.

An alternative method for determining the energy of the primary particle is to sum the energies of the different secondary components. The relation between the energies and the particle number is given by

$$E_0 = \varepsilon \int_0^\infty N_e dt + E_{h.i} + E_\mu,$$

where $E_{h.i}$ is the energy of the highly ionizing particles, and E_μ the energy of the muons. In order to obtain $N_e(t)$, it is necessary to know the high-altitude behaviour of the number of particles in the shower, λ_0 (figure 97). Since λ_0 depends slightly on the number of particles in the shower, one may use this value to obtain the values of the energy of the electron-photon component and the energy of the nuclear component that has been transferred to π^0-mesons. The energy of muons at sea level can be determined by examining their spectrum. To this quantity, one has to add the energy of the decaying muons, the energy loss on ionization and the energy of the neutrinos. If the number of nuclear-active particles in the shower and their dependence on altitude are known, one can calculate the number of nuclear disintegrations and their energy $E_{h.i}$. Estimations made by Greisen [18] shows that $E_0 = (14 \pm 3)N_e$ GeV, where N_e is the number of particles at sea level for showers with $N_e \sim 10^5$, or generally $E_0 = bN_e$ GeV (b depends on the observation level). At sea level, b depends weakly on energy since $E_0 \sim N^{0.85}$. If the distribution of showers over the number of particles is known, one can easily obtain the spectrum of the primary particles in the energy range of E 10^{15} eV.

We have seen that the shower spectrum with respect to the particle number, has the form of $K(>N) \sim N^{-x}$. Since $E_0 \sim N^{0.85}$ and $N \sim E_0^{1.17}$, then $n(>E_0) \sim E_0^{-1.17x}$. Consequently, the interval $10^4 < N < 10^7$ corresponds to the energy interval $14 \times 10^5 < E_0$ 1.4×10^7 GeV. In this interval, $x \sim 1.5$ and the exponent of the primary-particle spectrum $\gamma - 1 = 1.17\,x = 1.75$.

In the interval $1.4 \times 10^7 < E_0 < 1.4 \times 10^8$ GeV, the spectrum has another slope: $x \sim 2.0$. This yields $\gamma - 1 \simeq 2.3$. At $E_0 > 1.4 \times 10^8$ GeV, the spectrum apparantly becomes more weakly decaying again : $\gamma - 1 \sim 1.7$.

In this manner, various investigations made by means of different methods allow us to estimate the cosmic-radiation spectrum in the energy interval from 1 to 10^{11} GeV.

One of the possible reasons for the complicated behaviour of the cosmic-radiation spectrum is that very-high-energy particles cease to be kept in the Galaxy by the weak magnetic fields ($\sim 10^{-6} \div 10^{-5}$ gauss) and start to escape from it. This effect increases with increasing energy, which leads to the increase of the spectrum's slope. For nuclei, this effect starts to be important at higher energies, therefore the region of the "break" must be enriched with primary nuclei. Particles with an energy higher than 10^9 GeV are already not influenced by the Galaxial magnetic field (the radius of curvature of their motion is larger than the radius of the Galaxy) and hence they are free to penetrate the galaxial and intergalaxial space. Assuming that particles with an energy higher than 10^9 GeV have this origin, the exponent $\gamma - 1 = 1.7$ will define the spectrum of the metagalaxial cosmic rays (see chapter 10, section 3).

Questions and Problems

1. Compute the mean effective inelasticity coefficient for pion interactions in the atmosphere if the absorption path of pions is equal to 130 g/cm^2.
2. Find the relation between the absorption path and the interaction of a monoenergetic beam of primary protons.
3. Find the energy spectrum of pions at various depths in the atmosphere, assuming that the energy spectrum of pions, generated by pions in the interaction acts, is represented by a delta-function :

$$n_2(E, E_0) = n\delta\left(E - \frac{(1-\alpha)E_0}{n}\right),$$

where α is the energy fraction, lost by pions on the production of neutral pions, and n the multiplicity of charged pions.
4. How can the spectrum of photons at large heights in the atmosphere be constructed from the well-known spectrum of muons at sea level ?
5. Find the ratio between protons and neutrons of high energy (higher than 100 GeV) in cosmic rays at a height of 5 kms, assuming that primary radiation only consists of protons and that in each act of interaction the conserved nucleon flies off as a neutron with a probability of 50%. Take the interaction path equal to 85 g/cm^2, the inelasticity coefficient K = 0.5 and the differential exponent of the primary proton spectrum $\gamma = 2.7$.
6. What will be the difference in composition and intensity between cosmic rays at a depth of 20 m of soil under the surfaces of the Earth and the Moon? Assume the densities of the soils to be the same and equal to 2 g/cm^2.
7. At the expense of which processes are high-energy neutrinos produced in the soil ?
8. Qualitatively compare the properties of processes occuring when a proton of an energy higher than 10^3 GeV falls on a layer of air of a thickness equal to 10 nuclear interaction paths and on a similar layer of lead. What will be the difference between the radiations at the lower boundaries of the absorbers?

What will be the changes if the primary energy is increased to 10^7 GeV (assuming that the elementary act will not change) ?

9. Find the energy flux emerging from an ionization calorimeter of a thickness of 10λ (λ is the interaction path) if the inelasticity coefficient $K = 0.75$ and the primary energy is equal to 10^3 GeV. What is the fraction of the primary energy that leaves a calorimeter of this thickness at an energy of 10^3 GeV and of 10^6 GeV ? In the calculation, take into consideration only processes of pion production by pions and nucleons. Assume that pions consume in π°-meson production, only 1/3 of their energy.

PART THREE

ORIGIN OF COSMIC RAYS

Chapter 10

Origin of Cosmic Rays

1. Introduction [1,2]

The problem of the origin of cosmic rays was immediately raised after their discovery. For a long period of time, all theoretical approaches were very artificial because the properties of cosmic radiation outside the atmosphere limits were completely unknown. The problem of the origin of cosmic rays started to have an experimental basis in 1949, when the composition of primary cosmic radiation was investigated. It is now known that the major part of cosmic radiation is created outside the solar system, with the exception of low-energy particles ($E_o < 10$ GeV) which are partially generated on the sun during the moments of great outbursts, together with low-energy particles that occupy the geomagnetic trap. The properties of these particles were considered in chapters 7 and 8.

In this chapter, we shall briefly describe a hypothesis on the origin of cosmic rays, which has been mainly developed by V.L. Ginzburg and is now recognized by many scientists.

At the present time, any theory on the origin of cosmic rays must explain a whole series of well-established properties of the primary cosmic radiation. The most important of these properties are the following :

1) the total energy of cosmic rays,
2) the constant intensity of cosmic rays with respect to time,
3) the isotropy of the distribution of cosmic rays,
4) the energy spectrum $n(E)dE \sim E^{-\gamma} dE$, where $\gamma - 1 = 1.5 - 20$, and
5) the following composition of the primary radiation: the predominance of protons, the presence of nuclei of group L, the presence of heavy nuclei, and the small intensity of electrons and others.

Cosmic rays have a great role in the Universe. Alongside with matter, they belong to the basic elements of the Universe, where an equilibrium of three types of energies is apparently taking place. These types are, the energy density of the magnetic field, the energy density of cosmic rays and the energy density motion of matter :

$$\mathscr{E} \approx \mathscr{H} \approx \frac{\rho u^2}{2},$$

where $\mathscr{E}$ is the energy density of cosmic rays, $H = \frac{H^2}{8\pi}$ the energy density of the magnetic field and $\rho u^2/2 = nkT$ the energy density of the kinetic motion of matter. In a field of a magnetic intensity $H \sim 10^{-6}$ oersted, H 10^{-12} erg/cm^3. The energy densities of the kinetic motion of matter and of cosmic rays have values in this order of magnitude.

The total energy of cosmic rays may be obtained starting from the energy density of cosmic rays near the earth and the volume occupied by cosmic rays. The energy density of cosmic rays was considered in chapter 6 and found to be equal to $\mathscr{E} \simeq 0.9$ eV/cm$^3 \sim 10^{-12}$ erg/cm^3. The dimension of the region occupied by the cosmic radiation is equal to the dimension of the Galaxy, i.e. a sphere of a radius $R \sim 3 \div 5 \times 10^{22}$ cm. This yields a volume equal to $V = (3 \div 5) \times 10^{68}$ cm^3. The total energy of cosmic radiation is then equal to $W_{c.r} \sim 10^{68}$ eV $\sim 10^{56}$ erg. Cosmic rays moving in the inter-star space are subject to a nuclear interaction and after a few collisions loose their energy.

In order to determine the power of cosmic-ray sources, it is necessary to know their life-time, on which the accumulation time depends. The life-time is defined either by the exit of particles from the Galaxy or by their absorption at the expense of inelastic collisions. For nuclear components, the main role in these inelastic collisions is played by nuclear interactions with the atoms of the inter-star gas. Once the nuclear absorption path which for protons is equal to $L_p \sim 100$ g/cm^2, and matter density in the inter-sideral medium ρ ($\rho \sim 10^{-2}$ cm^{-3}) are known, one is able to estimate the time during which cosmic protons are absorbed.

Similar calculations could be carried out for nuclei heavier than protons. The results of calculations for various groups of nuclei till their nuclear absorption, are presented in table 33.

The estimation of the life time of cosmic rays could be done on the basis of the experimental data on the fraction of nuclei of group L in the primary radiation. It has already been mentioned in chapter 5 that the investigation of the quantity of nuclei of group L showed that cosmic rays pass a distance of approximately $1 \sim 5$ g/cm^2 before reaching the earth. Taking the density of the inter-sideral medium $\rho \sim 10^{-26}$ g/cm^3 and the velocity of particle motion to be nearly equal to the velocity of light, one can easily determine the life time of cosmic rays :

$$T = \frac{l}{\rho c} \approx \frac{5}{10^{-26} \cdot 3 \cdot 10^{10}} \approx 1{,}5 \cdot 10^{16} \text{ sec} \sim 5 \cdot 10^{8} \text{ years}$$

Adopting this latter value[1], and taking into consideration the relative stability of cosmic radiation in time, we conclude that the power of cosmic-ray sources is equal to

$$\mathcal{P} = \frac{W}{T} \sim \frac{10^{53}\ \text{erg}}{10^{16}\ \text{erg}} = 10^{10}\ \frac{\text{sec}}{\text{sec}}$$

Consequently, we have to find sources able to provide such a sufficiently powerful radiation

Table 33

Nucleus	p	α	L	M	H	Fe
Absorption Path, g/cm²	100	34	10	7,8	6,1	2,8
Life time, year	2.6×10^9	$1,7\cdot10^9$	$5,0\cdot10^8$	$4,0\cdot10^8$	$3,0\cdot10^8$	$1,4\cdot10^8$

2. Possible Sources of Cosmic Rays

The fact that the power of cosmic-ray sources $\sim 10^{40}$ erg/sec allows us to reject the assumption that stars like the sun, may be the source of cosmic-rays. The sun emits in one second no more than 10^{26} particles with an energy $\geqslant 10^9$ eV so that the power of the sun is equal to 10^{35} eV/sec $\approx 10^{23}$ erg/second. The Galaxy contains 10^{11} stars of the sun's type. Their total power (10^{34} erg/sec) is consequently by many orders of magnitude less than the required power. It is well known that the Galaxy contains a considerable number of stars significantly more powerful than the sun. Since the processes occuring in stars are still not sufficiently well known, the hypothesis that such large stars are the source of cosmic rays has supporters. V.L. Ginzburg however, showed that it was much easier to find the required energy in the

1) The age of the Galaxy is much greater than the life-time of cosmic rays ($T_{Galaxy} \sim 10^{10}$ years). In this respect, cosmic rays observed at present occured quite recently as compared to the time of existance of the Galaxy.

great phenomena responsible for the "super new stars" or "supernovas". "Super new stars" are tremendous ($\sim 5 \times 10^{18}$ cm) expanding gaseous nebulae, occuring as the result of the explosion of a star. One of the most famous supernovas is the crab-like nebula which exploded in 1054 as mentioned in middle-age chronicles.

There are two types of supernovas. The most powerful of them are the massive young stars of the second type. During the explosion, they throw a tremendous quantity of matter (exceeding several times the sun's mass) which fly away at a speed of ten thousand kms/sec. The energy of the explosion reaches 10^{50} or even 10^{52} ergs. A typical evidence for the generation of cosmic rays in the clouds of supernew stars is the powerful radio-wave radiation of these objects.

Electrons existing in the clouds of a supernova, where strong magnetic fields are acting ($\sim 10^3$ oersted in the clouds of the crab-like neubula), must move along curved trajectories (orbits). The electrons are thus accelerated and consequently must radiate electromagnetic waves. The spectrum of this magnetic bremsstraalung (of the supernovas° is a continuous spectrum. Observations by means of radio-telescopes show that the power consumed on the generation of electrons reaches 10^{38} erg/sec.

In the last few years, the non-galaxial sources of radio-wave radiation have been extensively studied. The most powerful among them are the radio-galaxies. When they occur, the energy separated reaches sometimes 10^{60} erg.

By measuring the radio-wave radiation flux, one can estimate the magnetic intensity in the source and consequently the energy of the magnetic field. At the expense of the interaction between the moving magnetic fields and the particles of the source (for instance those in the clouds of the supernovas), the energies of the magnetic fields and the particles must be equal. Therefore, the energy of cosmic rays in the source $W_{c.r.} \sim W_H$ where W_H is the energy of the magnetic field. The estimation of the total energy of cosmic rays in different sources (galaxial supernovas) yields a mean value approximately equal to 10^{49} erg.

Supernew stars in our Galaxy blaze up twice a century on the average. It is then easy to obtain that the mean power $P_{s.n}$ of supernovas in our Galaxy is equal to

$$\mathcal{P}_{c.r} = \frac{W_{c.r}}{T_s} \sim 10^{40} \text{ erg/sec}$$

where $\frac{1}{T}$ is the frequency of occurence of supernovas. We thus conclude that the power of the supernovas is sufficient for providing a constant intensity of cosmic rays in the Galaxy.

3. Cosmic-Ray Acceleration Mechanism

3.1. The Fermi mechanism

We know that cosmic rays involve very-high-energy particles. We thus have to know how such a large energy is concentrated on separate particles together with the search for the sources that produce cosmic rays.

Different authors approached this problem in different manners. Some of them considered that stars were the source of the relatively low-energy particles having an energy of $10^9 - 10^{11}$ eV, and that the acceleration of these particles up to cosmic energies takes place in the inter-sideral medium. Others (among them V.L. Ginzburg) assume that the acceleration takes place near the source, in the clouds of the supernovas. Several mechanisms for the interaction of particles with a magnetic field and leading to their acceleration have been suggested.

The betatron mechanism leads to an increase in particle energy if the field increases. In order to render this mechanism effective, it is necessary for the particles to leave the region where acceleration takes place, otherwise the field would decrease.

An alternative mechanism, considered by Fermi is based on the fact that particles can be accelerated by the inhomogeneities of the magnetic field. The magnetic fields are apparently connected with the gaseous clouds that move in the intersideral space. Within the limits of such a cloud, the "frozen" magnetic field could be considered quasi-homogeneous, while at the boundaries, the field varies strongly. Therefore, such clouds could be considered as a single unit.

The existance of clouds leads to the fact that the motion of charged particles in the Galaxy are very similar to the Brownian motion. In the spaces between the clouds, the particle moves almost linearly. When it collides with a cloud, it suddenly changes its direction of motion. Evidently, if the cloud was stationary in space, the change in the direction of the particle would not be accompanied by a change in energy, since the mass of the cloud is practically infinite as compared to the mass of the particle (only the momentum changes). Quite a different situation holds if the cloud is moving with a speed u. The latter problem is analogous to the change of internal energy of a gas during an adiabatic expansion or compression.

In an adiabatic compression, temperature increases and consequently the kinetic energy of the particles increase. In an expansion, the kinetic energy decreases. Accordingly, if the particle is moving to meet a cloud, it will loose energy. On the average, if the distribution of clouds and particles and their velocities in space are isotropic, the particle will aquire energy, i.e. be accelerated. The reason is that contrary collisions in which energy increases occur statistically more frequently than the cases when the particle overtakes a cloud. In the case of a head-on collision, the probability of a opposite and of an overtaking collision are $\frac{v+u}{2v}$ and $\frac{v-u}{2v}$ respectively (u is the velocity of cloud and v is the velocity of the particle). As a

result, the particle in each collision acquires, on the average, an energy equal to

$$\overline{\Delta E} \sim \frac{u^2}{c^2} E, \tag{10.1}$$

where E is the total energy of the particle and u is the velocity of the cloud. The velocity of the clouds $u \sim 10^6 \div 10^7$ cm/sec, so that $u^2/c^2 \quad 10^{-8}$ and $\overline{\Delta} E \sim 10$ eV.

3.2. The energy spectrum of particles

If the particles makes $1/\tau$ collisions per unit time, then the rate of energy change is given by

$$\frac{dE}{dt} = \frac{u^2}{c^2} \cdot \frac{E}{\tau}, \tag{10.2}$$

where τ is the time of flight between the gaseous clouds. Let be the mean path between collisions with the gaseous collisions and v is the velocity of the particles. Then

$$\frac{dE}{dt} = \frac{u^2 v}{c^2 l} E = \alpha E \text{ и } E = mc^2 e^{\alpha t}. \tag{10.3}$$

If the life-time of the particle is equal to T, then the probability to find a particle of an age t is equal to $dW = Ae^{-t/T} dt$. If the total probability $W = 1$, then $A = 1/T$ and $dW = e^{-t/T} dt/T$.

The differential probability, dW, is proportional to the number of particles of age t, i.e. with energy E. In other words dW defines the differential spectrum of the particles:

$$dW = \text{const}\, n(E)\, dE.$$

Using the relation between t and E, we obtain an explicit expression for the spectrum. From equation (10.3), we obtain

$$t = \frac{1}{\alpha} \ln E/mc^2;$$

$$dW = \frac{\exp[-(1/\alpha T) \ln E/mc^2]}{T} \cdot \frac{dE}{\alpha E} = \frac{1}{\alpha T}\left(\frac{E}{mc^2}\right)^{-1/\alpha T} \frac{dE}{E} = \frac{1}{\alpha T} \cdot \frac{(mc^2)^{1/\alpha T} dE}{E^{1/\alpha T + 1}} \tag{10.4}$$

Accordingly, the differential energy spectrum of cosmic particles will have the form of

$$\tilde{n}(E)\,dE = \text{const}\,E^{-\gamma}\,dE$$

where

$$\gamma = 1 + 1/\alpha T. \qquad (10.5)$$

In this manner the statistical mechanism of acceleration leads to a power spectrum. From the experiments, we know that the differential spectrum of cosmic radiation has an exponent $\gamma = 2.5 - 2.7$. We have found that the nuclear life time for a proton is equal to $T_p = 2.6 \times 10^9$ years $\sim 8 \times 10^{16}$ sec. From these data, we obtain

$$\alpha T = 0{,}6; \quad \alpha = \frac{0{,}6}{8 \cdot 10^{16}} \sim 10^{-17}\ \text{sec}^{-1}.$$

Quantity α mainly depends on the properties of the clouds and their distribution in space and hence should have the same values for all the particles. If the life-time T are defined by losses on nuclear collisions, then γ for alpha-particles will not be 2.7 but significantly less since the life-time of an alpha-particle is less (see table 33) than that of protons (because of the shorter absorption path). The situation for heavier nuclei is even worse. This is clearly in disagreement with the experimental facts, at least for not very high energies ($E < 10^3$ GeV). It means that the life-time is not defined by nuclear collisions but by the duration of the ejection of the particles.

If the acceleration of the particles takes place in limited regions of the Galaxy, for example, in the clouds of supernovas, then T will be the time during which the particle escapes from the region of acceleration and will be the same for all the particles if it is less than T_{Fe}, i.e.

$$T \ll T_{Fe} \sim \frac{1}{20} T_p.$$

In order that a particle is accelerated in the clouds of a supernova, it is necessary to assume that the magnetic field in these clouds has regions of inhomogeneities having small dimensions. Moreover, the speed of the gas in the clouds is ten times larger than the speed of the gaseous clouds. This leads to the fact that the rate of increase in energy, defined by the coefficient $\alpha = u^2 v/c^2 l$, will be several times larger in the clouds of the supernova than in the inter-sideral medium, where u is small and l is large. This difference may reach the value of 10^{10} times. It is therefore necessary to

note that the process of expansion of the cloud will make $\alpha \simeq \alpha(t)$ and

$$E = mc^2 \exp\left\{\int_0^t \alpha(t)\,dt\right\}.$$

Direct calculation shows that, for $\alpha \sim 10^{-7}$ sec^{-1}, a particle acquires an energy $E \sim 20$ mc^2 (i.e. 2×10^{10} eV for a proton) during a period of one year. The expansion of supernova clouds continues for a period $\sim 10^3$ years. During such a period, the particle has enough time to acquire an energy of 10^{13} mc^2 (10^{21} eV for a proton). Since energy is proportional to the mass, an electron will have an energy approximately 1800 times less than the energy of a proton. Moreover, the number of electrons decreases due to the losses on magnetic bremsstraalung. Photons will not be accelerated and will not be trapped by the magnetic field so that they will fly out of the Galaxy.

In conclusion, we have to note that α and T are different in different supernovas. The exponents γ of the particle spectra will therefore be different. Quantity γ however has the same value in all known supernovas, and is close to 2 - 3. The observed spectrum is the result of the addition of spectra from different stars. The number of simultaneously existing supernovas is sufficiently large. During the life-time of a single cosmic particle, the number of existing supernovas is equal to $10^8/50 = 2 \times 10^6$. A good averaging of particle spectra from different sources thus takes place.

3.3. The problem of particle injection

In the previous discussion, we did not consider the possibility of energy losses by particles, which compete with the acceleration procedure. If the energy loss on ionization in the inter-sideral medium during a time dt exceeds the energy acquired during this time, then acceleration will be impossible. Since the increase in energy is proportional to E, and the loss decreases with increase in energy generally speaking there will then be a critical energy, starting from which acceleration becomes possible. This critical energy will be called the injection energy and denoted by E_i.

In an ionized gas, it is necessary to take into consideration energy transfer to electrons. Starting from the condition

$$\alpha E > \left|\left(\frac{dE}{dt}\right)_{ion}\right|$$

we obtain

$$E_i = \frac{2\pi n Z^2 e}{mc\alpha} L_{ion} \simeq 7 \cdot 10^{-9} \frac{nZ^2}{c\alpha}.$$

For protons, this condition is fulfilled at $E > 10^2$ MeV while for iron nuclei, at $E > 300$ GeV. In this manner, iron nuclei cannot be accelerated in the inter-

sideral medium since particles with energies in hundreds of GeV are not emitted from stars. On the other hand, coefficient α is much larger in the supernova clouds. Hence, the injection energy there is less and acceleration is not only possible but in some cases is even indispensible.

A.A. Korčak and S.I. Syrovatskij /3/ considered this problem quantitatively. When a particle moves in an ionized gas, the largest energy loss takes place when the velocity of the particle is close to the velocity v_e of the electrons in the gas. If the acceleration mechanism is so effective that even at a proton energy of $E_p = m_p v_e^2/2$, the quantity $\alpha E_p > \Delta E^p_{max}$, where ΔE^p_{max} is the energy loss, acceleration will then be possible at any low energy. For nuclei, the maximum energy loss will be observed at an energy A times greater than for a proton :

$$E_A = \frac{A m_p v_e^2}{2}.$$

Consequently, the following condition could hold starting from a given value of α :

$$\alpha E_p < |\Delta E_{max}|, \text{ but } \alpha E_A > |\Delta E_{max}|$$

(see figure 99). In this case nuclei will be accelerated starting from the lowest energies whereas there will still be a threshold injection energy for protons. Such a situation probably exists to some extent, since, as mentioned in chapter 5, the fraction of heavy nuclei in cosmic radiation is much higher than their abundance in nature.

3.4. Electron sources

Experiments described in chapter 6 show that primary protons are only a small part of the cosmic-ray flux.

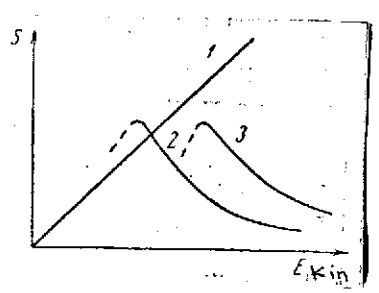

Figure 99. Illustration of the possibility of a particle acceleration without injection: 1- the rate of energy increase, 2- Ionization losses of protons as a function of the kinetic energy, 3- Ionization losses for heavy nuclei.

Electrons in cosmic rays could have two different origins. First, they could be accelerated in the same manner as protons, though the efficiency of acceleration will be less since the energy increment in each act is proportional to the mass. Among the directly accelerated electrons, the fraction of positions must be small.

A second source of electrons might be the production of electrons in the process $\pi \rightarrow \mu \rightarrow e$ initiated by pions occuring in nuclear collisions. The energy of such electrons is proportional to the energy of the nuclear-active particles. Together with electrons, positrons will be produced in an equal quantity.

It is therefore clear that the observation of the charge composition of the electron-positron component gives an information on the relative contribution of the possible sources. Experiments show that the intensity of electrons is roughly by an order of magnitude larger that what nuclear interactions can yield /4/ while the fraction of positrons does not exceed 10 ÷ 20%.

In this manner, direct acceleration is apparently responsible for the observed electron fluxes.

3.5. Photons /5/

Photons are scattered weakly in the inter-sideral medium and it is accordingly possible to search for discrete sources of γ- and X-rays. In particular, X-ray sources were discovered quite recently in the crab-like nebula and in some other Galaxies. For this reason, X-ray astronomy has become as important in value as optical astronomy. Together with the discrete sources, there should be a homogeneous γ-radiation from all parts of the inter-sideral medium resulting from nuclear interactions and from the cynchrotronic radiation by electrons. The theoretical estimation of the intensity of these photons yields a value of approximately 10^{-4} of the cosmic radiation's intensity.

Photons can acquire energy at the expense of the so-called Compton effect, in which electrons are scattered by photons. In this phenomenon, the electron gives part of its energy to the photons. This process is particularly effective near stars where the electron and photon fluxes are large.

3.6. Neutrinos /6/

We have already considered the neutrino sources in chapter 9, section 7. Low energy neutrinos occur in nuclear reactions in stars while high energy neutrinos are generated in the decay of pions and muons in the inter-sideral medium. The cosmic neutrino flux could reach a value of

$$\mathcal{J}_\nu (E > 1 \text{ GeV}) \lesssim 1 \ (\text{m}^2 \cdot \text{sec} \cdot \text{ster})^{-1}.$$

A hundred time more neutrinos are produced in the atmosphere.

3.7. The role of non-galaxial cosmic rays[1)]

Magnetic fields existing in the Galaxy are capable of trapping cosmic-ray particles if their energy is not very high. This condition can be mathematically formulated in the following manner : the radius of curvature of the particle trajectory must be much less than the dimensions of the Galaxy. Energy E_{cr}, corresponding to this condition is equal to $E_{cr} = (\rho c)_{cr} = 300\ H\rho$. Substituting $H \sim 10^{-6}$ oersted and $\rho = 10^{22}$ cm, we obtain $E_{cr} \sim 10^{18}$ eV. Consequently, at $E \simeq 10^{18}$ eV, particles cannot be kept in the Galaxy. The primary cosmic-ray spectrum involves particles with an energy $\sim 10^{20}$ eV. Such particles can penetrate freely through the Galaxy. It is therefore possible to assume that they occupy the space between the galaxies (the metagalaxial space).

The concentration of low-energy (E 10 GeV) particles in the metagalaxial space is small. Otherwise, one has to assume that a tremendous energy, exceeding all what the Galaxy can give, is concentrated on cosmic rays. A possible source, apart from all the sources mentioned above for the metagalaxial cosmic rays, could be the recently discovered cosmic objects known as quasars.

Particles with an energy less than 10^{15} eV can also escape from the Galaxy because their time of existence in the Galaxy (10^{8} sec) is much less than the time defined by nuclear collisions. If the energy is higher than 10^{15} eV, the rate of particle escape is increased (the period of stay in the Galaxy decreases). This fact find its reflection in the increase of the slope of the primary spectrum.

In chapter 5 (subsection 2.5) we discussed the possibility of cutting off the cosmic-ray spectrum at energies higher than 5×10^{19} eV because of collisions with ancient photons. Recently Mac Casker in Australia found evidence for the existance of primary particles with energies higher than 2×10^{20} eV while studying extensive atmospheric showers. Their spectrum apparantly does not become sharp at this energy. This puts us in a dramatic situation which certainly calls for new experimentation and new hypotheses. The reader can by himself search for a conclusion from this new situation.

APPENDICES

1. Some physical constants

Light velocity in vacuum	$c = 2.997925 \times 10^{8}$ m/sec.
Electron charge	$e = 1.60210 \times 10^{-19}$ Coulomb
Planck's constant	$h = 6.6256 \times 10^{-34}$ j/sec
	$\hbar = \frac{h}{2\pi} = 1.05450 \times 10^{-34}$ j/sec

1) For a more detailed discussion on this important subject, see Ref. [1].

Boltzmann's constant	$k = 1.38054 \times 10^{-23}$ j/k
Avogadro's number	$N_A = 6.02252 \times 10^{26}$ (kg mole)$^{-1}$
Classical electron radius	$r_e = \frac{e^2}{m_e c^2} = 2.8176 \times 10^{-15}$ m
Electron Compton wave length	$\lambda_e = \frac{h}{m_e c} = 2.4265 \times 10^{-12}$ m
Fine structure constant	$\alpha = \frac{e^2}{\hbar c} = 1/137.027$
Number of molecules in 1 cm^3 at normal conditions	$L = 2.687 \times 10^{19}$ cm^{-3}

2. Measuring units

1eV = 1.60210×10^{-7} j = 1.60210×10^{-12} erg

1 MeV = 10^6 eV

1 GeV = 10^9 eV

1 TeV = 10^{12} eV

3. Particle Masses

Electron	$m_e = 0.511$ MeV $= 9.109 \times 10^{-31}$ kg
Proton	$m_p = 1836\ m_e = 0.939$ GeV $= 1.672 \times 10^{-27}$ kg
Pions	$m_{\pi^\pm} = 273.2\ m_e = 139.63$ MeV
	$m_{\pi^0} = 264.2\ m_e = 135.0$ MeV
Muons	$m_\mu = 206.76\ m_e = 105.655$ MeV
Kaons	$m_{K^\pm} = 966.6\ m_e = 439.9$ MeV

4. Life-times

Pions	$\tau_{\pi^\pm} = 2.55 \times 10^{-8}$ sec
	$\tau_{\pi^0} = 2.1 \times 10^{-6}$ sec
Kaons	$\tau_{\mu^\pm} = 2.212 \times 10^{-6}$ sec
Muons	$\tau_{K^\pm} = 1.22 \times 10^{-8}$ sec
	$\tau_{K_1^0} = 1.00 \times 10^{-10}$ sec
	$\tau_{K_2^0} = 6.1 \times 10^{-8}$ sec

5. Relation between altitude from sea level, air column pressure and density

Table 1

Altitude over sea level, km	pressure g/cm²	Air density g/cm³·10³	Altitude over sea level km	pressure g/cm²	Air density g/cm³·10³
0	1030	1,225	5,50	513	0,697
0,5	969	1,167	—	—	—
1,0	914	1,112	6,0	478	0,660
1,5	860	1,058	7,0	417	0,590
2,0	808	1,006	8,0	362	0,525
2,25	783	0,981	9,0	312	0,466
2,50	759	0,957	10	268	0,413
2,75	735	0,933	11	230	0,364
3,00	712	0,909	12	196	0,311
3,25	690	0,886	13	168	0,265
3,50	668	0,863	14	143	0,227
3,75	646	0,841	15	122	0,194
4,00	626	0,819	16	104	0,165
4,25	606	0,798	17	89	0,141
4,50	586	0,777	18	76	0,121
4,75	567	0,756	19	65	0,103
5,00	549	0,736	20	55,5	0,088

6. Values of t-units and critical energies ε for various elements and complex materials

a) Elements

Table 2

element	z	A rounded	Density in g/cm³ at normal conditions	t, g/cm²	ε, M: without accounting for effective density	ε, M: with accounting for effective density
H	1	1	0,0899·10⁻³	62,8	350	—
He	2	4	0,1785·10⁻³	93,1	250	—
Li	3	7	0,534	83,3	180	138
Be	4	9	1,84	66,0	141	110
B	5	11	2,33	53,6	115	91
C	6	12	2,22 (графит)	43,3	97	77
N	7	14	1,25·10⁻³	38,6	85	—
O	8	16	1,429·10⁻³	34,6	75	—
F	9	19	1,69 10⁻³	33,4	67,5	—
Na	11	23	0,97	28,2	55,5	46,5
Al	13	27	2,7	24,3	47	40
Si	14	28	2,35	22,2	44	37,5
Ar	18	40	1,783·10⁻³	19,7	34	—
Ca	20	40	1,54	16,3	30,4	26,7
Fe	26	56	7,6—7,88	13,9	23,3	20,7
Cu	29	63,5	8,89	13,0	20,9	18,8
Br	35	80	1,139·10⁻³	11,5	17,2	15,7
Ag	47	108	10,5	9,0	12,7	11,9
Xe	54	131	5,85·10⁻³	8,5	11,0	—
W	74	184	19,3	6,8	8,3	8,1
Pb	82	207	11,34	6,4	7,5	7,4

b) Complex materials

Table 3

MATERIAL	Density g/cm²	t g/cm²	$\mathcal{E}$, MeV without accounting for effective density	$\mathcal{E}$, MeV Accounting for effective density
Air	$1{,}29\cdot10^{-3}$	37,1	81	—
Water	1,0	36,4	90	73
Lithium hydride (LiH)	0,6	80	207	157
Polystyrene $(C_8H_8)_m$	—	44,4	110	88
Clay $(Al_2SiO_3\cdot2SiO_3\cdot2H_2O)$	1,3÷2,5	28,8	60,9	50,6
Quartz (SiO_2)	2,65	27,4	56,2	47,3
Limestone ($CaCO_3$)	2,93	24,2	51,2	43,4
Salt (NaCl)	2,16	22,2	42,1	36,2
Nuclear Emulsion NIKFI-r	3,9	11,4	17,8	16,4

Table of Elementary Particles

Family	Particle	Spin (parity)	Isospin	Mass, MeV	Basic decay scheme	Mean Life time, sec
Photon	γ	1^-	—	0	—	Stable
Leptons	ν_e / ν_μ	1/2	—	0 {(<0,2 keV) / (<2 MeV)}	—	Stable
	e^-	1/2	—	0,5	—	Stable
	μ^+	1/2	—	105,7	$e^+\nu_e\nu_\mu$	$2{,}2\cdot10^{-6}$
Mesons	π^+	0^-	1	139,6	$\mu^+ + \bar{\nu}_\mu$	$2{,}6\cdot10^{-8}$
	π^0	0^-	1	135,0	$\gamma\gamma$, 98,8% γe^+e^-, 1,2%	$\sim0{,}9\cdot10^{-16}$
	K^+	0^-	1/2	493,8	$\mu+\bar{\nu}_\mu$(63,5%), $\pi^+\pi^0$ (21%), $2\pi^+$, π^- (5,5%)	$1{,}23\cdot10^{-8}$
	K^0	0^-	1/2	497,8	$K_1^0\to\pi^+\pi^-$ (69%), $2\pi^0$ (31%) $K_2^0\to$ {$\pi e\nu$ (37%), 3π (23%), $\pi\mu\nu$ (29%), $\pi^+\pi^-\pi^0$}	$K_1^0(0{,}88\cdot10^{-10})$ $K_2^0(5{,}8\cdot10^{-8})$
Baryons	p	1/2	1/2	938,3	—	Stable
	n	1/2	1/2	939,5	$pe^-\bar{\nu}_e$	$1{,}01\cdot10^3$
	Λ	1/2	0	1115,6	$p\pi^-$ (66%), $n\pi^0$ (34%)	$2{,}53\cdot10^{-10}$
	Σ^+	1/2	1	1189,5	$p\pi^0$ (53%), $n\pi^+$ (47%)	$0{,}81\cdot10^{-10}$
	Σ^0	1/2	1	1192,2	$\Lambda\gamma$	$<1\cdot10^{-14}$
	Σ^-	1/2	1	1197,3	$n\pi^-$ (99,8%)	$1{,}65\cdot10^{-10}$
	Ξ^0	1/2	1/2	1314,7	$\Lambda\pi^0$ (>99%)	$3{,}0\cdot10^{-10}$
	Ξ^-	1/2	1/2	1321,2	$\Lambda\pi^-$(>99%)	$1{,}75\cdot10^{-10}$
	Ω^-	3/2	0	1674±3	$\Xi\pi$ (~50%), $\Lambda\bar{K}$ (~50%)	$1{,}5\cdot10^{-10}$

Table of Some Resonances

Family	Hypercharge, isospin	symbol	rest energy	Energy width, MeV	Spin	Parity, G-parity	Basic decay scheme
Mesonic resonances	0; 0	η^0	549	0,002	0	—; +	2γ (39%); $3\pi^0$, $\pi^0 2\gamma$ (31%) $\pi^+\pi^-\pi^0$ (25%)
		ω^0	783	12	1	—; —	$\pi^+\pi^-\pi^0$ (90%); $\pi^0\gamma$ (<10%)
		$\eta'_{(x^0)}$	958	<4	0	—; +	$\eta 2\pi$ (76%); $\pi^+\pi^-\gamma$
		φ	1019	3	1	—; —	K^+K^- (47%); K_1K_2 (39%) $\pi^+\pi^-\pi^0$
		f	1260	140	2	+; +	2π
	0; 1	ρ	765	125	1	—; +	2π
		A_1	1070	80	1	+; —	$\rho\pi$
	1; 1/2	K^*	893	49	1	—	$K\pi$
Barionic resonances	1; 1/2	Ξ_δ	1530	7,3	3/2	+	$\pi\Xi$
		Ξ^{II}_α	1933	140	5/2	+	$\pi\Xi$; $\Lambda\widetilde{K}$
	0; 0	Λ_β	1405	36	1/2		$\pi\Sigma$
		Λ^I_γ	1519	16	3/2	—	$\pi\Sigma$ (55%); $\widetilde{K}N$ (29%) $\pi\pi\Lambda^0$ (16%)
		Λ_α	1815	~50	5/2	+	$\widetilde{K}N$ (75%); $\Lambda 2\pi$ (~15%) $\Sigma\pi$ (~10%)
	0; 1	Σ^I_δ	1381	~45	3/2	+	$\pi\Lambda^0$ (91%); $\pi\Sigma$ (9%)
		Σ_β	1767	~85	5/2	—	$\widetilde{K}N$ (~50%); $\pi\Lambda$ (~14%)
	1; 1/2	N_γ	1518	80	3/2	—	πN (~50%); $2\pi N$
		N^{II}_β	1688	100	5/2	—	πN (~35%); ΛK
		N^{II}_γ	2190	~200	7/2	—	πN (~30%); ΛK
	1; 3/2	Δ^I_δ	1236	120	3/2	+	πN
		Δ_β	1670	180	1/2	—	πN (~45%)
		Δ^{IV}_δ	2850	~300	15/2	+	πN

REFERENCES[1)]

CHAPTER 1

1. Skobel'cyn D.V., Cosmic rays (Kosmičeskie luci), M. ONTI, 1936
2. Dobrotin N.A., Cosmic rays (Kosmičeskie Luci). M., GITTL, 1954.
3. Cosmic rays (Kosmiceskie Luci). BSE, 2 ed., volume 23.
4. Janossi L., Cosmic rays (Kosmičeskie Luči). M., IL, 1949.
5. Dobrotin N.A., Cosmic rays (Kosmičeskie Luci). M., Izd-vo AN SSSR, 1963.
6. Rossi B., Cosmic rays (Kosmičeskie Luci). M., Atomisdat, 1966.
7. Ginzburg V.L., Cosmic rays at the earth and in the Universe (Kosmičeskie Luči u Zemli i vo Vselennoj). M., "Nauka", 1967.
8. Collection "Solar activity and cosmic rays" (Solnečnaja aktivnost' i kosmičeskie luči). M., IL., 1962.

CHAPTER 2

1*. Bohr N., Phil. Mag., 30, 581, 1915.
2*. Bethe H., Ann. der Phys., 5, 325, 1930.
3. See, for example, Kalašnikov et al;, Elementary particle detectors (Detektory elementarnyh častic). M., "Nauka", 1966.
4. Riston D., Experimental methods in high-energy physics (Eksperimental'nye metody v fizike vysokyh energij). M., "Nauka", 1964.
5. Belen'kij S.Z., Shower processes in cosmic rays (Lavinnye processy v. kosmičeskih lucah). M., Gostehizdat, 1948.
6. Gajtler V., Quantum theory of radiation (Kvantovaja teorija izlučenija). M., IL., 1964.
7. Dovženko O.I. and Pomanskij A.A., Transactions of FIAN, 26, 166, 1964.
8. Rossi B. and Grejzen K., Interaction of cosmic rays with matter (Vzaimodejstvie kosmičeskih lučej s veščestvom). M., IL, 1948.
9. Rossi B., High-energy particles (Časticy bolšyh energij). M., GITTL, 1965.
10. Belen'kij S.Z. and Ivanenko I.P., UFN, 60, 591, 1959.
11. Buslenko N.P., Golenko D.I., Sobol' I.M. et al, Method of statistical trials (Method statističeskih ispytanij). M., Fizmatgiz, 1962.
12*. See, for example, Nuovo Cim. Suppl., 1, 1087, 1963.
13. Pauell S., Fauler P. and Perkins D., Investigation of elementary particles by photographic methods (Issledovanie elementarnyh častic fotografičeskim metodom). M., IL, 1962.
14. Invanenko I.P., Doctor dissertation. M., FIAN, 1967.
15*. Emil'janov Ju. A. et al., Izv. AN SSSR, ser. fiz., 31, 1536, 1967.
16. Murzin V.S. and Saryčeva L.I., Cosmic rays and their interactions (Kosmičeskie luči i ih vsaimodejstvija). M., Atomizdat, 1968.

Chapter 3

1*. Guseva V.V., Dobrotin N.N. et al., Journ. Phys. Soc. Japan, 17, Suppl. AIII, 375, 1962.

2*. Alichanov A.N., Alichanjan A.I. and Weisenberg A.O., Journ. Phys. USSR, 11, 97, 1947.
3. Vajsenberg A.O., Mu-meson (Mju-mezon). M., "Nauka", 1964.
4. Rozental' I.L., UFN, 94, issue 1, 91, 1968.
5. See references /2,6/ to chapter 1 and /9/ to chapter 2.
6*. Anderson C.D. et al., Phys. Rev., 75, 1432, 1949.
7*. Ždanov G.B. et al., DAN SSSR, 65, 287, 1949.
8*. Conversi M. et al., Phys. Rev., 71, 209, 1947.
9. Markov M.A., Neutrino (Nejtrino). M., "Nauka", 1964.
10. Pontekorvo B.M., UFN, 79, 3, 1963.
11. Rajnes F., UFN, 77, 287, 1962.
12. See Ref. /13/ to chapter 2.
13. Markov M.A., Hyperons and K-mesons (Giperony i K-mezony). M., Fizmatgiz, 1958.
14. Grišin V.T., Resonance interactions of elementary particles (Rezonansnye vsaimodejstvija elementarnyh častic). UFN, 86, 71, 1965.
15. Zel'dovic Ja. B., Classification of elementary particles and quarks for pedestrians (Klassifikacija elementarnyh častic i kvarkov v izloženii dlja pešehodov), UFN, 8, 303, 1965.
16. Skačkov et al., Collection of problems in nuclear physics (Sbornik zadač po jadernoj fizike), M., Fizmatgiz, 1963.

Chapter 4

1. Baldin A.M., Gol'danskij V.I., Maksimenko V.V. and Rozental' I.L., Nuclear reaction kinematics (Kinimatica jadernyh reakcij). M., "Nauka", 1968.
2*. Veksler V.I., Dobrotin N.A., Zacepin G.T. et al., ŽETF, 19, 826, 1949.
3*. Bellitini G. et al., Nucl. Phys. 79, 609, 1966.
4*. Basilova P.N. et al., Izv. AN SSSR, ser. fiz., 30, 1610, 1966.
5*. Daniel R. et al., Nuovo Cinm. Suppl., 1, 1163, 1963.
6. Murzin V.C. and Saryčeva L.I., Cosmic rays and their interactions (Kosmiceskie lyči i ih vzaimodejstvija). M., Atomizdat, 1968.
7. Elton L., Nuclear dimensions (Razmery jader). M., IL, 1962.
8. Batašenkov V.S., Interaction cross-sections of elementary particles (Secenija vzaimodejstvija elementarnyh častic). M., "Nauka", 1966.
9*. Bradt H. and Piters B., in collection "Primary cosmic radiation" (Pervičnoe kosmičeskoe izlucenie). M., IL, 1956.
10. See reference /13/ to chapter 2.
11. Nuclear emulsions (Jadernye emul'sii). M., Fizmatgiz, 1961.
12*. Vernov et al., DAN SSSR, 81, 379, 1951; Grigorov N.L., UFN, 58, 599, 1956; Carahč'jan A.N. and Carahč'jan T.N., ŽETF, 35, 1088, 1958.
13*. Baradzej L.T. et al., Transactions of FIAN, 26, 224, 1964; Babajan H.P. et al., Izv. AN SSSR, ser. fiz., 28, 1184, 1964.
14. Grigorov N.L. et al., Cosmic investigations (Kosmičeskie issledovanija), 2, 724, 1964; Murzin V.S., In. Progress in Elem. Part. and Cosmic Rays, vol. 5, Amsterdam, North-Holl. Publ. Comp., 1967, p.247.

15*. Grigorov N.L. et al., Transactions of International Conference on Cosmic Rays (Trudy Mezdunarodnoj konferencii po kosmičeskim lučam), vol 1. M., Izd-vo AN SSSR, 1960, p.122.
16. Dajon M.I. et al., Spark chambers (Iskrovaja kamera). M., Atomizdat, 1967.
17*. Vernov S.N., Transactions of FIAN, issue 1, 25, 1945.
18*. Grigorov N.L. et al., Cosmic investigations (Kosmičeskie issledovanija), 5, 383, 1967.
19*. Danisz M. and Pniewski J., Phil. Mag., 44, 350, 1953.
20*. Grigorov N.L. et al., ŽETF, 35, 3, 1958.
21*. See reference /1/ to chapter 3.
22. Ciok P. et al., Nuovo Cim., 10, 741, 1958.
23. Volzenskaja V.A. and Saryčeva L.I., Izv. AN SSSR, ser. fiz. 30, 1594, 1966.
24*. Lohrmann E. et al., Phys. Rev., 122, 672, 1961.
25*. Koshiba M. et al., Nuovo Cim. Suppl., 1, 1091, 1963.
26. Fejnberg E.L. and Černavskij D.S., UFN, 80, 3, 1964.
27. Hajakava S., UFN, 89, 259, 1966.
28. Zacepin G.T., Izv. AN SSSR, 26, 1082, 1962.
29. Fejnberg E.L., UFN, 70, 333, 1960.
30*. Landau L.D., Izv. AN SSSR, ser. fiz., 17, 85, 1953.

Chapter 5

1*. Vernov S.N. et al., Transactions of International Conference on Cosmic Rays (Trudy Meždunarodnoj konferencii po kosmičeskim lucam), vol. 3. M., Izd-vo AN SSSR, 1960, p.17.
2*. See reference /13/ to chapter 2.
3*. Volodicev N.N. et al., Cosmic investigations (Kosmičeskie issledovanija), 5, 431, 1967.
4*. Kurnosova L.D., Izv. AN SSSR, ser. fiz., 31, 1214, 1967; Ginzburg V.L. et al., UFN, 82, 585, 1964.
5*. Rubcov V.I. and Zacepin V.L., Izv. AN SSSR, ser. fiz., 31, 1233, 1967.
6*. Daniel R. and Stephens S., Proc. Int. Conf. Cosmic Rays, vol. 1. London, 1965, p.335.
7*. Grigorov N.L. et al., Izv. AN SSSR, ser. fiz., 31, 1222, 1967.
8*. Greisen K., Phys. Rev. Lett. 16, 748, 1966; Zacepin G.T. and Kuz'min V.A., ŽETF Letters (Pis'ma v ZETF), 4, 114, 1966.

Chapter 6

1. See references /1, 4/ to chapter 1.
2. See references /4/ to chapter 1.
3*. Savenko I.A. et al., In collection: Artificial satellites (Isskustvennye sputniki Zemli), issue 10. M., Izd-vo AN SSSR, 1961, p.45.
4*. Quenby J. and Wenk G., Phil. Mag., 7, 1457, 1962.
5*. Brikker S.I. et al., DAN SSSR, 61, 629, 1948.

6*. Vernov S.N. et al., DAN SSSR, 68, 253, 1949.
7*. Vernov S.N. et al., Izv. AN SSSR, ser. fiz., 17, 13, 1953.
8*. Quenby J., Proc. Int. Conf. Cosmic Rays, vol. 1. London, 1965, p.3.
9. See reference /4/ to chapter 1.
10. Ginzburg V.L. and Syrovatskij S.I., Origin of cosmic rays (Proishoždenie kosmičeskih lucej). M., Izd-vo AN SSSR, 1963.

Chapter 7

1. Van Allen Dž, In collection: Radiational belts of the earth (Radiacionnye pojasa Zemli). M., IL, 1962, p.13.
2*. Vernov S.N. and Čudakov A.E., Transactions of International Conference on Cosmic Rays (Trudy Meždunarodnoj konferencii po kosmičeskim lučam), vol.3. M., Izd-vo AN SSSR, 1960, p.17.
3*. Van Allen Dž., Transactions of International Conference on Cosmic Rays (Trudy Meždunarodnoj Konferencii po kosmičeskim lučam), vol. 3, M., Izd-vo AN SSSR, 1960, p.5.
4*. Vernov S.N. et al., DAN SSSR, 120, 123, 1958.
5. Al'fven H., Cosmic electrodynamics (Kosmicesskaja electrodinamika) M., IL, 1952.
6. Collection: The near space (Okolozemnoe kosmičeskoe prostranstvo). M., "Mir", 1966, p.68.
7. Collection: Science in cosmus (Nauka v kosmuse). M., "Nauka", 1964, p.97.
8. Collection: The near space (Okolozemnoe kosmičeskoe prostranstvo). M., "Mir", 1966, p.72.
9. Collection: The near space (Okolozemnoe kosmičeskoe prostranstvo). M., "Mir", 1966, p. 74.
10. Rosser U., UFN, 85, 147, 1965.
11. Collection: The near space (Okolozemnoe prostranstvo). M., "Mir", 1966, p. 71.
12. Operation "Starfish" (Operacija "Morskaja zvezda"). M., Atomizdat, 1964.
13. Skuridin G.A. and Pletnev V.D., UFN, 85, 605, 1965.
14. Vernov S.N. and Cudakov A.E., Report in V assemby of IGY (Dokl. na V assamblee MGG). M., Izd-vo AN SSSR; Singer S.F., Phys. Rev. Let., 1, 171, 1958.
15. Tverskoj B.A., Dynamics of radiational belts (Dinamika radiacionnyh pojasov). M., "Nauka", 1968.
16. Collection: "Solar-terrestrial physics (Colnečnozemnaja fizika) Translated from English, edited by I.A. Žulin and G.A. Skuridin. M., "Mir", 1968.

Chapter 8

1. Geiss J., Proc. Int. Conf. on Cosmic Rays. Jaipur, vol. 3, 1964, p.434.
2. Libbi W., Radiocarbon dating, 2-nd Ed., Chicago University Press, 1963.
3. Libbi U.F., Radiocarbon atomic watches, In Science and humanity (Radiouglerod-atomnye casy. B kn. "Nauka u čelovečestvo"). M., "Znanie", 1962, p. 190.

4. Honda M. and Arnold J., Effects of cosmic rays on meteorites. Handbuch der Physik, Bd 46/2. Kosmische Stralung II. Berlin, Springer-Verlag, 1967.
5. Dorman L.I., Cosmic-ray variations (Variacii kosmičeskih lučej). M., Gostehizdat, 1957.
6. Dorman L.I., Cosmic-ray variations and the investigation of cosmus (Variacii kosmičeskih lučei i issledovanie kosmusa). M., Izd-vo AN SSSR, 1963.
7. Dorman L.I., Recent ideas about cosmic-ray variations. In collection: "Cosmic rays (results of IGY)" (Kosmiceskie luci (resultaty MGG). M., Izd-vo AN SSSR, 1961.
8. Parker E.N., The dynamical origin of the solar wind and cosmic ray variations. In: "Progress in Elem. Part. and Cosmic Ray Phys.", vol.9, North-Holl. Publ. Comp., 1967; see also reference /16/ to chapter 7.
9. Quenby J., The time variations of the cosmic rays intensity. Handbuch der Physik, Bd. 46/2. Berlin, Springer-Verlag 1967.

Chapter 9

1. Zacepin G.T., DAN SSSR, 67, 993, 1949.
2. Rozental' I.L., DAN SSSR, 80, 731, 1951.
3. Messel' G., In: Cosmic-ray physics (Fizika kosmičeskih Lucej), edited by Dž. Vil'son, volume 2. M., IL, 1956.
4. Grigorov N.L., UFN, 58, 599, 1956, ŽETF, 45, 1544, 1963; ŽETF, 45, 1920, 1963.
5*. Baradzej L.T., Rubcov V.I. and Smorodin Ju. A., Transactions FIAN, 26, M., "Nauka", 1964.
6. Yash Pal and Peters B., Mat. Fys. Medd.-Dan., 33, Nr. 15, 1964.
7. See reference /16/ to chapter 2.
8*. Kocarjan N.M. et al., ZETF, 35, 1335, 1958.
9*. Brook G., Meyer M. and Wolfendale A.W., Proc. Phys. Soc., 83, 871, 1964.
10*. Aurela A., Mac Keown and Wolfendale A.W., Proc. Phys. Soc., 89, 401, 1966.
11. Puppi Dž. and Dellaporta N., in: Cosmic ray physics (Fizika kosmičeskih lučej), edited by Dz. Vil'son, vol. 1. M., IL, 1954.
12. Schopper E., Lohrmann E. and Mauck G., Handbuch der Physik, Bd. 46/2, S. 371, 1967.
13. Ramana Murthy P.V. and Memon M.G., in: Progr. in Elem. Part. and Cosmic Rays, edited by J. Wilson, vol. 9, North-Holl. Publ. Comp., Amsterdam, 1967.
14. Fauler P. and Vol'fendajl A., in: Cosmic ray physics (Fizika Kosmičeskih lučej), edited by Vil'son Dž., vol. 4. M., IL, 1960.
15. Zacepin G.T. and Michalchi E.D., Proc. Int. Conf. Cosmic Rays, vol. 3. Kyoto, 1962, p. 356.
16. Yash Pal and Tandon S., Proc. Int. Conf. Cosmic Rays, vol. 2, London, 1965, p. 890.

17. Fujimoto H., Handbuck der Physik, Bd. 46/2. Berlin, Springer-Verlag, 1967.
18. Grejzen K., Cosmic-ray physics (Fizika kosmiceskih lučej), edited by Dž. Vil'son, vol. 3. M., IL, 1958, p. 7.
19. Nikol'skij S.I., UFN, 78, 365, 1962.
20. Vavilov Ju. N. et al., Transactions of NIAF, 26, 17, 1964.
21. Bothe et al., Phys. Zs., 38, 964, 1937.
22. Kamata K. and Nishimura J., Progr. Theor. Phys., Suppl. 6, 93, 1958; Nishimura J., Handbuch der Physik, Bd. 46/2. Berlin, Springer-Verlag, 1967.
23. Vernov S.N. and Hristiansen G.B., ŽETF, 35, 635, 1958.
24. Solov'eva V.I., Candidate dissertation. M., FIAN, 1964.
25. Clark G., Proc. Int. Conf. Cosmic Rays, vol. 2. London, 1965.
26. Fukui H., Jurn. Phys. Soc. Japan, 17, Suppl. A III, 220, 1962.
27. Vernov S.N. et al., Transactions of International Conference on Cosmic Rays (Trudy Meždunarodnoj konferencii po kosmičeskim lučam), vol. 2. M., Izd-vo AN SSSR, 1960, p. 123.
28. Zacepin G.T., Transactions of International Conference on Cosmic Rays (Trudy Meždunarodnoj konferencii po kosmičeskim lučam), vol. 2. M., Izd-vo AN SSSR, 1960, p. 212.
29. Abrosimov A.T. et al., Izv. AN SSSR, ser. fiz., 31, 1528, 1967.
30. Čudakov A.E. et al., Transactions of International Conference on Cosmic Rays (Trudy Meždunarodnoj konferencii po kosmičeskim lučam), vol. 2. M., Izd-vo AN SSSR, 1960, p. 50.
31. Jelley J.V., Progr. in Elem. Part. and Cosmic Rays, edited by J. Wilson. North-Holl. Publ. Comp., Amsterdam, 1967.

Chapter 10

1. Ginzburg V.L. and Syrovatskij S.I., Origin of cosmic rays (Proishoždenie kosmičeskih lučej). M., Izd-vo AN SSSR, 1963.
2. Ginzburg V.L., Cosmic rays at the earth and in the Universe (Kosmičeskie luci u Zemli i vo Vselennoj). M., "Nauka", 1967.
3. Korčak A.A. and Syrovatskij S.I., DAN SSSR, 122, 792, 1958.
4. See Reference [6] to chapter 5.
5. Ginzburg V.L., Modern astrophysics. In collection: "About what are physicists thinking?" (Nad cem dumajut fiziki?), issue 6. Astrophysics (Astrofizika). M., "Nauka" 1968; Ginzburg V.L. and Syrovatskij S.I., Gamma- and X-ray astronomy. In collection: "About what are physicists thinking?" (Nad čem dumajut fiziki?), issue 6. Astrophysics (Astrofizika). M., "Nauka", 1968, pp. 5-38.
6. Morrison F, Neutron astronomy. In collection: "About what are physicists thinking?" (Nad čem dumajut fiziki?) issue 6. Astrophysics (Astrofizika) M., "Nauka", 1968, pp. 39-50.